LA-UR-25-22398

Approved for public release; distribution is unlimited.

Title: MCNP® Code Version 6.3.1 Verification & Validation Testing

Author(s): Josey, Colin James
Clark, Alexander R.
Kulesza, Joel A.
Lively, Michael Aaron
Pearson, Eric J.
Rising, Michael Evan

Intended for: Report

Issued: 2025-03-24 (rev.1)

Los Alamos
NATIONAL LABORATORY

LA-UR-25-22398, Rev. 1

MCNP®

Code Version 6.3.1

Verification & Validation Testing

Document compiled from `git` hash `7d780ec54e` on March 19, 2025.

This document cannot be made Section-508 compliant (accessible to persons with disabilities) at this time. If you need help accessing this document, please email mcnp_help@lanl.gov.

Los Alamos
NATIONAL LABORATORY

MCNP® Code Version 6.3.1 Verification & Validation Testing

LA-UR-25-22398, Rev. 1

March 19, 2025

Los Alamos National Laboratory

Colin Josey
Alexander R. Clark
Joel A. Kulesza
Michael A. Lively
Eric J. Pearson
Michael E. Rising

Contents

Part I

Test Case Descriptions

1 Introduction

This report describes the verification and validation testing performed on MCNP® code version 6.3.1. The purpose of this report is to act as a compendium of test suite descriptions and results. Accordingly the document is divided into two parts. Part I (this part) describes each test suite in the following sections. Part II provides the results of testing each suite and comparisons to experimental and/or alternative computational results, as appropriate.

2 Validation

2.1 Criticality

In this suite, originally developed in 2004 in [1], 31 benchmark models from the International Criticality Safety Benchmark Evaluation Project (ICSBEP) Handbook [2] are run. These 31 problems include fast, intermediate, and thermal spectrums, problems with and without reflectors, and geometries with and without lattices. The k-eigenvalue is calculated with several nuclear data libraries (ENDF/B-VI.6, ENDF/B-VII.0, ENDF/B-VII.1, and ENDF/B-VIII.0) and compared against the benchmark measurement.

This suite has had minimal modifications since the original suite was developed. Materials for newer ENDF/B libraries have been generated by taking the latest material data and expanding natural elements into their isotopic compositions using the data from [3], which sources its compositions from [4]. Updates and corrections in the ICSBEP benchmarks after 2004 have not yet been incorporated.

2.2 Criticality Expanded

This suite, originally developed in 2011 [5] is an expanded version of the Criticality suite above. The set includes 119 problems from the ICSBEP Handbook. Material files are available for ENDF/B-VII.0, ENDF/B-VII.1, and ENDF/B-VIII.0.

For this document, the k-eigenvalues are re-verified against the 2015 revision of the ICSBEP handbook to check for transcription errors. The following discrepancies are addressed:

- heu-met-inter-006 Case 2 - k-eigenvalue is changed from 0.9997 (from Revision 3) to 1.0001 (from Revision 4). The actual model in the test suite is from Revision 4.
- ieu-met-fast-007 Case 4 - k-eigenvalue corrected from 1.0030 to 1.0300.

- leu-comp-therm-008 Case 1, 2, 5, 7, 8, 11 - The uncertainty is corrected from 0.0016 to 0.0012.
- mix-comp-therm-002 Case 30, 31, 32, 33, 34, 35 - The actual input file is the detailed model and not the simplified model. The eigenvalues and uncertainty are changed to the detailed model values.
- u233-sol-therm-001 Case 2-5 : k-eigenvalues corrected from 1.0000 to 1.0005, 1.0006, 0.9998, and 0.9999 respectively.
- u233-sol-therm-008 : k-eigenvalue corrected from 1.0000 to 1.0006.

Beyond these corrections, and with the exception of the addition of new nuclear data material cards, this suite is not revised relative to its original development.

2.3 LAQGSM: Los Alamos Quark-Gluon String Model

The original Los Alamos Quark-Gluon String Model (LAQGSM) test suite distributed with the MCNP6.1 code release has not been fully exercised since that release [6]. In that work, calculations were made and compared with 26 sets of experimental data. In the current work, only some sets of experimental data are compared.

Note that all prior experimental and calculated double-differential data used for comparison are converted to consistent units (millibarns $\cdot$ MeV^{-1} $\cdot$ sr^{-1}) with all energies expressed as MeV unless otherwise noted. In addition, all arbitrary multiplicative factors used for previously allowing multiple data sets to be differentiated on the same plot are removed from the raw data.

2.3.1 ^{40}Ar (1042 MeV/A) onto ^{40}Ca Double-differential Cross Section

This test (now named `DblDiff_Ar-40_1042_MeV_A_Ca-40` and formerly named `inpl05`) exercises the LAQGSM03.03 event generator for different NASA (shielding for missions in space) and FRIB (the U.S. DOE Facility for Rare Isotope Beams, a continuation and modification of the former Rare Isotope Production (RIA) project) applications.

This test problem models the double-differential proton spectra at 30°, 70°, 90°, 110°, and 150° from interaction of a 1042-MeV/A ^{40}Ar beam with a thin ^{40}Ca target to compare the results with experimental data.

The experimental data for this test problem were measured at the Berkeley Bevalac by an international team and are presented and discussed in [7]. The complete set of experimental data is tabulated on microfilm and is available from the Physics Auxiliary Publication Service of the American Institute of Physics as a 118-page PDF file by referencing the document number PRVCA-21-1321-117 (CPM reference: 8004E 1309). A set of standalone LAQGSM03.03 results are also available based on independent calculations made at LANL, but these alternative-code data are not presently used herein.

2.3.2 ^{12}C (290 MeV/A) onto ^{12}C Double-differential Cross Section

This test (now named `DblDiff_C-12_290_MeV_A_C-12` and formerly named `c290c`) exercises the LAQGSM03.03 event generator to calculate production of neutrons from intermediate energy carbon-beam induced reactions for different NASA (shielding for missions in space), medical (cancer treatment with a carbon-beam), FRIB (the U.S. DOE Facility for Rare Isotope Beams, a continuation and modification of the former Rare Isotope Production (RIA) project), and for some other U.S. DOE applications.

This test problem models the double-differential neutron spectra at 5°, 10°, 20°, 30°, 40°, 60°, and 80° from interaction of a 290-MeV/A ^{12}C beam with a thin ^{12}C target to compare the results with experimental data.

The experimental data for this test problem were measured at the Heavy Ion Medical Accelerator in Chiba (HIMAC) facility of the National Institute of Radiological Sciences (NIRS), Japan, and are presented and discussed in [8]. A set of calculated results are also available using a standalone version of the LAQGSM03.03 event generator, the Quantum Molecular Dynamics (QMD) code, the Heavy-Ion Code (HIC) code, and 2003 versions of the LAQGSM and LAQGSM03 codes [9], but these alternative-code data are not presently used herein.

2.3.3 ^{28}Si (600 MeV/A) onto ^{64}Cu Double-differential Cross Section

This test (now named `DblDiff_Si-28_600_MeV_A_Cu-64` and formerly named `Si600CuREP`) exercises the LAQGSM03.03 event generator for different NASA (shielding for missions in space), medical (cancer treatment with heavy-ions), and FRIB (the U.S. DOE Facility for Rare Isotope Beams, a continuation and modification of the former Rare Isotope Production (RIA) project) applications.

This test problem models the double-differential neutron spectra at 5°, 10°, 20°, 30°, 40°, 60°, and 80° from interaction of a 600-MeV/A ^{28}Si beam with a thin ^{64}Cu target to compare the results with experimental data.

The experimental data for this test problem are available in [10]. While the most precise representation of the experimental data values is a histogram with bin limits corresponding to the experimental configuration, the former approach of using point values with error bounds corresponding to the bin limits was used to be consistent with other test cases. Additionally, comparisons to other codes previously presented alongside these values (such as those in [6, 11]) are no longer plotted.

2.3.4 ^{20}Ne (800 MeV/A) onto ^{64}Cu Invariant Cross Section

This test (now named `Invariant_Ne-20_800_MeV_A_Cu-64` and formerly named `Ne800Cu`) exercises the LAQGSM03.03 event generator to calculate production of deuterons from intermediate energy heavy-ion induced reactions for different NASA (shielding for missions in space), medical (cancer treatment with heavy-ions), FRIB (the U.S. DOE Facility for Rare Isotope Beams, a continuation and modification of the former Rare Isotope Production (RIA) project), and for some other U.S. DOE applications.

This test problem models the deuteron invariant spectra at 30°, 45°, 60°, 90°, and 130° from interaction of a 800 MeV/A ^{20}Ne beam with a thin ^{64}Cu target to compare the results with experimental data.

The experimental data for this problem were measured at the Berkeley Bevalac by the Shoji Nagamiya Group [12] and are tabulated in [13].

A set of calculated results are also available using a standalone version of the LAQGSM03.03 event generator, but these alternative-code data are not presently used herein.

Note that to convert the calculated double-differential spectra to be consistent with the measured invariant spectra, one needs to calculate the mean deuteron kinetic energy for each energy bin, E_d, to compute the corresponding deuteron momentum, p_d, for each energy bin as

$$p_\mathrm{d} = \sqrt{\left(E_\mathrm{d} + m_\mathrm{d}\right)^2 - m_\mathrm{d}^2}, \tag{1}$$

where m_d is the mass of a deuteron in MeV (1875.61294257 MeV/c^2 [14]) and p_d has units of MeV/c. Then, the invariant spectra can be calculated from the double-differential spectra as

$$\frac{E\mathrm{d}^3\sigma}{\mathrm{d}p_\mathrm{d}^3} = \frac{1}{p_\mathrm{d}}\frac{\mathrm{d}^2\sigma}{\mathrm{d}E\mathrm{d}\Omega}, \tag{2}$$

which has units such as millibarn $\cdot$ steradian^{-1} $\cdot$ MeV^{-2} $\cdot$ c^3.

2.4 LLNL Pulsed Spheres

Lawrence Livermore National Laboratory (LLNL) performed a variety of pulsed-sphere measurements from the 1960s through the 1990s at the (now decomissioned) Insulated Core Transformer (ICT) accelerator. A deuteron beam impinges on a tritiated titanium target placed inside the sphere. The resultant (D,T) reactions nominally produce 14-MeV neutrons that propagate through the sphere. The produced neutron time-of-flight leakage spectra is observed by collimated detectors embedded in a concrete wall at some distance from the pulsed sphere and at some angle with respect to the deuteron beam [15]. Sometimes identical materials in different geometric configurations were used to investigate pulse-spectrum behavior resulting from attenuation through various thicknesses of the material. For this validation suite, six unique material and geometry configurations are selected for analysis (shown in Fig. 1). This is consistent with a recent analysis [16], though these configurations and others have been studied extensively [17–23].

All spheres feature a channel through half of the sphere that permits insertion of the target assembly used to produce the 14-MeV source neutrons. Assuming that the target assembly enters the sphere through the channel from the $+x$ direction, the detector package is positioned relative to the $-x$ direction. For each experiment, the detector is either a Pilot-B or NE213 scintillator and associated hardware. Note that the detector package is modeled as a ring detector within MCNP6 because of geometric and source symmetry. Details of each analyzed case are described next. Note that when describing the spherical geometry, the dimensions are typically given in terms of 14-MeV neutron mean-free paths (MFPs) along the flight path from the source to the detector.

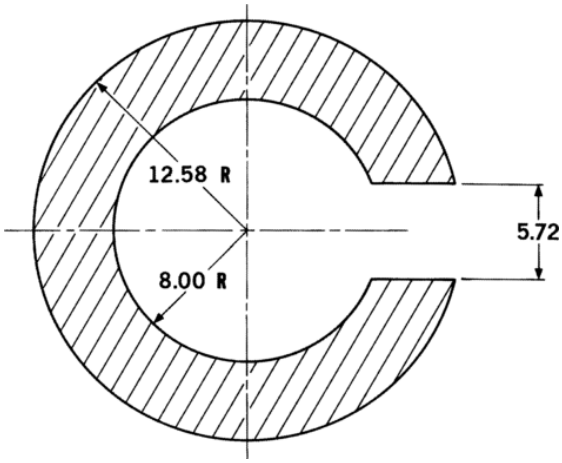

(a) Natural beryllium, 0.8 MFP.

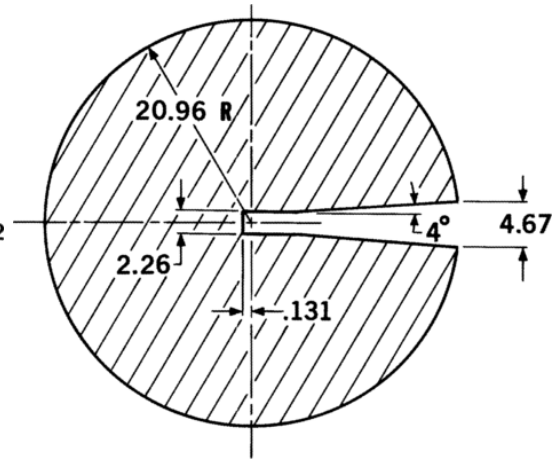

(b) Natural carbon, 2.9 MFP.

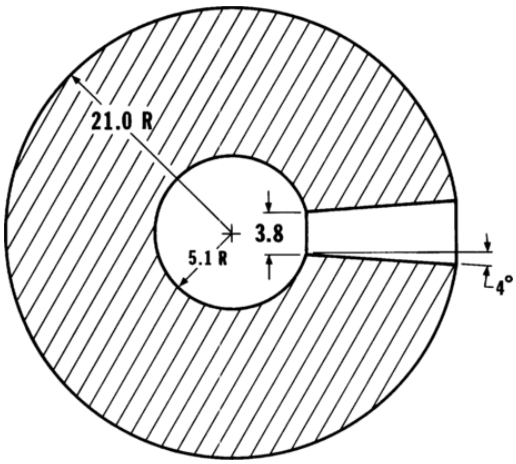

(c) Concrete mixture, 2.0 MFP.

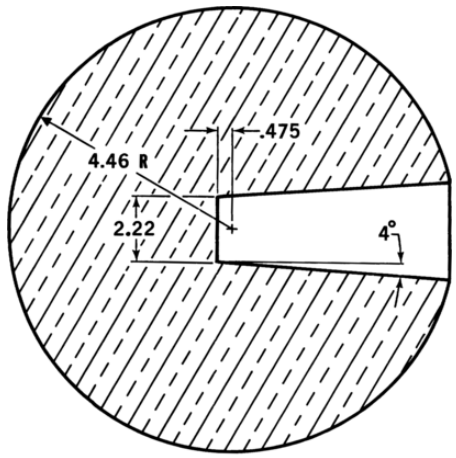

(d) Natural iron, 0.9 MFP.

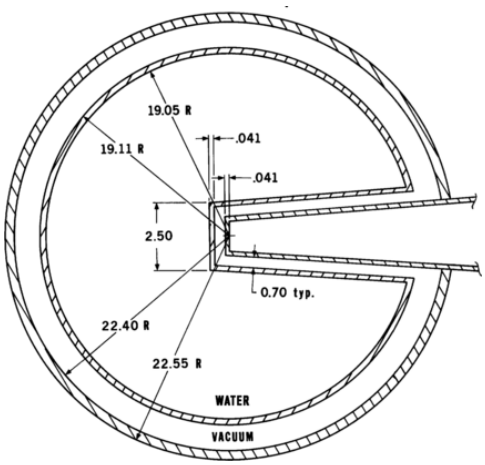

(e) Water, 1.9 MFP.

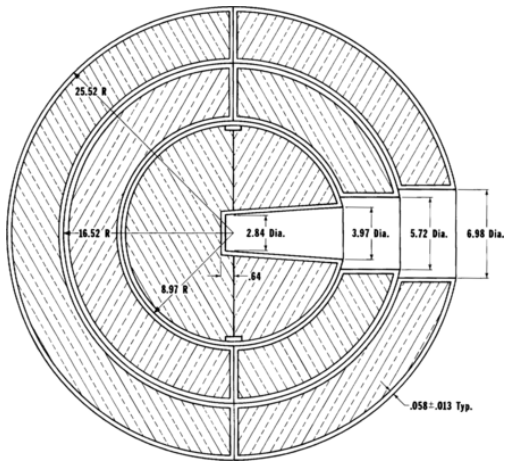

(f) Lithium-6, 1.6 MFP.

Figure 1: Pulsed sphere geometries reformatted from [15] (dimensions are centimeters).

2.4.1 Beryllium

The beryllium sphere with a thickness of 0.8 MFP (outer radius of 12.58 cm) consists of a spherical shell with a cylindrical channel and spherical hollow core. A Pilot-B detector with a 1.6-MeV cutoff energy and FWHM resolution of 4 ns is positioned 30° off-axis with a flight path distance of 765.2 cm. The detector captured results from 137–409 ns (corresponding to neutron energies of 16.7–1.8 MeV).

2.4.2 Carbon

The carbon sphere with a thickness of 2.9 MFP (outer radius of 20.96 cm) consists of a spherical shell with a cylindrical and tapered round channel leading to the center. An NE213 detector with a 1.6-MeV cutoff energy and FWHM resolution of 4 ns is positioned 30° off-axis with a flight path distance of 766.0 cm. The detector captured results from 141–409 ns (corresponding to neutron energies of 15.8–1.8 MeV).

2.4.3 Concrete

The concrete sphere with a thickness of 2.0 MFP (outer radius of 21 cm) consists of a spherical shell with a tapered round channel leading to a hollow spherical center cavity. An NE213 detector with a 1.6-MeV cutoff energy and FWHM resolution of 3 ns is positioned 120° off-axis with a flight path distance of 975.4 cm. The detector captured results from 185–491 ns (corresponding to neutron energies of 14.9–2.1 MeV).

2.4.4 Iron

The iron sphere with a thickness of 0.9 MFP (outer radius of 4.46 cm) consists of a spherical shell with a tapered round channel leading to the center. An NE213 detector with a 1.6-MeV cutoff energy and FWHM resolution of 3 ns is positioned 30° off-axis with a flight path distance of 766.0 cm. The detector captured results from 137–417 ns (corresponding to neutron energies of 16.8–1.8 MeV).

2.4.5 Water

The water sphere with a thickness of 1.9 MFP (outer radius of 22.55 cm) consists of a spherical steel shell (0.15 cm) filled with water surrounded by another steel shell (0.06 cm) with a vacuum between both shells. Each shell has a tapered round channel leading to the center. A Pilot-B detector with a 1.6-MeV cutoff energy and FWHM resolution of 5 ns is positioned 30° off-axis with a flight path distance of 754.0 cm. The detector captured results from 126–392 ns (corresponding to neutron energies of 19.3–1.9 MeV).

2.4.6 Lithium

The lithium-6 sphere with a thickness of 1.6 MFP (outer radius of 25.52 cm) consists of three steel shells (each 0.058 cm thick) with lithium filling the region between each shell. The inner shell has a tapered round channel leading to the center with the two outer shells having a cylindrical channel. A Pilot-B detector with a 1.6-MeV cutoff energy and FWHM resolution of 4 ns is positioned 30° off-axis with a flight path distance of 765.2 cm. The detector captured results from 133–409 ns (corresponding to neutron energies of 17.8–1.8 MeV).

2.5 Lockwood

The Lockwood Electron-transport Validation Suite is a collection of 334 calculations using eight materials of varying thickness bombarded by electrons at a variety of incident energies and angles. The principal reference for this work and the source of the experimental results used here is [24]. Other relevant publications that discuss this work are [25–33].

In Sandia's semi-infinite homogeneous media measurements, electrons were accelerated to between 0.05 and 1 MeV and impinged on thin foils at incident angles of 0°, 30°, and 60°. Energy deposition was measured using thermocouples on the calorimeter foil. The material thickness was varied by adding or removing additional front foils between the electron beam and calorimeter foil.

In [24], thicknesses are expressed as areal density quantities ($\mathrm{g \cdot cm^{-2}}$) or fractions of a mean range (abbreviated as FMR in [24]). The experimental setup is described as (from [p. 24 of 24]):

> The front foil, which is positioned 0.1 cm in front of the calorimeter foil, consists of either a single foil (see Figure III.3) or a stack of two or more foils of the material in which the measurement is being made. Because the thickness of the front foil is varied, the calorimeter foil measures energy deposition as a function of depth in the material. Thus, in determining the depth at which the dose is measured, one-half the calorimeter foil thickness is added to the thickness of the front foil. The minimum measurable depth is obtained with no front foil present, so that the electron beam strikes the calorimeter foil directly.

This approach is generally taken in the MCNP model of the experiment: the front foil and half the thickness of the calorimeter foil are used to calculate energy deposition (though the full thickness of the calorimeter is modeled). In the experiments and the MCNP calculations, an "infinite" plate of material is also positioned beyond the calorimeter foil with a 0.1 cm gap between the calorimeter and the infinite plate [p. 26 of 24]. Using the 1 MeV, 0° iron case as an example for calculating the material thicknesses needed for an MCNP model, one can begin by collecting the needed parameters:

$R = 0.606\ \mathrm{g \cdot cm^{-2}}$	the range in iron for 1.0 MeV electrons [p. 63 of 24],
$\Delta t_\mathrm{f} = 1.956 \times 10^{-2}\ \mathrm{g \cdot cm^{-2}}$	the thickness of the calorimeter foil [p. 64 of 24],
$f = 0.048$	the FMR value that one intends to model (chosen arbitrarily for this example from [p. 65 of 24]),

$\rho = 7.874\ \mathrm{g \cdot cm^{-3}}$ the density of the iron foil (as modeled in the MCNP input file).

The total thickness of material that corresponds to $f = 0.048$ is

$$\Delta t = \frac{fR}{\rho} = \frac{(0.048)\left(0.606\ \mathrm{g \cdot cm^{-2}}\right)}{7.874\ \mathrm{g \cdot cm^{-3}}} \approx 0.003694183388\ \mathrm{cm}. \tag{3}$$

The half thickness of the calorimeter foil is

$$\Delta t_{\mathrm{f,half}} = \frac{\Delta t_{\mathrm{f}}}{2\rho} = \frac{1.956 \times 10^{-2}\ \mathrm{g \cdot cm^{-2}}}{2(7.874\ \mathrm{g \cdot cm^{-3}})} \approx 0.001242062484\ \mathrm{cm}. \tag{4}$$

Therefore, the front foil thickness should be modeled as

$$\Delta t_{\mathrm{front}} = \Delta t - \Delta t_{\mathrm{f,half}} \approx 0.002452120904\ \mathrm{cm} \tag{5}$$

with a 0.1 cm gap between the rear of the front foil and the front of the calorimeter foil. The total calorimeter foil thickness of $\Delta t_{\mathrm{f}} = 0.002484124968$ cm is modeled. Finally, the "infinite" plate of material is modeled with a 0.1 cm gap between the rear of the calorimeter foil and the front of the "infinite" plate. The infinite material is modeled to fill the space from 0.1 cm beyond the calorimeter foil and $z = 5$ cm assuming that the foils are oriented perpendicular to the z axis and the front of the front foil is positioned at $z = 0$.

In summary, the front foil is modeled between $0 \leq z \leq \Delta t_{\mathrm{front}}$, the calorimeter is modeled between $\Delta t_{\mathrm{front}} + 0.1\ \mathrm{cm} \leq z \leq \Delta t_{\mathrm{front}} + 0.1\ \mathrm{cm} + \Delta t_{\mathrm{f}}$, and the infinite plate is modeled between $\Delta t_{\mathrm{front}} + 0.1\ \mathrm{cm} + \Delta t_{\mathrm{f}} + 0.1\ \mathrm{cm} \leq z \leq 5$ cm.

2.6 Rossi-α

The Rossi Validation Suite is a collection of 14 benchmarks in which the "KOPTS kinetics" computed Rossi-α is compared against experimental values. It must be noted that the input decks in this suite are ICSBEP benchmark models, while the Rossi-α values compared against are the raw experimental values. This is unlike the criticality validation suites, in which the reference value has been modified to incorporate corrections due to the benchmark model simplification process. The description of this suite can be found in [34].

These models were ported to the new V&V framework, and ENDF/B-VIII.0 data was added to the repository. The models themselves were unchanged, and materials were not examined against the original references to identify any newly available data that should be used. During the examination of Rossi-α sources, two values were adjusted.

- HEU-MET-FAST-073 values were noted to be inconsistent with all found citations. The Rossi-α was instead taken from [35], as it was the latest found experimental results for this experiment.
- U233-MET-FAST-006 was updated using the ICSBEP-2015 value.

All other experiments match either their original citation or are still present in ICSBEP-2015.

2.7 Electron Stopping Power

The Electron Stopping Power Validation Suite is a collection of 60 benchmarks in which single-event transport is used to compute electron stopping powers from 50 eV to 30 keV in various materials, including 38 elemental solids, 14 compound materials, 3 carbon allotropes, and 5 rare gas solids. MCNP calculations results are compared against semi-empirical data computed from experimental electron energy loss functions (ELF) measurements. Additionally, electron stopping powers are computed directly from the EPRDATA cross section library used in the calculations, and elemental solid stopping powers are compared to an empirical fitting function.

The stopping power calculation is performed by turning off electron elastic scattering (`PHYS:E 12J -1`) and writing all source, bank, and termination events to the PTRAC output file. Track lengths are estimated for each history by summing the distances between source events, change-of-direction events (i.e., ionization and bremsstrahlung collisions), and termination events for source electrons. At each value E_0 of initial electron energy, the range as a function of energy is fit locally by a simple quadratic function, $R(E) = a(E - E_0)^2 + b(E - E_0) + c$. Only the b parameter is needed and computed, and the electron stopping power is then $S_e \approx b^{-1}$.

The complete description of this suite and discussion of the results can be found in [36].

3 Verification

3.1 $k_{\mathbf{eff}}$ Verification

This suite, introduced in [37], contains 37 continuous energy and 68 multigroup k-eigenvalue analytic benchmarks. These simple models include k_∞, infinite slab, infinite cylinder, sphere, and two medium reflected infinite slab problems.

Some of the problems described in that document are excluded. First, continuous energy problems are generated only for one-group models. Second, any problem with P_2 Legendre moments is excluded. Finally, any problem with negative scattering probabilities is excluded, as these pose challenges for Monte Carlo transport.

The MCNP MCTAL file has a maximum of six digits of precision. However, on some problems, particularly the k_∞ problems, the resulting simulation uncertainty is far smaller than the last digit of precision. This poses a problem in performing statistical comparisons when the reference solution is non-zero past the precision of the MCNP output. The results in this document are printed to the precision available.

3.2 Kobayashi

This problem set contains six benchmarks that were designed by Kobayashi [38] to test how 3D discrete ordinates codes deal with ray effects in problems with void and shield regions. The problem set contains three distinct geometries that are each composed of a monoenergetic and isotropic

neutron source, uniformly distributed throughout a cube, that is bounded by void and shield material regions. In each problem, the shield material is either a pure absorber (designated "i") or one in which the scattering cross section is half of the total cross section (designated "ii"). Figure 2 shows octants of the problem geometries.

The first problem is a nested set of the three cubic regions. The second problem contains a central cubic neutron source, a rectangular void duct along one axis adjacent to the neutron source, and shield material encompassing them. The third problem contains a central cubic neutron source, a rectangular void duct with two 90-degree bends, and shield material encompassing them.

In discrete ordinates calculations, an octant of the geometry is simulated with reflective boundary conditions for computational efficiency. In MCNP calculations, however, the entire geometry is simulated. Despite the symmetry of each problem, MCNP point detector tallies produce erroneous results when using reflective boundary conditions.

Prior work [39] investigated this problem set using continuous energy (CE) and multigroup nuclear data, constructive solid geometry (CSG) and unstructured mesh (UM) geometry, and importance splitting turned on or off. This problem set, however, contains only the CE nuclear data, CSG, and importance splitting turned on, with importance splitting parameters given in [40].

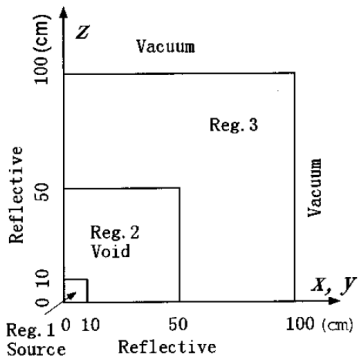

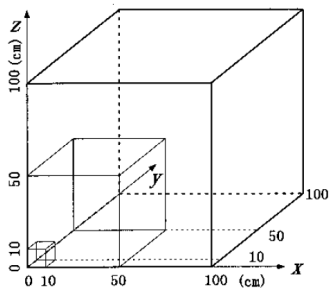

(a) Problem 1.

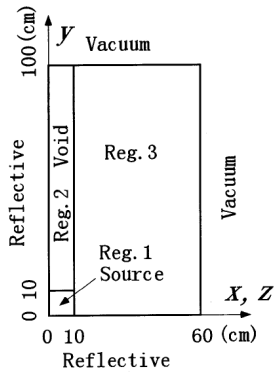

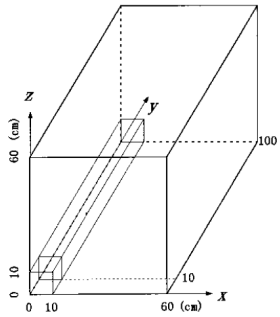

(b) Problem 2.

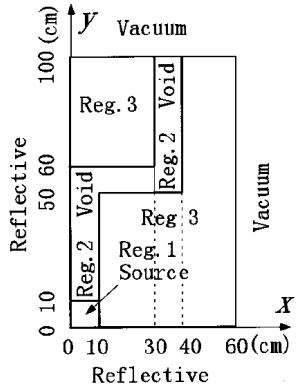

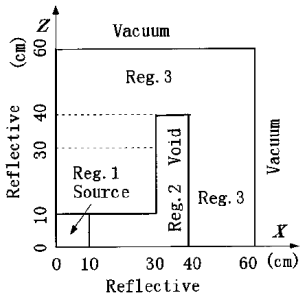

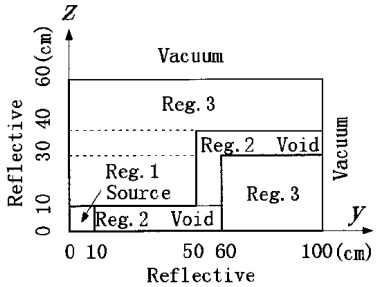

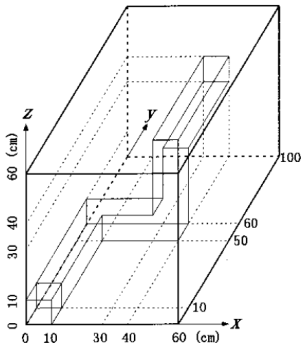

(c) Problem 3, view A.

(d) Problem 3, view B.

Figure 2: Kobayashi problem geometries reproduced from [38].

Part II

Test Case Results

This part describes the conditions under which each test suite is executed (computer hardware summary, runtime options, etc.) and the resulting values from the tests.

In all cases, the test cases are run on the LANL Rocinante supercomputer that is characterized by 380 computer nodes, where each node has dual 56-core processors and 256 GB of memory for a total of 42,560 cores and 97.28 TB of memory. Each processor is an Intel Xeon Platinum 8480 CPU operating at 2.0 GHz. Nodes communicate with an HPE Cray Slingshot11 interconnect. Job execution is managed with the Slurm Workload Manager.

4 Validation

4.1 Criticality

This test suite executes on 1 node, which uses 8 threads with 16 concurrent jobs, with a total Slurm allocation of no more than 10 minutes. An example `VnV.py` execution line is `./VnV.py execute_slurm --ntrd 8 --jobs 16 --time 10 --wait --calcdir_name criticality_$DATA`, where `$DATA` is an environment variable that identifies which evaluated nuclear data set to use.

The following figures and tables are results for the Criticality benchmark suite. The plots display k_{eff} values and their uncertainties. The tables provide benchmark and calculated values and uncertainties. This suite contains 31 ICSBEP Handbook problems that are meant to span a "wide variety of fissile isotopes, spectra, compositions, and configurations" [1].

4.1.1 ENDF/B-VI.6

For the validation criticality (ENDF/B-VI.6) benchmarks, the benchmark data and calculation results are plotted in Fig. 3 with individual values listed in Table 1.

4.1.2 ENDF/B-VII.0

For the validation criticality (ENDF/B-VII.0) benchmarks, the benchmark data and calculation results are plotted in Fig. 4 with individual values listed in Table 2.

4.1.3 ENDF/B-VII.1

For the validation criticality (ENDF/B-VII.1) benchmarks, the benchmark data and calculation results are plotted in Fig. 5 with individual values listed in Table 3.

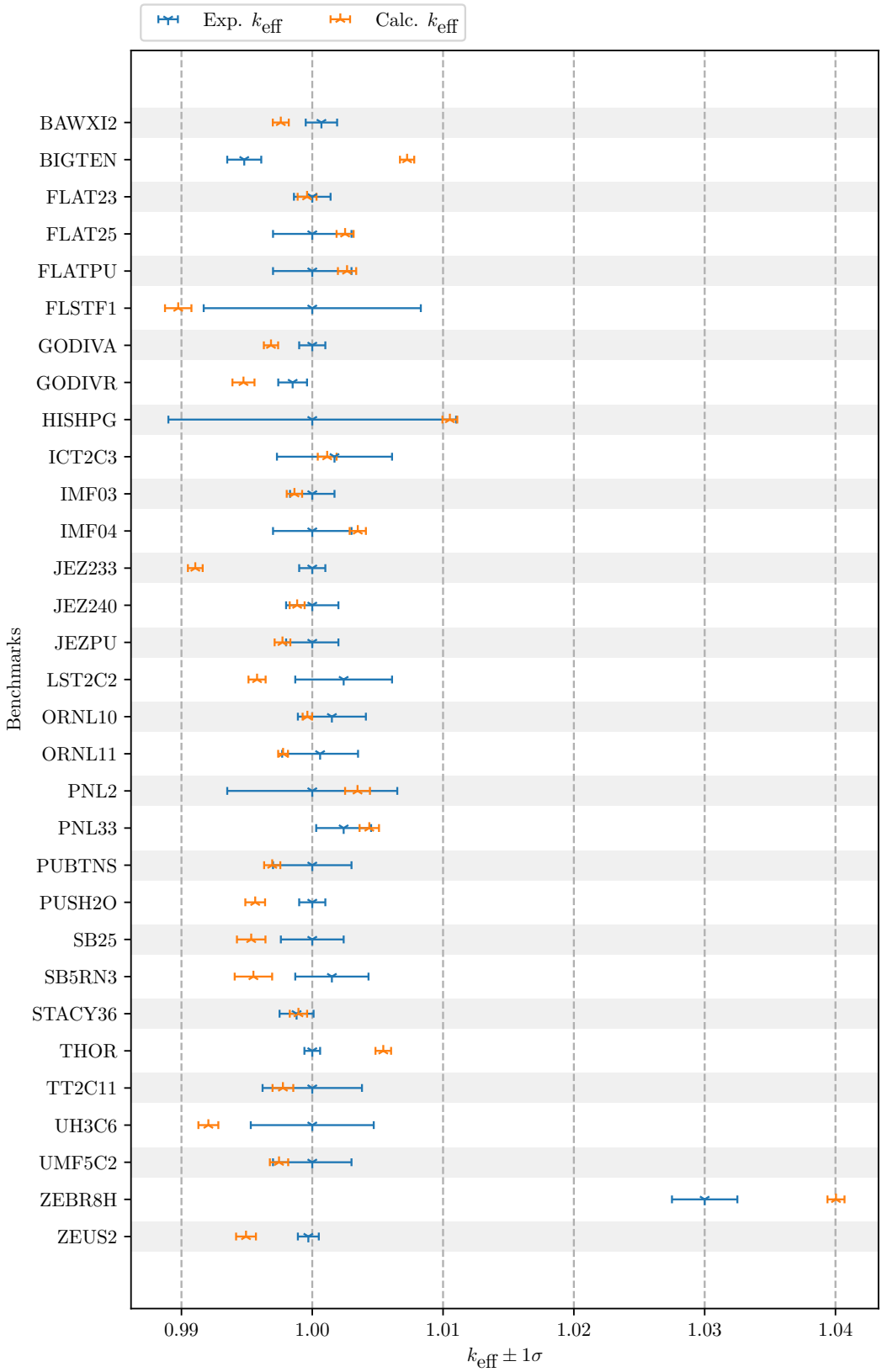

Figure 3: Criticality (ENDF/B-VI.6) Benchmark Results

Table 1: Criticality (ENDF/B-VI.6) Benchmark Results

	Exp. k_{eff}	Exp. unc.	Calc. k_{eff}	Calc. unc.
BAWXI2	1.0007	0.0012	0.997 594	0.000 611
BIGTEN	0.9948	0.0013	1.007 25	0.000 545
FLAT23	1.0000	0.0014	0.999 604	0.000 723
FLAT25	1.0000	0.0030	1.002 51	0.000 652
FLATPU	1.0000	0.0030	1.002 66	0.000 699
FLSTF1	1.0000	0.0083	0.989 752	0.001 010
GODIVA	1.0000	0.0010	0.996 845	0.000 546
GODIVR	0.9985	0.0011	0.994 741	0.000 843
HISHPG	1.0000	0.0110	1.010 52	0.000 567
ICT2C3	1.0017	0.0044	1.001 14	0.000 720
IMF03	1.0000	0.0017	0.998 637	0.000 588
IMF04	1.0000	0.0030	1.003 48	0.000 621
JEZ233	1.0000	0.0010	0.991 058	0.000 564
JEZ240	1.0000	0.0020	0.998 845	0.000 569
JEZPU	1.0000	0.0020	0.997 723	0.000 601
LST2C2	1.0024	0.0037	0.995 780	0.000 655
ORNL10	1.0015	0.0026	0.999 627	0.000 363
ORNL11	1.0006	0.0029	0.997 769	0.000 375
PNL2	1.0000	0.0065	1.003 46	0.000 950
PNL33	1.0024	0.0021	1.004 36	0.000 742
PUBTNS	1.0000	0.0030	0.996 939	0.000 619
PUSH2O	1.0000	0.0010	0.995 638	0.000 755
SB25	1.0000	0.0024	0.995 332	0.001 090
SB5RN3	1.0015	0.0028	0.995 501	0.001 432
STACY36	0.9988	0.0013	0.998 943	0.000 663
THOR	1.0000	0.0006	1.005 43	0.000 596
TT2C11	1.0000	0.0038	0.997 756	0.000 793
UH3C6	1.0000	0.0047	0.992 057	0.000 762
UMF5C2	1.0000	0.0030	0.997 459	0.000 700
ZEBR8H	1.0300	0.0025	1.040 04	0.000 651
ZEUS2	0.9997	0.0008	0.994 935	0.000 758

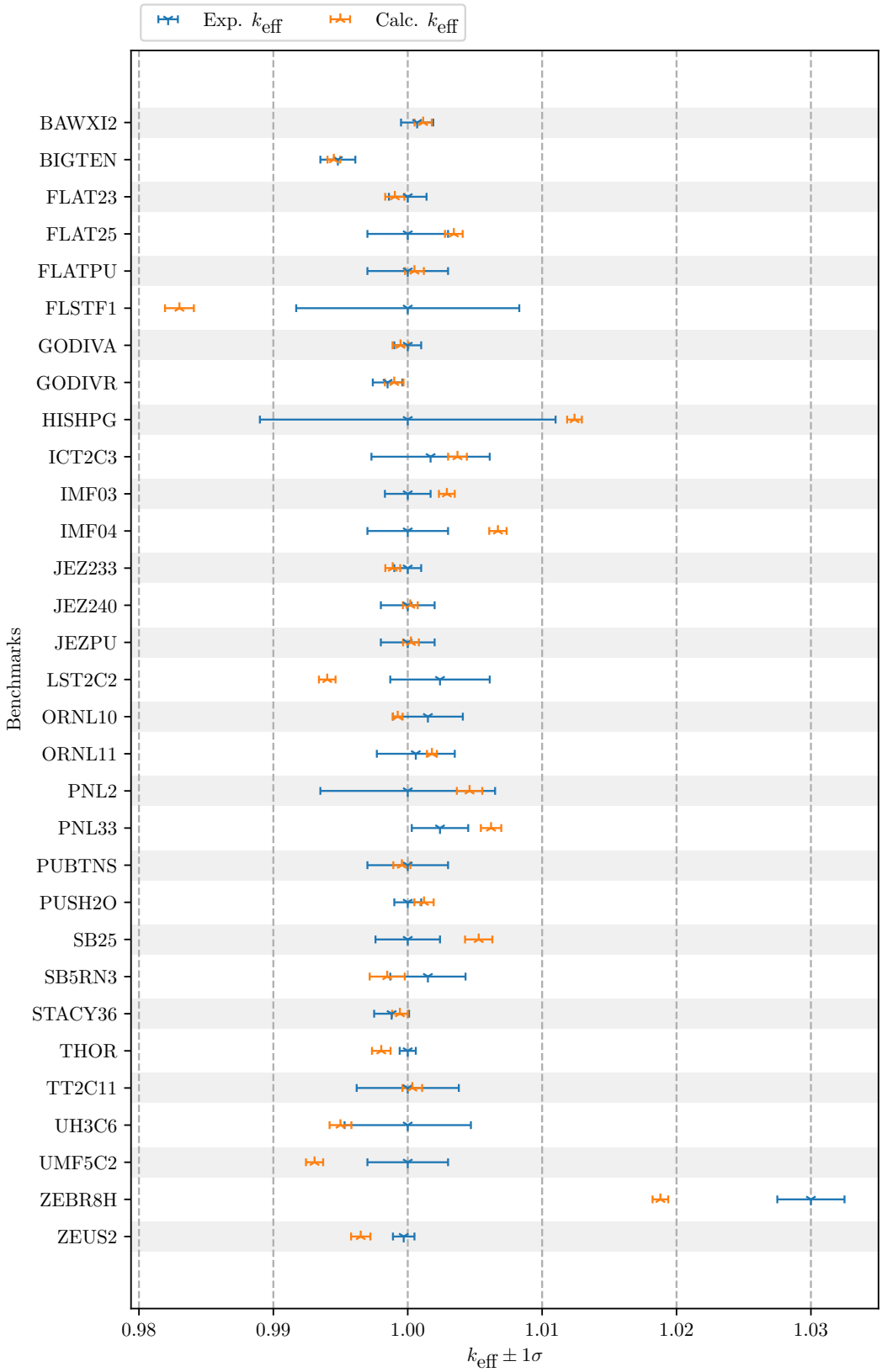

Figure 4: Criticality (ENDF/B-VII.0) Benchmark Results

Table 2: Criticality (ENDF/B-VII.0) Benchmark Results

	Exp. k_{eff}	Exp. unc.	Calc. k_{eff}	Calc. unc.
BAWXI2	1.0007	0.0012	1.001 15	0.000 642
BIGTEN	0.9948	0.0013	0.994 501	0.000 471
FLAT23	1.0000	0.0014	0.999 039	0.000 716
FLAT25	1.0000	0.0030	1.003 43	0.000 658
FLATPU	1.0000	0.0030	1.000 50	0.000 699
FLSTF1	1.0000	0.0083	0.983 012	0.001 074
GODIVA	1.0000	0.0010	0.999 463	0.000 593
GODIVR	0.9985	0.0011	0.998 992	0.000 694
HISHPG	1.0000	0.0110	1.012 41	0.000 547
ICT2C3	1.0017	0.0044	1.003 70	0.000 698
IMF03	1.0000	0.0017	1.002 91	0.000 587
IMF04	1.0000	0.0030	1.006 71	0.000 647
JEZ233	1.0000	0.0010	0.998 885	0.000 554
JEZ240	1.0000	0.0020	1.000 19	0.000 551
JEZPU	1.0000	0.0020	1.000 24	0.000 588
LST2C2	1.0024	0.0037	0.994 009	0.000 618
ORNL10	1.0015	0.0026	0.999 255	0.000 367
ORNL11	1.0006	0.0029	1.001 80	0.000 368
PNL2	1.0000	0.0065	1.004 60	0.000 948
PNL33	1.0024	0.0021	1.006 20	0.000 759
PUBTNS	1.0000	0.0030	0.999 564	0.000 636
PUSH2O	1.0000	0.0010	1.001 21	0.000 718
SB25	1.0000	0.0024	1.005 28	0.001 015
SB5RN3	1.0015	0.0028	0.998 473	0.001 306
STACY36	0.9988	0.0013	0.999 417	0.000 584
THOR	1.0000	0.0006	0.998 030	0.000 690
TT2C11	1.0000	0.0038	1.000 34	0.000 732
UH3C6	1.0000	0.0047	0.994 995	0.000 811
UMF5C2	1.0000	0.0030	0.993 067	0.000 638
ZEBR8H	1.0300	0.0025	1.018 80	0.000 583
ZEUS2	0.9997	0.0008	0.996 502	0.000 720

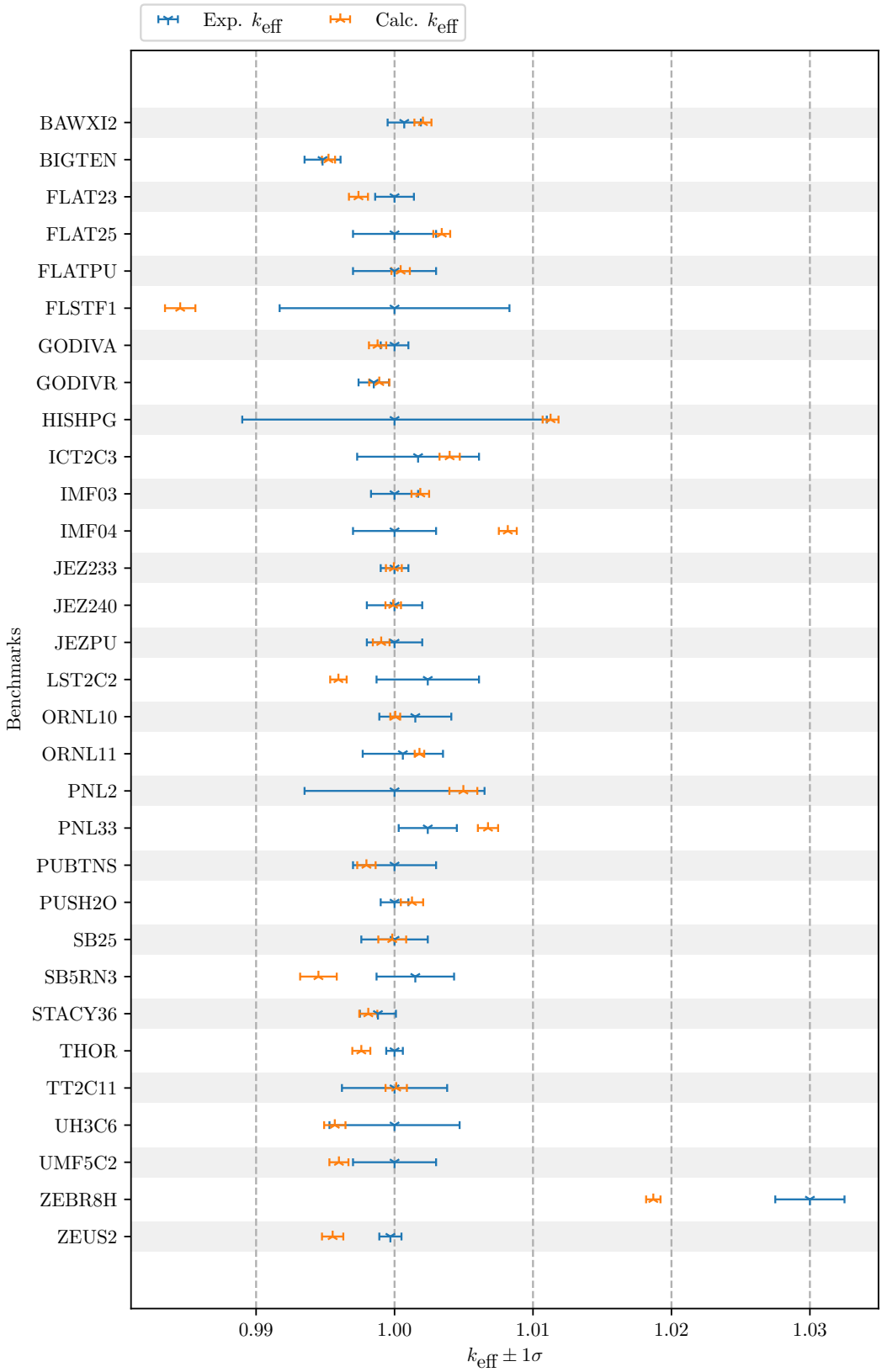

Figure 5: Criticality (ENDF/B-VII.1) Benchmark Results

Table 3: Criticality (ENDF/B-VII.1) Benchmark Results

	Exp. k_{eff}	Exp. unc.	Calc. k_{eff}	Calc. unc.
BAWXI2	1.0007	0.0012	1.002 05	0.000 616
BIGTEN	0.9948	0.0013	0.995 230	0.000 474
FLAT23	1.0000	0.0014	0.997 394	0.000 687
FLAT25	1.0000	0.0030	1.003 41	0.000 610
FLATPU	1.0000	0.0030	1.000 44	0.000 665
FLSTF1	1.0000	0.0083	0.984 518	0.001 098
GODIVA	1.0000	0.0010	0.998 775	0.000 624
GODIVR	0.9985	0.0011	0.998 897	0.000 729
HISHPG	1.0000	0.0110	1.011 27	0.000 573
ICT2C3	1.0017	0.0044	1.003 98	0.000 731
IMF03	1.0000	0.0017	1.001 86	0.000 637
IMF04	1.0000	0.0030	1.008 18	0.000 647
JEZ233	1.0000	0.0010	0.999 950	0.000 572
JEZ240	1.0000	0.0020	0.999 904	0.000 561
JEZPU	1.0000	0.0020	0.999 036	0.000 605
LST2C2	1.0024	0.0037	0.995 946	0.000 594
ORNL10	1.0015	0.0026	1.000 05	0.000 357
ORNL11	1.0006	0.0029	1.001 80	0.000 345
PNL2	1.0000	0.0065	1.004 97	0.001 007
PNL33	1.0024	0.0021	1.006 75	0.000 731
PUBTNS	1.0000	0.0030	0.997 969	0.000 664
PUSH2O	1.0000	0.0010	1.001 26	0.000 806
SB25	1.0000	0.0024	0.999 834	0.001 007
SB5RN3	1.0015	0.0028	0.994 503	0.001 322
STACY36	0.9988	0.0013	0.998 104	0.000 650
THOR	1.0000	0.0006	0.997 600	0.000 651
TT2C11	1.0000	0.0038	1.000 12	0.000 771
UH3C6	1.0000	0.0047	0.995 685	0.000 771
UMF5C2	1.0000	0.0030	0.995 983	0.000 688
ZEBR8H	1.0300	0.0025	1.018 69	0.000 519
ZEUS2	0.9997	0.0008	0.995 529	0.000 769

4.1.4 ENDF/B-VIII.0

For the validation criticality (ENDF/B-VIII.0) benchmarks, the benchmark data and calculation results are plotted in Fig. 6 with individual values listed in Table 4.

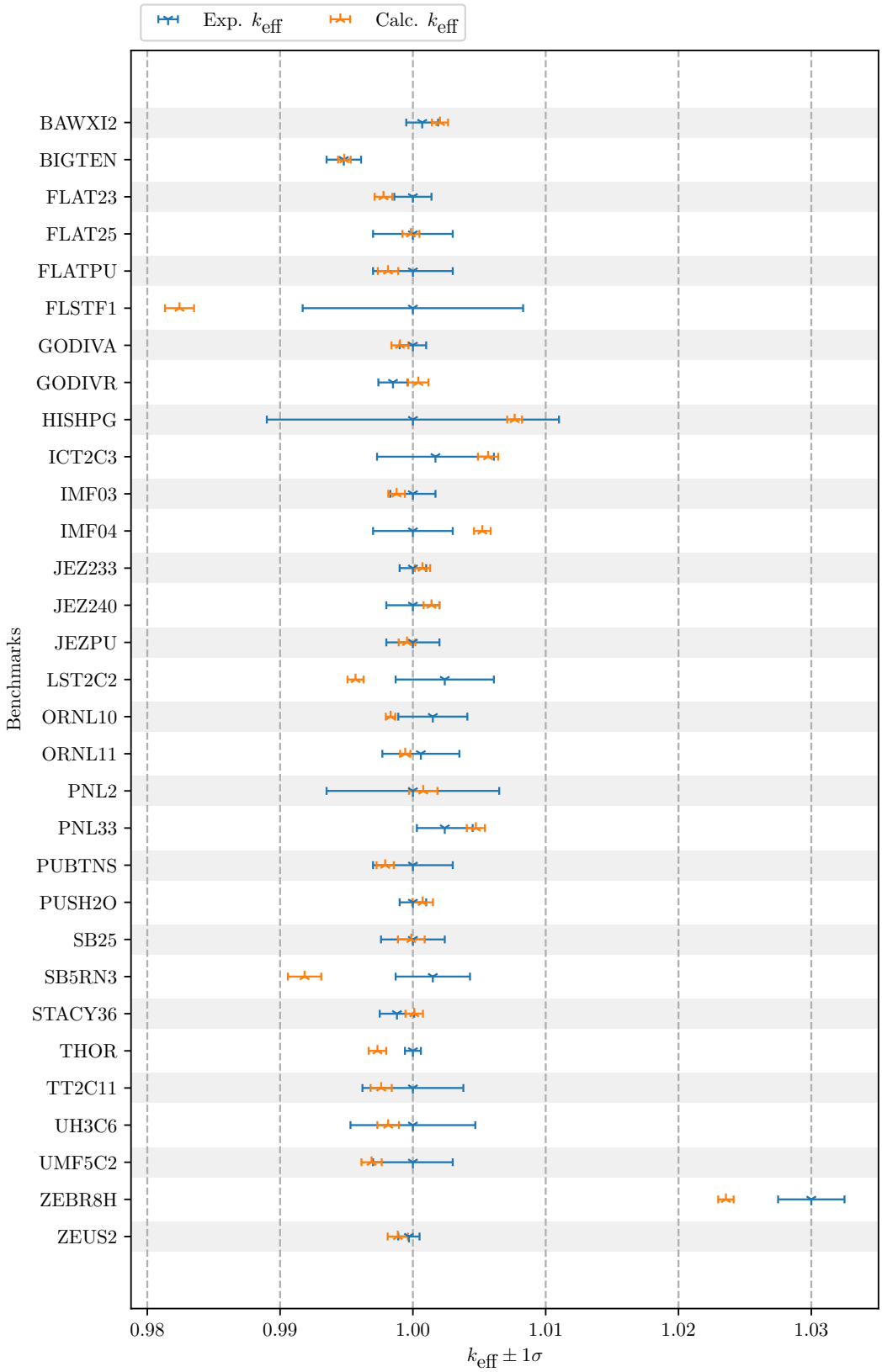

Figure 6: Criticality (ENDF/B-VIII.0) Benchmark Results

Table 4: Criticality (ENDF/B-VIII.0) Benchmark Results

	Exp. k_{eff}	Exp. unc.	Calc. k_{eff}	Calc. unc.
BAWXI2	1.0007	0.0012	1.002 04	0.000 605
BIGTEN	0.9948	0.0013	0.994 839	0.000 475
FLAT23	1.0000	0.0014	0.997 786	0.000 666
FLAT25	1.0000	0.0030	0.999 852	0.000 637
FLATPU	1.0000	0.0030	0.998 127	0.000 765
FLSTF1	1.0000	0.0083	0.982 427	0.001 093
GODIVA	1.0000	0.0010	0.999 026	0.000 641
GODIVR	0.9985	0.0011	1.000 41	0.000 764
HISHPG	1.0000	0.0110	1.007 66	0.000 560
ICT2C3	1.0017	0.0044	1.005 66	0.000 763
IMF03	1.0000	0.0017	0.998 772	0.000 624
IMF04	1.0000	0.0030	1.005 23	0.000 627
JEZ233	1.0000	0.0010	1.000 72	0.000 581
JEZ240	1.0000	0.0020	1.001 40	0.000 595
JEZPU	1.0000	0.0020	0.999 557	0.000 626
LST2C2	1.0024	0.0037	0.995 681	0.000 605
ORNL10	1.0015	0.0026	0.998 318	0.000 358
ORNL11	1.0006	0.0029	0.999 421	0.000 387
PNL2	1.0000	0.0065	1.000 78	0.001 069
PNL33	1.0024	0.0021	1.004 74	0.000 681
PUBTNS	1.0000	0.0030	0.997 913	0.000 648
PUSH2O	1.0000	0.0010	1.000 73	0.000 781
SB25	1.0000	0.0024	0.999 882	0.001 006
SB5RN3	1.0015	0.0028	0.991 841	0.001 256
STACY36	0.9988	0.0013	1.000 10	0.000 658
THOR	1.0000	0.0006	0.997 333	0.000 663
TT2C11	1.0000	0.0038	0.997 611	0.000 795
UH3C6	1.0000	0.0047	0.998 138	0.000 814
UMF5C2	1.0000	0.0030	0.996 887	0.000 761
ZEBR8H	1.0300	0.0025	1.023 57	0.000 580
ZEUS2	0.9997	0.0008	0.998 864	0.000 762

4.2 Criticality Expanded

This test suite executes on 1 node, which uses 8 threads with 14 concurrent jobs, with a total Slurm allocation of no more than 30 minutes. An example `VnV.py` execution line is `./VnV.py execute_slurm --ntrd 8 --jobs 14 --time 30 --wait --calcdir_name crit_expanded_$DATA`, where `$DATA` is an environment variable that identifies which evaluated nuclear data set to use.

The following figures and tables are results for the Criticality Expanded benchmark suite. The plots display k_{eff} values and their uncertainties. The tables provide benchmark and calculated values and uncertainties.

4.2.1 ENDF/B-VII.0

For the validation criticality expanded (ENDF/B-VII.0) benchmarks, the benchmark data and calculation results are plotted in Fig. 7 with individual values listed in Table 5.

Table 5: Criticality Expanded (ENDF/B-VII.0) Benchmark Results

	Exp. k_{eff}	Exp. unc.	Calc. k_{eff}	Calc. unc.
heu-comp-inter-003-case-6	1.0000	0.0047	0.995 216	0.000 338
heu-met-fast-001	1.0000	0.0010	0.999 278	0.000 255
heu-met-fast-003-case-1	1.0000	0.0050	0.995 355	0.000 280
heu-met-fast-003-case-10	1.0000	0.0050	1.012 91	0.000 296
heu-met-fast-003-case-11	1.0000	0.0050	1.016 59	0.000 287
heu-met-fast-003-case-12	1.0000	0.0030	1.008 34	0.000 286
heu-met-fast-003-case-2	1.0000	0.0050	0.994 215	0.000 283
heu-met-fast-003-case-3	1.0000	0.0050	0.999 412	0.000 267
heu-met-fast-003-case-4	1.0000	0.0030	0.997 089	0.000 287
heu-met-fast-003-case-5	1.0000	0.0030	1.000 80	0.000 276
heu-met-fast-003-case-6	1.0000	0.0030	1.001 71	0.000 302
heu-met-fast-003-case-7	1.0000	0.0030	1.002 65	0.000 288
heu-met-fast-003-case-8	1.0000	0.0050	1.008 08	0.000 288
heu-met-fast-003-case-9	1.0000	0.0050	1.009 47	0.000 288
heu-met-fast-004-case-1	1.0020	0.0010	1.002 80	0.000 347
heu-met-fast-008	0.9989	0.0016	0.995 704	0.000 261
heu-met-fast-009-case-1	0.9992	0.0015	0.995 660	0.000 282
heu-met-fast-009-case-2	0.9992	0.0015	0.995 499	0.000 294
heu-met-fast-011	0.9989	0.0015	0.998 422	0.000 354
heu-met-fast-012	0.9992	0.0018	0.998 177	0.000 270
heu-met-fast-013	0.9990	0.0015	0.997 686	0.000 269
heu-met-fast-014	0.9989	0.0017	0.998 213	0.000 278
heu-met-fast-015	0.9996	0.0017	0.994 271	0.000 273
heu-met-fast-018-case-2	1.0000	0.0014	0.999 930	0.000 259
heu-met-fast-019-case-2	1.0000	0.0028	1.007 13	0.000 290

Continued on next page

Table 5: Criticality Expanded (ENDF/B-VII.0) Benchmark Results

	Exp. k_{eff}	Exp. unc.	Calc. k_{eff}	Calc. unc.
heu-met-fast-020-case-2	1.0000	0.0028	1.000 78	0.000 294
heu-met-fast-021-case-2	1.0000	0.0024	0.996 932	0.000 270
heu-met-fast-022-case-2	1.0000	0.0019	0.997 650	0.000 275
heu-met-fast-026-case-c-11	1.0000	0.0038	1.003 46	0.000 343
heu-met-fast-028	1.0000	0.0030	1.003 20	0.000 298
heu-met-inter-006-case-1	0.9977	0.0008	0.993 366	0.000 356
heu-met-inter-006-case-2	1.0001	0.0008	0.996 926	0.000 337
heu-met-inter-006-case-3	1.0015	0.0009	1.001 02	0.000 335
heu-met-inter-006-case-4	1.0016	0.0008	1.008 15	0.000 324
heu-sol-therm-013-case-1	1.0012	0.0026	0.998 477	0.000 258
heu-sol-therm-013-case-2	1.0007	0.0036	0.997 542	0.000 264
heu-sol-therm-013-case-3	1.0009	0.0036	0.994 173	0.000 284
heu-sol-therm-013-case-4	1.0003	0.0036	0.995 710	0.000 296
heu-sol-therm-032	1.0015	0.0026	0.999 060	0.000 168
ieu-comp-therm-002-case-3	1.0017	0.0044	1.003 42	0.000 342
ieu-met-fast-001-case-1	0.9989	0.0010	1.000 85	0.000 272
ieu-met-fast-001-case-2	0.9997	0.0010	1.001 28	0.000 260
ieu-met-fast-001-case-3	0.9993	0.0005	1.001 42	0.000 270
ieu-met-fast-001-case-4	1.0002	0.0005	1.001 46	0.000 258
ieu-met-fast-002	1.0000	0.0030	0.999 081	0.000 252
ieu-met-fast-003-case-2	1.0000	0.0017	1.002 86	0.000 268
ieu-met-fast-004-case-2	1.0000	0.0030	1.007 53	0.000 281
ieu-met-fast-005-case-2	1.0000	0.0021	1.001 84	0.000 269
ieu-met-fast-006-case-2	1.0000	0.0023	0.995 649	0.000 270
ieu-met-fast-007-case-4	1.0049	0.0008	1.005 03	0.000 238
leu-comp-therm-008-case-1	1.0007	0.0012	1.001 26	0.000 285
leu-comp-therm-008-case-11	1.0007	0.0012	1.001 01	0.000 308
leu-comp-therm-008-case-2	1.0007	0.0012	1.000 88	0.000 301
leu-comp-therm-008-case-5	1.0007	0.0012	1.001 18	0.000 282
leu-comp-therm-008-case-7	1.0007	0.0012	0.999 952	0.000 291
leu-comp-therm-008-case-8	1.0007	0.0012	0.999 760	0.000 307
leu-sol-therm-002-case-1	1.0038	0.0040	1.000 02	0.000 249
leu-sol-therm-002-case-2	1.0024	0.0037	0.995 941	0.000 283
leu-sol-therm-007-case-14	0.9961	0.0009	0.994 946	0.000 296
leu-sol-therm-007-case-30	0.9973	0.0009	0.997 707	0.000 312
leu-sol-therm-007-case-32	0.9985	0.0010	0.995 794	0.000 288
leu-sol-therm-007-case-36	0.9988	0.0011	0.998 600	0.000 268
leu-sol-therm-007-case-49	0.9983	0.0011	0.997 519	0.000 278
mix-comp-therm-002-case-pnl30	1.0010	0.0059	1.000 63	0.000 333
mix-comp-therm-002-case-pnl31	1.0009	0.0045	1.002 41	0.000 324
mix-comp-therm-002-case-pnl32	1.0024	0.0029	1.003 23	0.000 330
mix-comp-therm-002-case-pnl33	1.0024	0.0021	1.006 91	0.000 321

Continued on next page

Table 5: Criticality Expanded (ENDF/B-VII.0) Benchmark Results

	Exp. k_{eff}	Exp. unc.	Calc. k_{eff}	Calc. unc.
mix-comp-therm-002-case-pnl34	1.0038	0.0022	1.004 41	0.000 322
mix-comp-therm-002-case-pnl35	1.0029	0.0024	1.006 87	0.000 306
mix-met-fast-001	1.0000	0.0016	0.999 335	0.000 258
mix-met-fast-003	0.9993	0.0016	1.000 76	0.000 281
mix-met-fast-008-case-7	1.0300	0.0025	1.019 04	0.000 185
pu-comp-inter-001	1.0000	0.0110	1.012 04	0.000 248
pu-met-fast-001	1.0000	0.0020	1.000 02	0.000 257
pu-met-fast-002	1.0000	0.0020	0.999 851	0.000 265
pu-met-fast-003-case-103	1.0000	0.0030	0.998 056	0.000 291
pu-met-fast-005	1.0000	0.0013	1.009 24	0.000 289
pu-met-fast-006	1.0000	0.0030	0.999 489	0.000 303
pu-met-fast-008-case-2	1.0000	0.0006	0.997 722	0.000 274
pu-met-fast-009	1.0000	0.0027	1.005 27	0.000 280
pu-met-fast-010	1.0000	0.0018	1.000 05	0.000 285
pu-met-fast-011	1.0000	0.0010	1.000 62	0.000 344
pu-met-fast-018	1.0000	0.0030	0.996 454	0.000 280
pu-met-fast-019	0.9992	0.0015	0.997 517	0.000 289
pu-met-fast-020	0.9993	0.0017	0.998 089	0.000 291
pu-met-fast-021-case-1	1.0000	0.0026	1.002 07	0.000 281
pu-met-fast-021-case-2	1.0000	0.0026	0.993 149	0.000 291
pu-met-fast-022-case-2	1.0000	0.0021	0.998 319	0.000 275
pu-met-fast-023-case-2	1.0000	0.0020	0.999 342	0.000 286
pu-met-fast-024-case-2	1.0000	0.0020	1.001 88	0.000 286
pu-met-fast-025-case-2	1.0000	0.0020	0.998 785	0.000 272
pu-met-fast-026-case-2	1.0000	0.0024	0.998 466	0.000 294
pu-sol-therm-009-case-3a	1.0000	0.0033	1.018 95	0.000 169
pu-sol-therm-011-case-16-5	1.0000	0.0052	1.005 99	0.000 408
pu-sol-therm-011-case-18-1	1.0000	0.0052	0.994 345	0.000 364
pu-sol-therm-011-case-18-6	1.0000	0.0052	0.999 643	0.000 384
pu-sol-therm-018-case-9	1.0000	0.0034	1.003 07	0.000 316
pu-sol-therm-021-case-1	1.0000	0.0032	1.004 32	0.000 404
pu-sol-therm-021-case-3	1.0000	0.0065	1.004 39	0.000 459
pu-sol-therm-034-case-1	1.0000	0.0062	0.999 905	0.000 405
u233-comp-therm-001-case-3	1.0000	0.0024	1.004 64	0.000 443
u233-comp-therm-001-case-6	1.0015	0.0028	1.000 31	0.000 397
u233-met-fast-001	1.0000	0.0010	0.999 298	0.000 260
u233-met-fast-002-case-1	1.0000	0.0010	0.998 696	0.000 263
u233-met-fast-002-case-2	1.0000	0.0011	1.000 54	0.000 288
u233-met-fast-003-case-1	1.0000	0.0010	0.999 710	0.000 273
u233-met-fast-003-case-2	1.0000	0.0010	1.000 12	0.000 276
u233-met-fast-004-case-1	1.0000	0.0007	1.005 06	0.000 283
u233-met-fast-004-case-2	1.0000	0.0008	1.005 14	0.000 293

Continued on next page

Table 5: Criticality Expanded (ENDF/B-VII.0) Benchmark Results

	Exp. k_{eff}	Exp. unc.	Calc. k_{eff}	Calc. unc.
u233-met-fast-005-case-1	1.0000	0.0030	0.994 363	0.000 275
u233-met-fast-005-case-2	1.0000	0.0030	0.992 541	0.000 300
u233-met-fast-006	1.0000	0.0014	0.999 390	0.000 303
u233-sol-inter-001-case-1	1.0000	0.0083	0.984 767	0.000 503
u233-sol-therm-001-case-1	1.0000	0.0031	1.001 49	0.000 252
u233-sol-therm-001-case-2	1.0005	0.0033	1.001 14	0.000 266
u233-sol-therm-001-case-3	1.0006	0.0033	1.000 89	0.000 253
u233-sol-therm-001-case-4	0.9998	0.0033	1.001 86	0.000 270
u233-sol-therm-001-case-5	0.9999	0.0033	0.999 581	0.000 274
u233-sol-therm-008	1.0006	0.0029	1.001 42	0.000 170

4.2.2 ENDF/B-VII.1

For the validation criticality expanded (ENDF/B-VII.1) benchmarks, the benchmark data and calculation results are plotted in Fig. 8 with individual values listed in Table 6.

Table 6: Criticality Expanded (ENDF/B-VII.1) Benchmark Results

	Exp. k_{eff}	Exp. unc.	Calc. k_{eff}	Calc. unc.
heu-comp-inter-003-case-6	1.0000	0.0047	0.994 948	0.000 361
heu-met-fast-001	1.0000	0.0010	0.999 359	0.000 278
heu-met-fast-003-case-1	1.0000	0.0050	0.994 873	0.000 281
heu-met-fast-003-case-10	1.0000	0.0050	1.005 25	0.000 279
heu-met-fast-003-case-11	1.0000	0.0050	1.009 38	0.000 306
heu-met-fast-003-case-12	1.0000	0.0030	1.008 72	0.000 289
heu-met-fast-003-case-2	1.0000	0.0050	0.994 469	0.000 270
heu-met-fast-003-case-3	1.0000	0.0050	0.998 909	0.000 278
heu-met-fast-003-case-4	1.0000	0.0030	0.997 454	0.000 288
heu-met-fast-003-case-5	1.0000	0.0030	1.001 17	0.000 284
heu-met-fast-003-case-6	1.0000	0.0030	1.002 02	0.000 290
heu-met-fast-003-case-7	1.0000	0.0030	1.001 91	0.000 300
heu-met-fast-003-case-8	1.0000	0.0050	1.002 28	0.000 275
heu-met-fast-003-case-9	1.0000	0.0050	1.002 27	0.000 309
heu-met-fast-004-case-1	1.0020	0.0010	1.003 39	0.000 331
heu-met-fast-008	0.9989	0.0016	0.996 196	0.000 272
heu-met-fast-009-case-1	0.9992	0.0015	0.997 684	0.000 284
heu-met-fast-009-case-2	0.9992	0.0015	0.996 613	0.000 299
heu-met-fast-011	0.9989	0.0015	0.998 739	0.000 358
heu-met-fast-012	0.9992	0.0018	0.998 440	0.000 279
heu-met-fast-013	0.9990	0.0015	0.997 468	0.000 275

Continued on next page

Table 6: Criticality Expanded (ENDF/B-VII.1) Benchmark Results

	Exp. k_{eff}	Exp. unc.	Calc. k_{eff}	Calc. unc.
heu-met-fast-014	0.9989	0.0017	0.997 459	0.000 269
heu-met-fast-015	0.9996	0.0017	0.994 692	0.000 282
heu-met-fast-018-case-2	1.0000	0.0014	0.999 531	0.000 271
heu-met-fast-019-case-2	1.0000	0.0028	1.006 86	0.000 292
heu-met-fast-020-case-2	1.0000	0.0028	1.000 57	0.000 303
heu-met-fast-021-case-2	1.0000	0.0024	0.997 921	0.000 267
heu-met-fast-022-case-2	1.0000	0.0019	0.997 591	0.000 270
heu-met-fast-026-case-c-11	1.0000	0.0038	1.003 15	0.000 333
heu-met-fast-028	1.0000	0.0030	1.002 71	0.000 305
heu-met-inter-006-case-1	0.9977	0.0008	0.992 282	0.000 347
heu-met-inter-006-case-2	1.0001	0.0008	0.997 022	0.000 329
heu-met-inter-006-case-3	1.0015	0.0009	1.000 74	0.000 318
heu-met-inter-006-case-4	1.0016	0.0008	1.007 13	0.000 319
heu-sol-therm-013-case-1	1.0012	0.0026	0.998 495	0.000 260
heu-sol-therm-013-case-2	1.0007	0.0036	0.996 913	0.000 275
heu-sol-therm-013-case-3	1.0009	0.0036	0.993 898	0.000 265
heu-sol-therm-013-case-4	1.0003	0.0036	0.995 293	0.000 293
heu-sol-therm-032	1.0015	0.0026	0.999 168	0.000 174
ieu-comp-therm-002-case-3	1.0017	0.0044	1.003 46	0.000 328
ieu-met-fast-001-case-1	0.9989	0.0010	1.000 89	0.000 281
ieu-met-fast-001-case-2	0.9997	0.0010	0.999 869	0.000 292
ieu-met-fast-001-case-3	0.9993	0.0005	1.001 12	0.000 289
ieu-met-fast-001-case-4	1.0002	0.0005	1.001 50	0.000 259
ieu-met-fast-002	1.0000	0.0030	0.999 145	0.000 252
ieu-met-fast-003-case-2	1.0000	0.0017	1.002 75	0.000 278
ieu-met-fast-004-case-2	1.0000	0.0030	1.007 59	0.000 267
ieu-met-fast-005-case-2	1.0000	0.0021	1.002 36	0.000 279
ieu-met-fast-006-case-2	1.0000	0.0023	0.995 831	0.000 283
ieu-met-fast-007-case-4	1.0049	0.0008	1.004 76	0.000 223
leu-comp-therm-008-case-1	1.0007	0.0012	1.000 68	0.000 303
leu-comp-therm-008-case-11	1.0007	0.0012	1.001 23	0.000 295
leu-comp-therm-008-case-2	1.0007	0.0012	1.000 67	0.000 304
leu-comp-therm-008-case-5	1.0007	0.0012	1.001 02	0.000 291
leu-comp-therm-008-case-7	1.0007	0.0012	1.000 29	0.000 291
leu-comp-therm-008-case-8	1.0007	0.0012	0.999 497	0.000 289
leu-sol-therm-002-case-1	1.0038	0.0040	0.999 437	0.000 258
leu-sol-therm-002-case-2	1.0024	0.0037	0.996 410	0.000 279
leu-sol-therm-007-case-14	0.9961	0.0009	0.994 668	0.000 315
leu-sol-therm-007-case-30	0.9973	0.0009	0.997 144	0.000 320
leu-sol-therm-007-case-32	0.9985	0.0010	0.995 853	0.000 278
leu-sol-therm-007-case-36	0.9988	0.0011	0.998 949	0.000 292
leu-sol-therm-007-case-49	0.9983	0.0011	0.997 226	0.000 261

Continued on next page

Table 6: Criticality Expanded (ENDF/B-VII.1) Benchmark Results

	Exp. k_{eff}	Exp. unc.	Calc. k_{eff}	Calc. unc.
mix-comp-therm-002-case-pnl30	1.0010	0.0059	1.000 70	0.000 327
mix-comp-therm-002-case-pnl31	1.0009	0.0045	1.001 91	0.000 333
mix-comp-therm-002-case-pnl32	1.0024	0.0029	1.002 26	0.000 338
mix-comp-therm-002-case-pnl33	1.0024	0.0021	1.006 44	0.000 347
mix-comp-therm-002-case-pnl34	1.0038	0.0022	1.003 71	0.000 309
mix-comp-therm-002-case-pnl35	1.0029	0.0024	1.005 47	0.000 333
mix-met-fast-001	1.0000	0.0016	0.999 802	0.000 263
mix-met-fast-003	0.9993	0.0016	1.000 43	0.000 279
mix-met-fast-008-case-7	1.0300	0.0025	1.018 83	0.000 176
pu-comp-inter-001	1.0000	0.0110	1.012 00	0.000 248
pu-met-fast-001	1.0000	0.0020	0.999 349	0.000 259
pu-met-fast-002	1.0000	0.0020	1.000 34	0.000 266
pu-met-fast-003-case-103	1.0000	0.0030	0.999 042	0.000 308
pu-met-fast-005	1.0000	0.0013	1.001 90	0.000 266
pu-met-fast-006	1.0000	0.0030	1.000 06	0.000 304
pu-met-fast-008-case-2	1.0000	0.0006	0.997 658	0.000 283
pu-met-fast-009	1.0000	0.0027	1.004 77	0.000 262
pu-met-fast-010	1.0000	0.0018	0.999 585	0.000 282
pu-met-fast-011	1.0000	0.0010	0.999 974	0.000 332
pu-met-fast-018	1.0000	0.0030	0.999 291	0.000 289
pu-met-fast-019	0.9992	0.0015	1.000 39	0.000 280
pu-met-fast-020	0.9993	0.0017	0.997 941	0.000 300
pu-met-fast-021-case-1	1.0000	0.0026	1.004 70	0.000 303
pu-met-fast-021-case-2	1.0000	0.0026	0.993 449	0.000 280
pu-met-fast-022-case-2	1.0000	0.0021	0.998 418	0.000 255
pu-met-fast-023-case-2	1.0000	0.0020	0.999 428	0.000 261
pu-met-fast-024-case-2	1.0000	0.0020	1.002 46	0.000 295
pu-met-fast-025-case-2	1.0000	0.0020	0.999 126	0.000 270
pu-met-fast-026-case-2	1.0000	0.0024	0.998 666	0.000 288
pu-sol-therm-009-case-3a	1.0000	0.0033	1.019 06	0.000 178
pu-sol-therm-011-case-16-5	1.0000	0.0052	1.005 36	0.000 400
pu-sol-therm-011-case-18-1	1.0000	0.0052	0.994 132	0.000 350
pu-sol-therm-011-case-18-6	1.0000	0.0052	1.000 52	0.000 367
pu-sol-therm-018-case-9	1.0000	0.0034	1.002 60	0.000 329
pu-sol-therm-021-case-1	1.0000	0.0032	1.005 26	0.000 410
pu-sol-therm-021-case-3	1.0000	0.0065	1.004 32	0.000 445
pu-sol-therm-034-case-1	1.0000	0.0062	1.000 65	0.000 407
u233-comp-therm-001-case-3	1.0000	0.0024	1.002 97	0.000 446
u233-comp-therm-001-case-6	1.0015	0.0028	0.998 775	0.000 404
u233-met-fast-001	1.0000	0.0010	0.999 948	0.000 283
u233-met-fast-002-case-1	1.0000	0.0010	0.998 276	0.000 263
u233-met-fast-002-case-2	1.0000	0.0011	1.000 30	0.000 286

Continued on next page

Table 6: Criticality Expanded (ENDF/B-VII.1) Benchmark Results

	Exp. k_{eff}	Exp. unc.	Calc. k_{eff}	Calc. unc.
u233-met-fast-003-case-1	1.0000	0.0010	0.999 488	0.000 292
u233-met-fast-003-case-2	1.0000	0.0010	0.999 543	0.000 275
u233-met-fast-004-case-1	1.0000	0.0007	0.998 768	0.000 282
u233-met-fast-004-case-2	1.0000	0.0008	0.995 574	0.000 308
u233-met-fast-005-case-1	1.0000	0.0030	0.995 887	0.000 288
u233-met-fast-005-case-2	1.0000	0.0030	0.995 211	0.000 308
u233-met-fast-006	1.0000	0.0014	0.998 403	0.000 308
u233-sol-inter-001-case-1	1.0000	0.0083	0.984 517	0.000 473
u233-sol-therm-001-case-1	1.0000	0.0031	1.000 96	0.000 261
u233-sol-therm-001-case-2	1.0005	0.0033	1.001 03	0.000 268
u233-sol-therm-001-case-3	1.0006	0.0033	1.000 68	0.000 266
u233-sol-therm-001-case-4	0.9998	0.0033	1.000 74	0.000 267
u233-sol-therm-001-case-5	0.9999	0.0033	0.999 632	0.000 270
u233-sol-therm-008	1.0006	0.0029	1.001 56	0.000 175

4.2.3 ENDF/B-VIII.0

For the validation criticality expanded (ENDF/B-VIII.0) benchmarks, the benchmark data and calculation results are plotted in Fig. 9 with individual values listed in Table 7.

Table 7: Criticality Expanded (ENDF/B-VIII.0) Benchmark Results

	Exp. k_{eff}	Exp. unc.	Calc. k_{eff}	Calc. unc.
heu-comp-inter-003-case-6	1.0000	0.0047	0.997 539	0.000 353
heu-met-fast-001	1.0000	0.0010	0.999 834	0.000 270
heu-met-fast-003-case-1	1.0000	0.0050	0.993 220	0.000 269
heu-met-fast-003-case-10	1.0000	0.0050	1.003 62	0.000 296
heu-met-fast-003-case-11	1.0000	0.0050	1.008 50	0.000 297
heu-met-fast-003-case-12	1.0000	0.0030	0.998 779	0.000 289
heu-met-fast-003-case-2	1.0000	0.0050	0.991 856	0.000 297
heu-met-fast-003-case-3	1.0000	0.0050	0.996 786	0.000 278
heu-met-fast-003-case-4	1.0000	0.0030	0.994 859	0.000 268
heu-met-fast-003-case-5	1.0000	0.0030	0.999 360	0.000 292
heu-met-fast-003-case-6	1.0000	0.0030	0.999 834	0.000 291
heu-met-fast-003-case-7	1.0000	0.0030	0.999 749	0.000 309
heu-met-fast-003-case-8	1.0000	0.0050	1.000 68	0.000 286
heu-met-fast-003-case-9	1.0000	0.0050	1.000 56	0.000 281
heu-met-fast-004-case-1	1.0020	0.0010	1.002 37	0.000 344
heu-met-fast-008	0.9989	0.0016	0.995 305	0.000 272
heu-met-fast-009-case-1	0.9992	0.0015	0.996 325	0.000 273

Continued on next page

Table 7: Criticality Expanded (ENDF/B-VIII.0) Benchmark Results

	Exp. k_{eff}	Exp. unc.	Calc. k_{eff}	Calc. unc.
heu-met-fast-009-case-2	0.9992	0.0015	0.994 924	0.000 284
heu-met-fast-011	0.9989	0.0015	0.996 594	0.000 326
heu-met-fast-012	0.9992	0.0018	0.997 269	0.000 270
heu-met-fast-013	0.9990	0.0015	0.999 065	0.000 285
heu-met-fast-014	0.9989	0.0017	0.994 851	0.000 277
heu-met-fast-015	0.9996	0.0017	0.994 417	0.000 260
heu-met-fast-018-case-2	1.0000	0.0014	0.999 136	0.000 262
heu-met-fast-019-case-2	1.0000	0.0028	1.006 22	0.000 262
heu-met-fast-020-case-2	1.0000	0.0028	1.000 00	0.000 288
heu-met-fast-021-case-2	1.0000	0.0024	1.000 36	0.000 279
heu-met-fast-022-case-2	1.0000	0.0019	0.997 428	0.000 272
heu-met-fast-026-case-c-11	1.0000	0.0038	1.001 21	0.000 351
heu-met-fast-028	1.0000	0.0030	1.001 13	0.000 286
heu-met-inter-006-case-1	0.9977	0.0008	0.995 337	0.000 326
heu-met-inter-006-case-2	1.0001	0.0008	1.000 40	0.000 341
heu-met-inter-006-case-3	1.0015	0.0009	1.003 21	0.000 364
heu-met-inter-006-case-4	1.0016	0.0008	1.005 53	0.000 312
heu-sol-therm-013-case-1	1.0012	0.0026	0.998 131	0.000 256
heu-sol-therm-013-case-2	1.0007	0.0036	0.997 469	0.000 269
heu-sol-therm-013-case-3	1.0009	0.0036	0.993 859	0.000 292
heu-sol-therm-013-case-4	1.0003	0.0036	0.996 239	0.000 279
heu-sol-therm-032	1.0015	0.0026	0.998 674	0.000 166
ieu-comp-therm-002-case-3	1.0017	0.0044	1.004 54	0.000 307
ieu-met-fast-001-case-1	0.9989	0.0010	0.999 613	0.000 274
ieu-met-fast-001-case-2	0.9997	0.0010	0.999 281	0.000 282
ieu-met-fast-001-case-3	0.9993	0.0005	0.998 862	0.000 280
ieu-met-fast-001-case-4	1.0002	0.0005	0.999 460	0.000 285
ieu-met-fast-002	1.0000	0.0030	0.996 158	0.000 238
ieu-met-fast-003-case-2	1.0000	0.0017	1.000 30	0.000 278
ieu-met-fast-004-case-2	1.0000	0.0030	1.004 54	0.000 296
ieu-met-fast-005-case-2	1.0000	0.0021	1.001 33	0.000 287
ieu-met-fast-006-case-2	1.0000	0.0023	0.993 957	0.000 287
ieu-met-fast-007-case-4	1.0049	0.0008	1.004 21	0.000 228
leu-comp-therm-008-case-1	1.0007	0.0012	1.000 92	0.000 285
leu-comp-therm-008-case-11	1.0007	0.0012	1.000 70	0.000 299
leu-comp-therm-008-case-2	1.0007	0.0012	1.000 96	0.000 293
leu-comp-therm-008-case-5	1.0007	0.0012	0.999 887	0.000 296
leu-comp-therm-008-case-7	1.0007	0.0012	0.999 708	0.000 302
leu-comp-therm-008-case-8	1.0007	0.0012	0.999 297	0.000 299
leu-sol-therm-002-case-1	1.0038	0.0040	1.000 52	0.000 249
leu-sol-therm-002-case-2	1.0024	0.0037	0.995 899	0.000 283
leu-sol-therm-007-case-14	0.9961	0.0009	0.995 846	0.000 308

Continued on next page

Table 7: Criticality Expanded (ENDF/B-VIII.0) Benchmark Results

	Exp. k_{eff}	Exp. unc.	Calc. k_{eff}	Calc. unc.
leu-sol-therm-007-case-30	0.9973	0.0009	0.997 117	0.000 283
leu-sol-therm-007-case-32	0.9985	0.0010	0.996 595	0.000 302
leu-sol-therm-007-case-36	0.9988	0.0011	0.999 979	0.000 275
leu-sol-therm-007-case-49	0.9983	0.0011	0.997 363	0.000 269
mix-comp-therm-002-case-pnl30	1.0010	0.0059	1.000 05	0.000 312
mix-comp-therm-002-case-pnl31	1.0009	0.0045	1.001 16	0.000 344
mix-comp-therm-002-case-pnl32	1.0024	0.0029	1.001 24	0.000 341
mix-comp-therm-002-case-pnl33	1.0024	0.0021	1.005 08	0.000 314
mix-comp-therm-002-case-pnl34	1.0038	0.0022	1.001 84	0.000 309
mix-comp-therm-002-case-pnl35	1.0029	0.0024	1.003 62	0.000 318
mix-met-fast-001	1.0000	0.0016	0.999 492	0.000 281
mix-met-fast-003	0.9993	0.0016	1.000 47	0.000 272
mix-met-fast-008-case-7	1.0300	0.0025	1.023 14	0.000 179
pu-comp-inter-001	1.0000	0.0110	1.007 38	0.000 239
pu-met-fast-001	1.0000	0.0020	0.999 816	0.000 256
pu-met-fast-002	1.0000	0.0020	1.001 21	0.000 274
pu-met-fast-003-case-103	1.0000	0.0030	0.998 681	0.000 291
pu-met-fast-005	1.0000	0.0013	0.999 445	0.000 291
pu-met-fast-006	1.0000	0.0030	0.998 806	0.000 315
pu-met-fast-008-case-2	1.0000	0.0006	0.997 301	0.000 271
pu-met-fast-009	1.0000	0.0027	1.004 63	0.000 285
pu-met-fast-010	1.0000	0.0018	0.997 602	0.000 280
pu-met-fast-011	1.0000	0.0010	1.000 72	0.000 357
pu-met-fast-018	1.0000	0.0030	0.997 848	0.000 288
pu-met-fast-019	0.9992	0.0015	0.999 479	0.000 292
pu-met-fast-020	0.9993	0.0017	0.996 468	0.000 292
pu-met-fast-021-case-1	1.0000	0.0026	1.003 54	0.000 309
pu-met-fast-021-case-2	1.0000	0.0026	0.992 053	0.000 299
pu-met-fast-022-case-2	1.0000	0.0021	0.998 039	0.000 261
pu-met-fast-023-case-2	1.0000	0.0020	0.998 136	0.000 274
pu-met-fast-024-case-2	1.0000	0.0020	1.001 05	0.000 307
pu-met-fast-025-case-2	1.0000	0.0020	1.000 40	0.000 262
pu-met-fast-026-case-2	1.0000	0.0024	1.001 64	0.000 276
pu-sol-therm-009-case-3a	1.0000	0.0033	1.013 22	0.000 178
pu-sol-therm-011-case-16-5	1.0000	0.0052	0.999 977	0.000 403
pu-sol-therm-011-case-18-1	1.0000	0.0052	0.987 837	0.000 326
pu-sol-therm-011-case-18-6	1.0000	0.0052	0.994 488	0.000 366
pu-sol-therm-018-case-9	1.0000	0.0034	1.000 08	0.000 312
pu-sol-therm-021-case-1	1.0000	0.0032	0.998 828	0.000 409
pu-sol-therm-021-case-3	1.0000	0.0065	0.999 768	0.000 425
pu-sol-therm-034-case-1	1.0000	0.0062	0.996 915	0.000 392
u233-comp-therm-001-case-3	1.0000	0.0024	1.000 02	0.000 472

Continued on next page

Table 7: Criticality Expanded (ENDF/B-VIII.0) Benchmark Results

	Exp. k_{eff}	Exp. unc.	Calc. k_{eff}	Calc. unc.
u233-comp-therm-001-case-6	1.0015	0.0028	0.996 206	0.000 398
u233-met-fast-001	1.0000	0.0010	1.000 54	0.000 252
u233-met-fast-002-case-1	1.0000	0.0010	1.000 51	0.000 271
u233-met-fast-002-case-2	1.0000	0.0011	1.002 24	0.000 274
u233-met-fast-003-case-1	1.0000	0.0010	0.999 106	0.000 256
u233-met-fast-003-case-2	1.0000	0.0010	0.999 961	0.000 282
u233-met-fast-004-case-1	1.0000	0.0007	0.999 381	0.000 259
u233-met-fast-004-case-2	1.0000	0.0008	0.996 599	0.000 284
u233-met-fast-005-case-1	1.0000	0.0030	0.997 524	0.000 275
u233-met-fast-005-case-2	1.0000	0.0030	0.997 854	0.000 286
u233-met-fast-006	1.0000	0.0014	0.999 777	0.000 293
u233-sol-inter-001-case-1	1.0000	0.0083	0.981 908	0.000 455
u233-sol-therm-001-case-1	1.0000	0.0031	0.999 461	0.000 250
u233-sol-therm-001-case-2	1.0005	0.0033	0.999 712	0.000 245
u233-sol-therm-001-case-3	1.0006	0.0033	0.999 001	0.000 253
u233-sol-therm-001-case-4	0.9998	0.0033	0.999 446	0.000 273
u233-sol-therm-001-case-5	0.9999	0.0033	0.998 528	0.000 280
u233-sol-therm-008	1.0006	0.0029	0.999 786	0.000 177

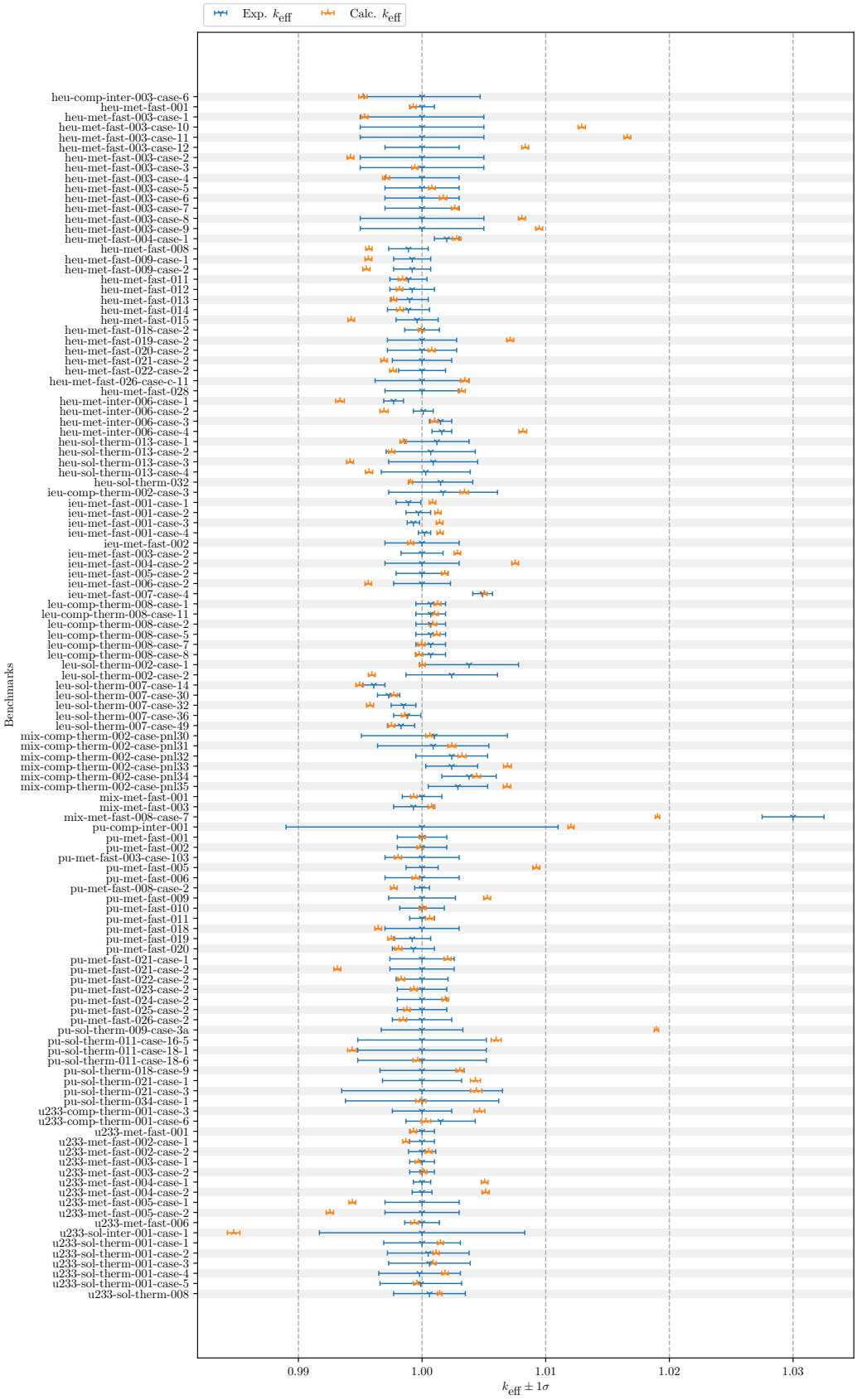

Figure 7: Criticality Expanded (ENDF/B-VII.0) Benchmark Results

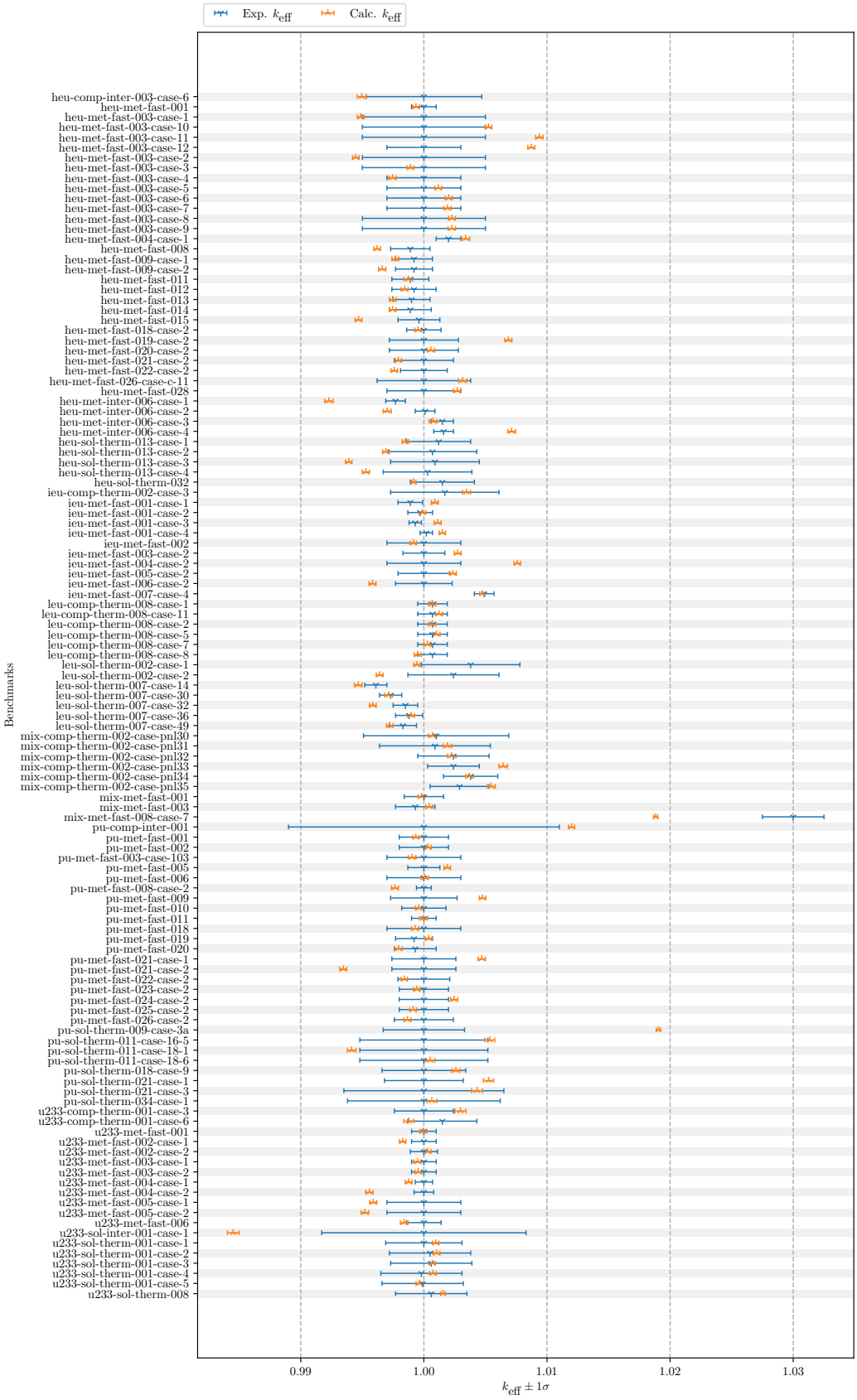

Figure 8: Criticality Expanded (ENDF/B-VII.1) Benchmark Results

Figure 9: Criticality Expanded (ENDF/B-VIII.0) Benchmark Results

4.3 LAQGSM: Los Alamos Quark-Gluon String Model

This test suite executes on 1 node, which uses 114 MPI ranks, with a total Slurm allocation of no more than 40 minutes. An example `VnV.py` execution line is `./VnV.py execute_slurm --nmpi 114 --time 40 --wait --calcdir_name laqgsm`.

4.3.1 ^{40}Ar (1042 MeV/A) onto ^{40}Ca Double-differential Cross Section

This experiment is a double-differential cross-section measurement. Historically, calculated and experimental results were compared visually, and that is the approach provided here such that no additional measures of agreement are provided. The results are shown in Fig. 10.

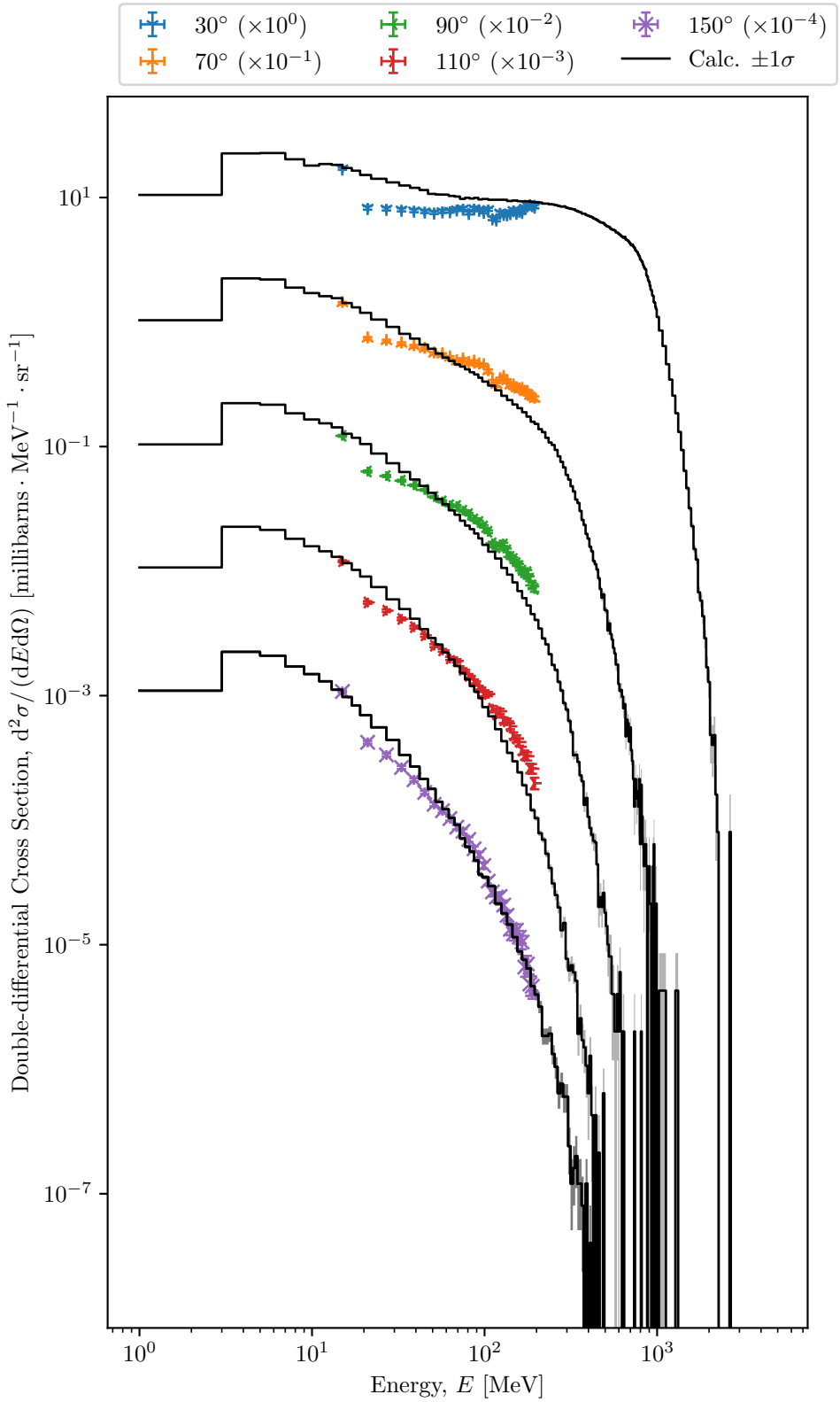

Figure 10: ^{40}Ar (1042 MeV/A) onto ^{40}Ca Double-differential Cross Section

4.3.2 ^{12}C (290 MeV/A) onto ^{12}C Double-differential Cross Section

This experiment is a double-differential cross-section measurement. Historically, calculated and experimental results were compared visually, and that is the approach provided here such that no additional measures of agreement are provided. The results are shown in Fig. 11.

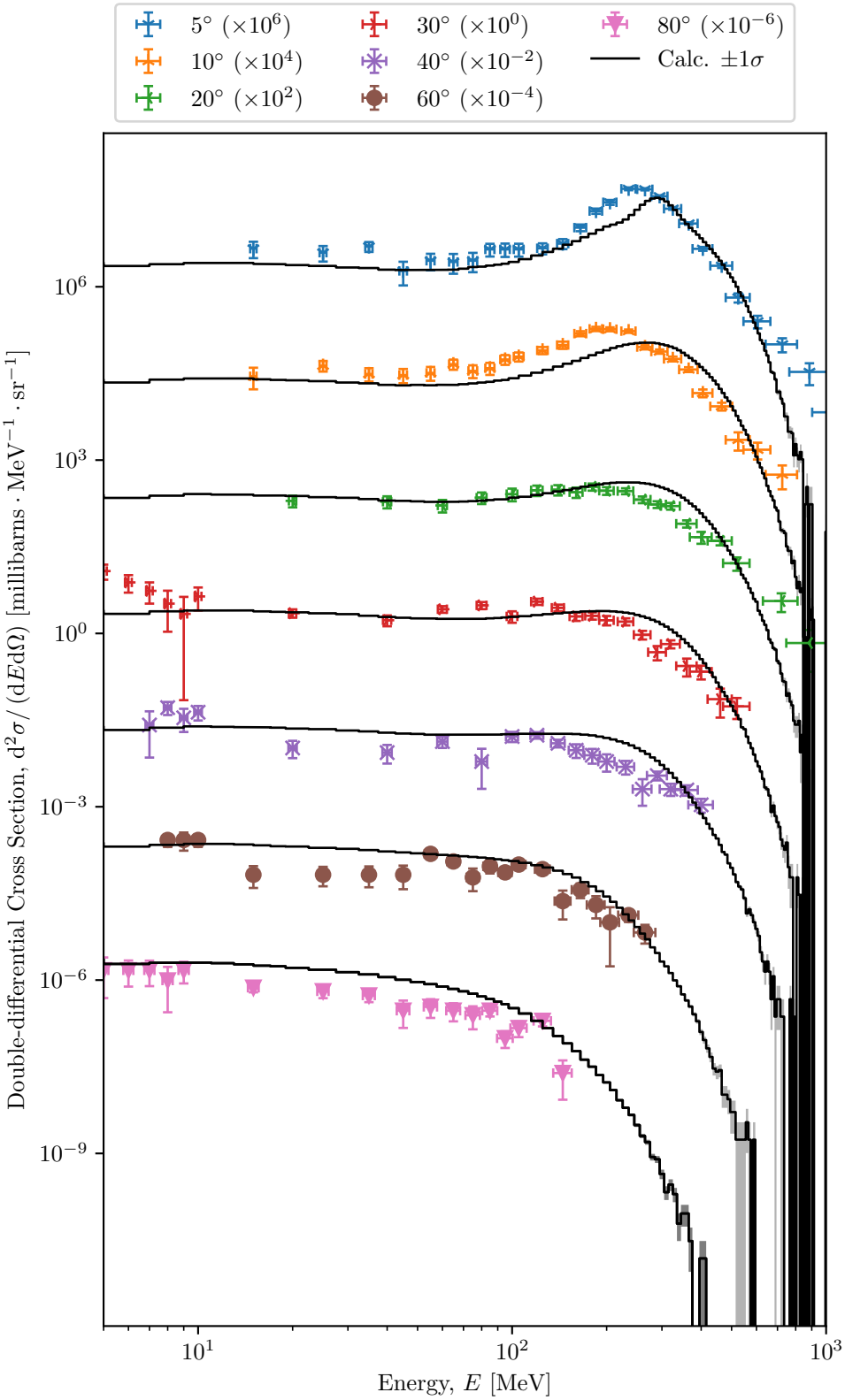

Figure 11: ^{12}C (290 MeV/A) onto ^{12}C Double-differential Cross Section

4.3.3 ^{28}Si (600 MeV/A) onto ^{64}Cu Double-differential Cross Section

This experiment is a double-differential cross-section measurement. Historically, calculated and experimental results were compared visually, and that is the approach provided here such that no additional measures of agreement are provided. The results are shown in Fig. 12.

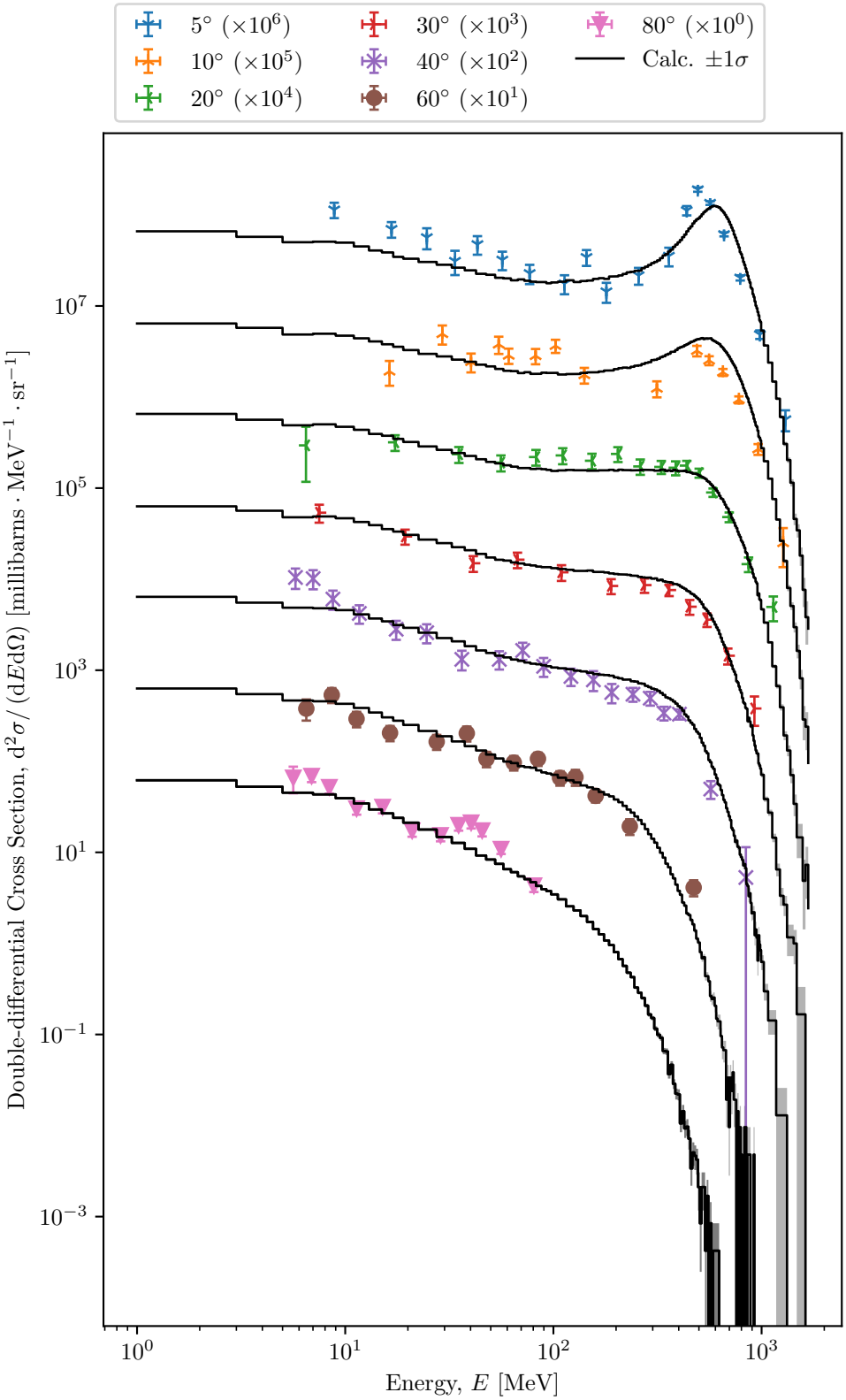

Figure 12: ^{28}Si (600 MeV/A) onto ^{64}Cu Double-differential Cross Section

4.3.4 ^{20}Ne (800 MeV/A) onto ^{64}Cu Deuteron Invariant Cross Section

This experiment is a invariant cross-section measurement. Historically, calculated and experimental results were compared visually, and that is the approach provided here such that no additional measures of agreement are provided. The results are shown in Fig. 13.

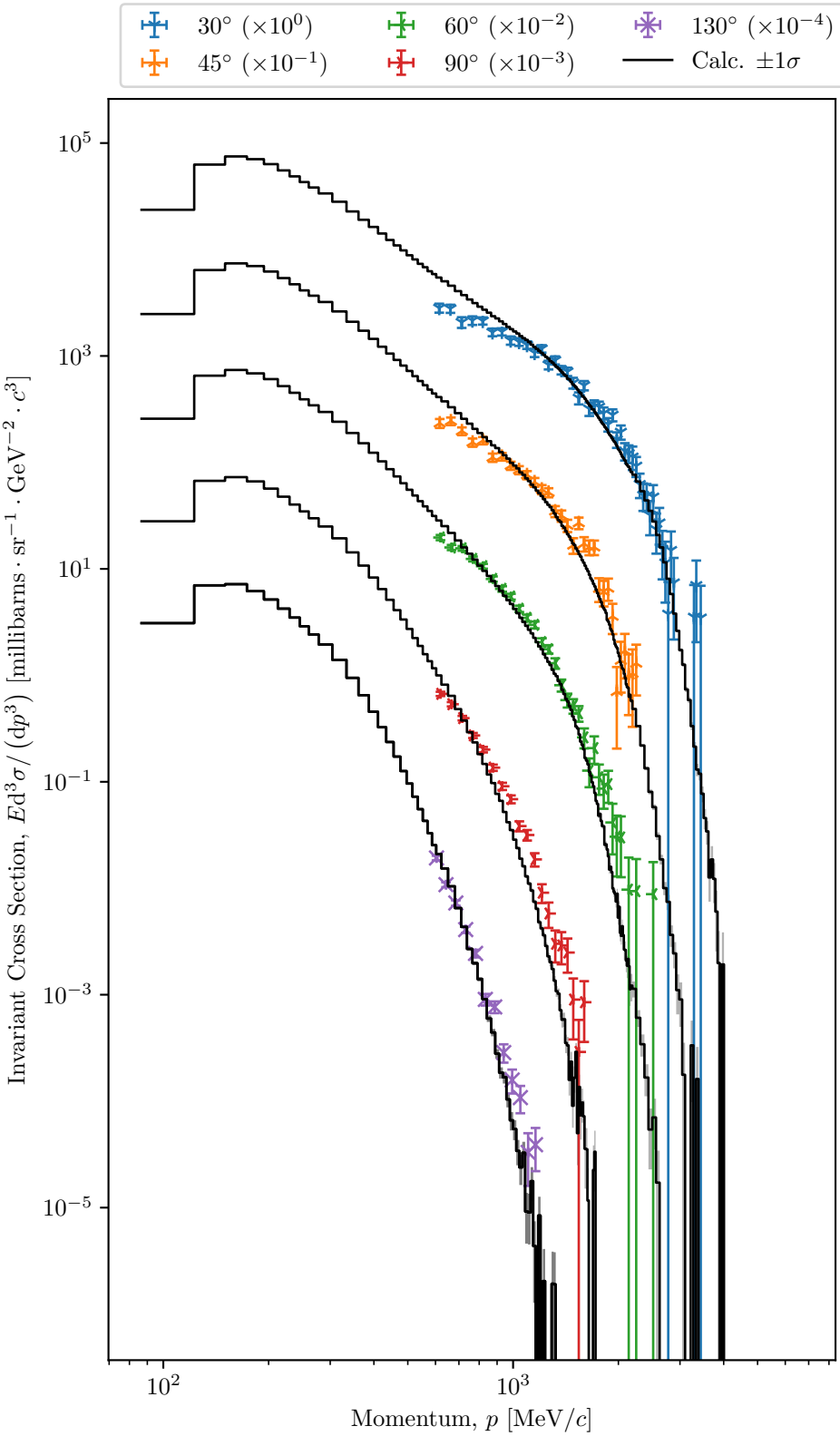

Figure 13: ^{20}Ne (800 MeV/A) onto ^{64}Cu Deuteron Invariant Cross Section

4.4 LLNL Pulsed Spheres

This test suite executes on 1 node, which uses 14 threads and 8 concurrent jobs, with a total Slurm allocation of no more than 8 minutes. An example `VnV.py` execution line is `./VnV.py execute_slurm --ntrd 14 --jobs 8 --time 8 --wait --calcdir_name pulsed_spheres_$DATA`, where `$DATA` is an environment variable that identifies which evaluated nuclear data set to use.

4.4.1 ENDF/B-VI.6

Results from neutron pulsed spheres of six different materials are presented. For each material, the neutron time-of-flight spectra calculated from both CSG models and measured experimentally are plotted together and the average ratio of calculation results over experimental results with the associated one-standard-deviation uncertainty is presented. Uncertainty propagation is done with the assumption of normally distributed uncertainties. A summary for all sphere materials is given at the conclusion of this section.

Beryllium The time-of-flight spectra for a 0.8 MFP (14-MeV neutron) thick beryllium pulsed sphere modeled with legacy and detailed CSG is given in Fig. 14. The legacy model has an average ratio of calculation to measured results of $1.0017 \pm 5.90\%$ and the detailed model has an average ratio of $0.9942 \pm 5.14\%$.

Carbon The time-of-flight spectra for a 2.9 MFP (14-MeV neutron) thick carbon pulsed sphere modeled with legacy and detailed CSG is given in Fig. 15. The legacy model has an average ratio of calculation to measured results of $0.9645 \pm 4.05\%$ and the detailed model has an average ratio of $0.9603 \pm 3.58\%$.

Concrete The time-of-flight spectra for a 2.0 MFP (14-MeV neutron) thick concrete pulsed sphere modeled with legacy and detailed CSG is given in Fig. 16. The legacy model has an average ratio of calculation to measured results of $1.0117 \pm 5.77\%$ and the detailed model has an average ratio of $0.9919 \pm 5.11\%$.

Iron The time-of-flight spectra for a 0.9 MFP (14-MeV neutron) thick iron pulsed sphere modeled with legacy and detailed CSG is given in Fig. 17. The legacy model has an average ratio of calculation to measured results of $0.9743 \pm 5.71\%$ and the detailed model has an average ratio of $0.9451 \pm 4.23\%$.

Lithium-6 The time-of-flight spectra for a 1.6 MFP (14-MeV neutron) thick lithium-6 pulsed sphere modeled with legacy and detailed CSG is given in Fig. 18. The legacy model has an average ratio of calculation to measured results of $1.0974 \pm 5.97\%$ and the detailed model has an average ratio of $1.0917 \pm 5.38\%$.

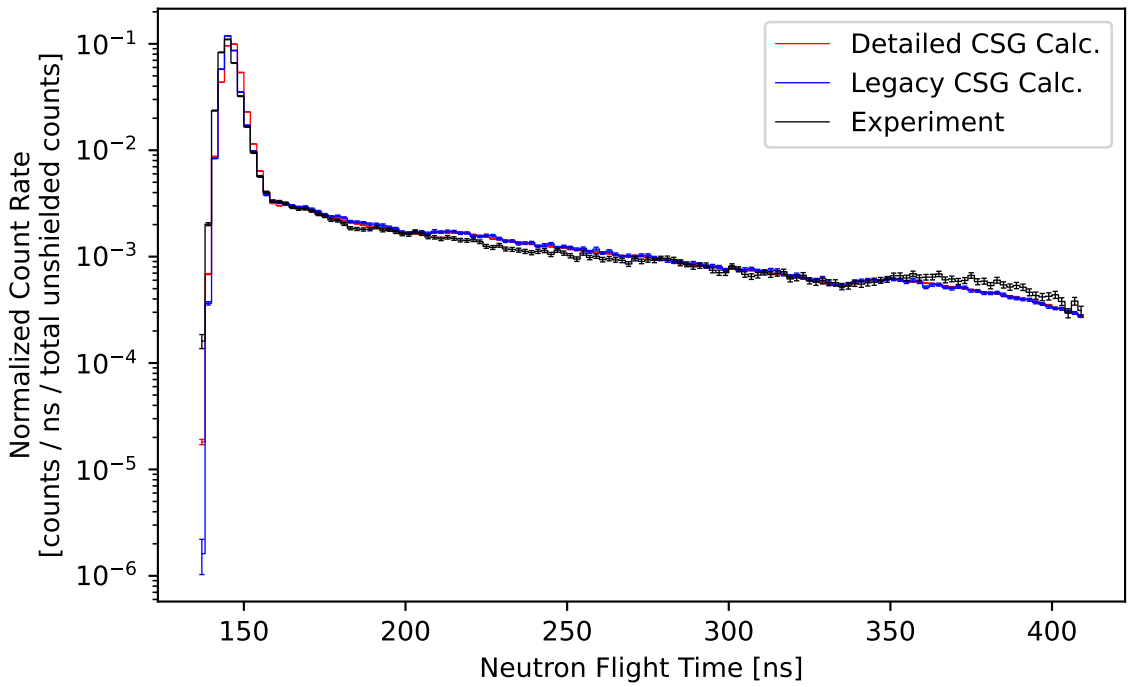

Figure 14: Comparison of the measured and calculated (ENDF/B-VI.6) normalized count rate of neutrons escaping from a 0.8 MFP (14-MeV neutron) thick sphere of beryllium plotted against flight time.

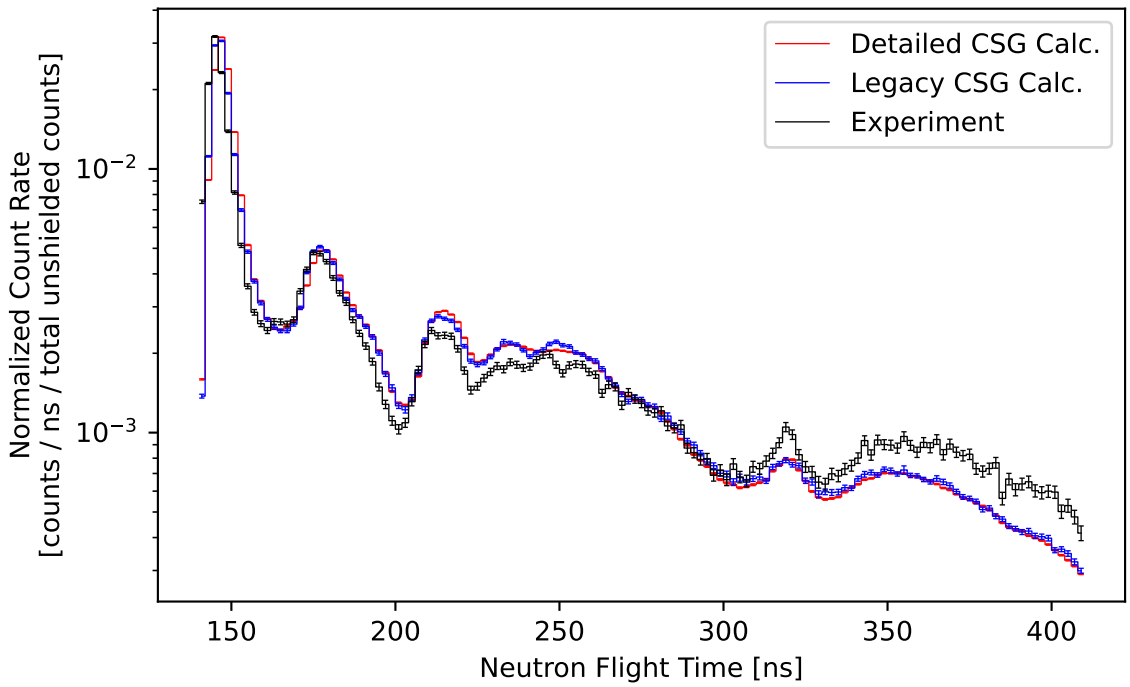

Figure 15: Comparison of the measured and calculated (ENDF/B-VI.6) normalized count rate of neutrons escaping from a 2.9 MFP (14-MeV neutron) thick sphere of carbon plotted against flight time.

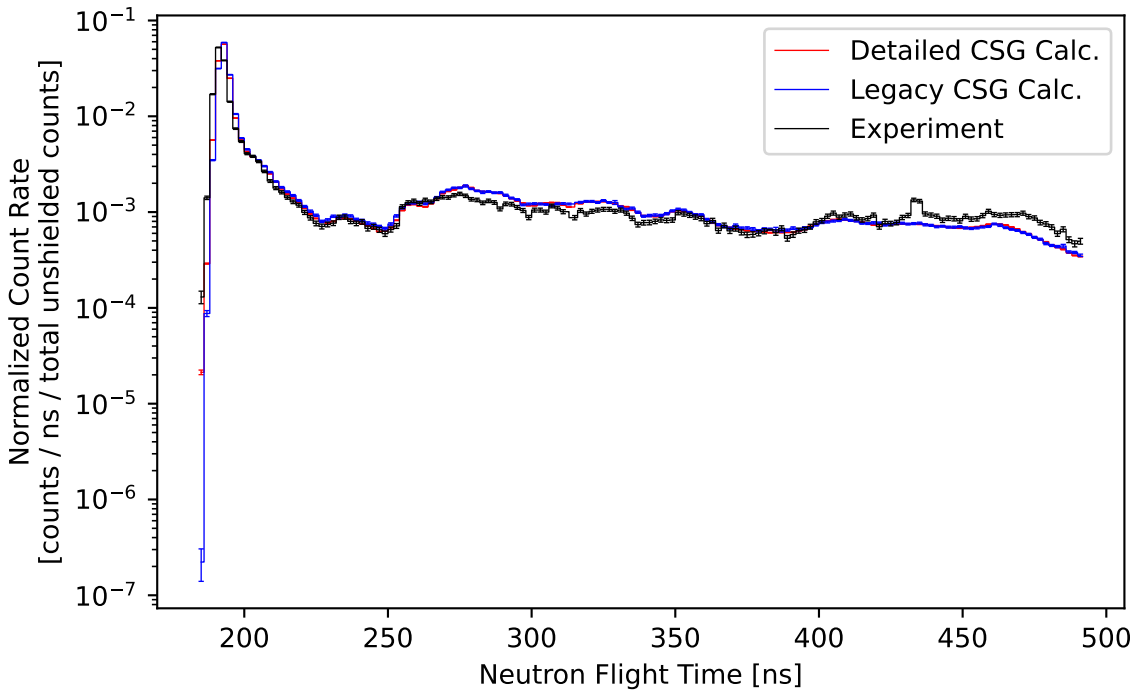

Figure 16: Comparison of the measured and calculated (ENDF/B-VI.6) normalized count rate of neutrons escaping from a 2.0 MFP (14-MeV neutron) thick sphere of concrete plotted against flight time.

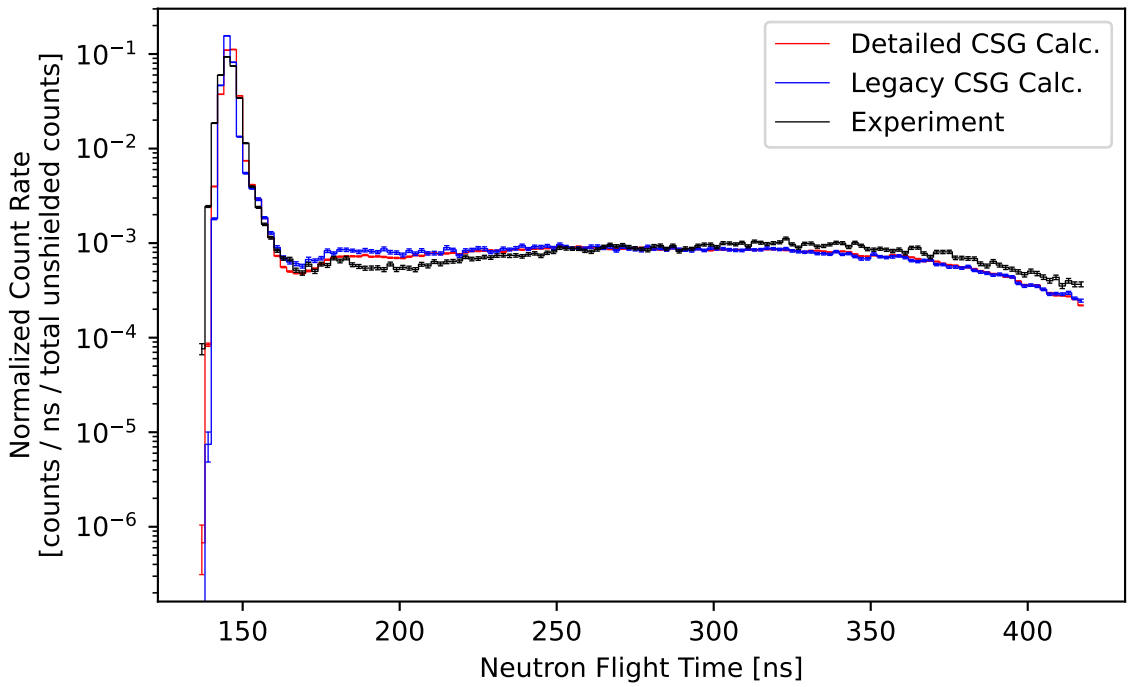

Figure 17: Comparison of the measured and calculated (ENDF/B-VI.6) normalized count rate of neutrons escaping from a 0.9 MFP (14-MeV neutron) thick sphere of iron plotted against flight time.

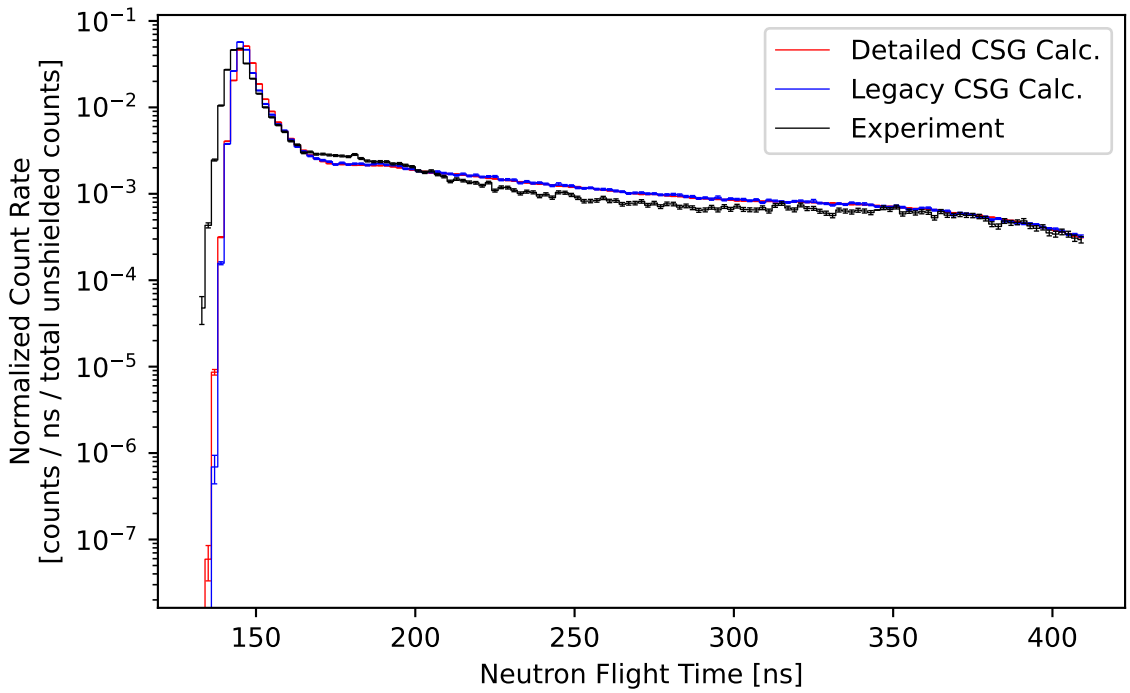

Figure 18: Comparison of the measured and calculated (ENDF/B-VI.6) normalized count rate of neutrons escaping from a 1.6 MFP (14-MeV neutron) thick sphere of lithium-6 plotted against flight time.

Water The time-of-flight spectra for a 1.9 MFP (14-MeV neutron) thick water pulsed sphere modeled with legacy and detailed CSG is given in Fig. 19. The legacy model has an average ratio of calculation to measured results of $1.0875 \pm 27.52\%$ and the detailed model has an average ratio of $1.0442 \pm 23.53\%$.

Note that the uncertainty in the average ratio of calculated to experimental time-of-flight results is calculated by propagating both the calculation result uncertainty and the experimental measurement uncertainty. From Fig. 19 one sees more measurement uncertainty compared to other materials, this is the cause of the high average ratio uncertainty for this material.

Summary A summary of the experiment characteristics and the averaged calculation to experiment ratio is given for each benchmark in Table 8.

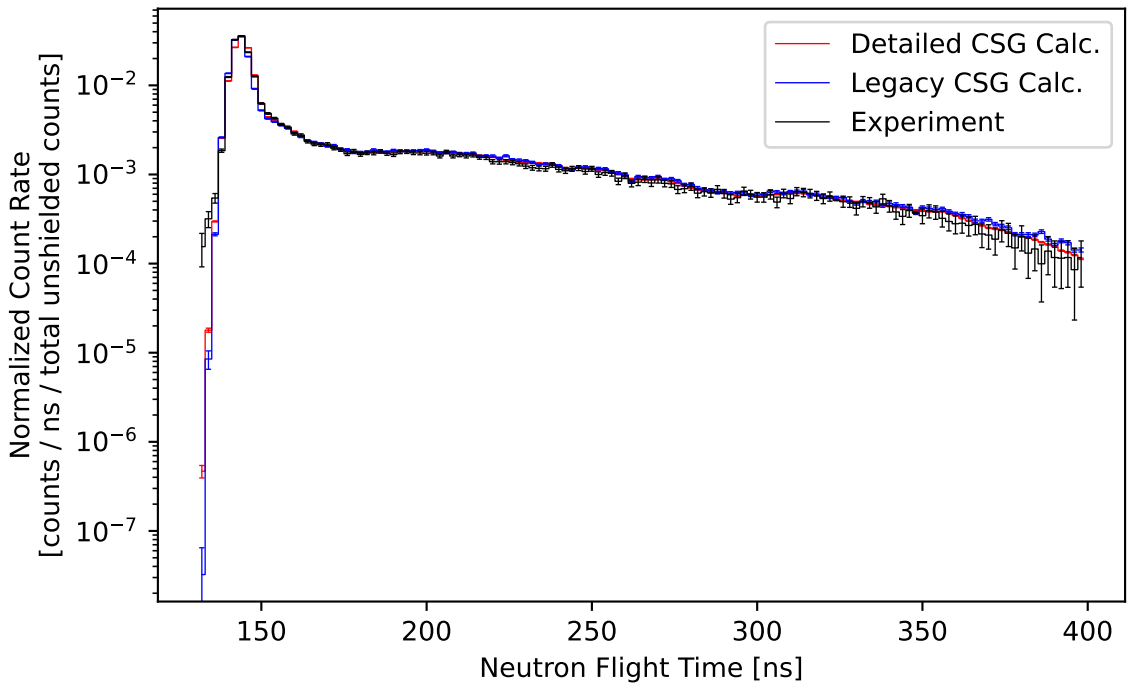

Figure 19: Comparison of the measured and calculated (ENDF/B-VI.6) normalized count rate of neutrons escaping from a 1.9 MFP (14-MeV neutron) thick sphere of water plotted against flight time.

Table 8: Characteristics and Calculation (C) to Experimental (E) Ratios of All Benchmarks using ENDF/B-VI.6

CSG Model	Material	Thickness	Flight Distance	Degrees Off Axis	C/E Val.	C/E Unc. [%]
detailed	beryllium	0.8 MFP (14-MeV neutron)	765.2 cm	30	0.9942	5.14
simple	beryllium	0.8 MFP (14-MeV neutron)	765.2 cm	30	1.0017	5.90
detailed	carbon	2.9 MFP (14-MeV neutron)	766.0 cm	30	0.9603	3.58
simple	carbon	2.9 MFP (14-MeV neutron)	766.0 cm	30	0.9645	4.05
detailed	concrete	2.0 MFP (14-MeV neutron)	975.4 cm	120	0.9919	5.11
simple	concrete	2.0 MFP (14-MeV neutron)	975.4 cm	120	1.0117	5.77
detailed	iron	0.9 MFP (14-MeV neutron)	766.0 cm	30	0.9451	4.23
simple	iron	0.9 MFP (14-MeV neutron)	766.0 cm	30	0.9743	5.71
detailed	lithium-6	1.6 MFP (14-MeV neutron)	765.2 cm	30	1.0917	5.38
simple	lithium-6	1.6 MFP (14-MeV neutron)	765.2 cm	30	1.0974	5.97
detailed	water	1.9 MFP (14-MeV neutron)	754.0 cm	30	1.0442	23.53
simple	water	1.9 MFP (14-MeV neutron)	754.0 cm	30	1.0875	27.52

4.4.2 ENDF/B-VII.0

Results from neutron pulsed spheres of six different materials are presented. For each material, the neutron time-of-flight spectra calculated from both CSG models and measured experimentally are plotted together and the average ratio of calculation results over experimental results with the associated one-standard-deviation uncertainty is presented. Uncertainty propagation is done with the assumption of normally distributed uncertainties. A summary for all sphere materials is given at the conclusion of this section.

Beryllium The time-of-flight spectra for a 0.8 MFP (14-MeV neutron) thick beryllium pulsed sphere modeled with legacy and detailed CSG is given in Fig. 20. The legacy model has an average ratio of calculation to measured results of $1.0026 \pm 6.15\%$ and the detailed model has an average ratio of $0.9921 \pm 5.15\%$.

Carbon The time-of-flight spectra for a 2.9 MFP (14-MeV neutron) thick carbon pulsed sphere modeled with legacy and detailed CSG is given in Fig. 21. The legacy model has an average ratio of calculation to measured results of $0.9648 \pm 4.06\%$ and the detailed model has an average ratio of $0.9604 \pm 3.58\%$.

Concrete The time-of-flight spectra for a 2.0 MFP (14-MeV neutron) thick concrete pulsed sphere modeled with legacy and detailed CSG is given in Fig. 22. The legacy model has an average ratio of calculation to measured results of $0.9953 \pm 5.73\%$ and the detailed model has an average ratio of $0.9753 \pm 5.02\%$.

Iron The time-of-flight spectra for a 0.9 MFP (14-MeV neutron) thick iron pulsed sphere modeled with legacy and detailed CSG is given in Fig. 23. The legacy model has an average ratio of calculation to measured results of $0.9755 \pm 5.74\%$ and the detailed model has an average ratio of $0.9451 \pm 4.23\%$.

Lithium-6 The time-of-flight spectra for a 1.6 MFP (14-MeV neutron) thick lithium-6 pulsed sphere modeled with legacy and detailed CSG is given in Fig. 24. The legacy model has an average ratio of calculation to measured results of $1.1042 \pm 6.03\%$ and the detailed model has an average ratio of $1.0994 \pm 5.44\%$.

Water The time-of-flight spectra for a 1.9 MFP (14-MeV neutron) thick water pulsed sphere modeled with legacy and detailed CSG is given in Fig. 25. The legacy model has an average ratio of calculation to measured results of $1.0946 \pm 28.06\%$ and the detailed model has an average ratio of $1.0514 \pm 24.47\%$.

Note that the uncertainty in the average ratio of calculated to experimental time-of-flight results is calculated by propagating both the calculation result uncertainty and the experimental measurement uncertainty. From Fig. 25 one sees more measurement uncertainty compared to other materials, this is the cause of the high average ratio uncertainty for this material.

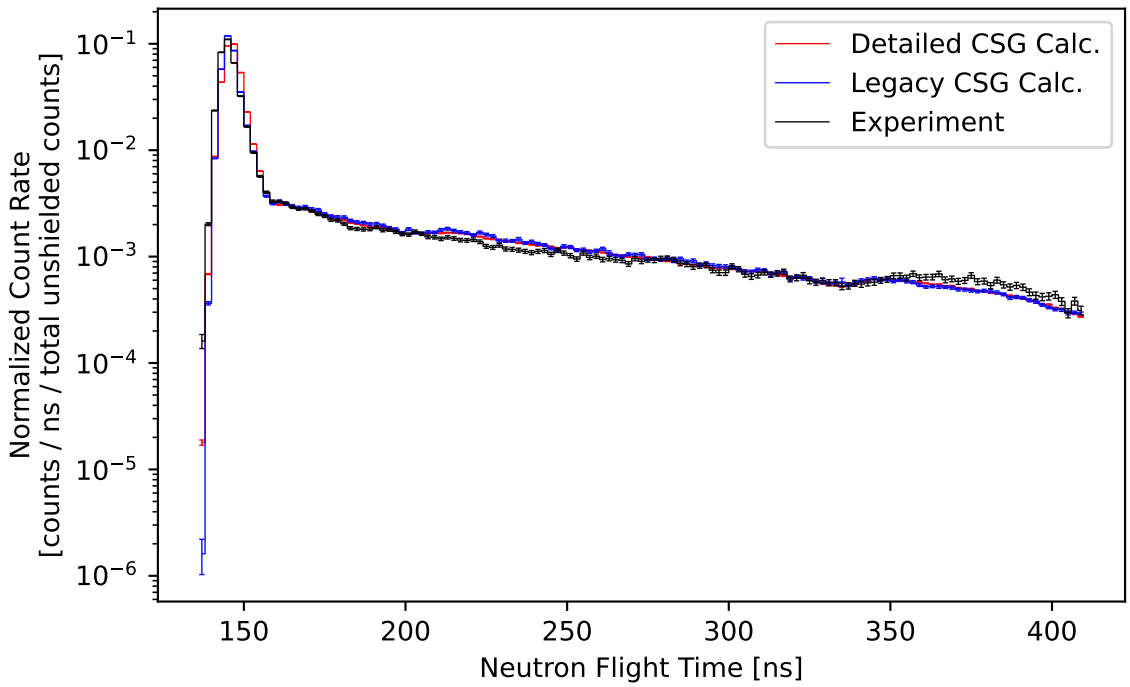

Figure 20: Comparison of the measured and calculated (ENDF/B-VII.0) normalized count rate of neutrons escaping from a 0.8 MFP (14-MeV neutron) thick sphere of beryllium plotted against flight time.

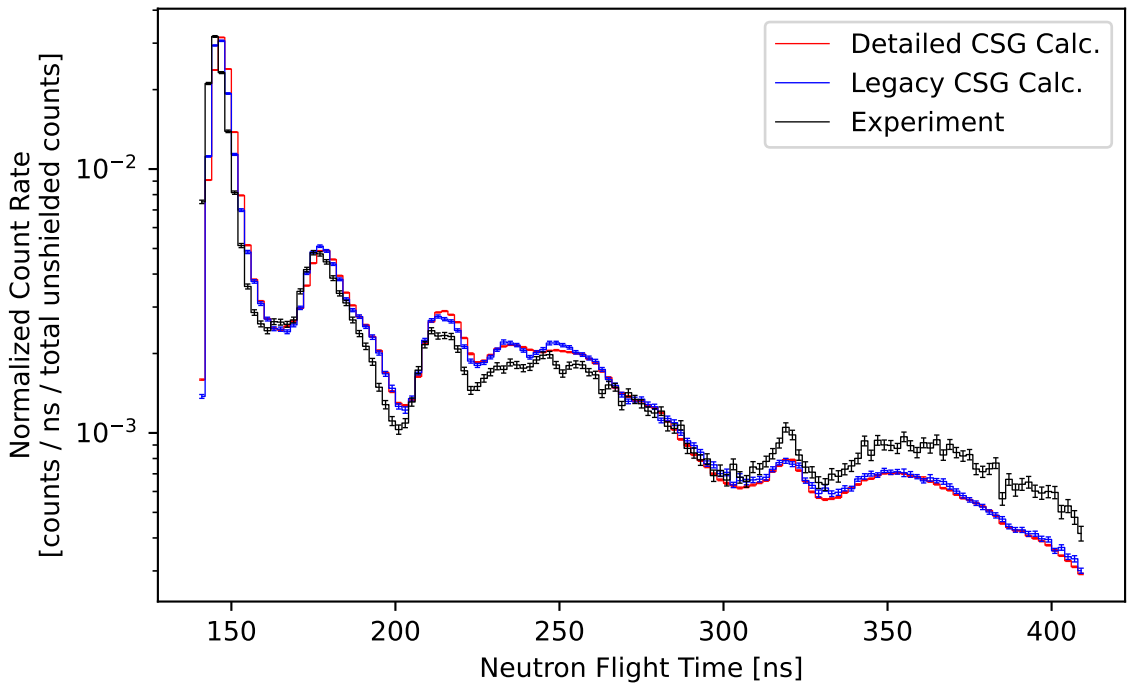

Figure 21: Comparison of the measured and calculated (ENDF/B-VII.0) normalized count rate of neutrons escaping from a 2.9 MFP (14-MeV neutron) thick sphere of carbon plotted against flight time.

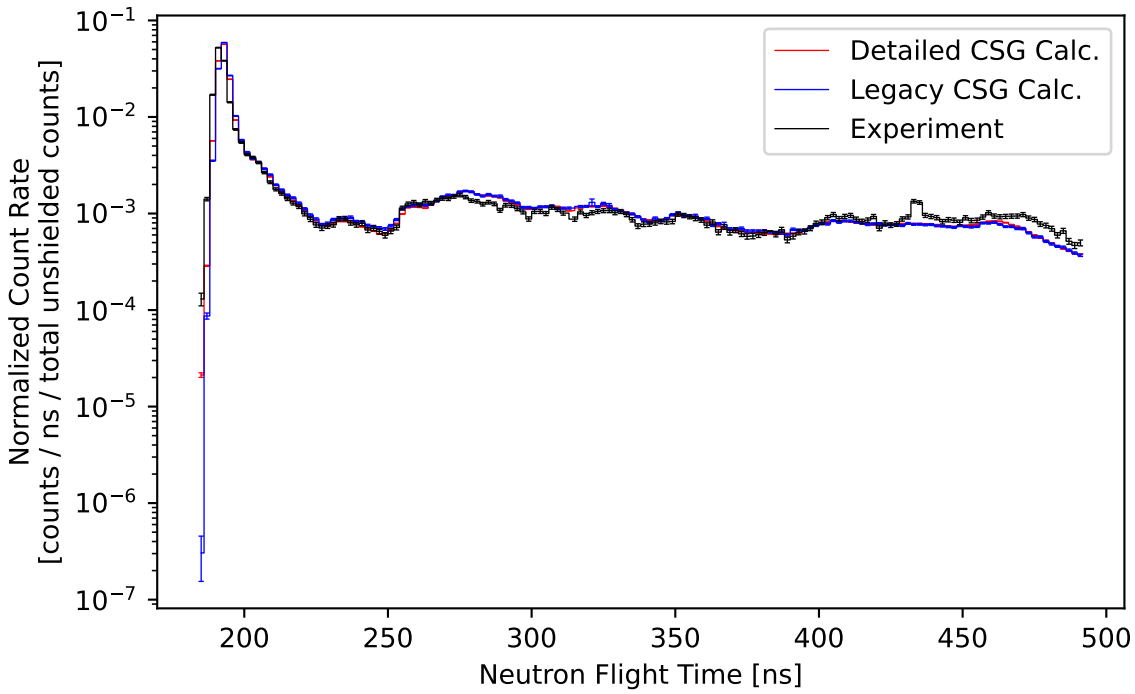

Figure 22: Comparison of the measured and calculated (ENDF/B-VII.0) normalized count rate of neutrons escaping from a 2.0 MFP (14-MeV neutron) thick sphere of concrete plotted against flight time.

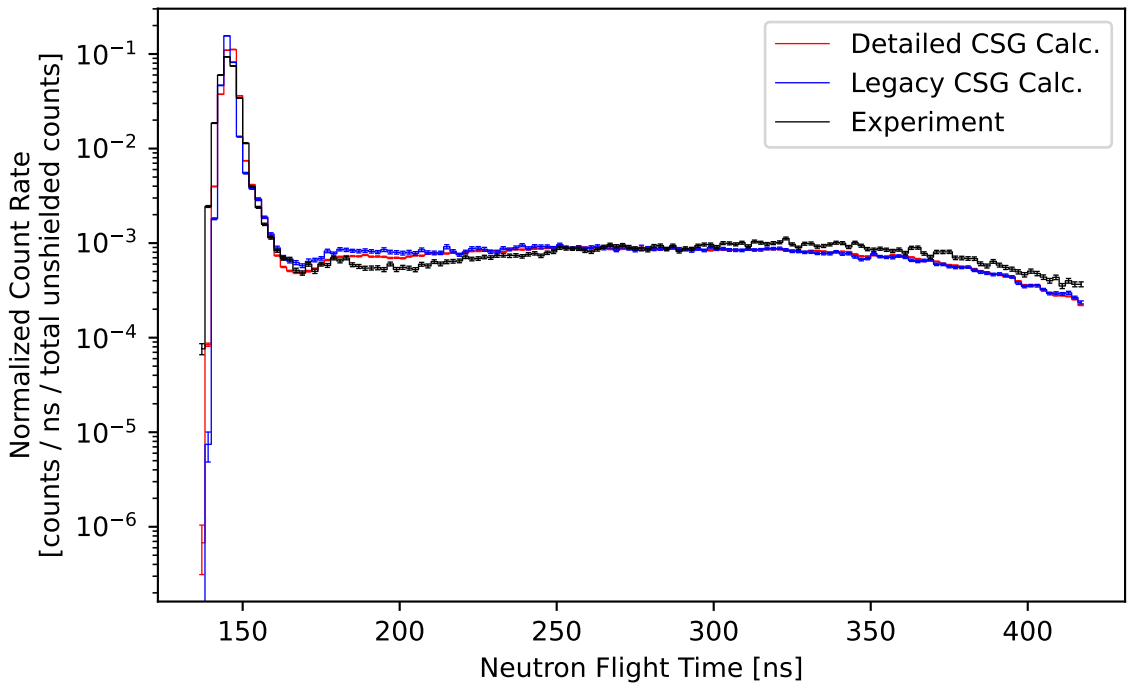

Figure 23: Comparison of the measured and calculated (ENDF/B-VII.0) normalized count rate of neutrons escaping from a 0.9 MFP (14-MeV neutron) thick sphere of iron plotted against flight time.

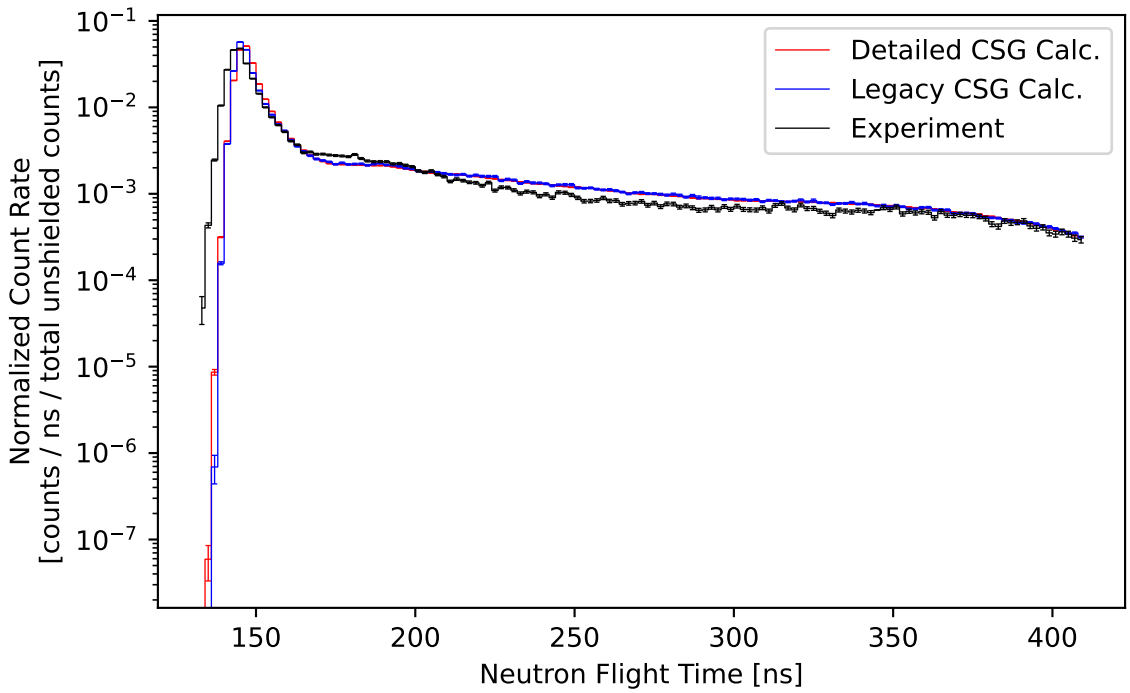

Figure 24: Comparison of the measured and calculated (ENDF/B-VII.0) normalized count rate of neutrons escaping from a 1.6 MFP (14-MeV neutron) thick sphere of lithium-6 plotted against flight time.

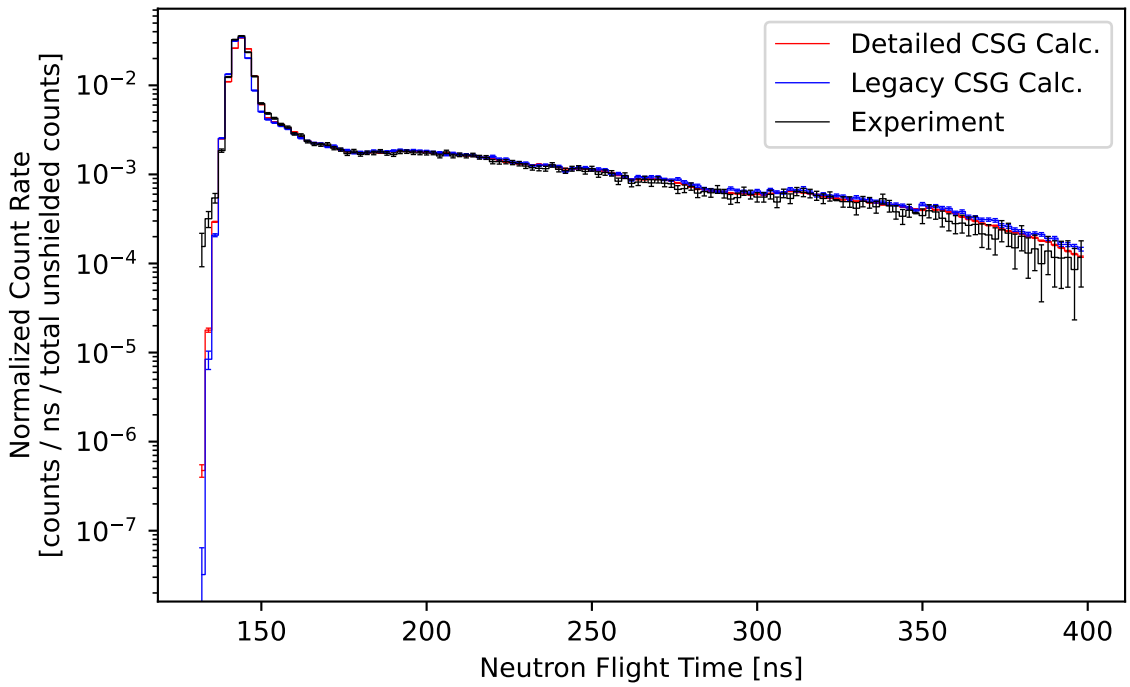

Figure 25: Comparison of the measured and calculated (ENDF/B-VII.0) normalized count rate of neutrons escaping from a 1.9 MFP (14-MeV neutron) thick sphere of water plotted against flight time.

Summary A summary of the experiment characteristics and the averaged calculation to experiment ratio is given for each benchmark in Table 9.

Table 9: Characteristics and Calculation (C) to Experimental (E) Ratios of All Benchmarks using ENDF/B-VII.0

CSG Model	Material	Thickness	Flight Distance	Degrees Off Axis	C/E Val.	C/E Unc. [%]
detailed	beryllium	0.8 MFP (14-MeV neutron)	765.2 cm	30	0.9921	5.15
simple	beryllium	0.8 MFP (14-MeV neutron)	765.2 cm	30	1.0026	6.15
detailed	carbon	2.9 MFP (14-MeV neutron)	766.0 cm	30	0.9604	3.58
simple	carbon	2.9 MFP (14-MeV neutron)	766.0 cm	30	0.9648	4.06
detailed	concrete	2.0 MFP (14-MeV neutron)	975.4 cm	120	0.9753	5.02
simple	concrete	2.0 MFP (14-MeV neutron)	975.4 cm	120	0.9953	5.73
detailed	iron	0.9 MFP (14-MeV neutron)	766.0 cm	30	0.9451	4.23
simple	iron	0.9 MFP (14-MeV neutron)	766.0 cm	30	0.9755	5.74
detailed	lithium-6	1.6 MFP (14-MeV neutron)	765.2 cm	30	1.0994	5.44
simple	lithium-6	1.6 MFP (14-MeV neutron)	765.2 cm	30	1.1042	6.03
detailed	water	1.9 MFP (14-MeV neutron)	754.0 cm	30	1.0514	24.47
simple	water	1.9 MFP (14-MeV neutron)	754.0 cm	30	1.0946	28.06

4.4.3 ENDF/B-VII.1

Results from neutron pulsed spheres of six different materials are presented. For each material, the neutron time-of-flight spectra calculated from both CSG models and measured experimentally are plotted together and the average ratio of calculation results over experimental results with the associated one-standard-deviation uncertainty is presented. Uncertainty propagation is done with the assumption of normally distributed uncertainties. A summary for all sphere materials is given at the conclusion of this section.

Beryllium The time-of-flight spectra for a 0.8 MFP (14-MeV neutron) thick beryllium pulsed sphere modeled with legacy and detailed CSG is given in Fig. 26. The legacy model has an average ratio of calculation to measured results of $1.0034 \pm 6.16\%$ and the detailed model has an average ratio of $0.9957 \pm 5.18\%$.

Carbon The time-of-flight spectra for a 2.9 MFP (14-MeV neutron) thick carbon pulsed sphere modeled with legacy and detailed CSG is given in Fig. 27. The legacy model has an average ratio of calculation to measured results of $0.9648 \pm 4.06\%$ and the detailed model has an average ratio of $0.9610 \pm 3.58\%$.

Concrete The time-of-flight spectra for a 2.0 MFP (14-MeV neutron) thick concrete pulsed sphere modeled with legacy and detailed CSG is given in Fig. 28. The legacy model has an average ratio of calculation to measured results of $0.9955 \pm 5.72\%$ and the detailed model has an average ratio of $0.9753 \pm 5.02\%$.

Iron The time-of-flight spectra for a 0.9 MFP (14-MeV neutron) thick iron pulsed sphere modeled with legacy and detailed CSG is given in Fig. 29. The legacy model has an average ratio of calculation to measured results of $0.9745 \pm 5.73\%$ and the detailed model has an average ratio of $0.9488 \pm 4.24\%$.

Lithium-6 The time-of-flight spectra for a 1.6 MFP (14-MeV neutron) thick lithium-6 pulsed sphere modeled with legacy and detailed CSG is given in Fig. 30. The legacy model has an average ratio of calculation to measured results of $1.0991 \pm 5.99\%$ and the detailed model has an average ratio of $1.0957 \pm 5.42\%$.

Water The time-of-flight spectra for a 1.9 MFP (14-MeV neutron) thick water pulsed sphere modeled with legacy and detailed CSG is given in Fig. 31. The legacy model has an average ratio of calculation to measured results of $1.0945 \pm 28.08\%$ and the detailed model has an average ratio of $1.0519 \pm 24.43\%$.

Note that the uncertainty in the average ratio of calculated to experimental time-of-flight results is calculated by propagating both the calculation result uncertainty and the experimental measurement uncertainty. From Fig. 31 one sees more measurement uncertainty compared to other materials, this is the cause of the high average ratio uncertainty for this material.

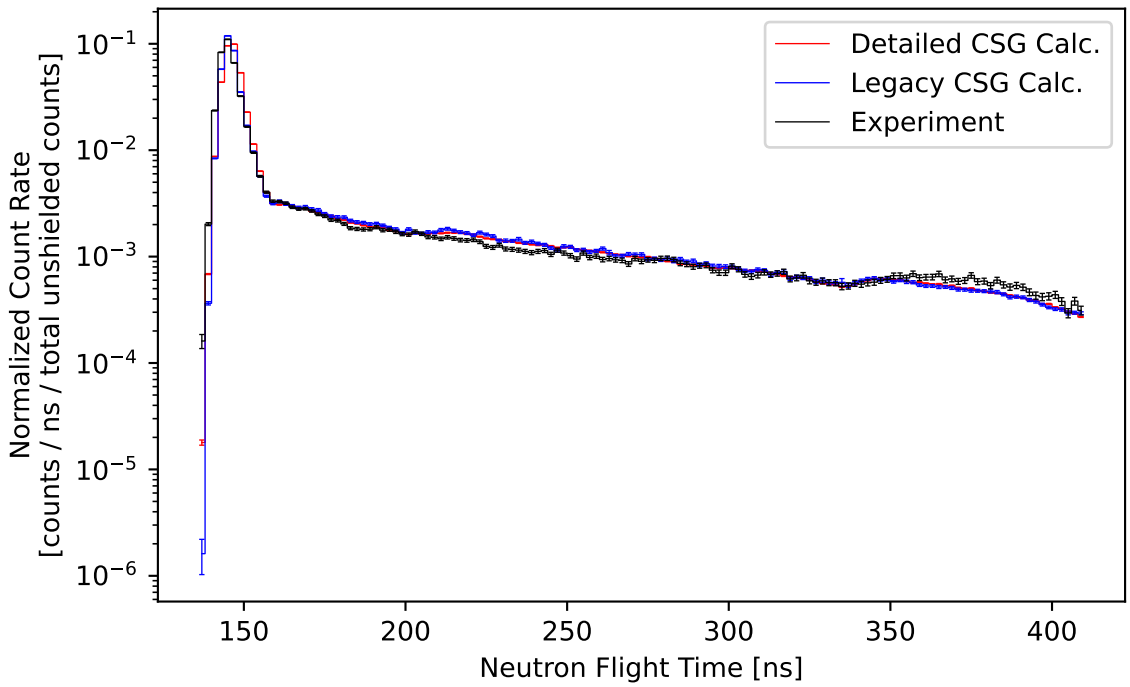

Figure 26: Comparison of the measured and calculated (ENDF/B-VII.1) normalized count rate of neutrons escaping from a 0.8 MFP (14-MeV neutron) thick sphere of beryllium plotted against flight time.

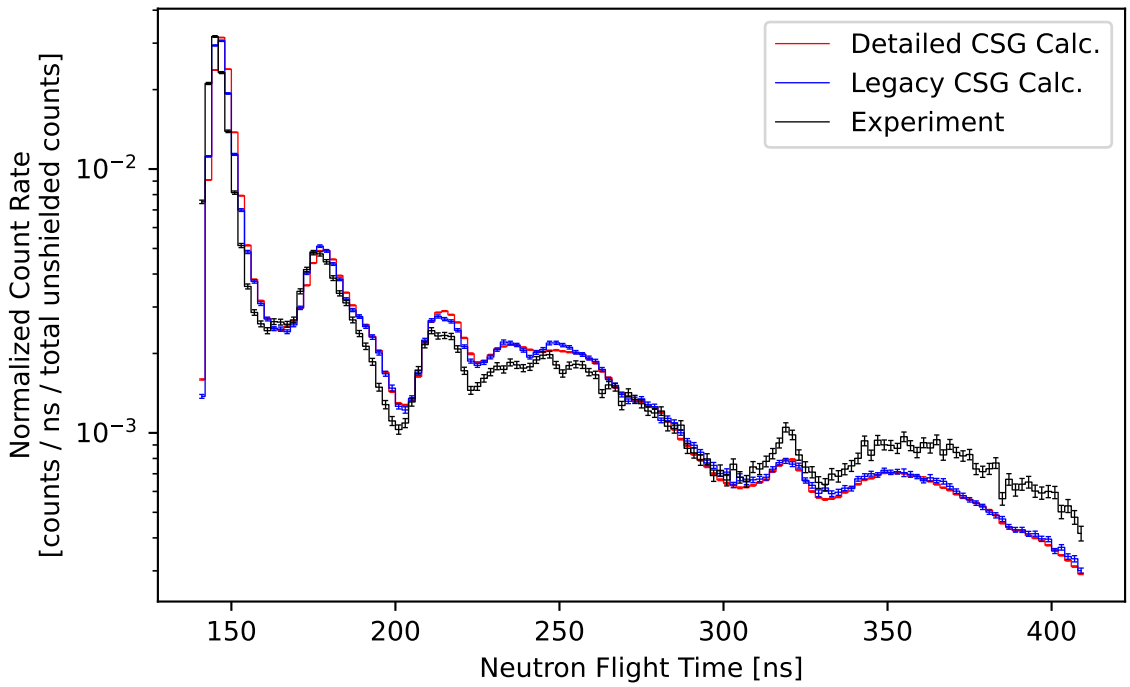

Figure 27: Comparison of the measured and calculated (ENDF/B-VII.1) normalized count rate of neutrons escaping from a 2.9 MFP (14-MeV neutron) thick sphere of carbon plotted against flight time.

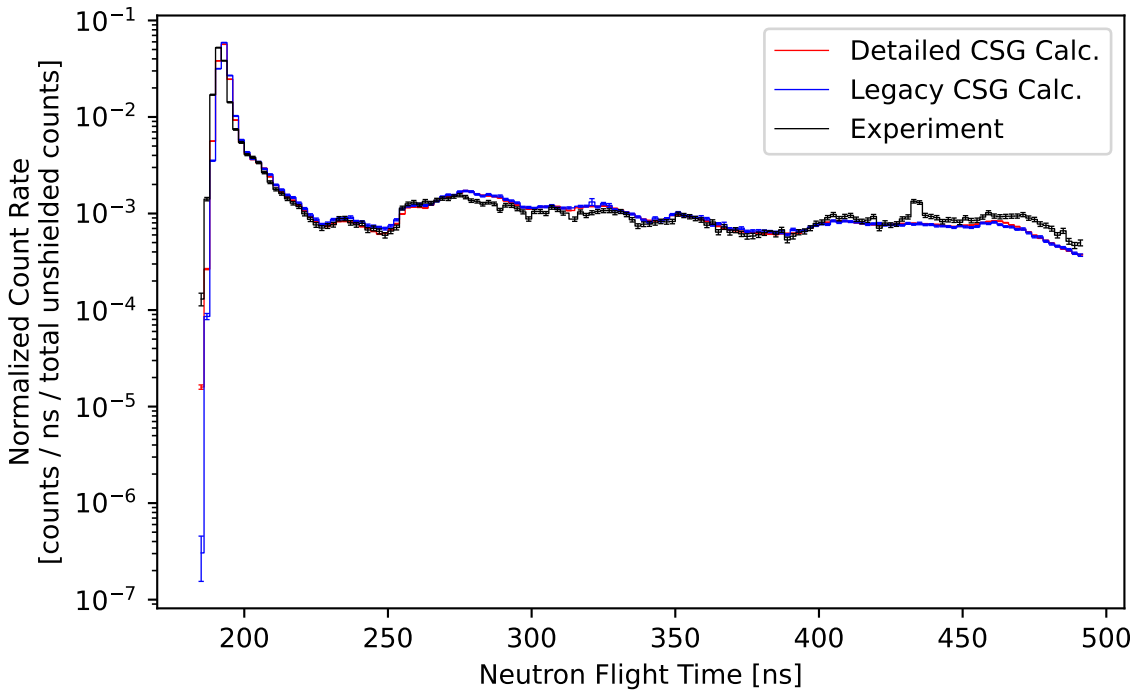

Figure 28: Comparison of the measured and calculated (ENDF/B-VII.1) normalized count rate of neutrons escaping from a 2.0 MFP (14-MeV neutron) thick sphere of concrete plotted against flight time.

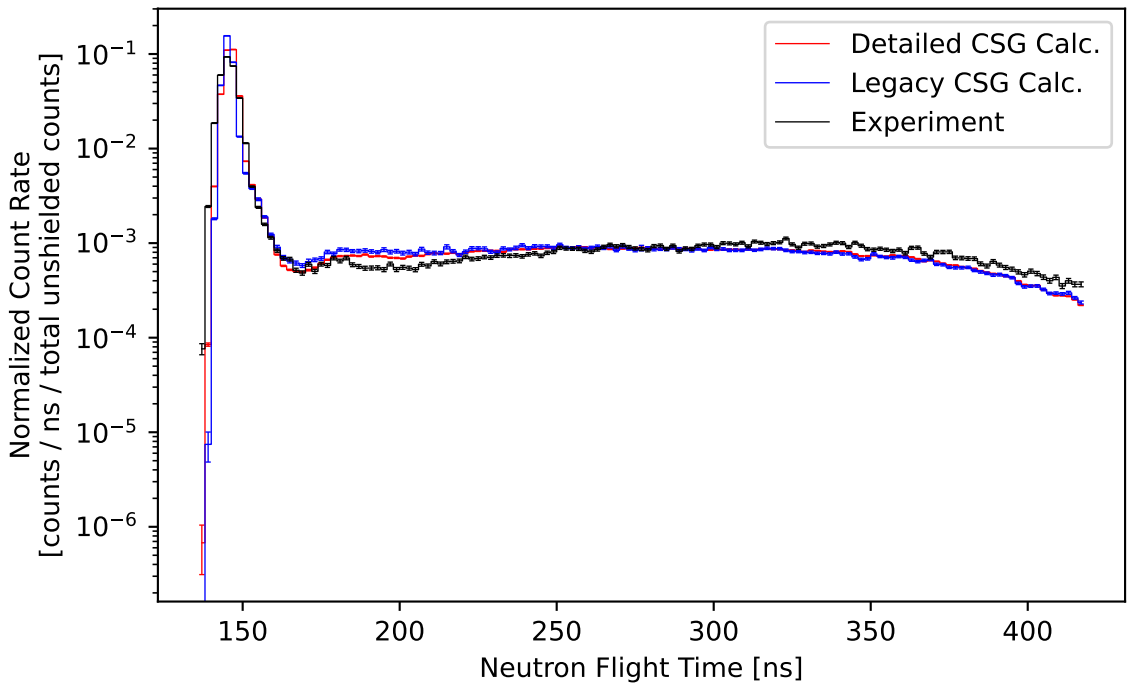

Figure 29: Comparison of the measured and calculated (ENDF/B-VII.1) normalized count rate of neutrons escaping from a 0.9 MFP (14-MeV neutron) thick sphere of iron plotted against flight time.

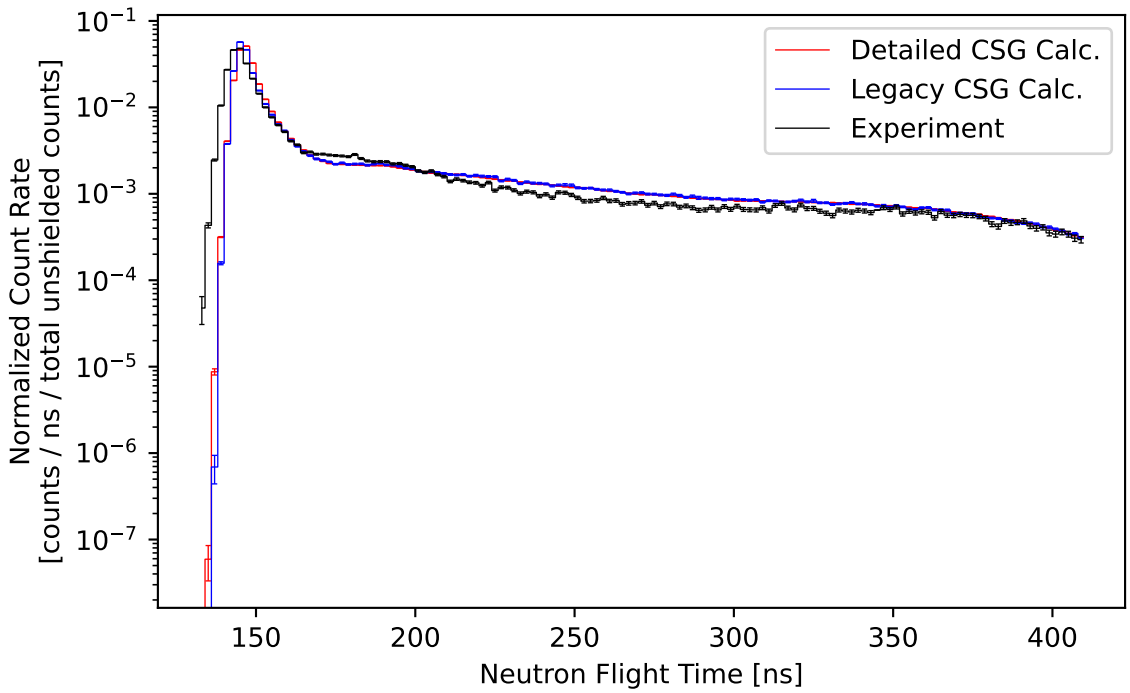

Figure 30: Comparison of the measured and calculated (ENDF/B-VII.1) normalized count rate of neutrons escaping from a 1.6 MFP (14-MeV neutron) thick sphere of lithium-6 plotted against flight time.

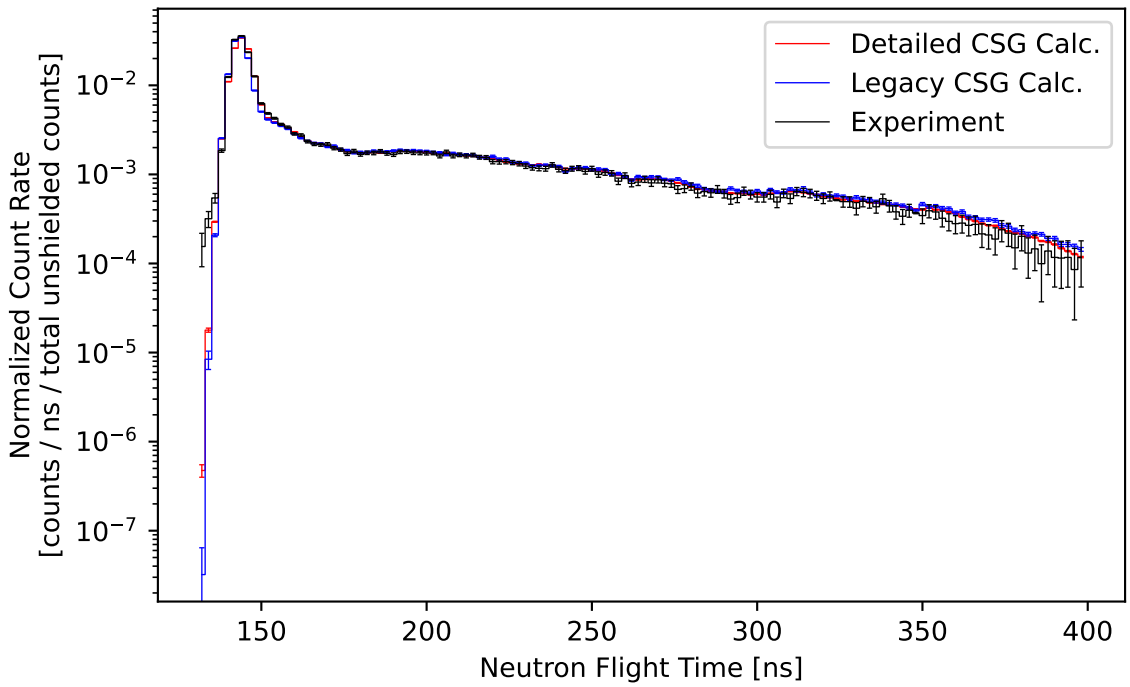

Figure 31: Comparison of the measured and calculated (ENDF/B-VII.1) normalized count rate of neutrons escaping from a 1.9 MFP (14-MeV neutron) thick sphere of water plotted against flight time.

Summary A summary of the experiment characteristics and the averaged calculation to experiment ratio is given for each benchmark in Table 10.

Table 10: Characteristics and Calculation (C) to Experimental (E) Ratios of All Benchmarks using ENDF/B-VII.1

CSG Model	Material	Thickness	Flight Distance	Degrees Off Axis	C/E Val.	C/E Unc. [%]
detailed	beryllium	0.8 MFP (14-MeV neutron)	765.2 cm	30	0.9957	5.18
simple	beryllium	0.8 MFP (14-MeV neutron)	765.2 cm	30	1.0034	6.16
detailed	carbon	2.9 MFP (14-MeV neutron)	766.0 cm	30	0.9610	3.58
simple	carbon	2.9 MFP (14-MeV neutron)	766.0 cm	30	0.9648	4.06
detailed	concrete	2.0 MFP (14-MeV neutron)	975.4 cm	120	0.9753	5.02
simple	concrete	2.0 MFP (14-MeV neutron)	975.4 cm	120	0.9955	5.72
detailed	iron	0.9 MFP (14-MeV neutron)	766.0 cm	30	0.9488	4.24
simple	iron	0.9 MFP (14-MeV neutron)	766.0 cm	30	0.9745	5.73
detailed	lithium-6	1.6 MFP (14-MeV neutron)	765.2 cm	30	1.0957	5.42
simple	lithium-6	1.6 MFP (14-MeV neutron)	765.2 cm	30	1.0991	5.99
detailed	water	1.9 MFP (14-MeV neutron)	754.0 cm	30	1.0519	24.43
simple	water	1.9 MFP (14-MeV neutron)	754.0 cm	30	1.0945	28.08

4.4.4 ENDF/B-VIII.0

Results from neutron pulsed spheres of six different materials are presented. For each material, the neutron time-of-flight spectra calculated from both CSG models and measured experimentally are plotted together and the average ratio of calculation results over experimental results with the associated one-standard-deviation uncertainty is presented. Uncertainty propagation is done with the assumption of normally distributed uncertainties. A summary for all sphere materials is given at the conclusion of this section.

Beryllium The time-of-flight spectra for a 0.8 MFP (14-MeV neutron) thick beryllium pulsed sphere modeled with legacy and detailed CSG is given in Fig. 32. The legacy model has an average ratio of calculation to measured results of $1.0408 \pm 6.51\%$ and the detailed model has an average ratio of $1.0305 \pm 5.32\%$.

Carbon The time-of-flight spectra for a 2.9 MFP (14-MeV neutron) thick carbon pulsed sphere modeled with legacy and detailed CSG is given in Fig. 33. The legacy model has an average ratio of calculation to measured results of $0.9738 \pm 4.12\%$ and the detailed model has an average ratio of $0.9666 \pm 3.60\%$.

Concrete The time-of-flight spectra for a 2.0 MFP (14-MeV neutron) thick concrete pulsed sphere modeled with legacy and detailed CSG is given in Fig. 34. The legacy model has an average ratio of calculation to measured results of $0.9816 \pm 5.70\%$ and the detailed model has an average ratio of $0.9599 \pm 4.95\%$.

Iron The time-of-flight spectra for a 0.9 MFP (14-MeV neutron) thick iron pulsed sphere modeled with legacy and detailed CSG is given in Fig. 35. The legacy model has an average ratio of calculation to measured results of $0.8983 \pm 5.45\%$ and the detailed model has an average ratio of $0.8696 \pm 3.89\%$.

Lithium-6 The time-of-flight spectra for a 1.6 MFP (14-MeV neutron) thick lithium-6 pulsed sphere modeled with legacy and detailed CSG is given in Fig. 36. The legacy model has an average ratio of calculation to measured results of $1.0840 \pm 5.93\%$ and the detailed model has an average ratio of $1.0792 \pm 5.32\%$.

Water The time-of-flight spectra for a 1.9 MFP (14-MeV neutron) thick water pulsed sphere modeled with legacy and detailed CSG is given in Fig. 37. The legacy model has an average ratio of calculation to measured results of $1.0831 \pm 27.86\%$ and the detailed model has an average ratio of $1.0402 \pm 24.25\%$.

Note that the uncertainty in the average ratio of calculated to experimental time-of-flight results is calculated by propagating both the calculation result uncertainty and the experimental measurement uncertainty. From Fig. 37 one sees more measurement uncertainty compared to other materials, this is the cause of the high average ratio uncertainty for this material.

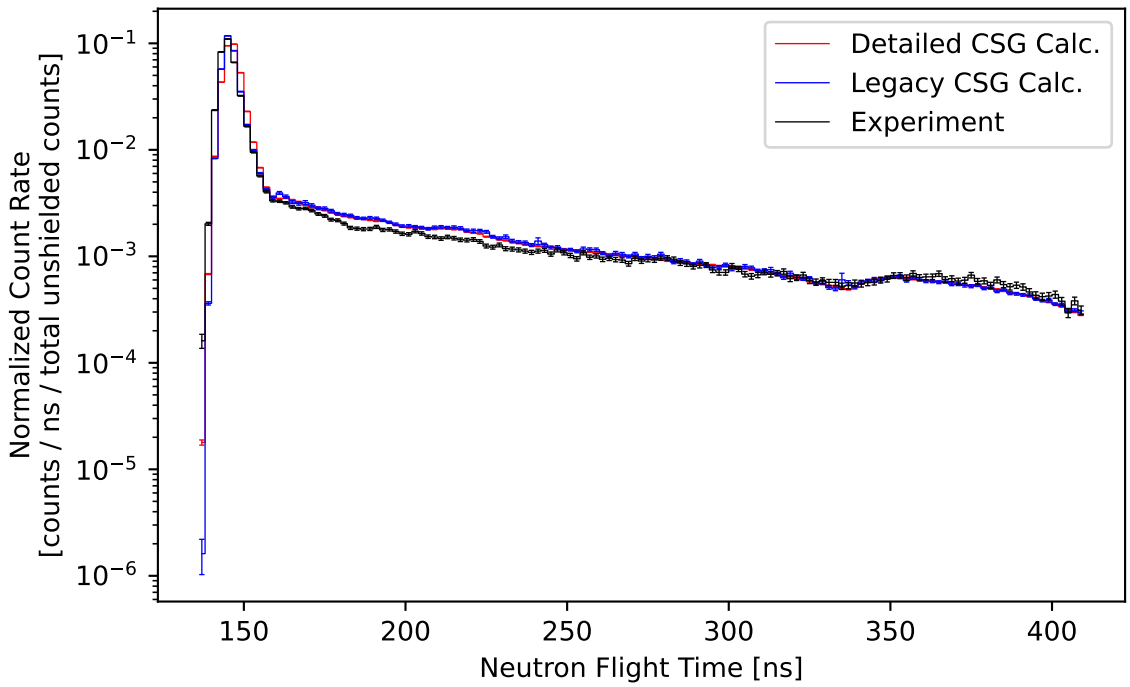

Figure 32: Comparison of the measured and calculated (ENDF/B-VIII.0) normalized count rate of neutrons escaping from a 0.8 MFP (14-MeV neutron) thick sphere of beryllium plotted against flight time.

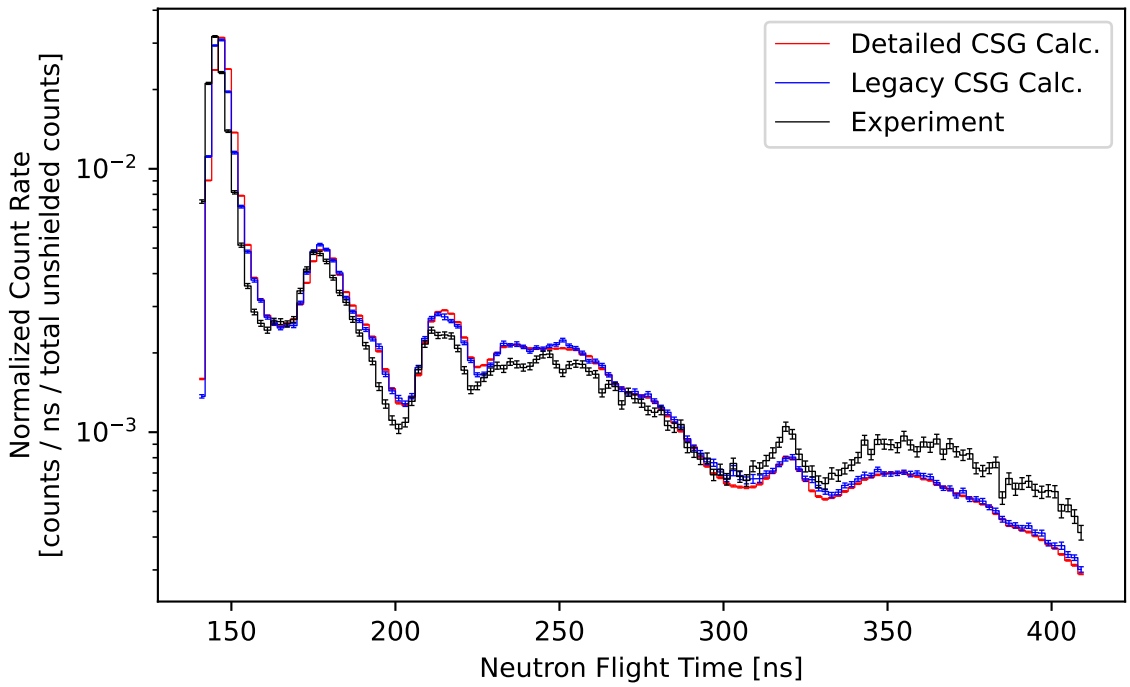

Figure 33: Comparison of the measured and calculated (ENDF/B-VIII.0) normalized count rate of neutrons escaping from a 2.9 MFP (14-MeV neutron) thick sphere of carbon plotted against flight time.

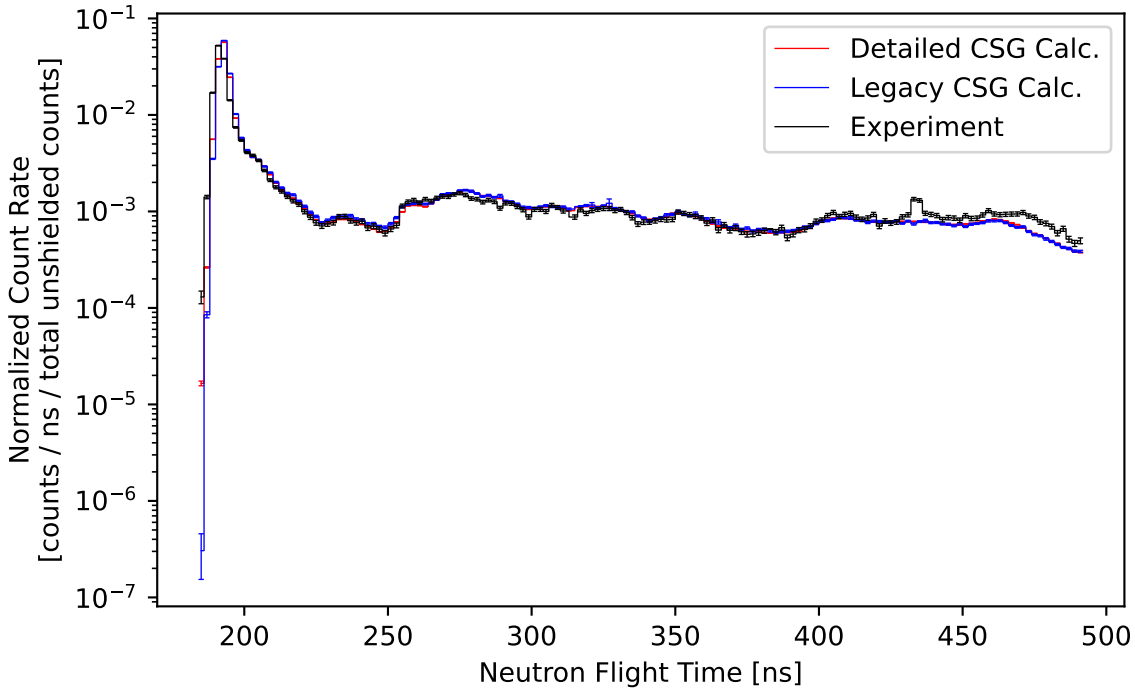

Figure 34: Comparison of the measured and calculated (ENDF/B-VIII.0) normalized count rate of neutrons escaping from a 2.0 MFP (14-MeV neutron) thick sphere of concrete plotted against flight time.

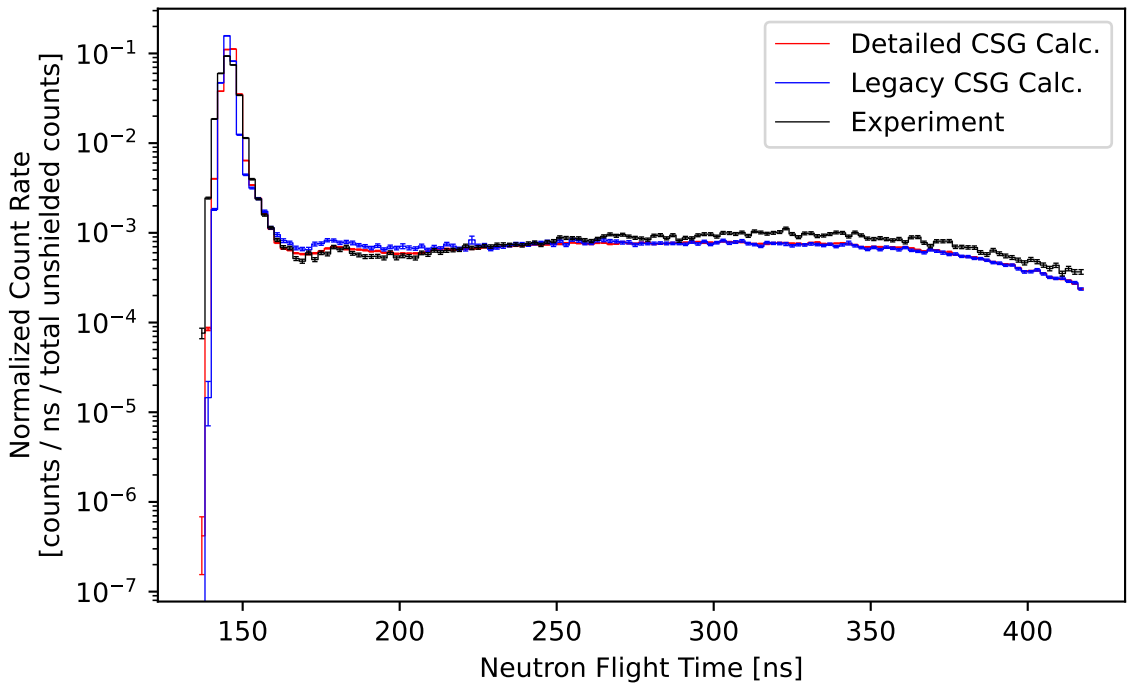

Figure 35: Comparison of the measured and calculated (ENDF/B-VIII.0) normalized count rate of neutrons escaping from a 0.9 MFP (14-MeV neutron) thick sphere of iron plotted against flight time.

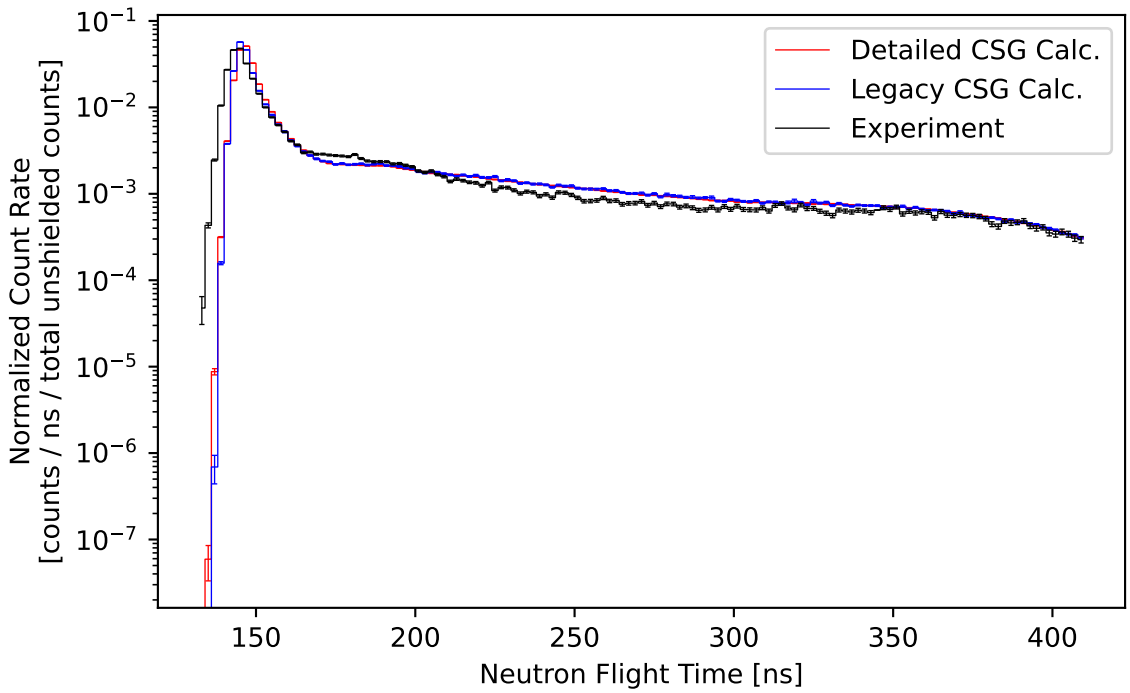

Figure 36: Comparison of the measured and calculated (ENDF/B-VIII.0) normalized count rate of neutrons escaping from a 1.6 MFP (14-MeV neutron) thick sphere of lithium-6 plotted against flight time.

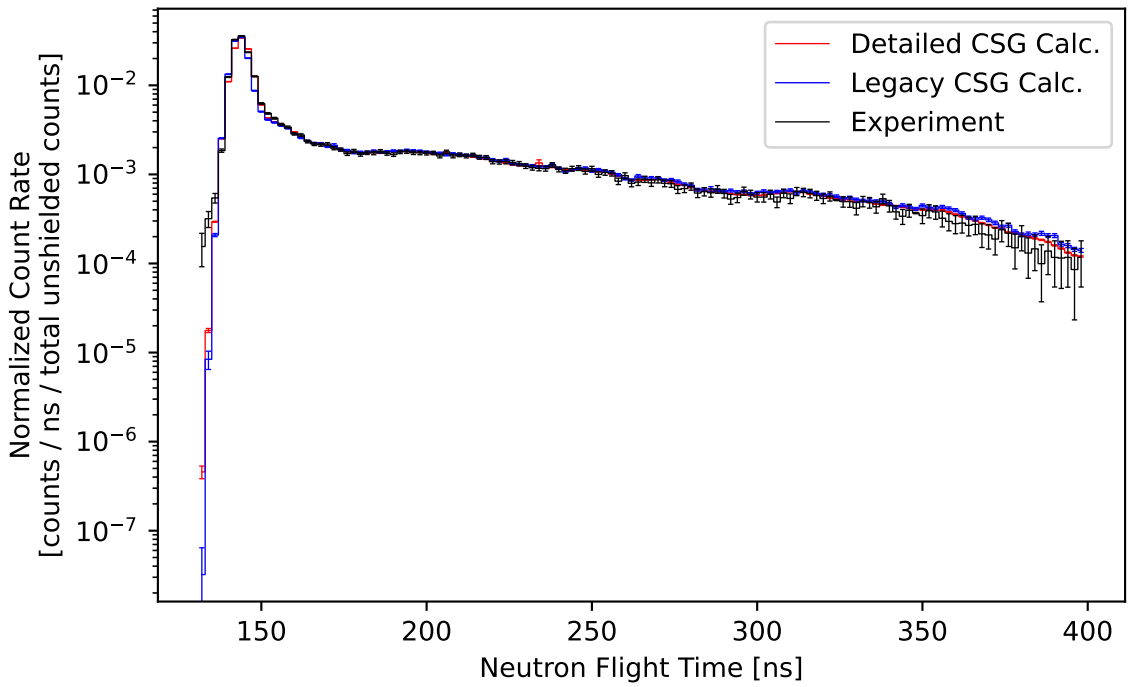

Figure 37: Comparison of the measured and calculated (ENDF/B-VIII.0) normalized count rate of neutrons escaping from a 1.9 MFP (14-MeV neutron) thick sphere of water plotted against flight time.

Summary A summary of the experiment characteristics and the averaged calculation to experiment ratio is given for each benchmark in Table 11.

Table 11: Characteristics and Calculation (C) to Experimental (E) Ratios of All Benchmarks using ENDF/B-VIII.0

CSG Model	Material	Thickness	Flight Distance	Degrees Off Axis	C/E Val.	C/E Unc. [%]
detailed	beryllium	0.8 MFP (14-MeV neutron)	765.2 cm	30	1.0305	5.32
simple	beryllium	0.8 MFP (14-MeV neutron)	765.2 cm	30	1.0408	6.51
detailed	carbon	2.9 MFP (14-MeV neutron)	766.0 cm	30	0.9666	3.60
simple	carbon	2.9 MFP (14-MeV neutron)	766.0 cm	30	0.9738	4.12
detailed	concrete	2.0 MFP (14-MeV neutron)	975.4 cm	120	0.9599	4.95
simple	concrete	2.0 MFP (14-MeV neutron)	975.4 cm	120	0.9816	5.70
detailed	iron	0.9 MFP (14-MeV neutron)	766.0 cm	30	0.8696	3.89
simple	iron	0.9 MFP (14-MeV neutron)	766.0 cm	30	0.8983	5.45
detailed	lithium-6	1.6 MFP (14-MeV neutron)	765.2 cm	30	1.0792	5.32
simple	lithium-6	1.6 MFP (14-MeV neutron)	765.2 cm	30	1.0840	5.93
detailed	water	1.9 MFP (14-MeV neutron)	754.0 cm	30	1.0402	24.25
simple	water	1.9 MFP (14-MeV neutron)	754.0 cm	30	1.0831	27.86

4.5 Lockwood

Each benchmark problem compares the experiment data to both the calculated results using the condensed history algorithm and the calculated results using the single event electron transport algorithm. Both calculation algorithms use the electron-photon-relaxation data library EPRDATA14 [41]. This test suite sequentially executes 16 inputs per node, where each node uses 114 MPI ranks, with a total Slurm allocation of no more than 70 minutes per node. An example `VnV.py` execution line is `./VnV.py execute_slurm --nmpi 114 --time 70 --stride 16 --wait --calcdir_name lockwood`.

4.5.1 Aluminum

The Aluminum cases break down into 2 angles and 3 energies. The condensed-history results are given in Table 12 and the single-event results are given in Table 13. For each energy and direction, plots of results versus measured values are given in Figures 38–43.

For the 0.3 MeV case at 0 degrees, the condensed-history results have an average calculated-over-measured value of 0.996±0.066% (overall average standard deviation) and the single-event results have an average calculated-over-measured value of $0.994 \pm 0.066\%$ (overall average standard deviation).

For the 0.3 MeV case at 60 degrees, the condensed-history results have an average calculated-over-measured value of $1.020 \pm 0.053\%$ (overall average standard deviation) and the single-event results have an average calculated-over-measured value of $0.972 \pm 0.050\%$ (overall average standard deviation).

For the 0.5 MeV case at 0 degrees, the condensed-history results have an average calculated-over-measured value of 0.992±0.080% (overall average standard deviation) and the single-event results have an average calculated-over-measured value of $0.990 \pm 0.079\%$ (overall average standard deviation).

For the 0.5 MeV case at 60 degrees, the condensed-history results have an average calculated-over-measured value of $1.036 \pm 0.059\%$ (overall average standard deviation) and the single-event results have an average calculated-over-measured value of $1.012 \pm 0.055\%$ (overall average standard deviation).

For the 1.0 MeV case at 0 degrees, the condensed-history results have an average calculated-over-measured value of 1.013±0.101% (overall average standard deviation) and the single-event results have an average calculated-over-measured value of $1.011 \pm 0.086\%$ (overall average standard deviation).

For the 1.0 MeV case at 60 degrees, the condensed-history results have an average calculated-over-measured value of $1.063 \pm 0.076\%$ (overall average standard deviation) and the single-event results have an average calculated-over-measured value of $1.062 \pm 0.058\%$ (overall average standard deviation).

4.5.2 Beryllium

The Beryllium cases break down into 1 angle and 5 energies. The condensed-history results are given in Table 14 and the single-event results are given in Table 15. For each energy and direction, plots of results versus measured values are given in Figures 44–48.

For the 0.05 MeV case at 0 degrees, the condensed-history results have an average calculated-over-measured value of $0.649 \pm 0.095\%$ (overall average standard deviation) and the single-event results have an average calculated-over-measured value of $0.614 \pm 0.110\%$ (overall average standard deviation).

For the 0.1 MeV case at 0 degrees, the condensed-history results have an average calculated-over-measured value of $0.919 \pm 0.041\%$ (overall average standard deviation) and the single-event results have an average calculated-over-measured value of $0.901 \pm 0.048\%$ (overall average standard deviation).

For the 0.3 MeV case at 0 degrees, the condensed-history results have an average calculated-over-measured value of $0.907 \pm 0.095\%$ (overall average standard deviation) and the single-event results have an average calculated-over-measured value of $0.862 \pm 0.117\%$ (overall average standard deviation).

For the 0.5 MeV case at 0 degrees, the condensed-history results have an average calculated-over-measured value of $0.937 \pm 0.098\%$ (overall average standard deviation) and the single-event results have an average calculated-over-measured value of $0.876 \pm 0.115\%$ (overall average standard deviation).

For the 1.0 MeV case at 0 degrees, the condensed-history results have an average calculated-over-measured value of $0.994 \pm 0.105\%$ (overall average standard deviation) and the single-event results have an average calculated-over-measured value of $0.940 \pm 0.103\%$ (overall average standard deviation).

4.5.3 Carbon

The Carbon cases break down into 1 angle and 1 energy. The condensed-history results are given in Table 16 and the single-event results are given in Table 17. For each energy and direction, plots of results versus measured values are given in Figure 49.

For the 1.0 MeV case at 0 degrees, the condensed-history results have an average calculated-over-measured value of $1.010 \pm 0.074\%$ (overall average standard deviation) and the single-event results have an average calculated-over-measured value of $0.978 \pm 0.080\%$ (overall average standard deviation).

4.5.4 Copper

The Copper cases break down into 1 angle and 2 energies. The condensed-history results are given in Table 18 and the single-event results are given in Table 19. For each energy and direction, plots of results versus measured values are given in Figures 50–51.

For the 0.3 MeV case at 0 degrees, the condensed-history results have an average calculated-over-measured value of $1.020 \pm 0.053\%$ (overall average standard deviation) and the single-event results have an average calculated-over-measured value of $0.993 \pm 0.055\%$ (overall average standard deviation).

For the 0.5 MeV case at 0 degrees, the condensed-history results have an average calculated-over-measured value of $1.028 \pm 0.057\%$ (overall average standard deviation) and the single-event results have an average calculated-over-measured value of $1.030 \pm 0.056\%$ (overall average standard deviation).

4.5.5 Iron

The Iron cases break down into 1 angle and 3 energies. The condensed-history results are given in Table 20 and the single-event results are given in Table 21. For each energy and direction, plots of results versus measured values are given in Figures 52–54.

For the 0.3 MeV case at 0 degrees, the condensed-history results have an average calculated-over-measured value of 0.926±0.153% (overall average standard deviation) and the single-event results have an average calculated-over-measured value of $0.888 \pm 0.159\%$ (overall average standard deviation).

For the 0.5 MeV case at 0 degrees, the condensed-history results have an average calculated-over-measured value of 1.079±0.052% (overall average standard deviation) and the single-event results have an average calculated-over-measured value of $1.075 \pm 0.052\%$ (overall average standard deviation).

For the 1.0 MeV case at 0 degrees, the condensed-history results have an average calculated-over-measured value of 1.069±0.064% (overall average standard deviation) and the single-event results have an average calculated-over-measured value of $1.077 \pm 0.060\%$ (overall average standard deviation).

4.5.6 Molybdenum

The Molybdenum cases break down into 2 angles and 4 energies. The condensed-history results are given in Table 22 and the single-event results are given in Table 23. For each energy and direction, plots of results versus measured values are given in Figures 55–61.

For the 0.1 MeV case at 0 degrees, the condensed-history results have an average calculated-over-measured value of 1.065±0.052% (overall average standard deviation) and the single-event results have an average calculated-over-measured value of $1.024 \pm 0.056\%$ (overall average standard deviation).

For the 0.3 MeV case at 0 degrees, the condensed-history results have an average calculated-over-measured value of 1.097±0.068% (overall average standard deviation) and the single-event results have an average calculated-over-measured value of $1.073 \pm 0.066\%$ (overall average standard deviation).

For the 0.3 MeV case at 60 degrees, the condensed-history results have an average calculated-over-measured value of $1.086 \pm 0.074\%$ (overall average standard deviation) and the single-event results have an average calculated-over-measured value of $1.026 \pm 0.074\%$ (overall average standard deviation).

For the 0.5 MeV case at 0 degrees, the condensed-history results have an average calculated-over-measured value of 1.053±0.078% (overall average standard deviation) and the single-event results have an average calculated-over-measured value of $1.047 \pm 0.072\%$ (overall average standard deviation).

For the 0.5 MeV case at 60 degrees, the condensed-history results have an average calculated-over-measured value of $1.081 \pm 0.090\%$ (overall average standard deviation) and the single-event results have an average calculated-over-measured value of $1.049 \pm 0.087\%$ (overall average standard deviation).

For the 1.0 MeV case at 0 degrees, the condensed-history results have an average calculated-over-measured value of 1.022±0.095% (overall average standard deviation) and the single-event results have an average calculated-over-measured value of $1.011 \pm 0.073\%$ (overall average standard deviation).

For the 1.0 MeV case at 60 degrees, the condensed-history results have an average calculated-over-measured value of $1.099 \pm 0.090\%$ (overall average standard deviation) and the single-event results have an average calculated-over-measured value of $1.072 \pm 0.069\%$ (overall average standard deviation).

4.5.7 Tantalum

The Tantalum cases break down into 3 angles and 3 energies. The condensed-history results are given in Table 24 and the single-event results are given in Table 25. For each energy and direction, plots of results versus measured values are given in Figures 62–67.

For the 0.3 MeV case at 0 degrees, the condensed-history results have an average calculated-over-measured value of $0.930 \pm 0.116\%$ (overall average standard deviation) and the single-event results have an average calculated-over-measured value of $0.933 \pm 0.112\%$ (overall average standard deviation).

For the 0.5 MeV case at 0 degrees, the condensed-history results have an average calculated-over-measured value of $0.865 \pm 0.276\%$ (overall average standard deviation) and the single-event results have an average calculated-over-measured value of $0.933 \pm 0.239\%$ (overall average standard deviation).

For the 0.5 MeV case at 30 degrees, the condensed-history results have an average calculated-over-measured value of $1.032 \pm 0.063\%$ (overall average standard deviation) and the single-event results have an average calculated-over-measured value of $1.012 \pm 0.061\%$ (overall average standard deviation).

For the 0.5 MeV case at 60 degrees, the condensed-history results have an average calculated-over-measured value of $1.070 \pm 0.077\%$ (overall average standard deviation) and the single-event results have an average calculated-over-measured value of $1.035 \pm 0.076\%$ (overall average standard deviation).

For the 1.0 MeV case at 0 degrees, the condensed-history results have an average calculated-over-measured value of $1.050 \pm 0.066\%$ (overall average standard deviation) and the single-event results have an average calculated-over-measured value of $1.022 \pm 0.058\%$ (overall average standard deviation).

For the 1.0 MeV case at 60 degrees, the condensed-history results have an average calculated-over-measured value of $1.059 \pm 0.073\%$ (overall average standard deviation) and the single-event results have an average calculated-over-measured value of $1.031 \pm 0.067\%$ (overall average standard deviation).

4.5.8 Uranium

The Uranium cases break down into 2 angles and 3 energies. The condensed-history results are given in Table 26 and the single-event results are given in Table 27. For each energy and direction, plots of results versus measured values are given in Figures 68–71.

For the 0.3 MeV case at 0 degrees, the condensed-history results have an average calculated-over-measured value of $1.034 \pm 0.062\%$ (overall average standard deviation) and the single-event results have an average calculated-over-measured value of $1.005 \pm 0.062\%$ (overall average standard deviation).

For the 0.5 MeV case at 0 degrees, the condensed-history results have an average calculated-over-measured value of $1.035 \pm 0.068\%$ (overall average standard deviation) and the single-event results have an average calculated-over-measured value of $1.020 \pm 0.065\%$ (overall average standard deviation).

For the 1.0 MeV case at 0 degrees, the condensed-history results have an average calculated-over-measured value of $1.019 \pm 0.077\%$ (overall average standard deviation) and the single-event results have an average calculated-over-measured value of $1.004 \pm 0.067\%$ (overall average standard deviation).

For the 1.0 MeV case at 60 degrees, the condensed-history results have an average calculated-over-measured value of $1.056 \pm 0.079\%$ (overall average standard deviation) and the single-event results have an average calculated-over-measured value of $1.015 \pm 0.070\%$ (overall average standard deviation).

Table 12: Aluminum Condensed History Results

Angle	Energy	FMR	Exp. [MeV]	Calc. [MeV]	C/E
0°	0.3 MeV	0.022400	0.01424±1.4%	0.01432±0.1%	1.01
0°	0.3 MeV	0.083100	0.01975±1.4%	0.01992±0.1%	1.01
0°	0.3 MeV	0.226000	0.02485±1.4%	0.02606±0.1%	1.05
0°	0.3 MeV	0.422000	0.01904±1.4%	0.01908±0.2%	1.00
0°	0.3 MeV	0.501000	0.01555±1.4%	0.01421±0.2%	0.91
0°	0.5 MeV	0.010800	0.01066±1.4%	0.01068±0.2%	1.00
0°	0.5 MeV	0.109000	0.01717±1.4%	0.01788±0.1%	1.04
0°	0.5 MeV	0.242000	0.02060±1.4%	0.02108±0.1%	1.02
0°	0.5 MeV	0.424000	0.01550±1.4%	0.01529±0.2%	0.99
0°	0.5 MeV	0.538000	0.01060±1.4%	0.00964±0.2%	0.91
0°	1.0 MeV	0.004500	0.00823±1.4%	0.00848±0.2%	1.03
0°	1.0 MeV	0.115000	0.01379±1.4%	0.01455±0.2%	1.06
0°	1.0 MeV	0.253000	0.01656±1.4%	0.01727±0.2%	1.04
0°	1.0 MeV	0.431000	0.01273±1.4%	0.01264±0.2%	0.99
0°	1.0 MeV	0.552000	0.00823±1.4%	0.00777±0.3%	0.94
60°	0.3 MeV	0.022000	0.03257±1.4%	0.03426±0.1%	1.05
60°	0.3 MeV	0.033000	0.03313±1.4%	0.03496±0.1%	1.06
60°	0.3 MeV	0.066000	0.03055±1.4%	0.03023±0.1%	0.99
60°	0.3 MeV	0.121000	0.02495±1.4%	0.02486±0.1%	1.00
60°	0.3 MeV	0.160000	0.02237±1.4%	0.02249±0.1%	1.01
60°	0.5 MeV	0.011000	0.02666±1.4%	0.02773±0.1%	1.04
60°	0.5 MeV	0.018000	0.02884±1.4%	0.03012±0.1%	1.04
60°	0.5 MeV	0.059000	0.02540±1.4%	0.02592±0.1%	1.02
60°	0.5 MeV	0.077000	0.02293±1.4%	0.02393±0.1%	1.04
60°	0.5 MeV	0.109000	0.02055±1.4%	0.02122±0.1%	1.03
60°	1.0 MeV	0.005000	0.02101±1.4%	0.02115±0.2%	1.01
60°	1.0 MeV	0.009000	0.02308±1.4%	0.02556±0.2%	1.11
60°	1.0 MeV	0.024000	0.02474±1.4%	0.02653±0.2%	1.07
60°	1.0 MeV	0.084000	0.01899±1.4%	0.02033±0.2%	1.07
60°	1.0 MeV	0.115000	0.01697±1.4%	0.01794±0.2%	1.06

Table 13: Aluminum Single Event Results

Angle	Energy	FMR	Exp. [MeV]	Calc. [MeV]	C/E
0°	0.3 MeV	0.022400	0.01424±1.4%	0.01510±0.1%	1.06
0°	0.3 MeV	0.083100	0.01975±1.4%	0.02130±0.1%	1.08
0°	0.3 MeV	0.226000	0.02485±1.4%	0.02598±0.1%	1.05
0°	0.3 MeV	0.422000	0.01904±1.4%	0.01790±0.2%	0.94
0°	0.3 MeV	0.501000	0.01555±1.4%	0.01311±0.2%	0.84
0°	0.5 MeV	0.010800	0.01066±1.4%	0.01137±0.1%	1.07
0°	0.5 MeV	0.109000	0.01717±1.4%	0.01935±0.1%	1.13
0°	0.5 MeV	0.242000	0.02060±1.4%	0.02106±0.1%	1.02
0°	0.5 MeV	0.424000	0.01550±1.4%	0.01434±0.2%	0.92
0°	0.5 MeV	0.538000	0.01060±1.4%	0.00861±0.3%	0.81
0°	1.0 MeV	0.004500	0.00823±1.4%	0.00889±0.1%	1.08
0°	1.0 MeV	0.115000	0.01379±1.4%	0.01593±0.1%	1.16
0°	1.0 MeV	0.253000	0.01656±1.4%	0.01755±0.1%	1.06
0°	1.0 MeV	0.431000	0.01273±1.4%	0.01196±0.2%	0.94
0°	1.0 MeV	0.552000	0.00823±1.4%	0.00677±0.3%	0.82
60°	0.3 MeV	0.022000	0.03257±1.4%	0.03330±0.1%	1.02
60°	0.3 MeV	0.033000	0.03313±1.4%	0.03307±0.1%	1.00
60°	0.3 MeV	0.066000	0.03055±1.4%	0.02843±0.1%	0.93
60°	0.3 MeV	0.121000	0.02495±1.4%	0.02362±0.1%	0.95
60°	0.3 MeV	0.160000	0.02237±1.4%	0.02151±0.1%	0.96
60°	0.5 MeV	0.011000	0.02666±1.4%	0.02856±0.1%	1.07
60°	0.5 MeV	0.018000	0.02884±1.4%	0.02989±0.1%	1.04
60°	0.5 MeV	0.059000	0.02540±1.4%	0.02467±0.1%	0.97
60°	0.5 MeV	0.077000	0.02293±1.4%	0.02274±0.1%	0.99
60°	0.5 MeV	0.109000	0.02055±1.4%	0.02030±0.1%	0.99
60°	1.0 MeV	0.005000	0.02101±1.4%	0.02302±0.1%	1.10
60°	1.0 MeV	0.009000	0.02308±1.4%	0.02660±0.1%	1.15
60°	1.0 MeV	0.024000	0.02474±1.4%	0.02537±0.1%	1.03
60°	1.0 MeV	0.084000	0.01899±1.4%	0.01939±0.1%	1.02
60°	1.0 MeV	0.115000	0.01697±1.4%	0.01720±0.2%	1.01

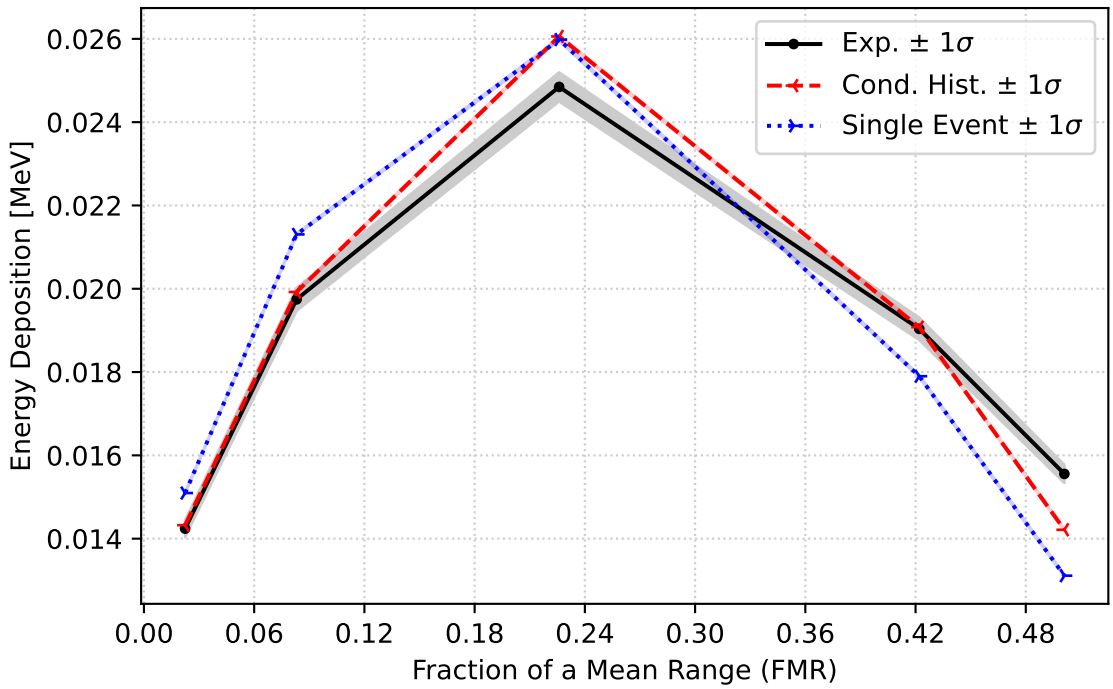

Figure 38: Aluminum 0-degree 0.3 MeV Results

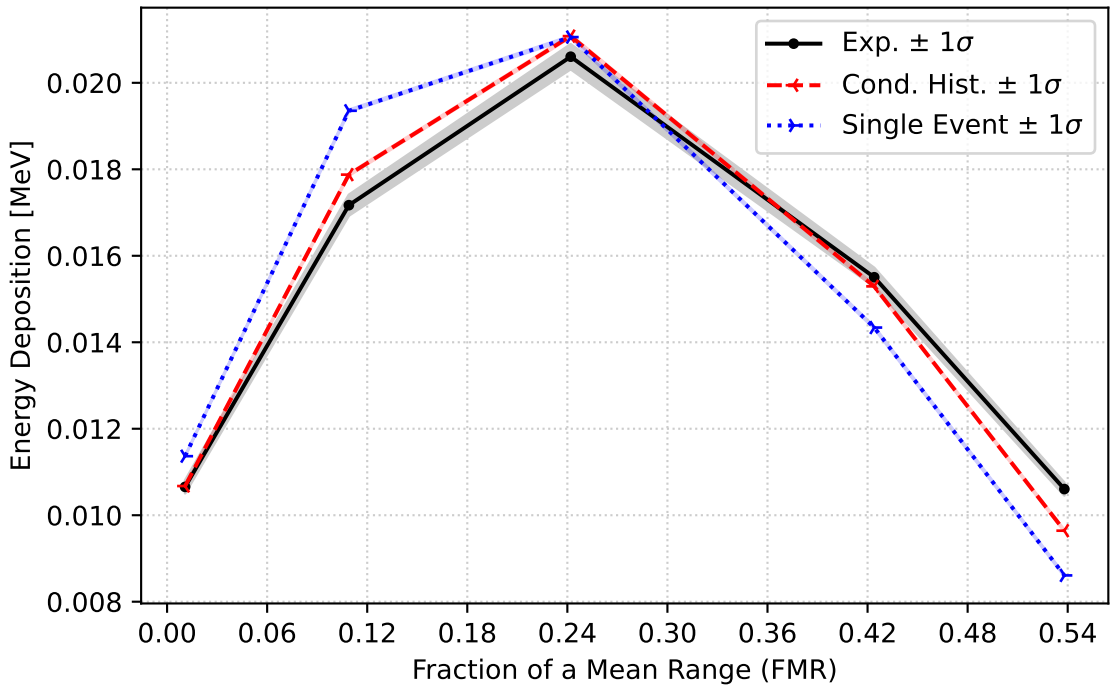

Figure 39: Aluminum 0-degree 0.5 MeV Results

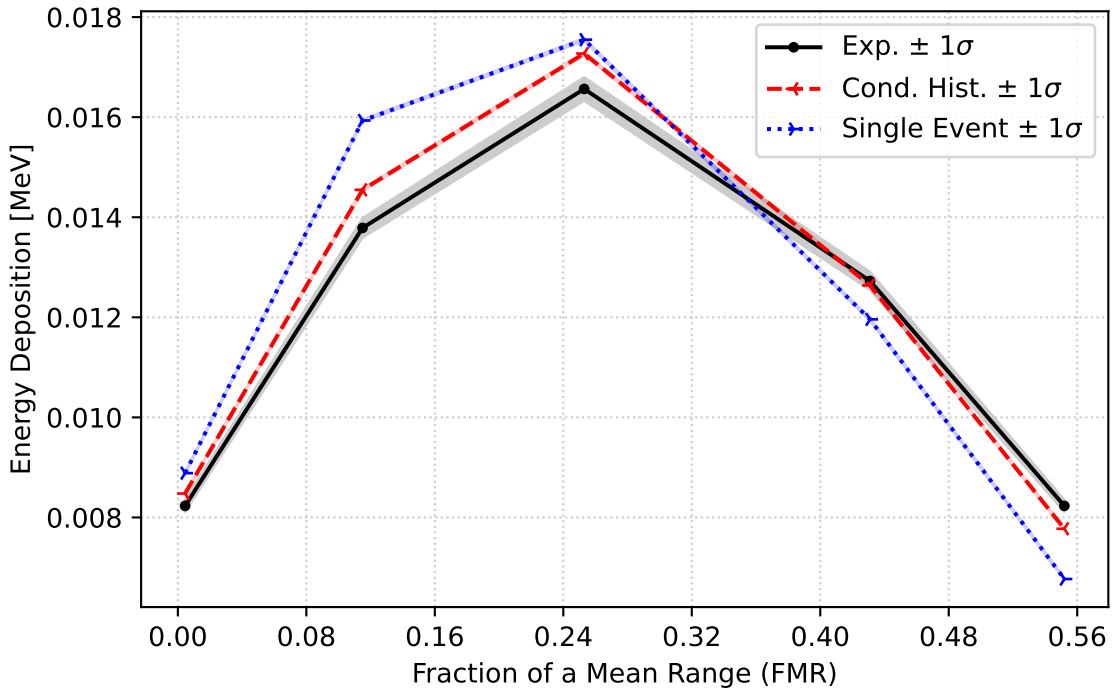

Figure 40: Aluminum 0-degree 1.0 MeV Results

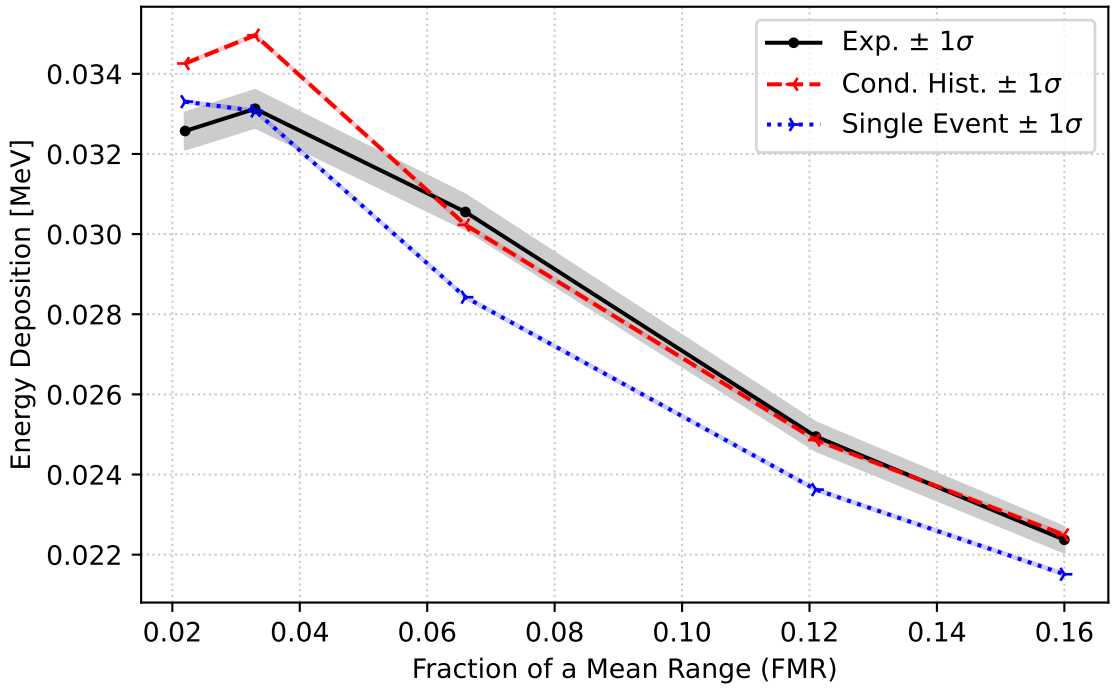

Figure 41: Aluminum 60-degree 0.3 MeV Results

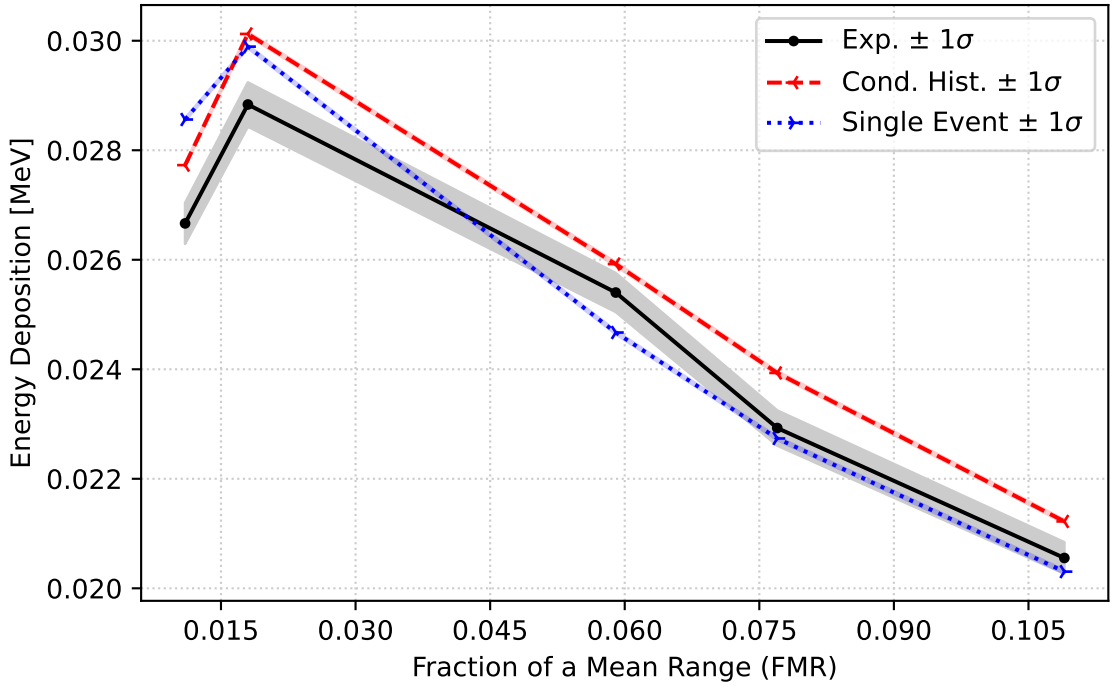

Figure 42: Aluminum 60-degree 0.5 MeV Results

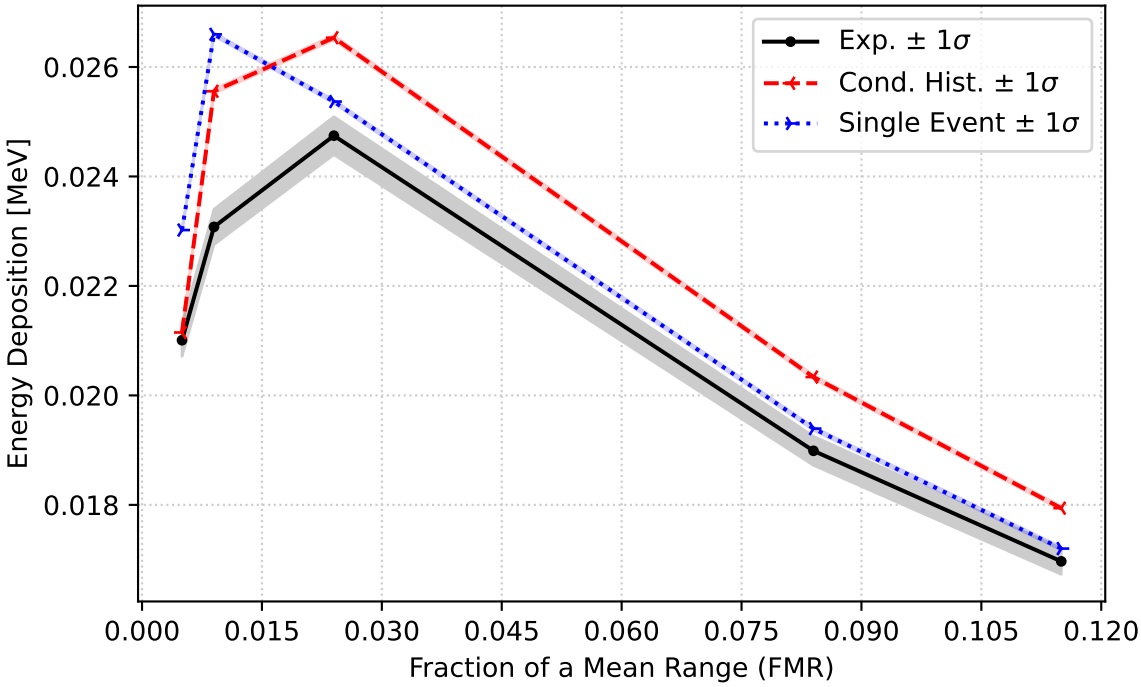

Figure 43: Aluminum 60-degree 1.0 MeV Results

Table 14: Beryllium Condensed History Results

Angle	Energy	FMR	Exp. [MeV]	Calc. [MeV]	C/E
0°	0.05 MeV	0.396000	0.04882±1.6%	0.04834±0.0%	0.99
0°	0.05 MeV	1.104000	0.01456±1.6%	0.00447±0.2%	0.31
0°	0.1 MeV	0.127000	0.02236±1.6%	0.02289±0.1%	1.02
0°	0.1 MeV	0.353000	0.03400±1.6%	0.03620±0.1%	1.06
0°	0.1 MeV	0.499000	0.03833±1.6%	0.03960±0.1%	1.03
0°	0.1 MeV	0.726000	0.02796±1.6%	0.02401±0.1%	0.86
0°	0.1 MeV	0.819000	0.02197±1.6%	0.01355±0.1%	0.62
0°	0.3 MeV	0.022000	0.00979±1.6%	0.00973±0.1%	0.99
0°	0.3 MeV	0.251000	0.01534±1.6%	0.01555±0.1%	1.01
0°	0.3 MeV	0.459000	0.01997±1.6%	0.02077±0.1%	1.04
0°	0.3 MeV	0.773000	0.01296±1.6%	0.01104±0.2%	0.85
0°	0.3 MeV	0.901000	0.00531±1.6%	0.00338±0.4%	0.64
0°	0.5 MeV	0.011000	0.00813±1.6%	0.00791±0.2%	0.97
0°	0.5 MeV	0.219000	0.01193±1.6%	0.01178±0.1%	0.99
0°	0.5 MeV	0.525000	0.01578±1.6%	0.01638±0.1%	1.04
0°	0.5 MeV	0.736000	0.01101±1.6%	0.01048±0.2%	0.95
0°	0.5 MeV	0.872000	0.00521±1.6%	0.00385±0.4%	0.74
0°	1.0 MeV	0.004000	0.00672±1.6%	0.00675±0.3%	1.00
0°	1.0 MeV	0.257000	0.01023±1.6%	0.01040±0.2%	1.02
0°	1.0 MeV	0.492000	0.01271±1.6%	0.01316±0.2%	1.04
0°	1.0 MeV	0.648000	0.01096±1.6%	0.01116±0.2%	1.02
0°	1.0 MeV	0.822000	0.00570±1.6%	0.00511±0.3%	0.90

Table 15: Beryllium Single Event Results

Angle	Energy	FMR	Exp. [MeV]	Calc. [MeV]	C/E
0°	0.05 MeV	0.396000	0.04882±1.6%	0.04840±0.0%	0.99
0°	0.05 MeV	1.104000	0.01456±1.6%	0.00345±0.2%	0.24
0°	0.1 MeV	0.127000	0.02236±1.6%	0.02576±0.1%	1.15
0°	0.1 MeV	0.353000	0.03400±1.6%	0.03892±0.1%	1.14
0°	0.1 MeV	0.499000	0.03833±1.6%	0.03879±0.1%	1.01
0°	0.1 MeV	0.726000	0.02796±1.6%	0.02007±0.1%	0.72
0°	0.1 MeV	0.819000	0.02197±1.6%	0.01046±0.2%	0.48
0°	0.3 MeV	0.022000	0.00979±1.6%	0.01030±0.1%	1.05
0°	0.3 MeV	0.251000	0.01534±1.6%	0.01773±0.1%	1.16
0°	0.3 MeV	0.459000	0.01997±1.6%	0.02103±0.1%	1.05
0°	0.3 MeV	0.773000	0.01296±1.6%	0.00877±0.2%	0.68
0°	0.3 MeV	0.901000	0.00531±1.6%	0.00199±0.5%	0.37
0°	0.5 MeV	0.011000	0.00813±1.6%	0.00842±0.1%	1.04
0°	0.5 MeV	0.219000	0.01193±1.6%	0.01383±0.1%	1.16
0°	0.5 MeV	0.525000	0.01578±1.6%	0.01581±0.1%	1.00
0°	0.5 MeV	0.736000	0.01101±1.6%	0.00835±0.2%	0.76
0°	0.5 MeV	0.872000	0.00521±1.6%	0.00222±0.5%	0.43
0°	1.0 MeV	0.004000	0.00672±1.6%	0.00713±0.1%	1.06
0°	1.0 MeV	0.257000	0.01023±1.6%	0.01243±0.1%	1.21
0°	1.0 MeV	0.492000	0.01271±1.6%	0.01313±0.2%	1.03
0°	1.0 MeV	0.648000	0.01096±1.6%	0.00944±0.2%	0.86
0°	1.0 MeV	0.822000	0.00570±1.6%	0.00302±0.4%	0.53

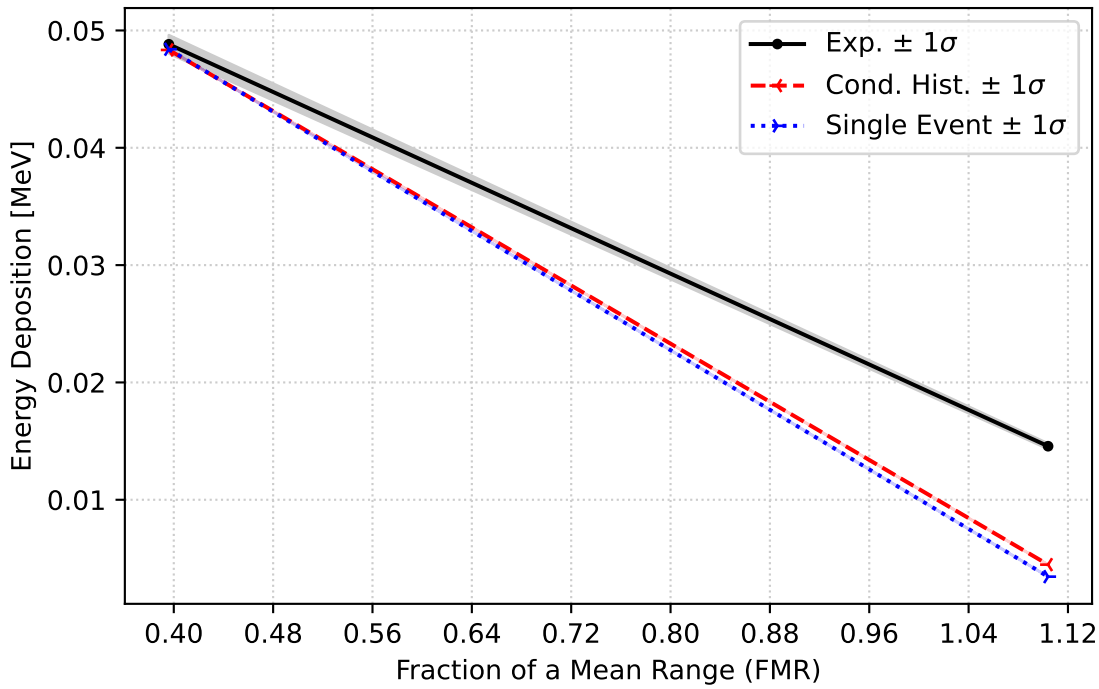

Figure 44: Beryllium 0-degree 0.05 MeV Results

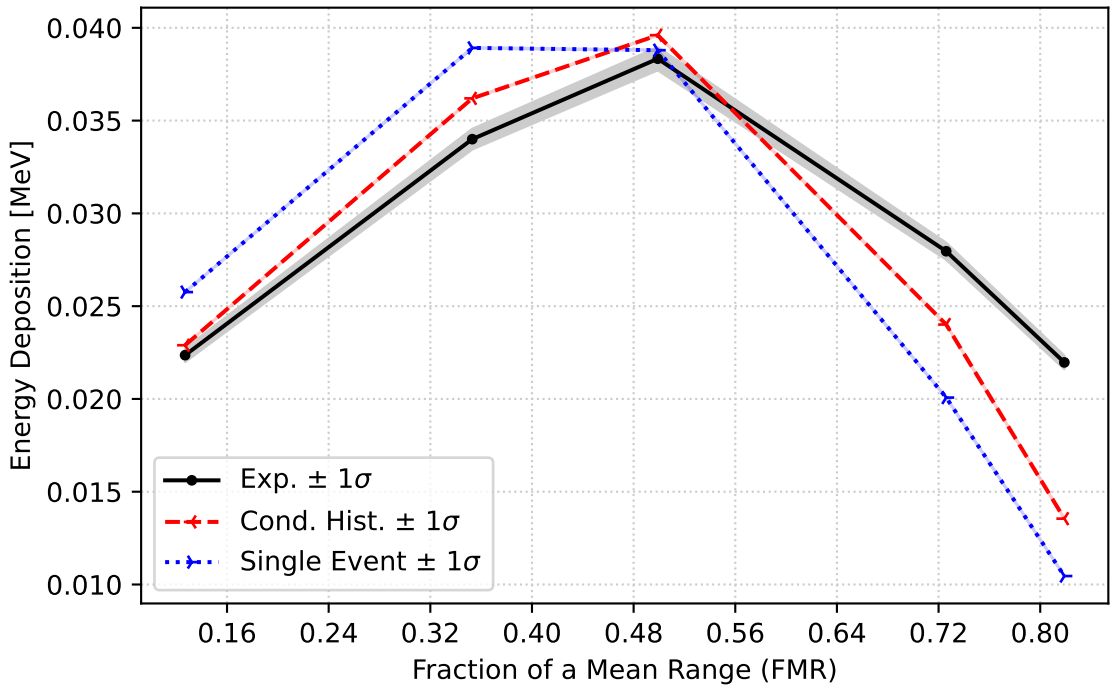

Figure 45: Beryllium 0-degree 0.1 MeV Results

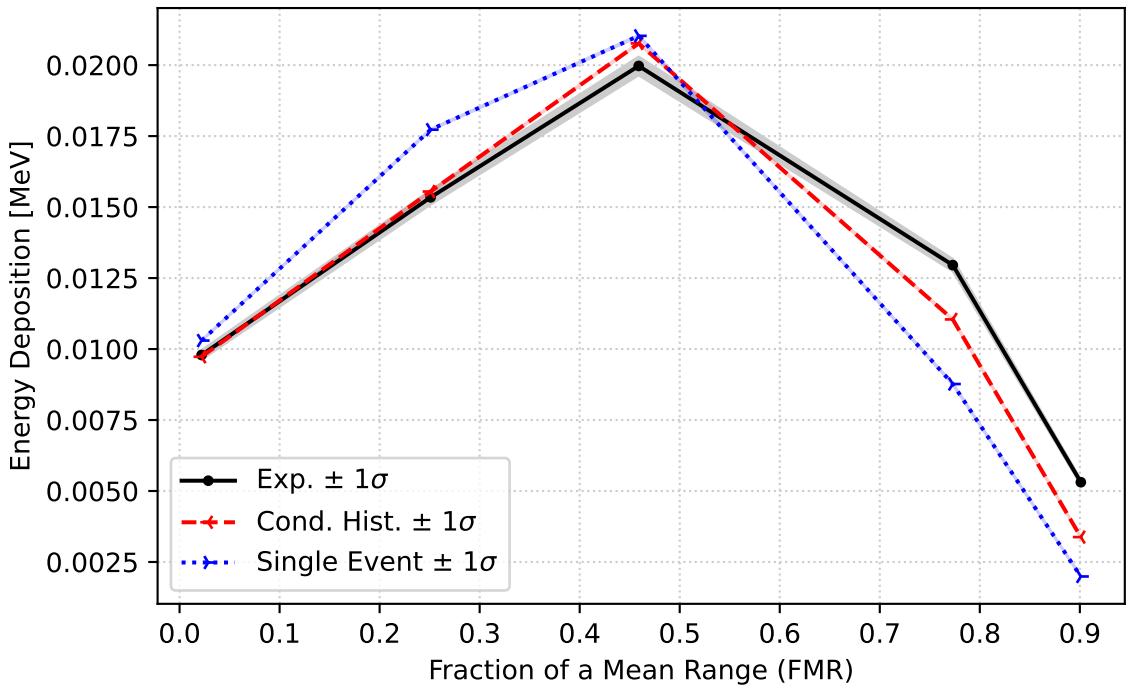

Figure 46: Beryllium 0-degree 0.3 MeV Results

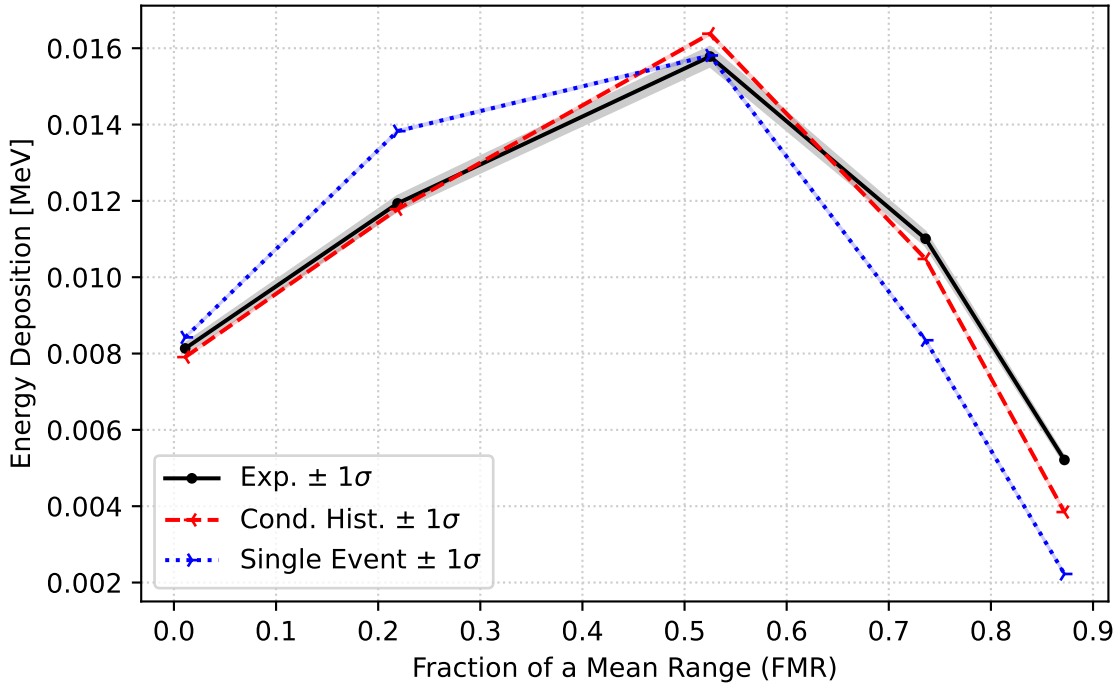

Figure 47: Beryllium 0-degree 0.5 MeV Results

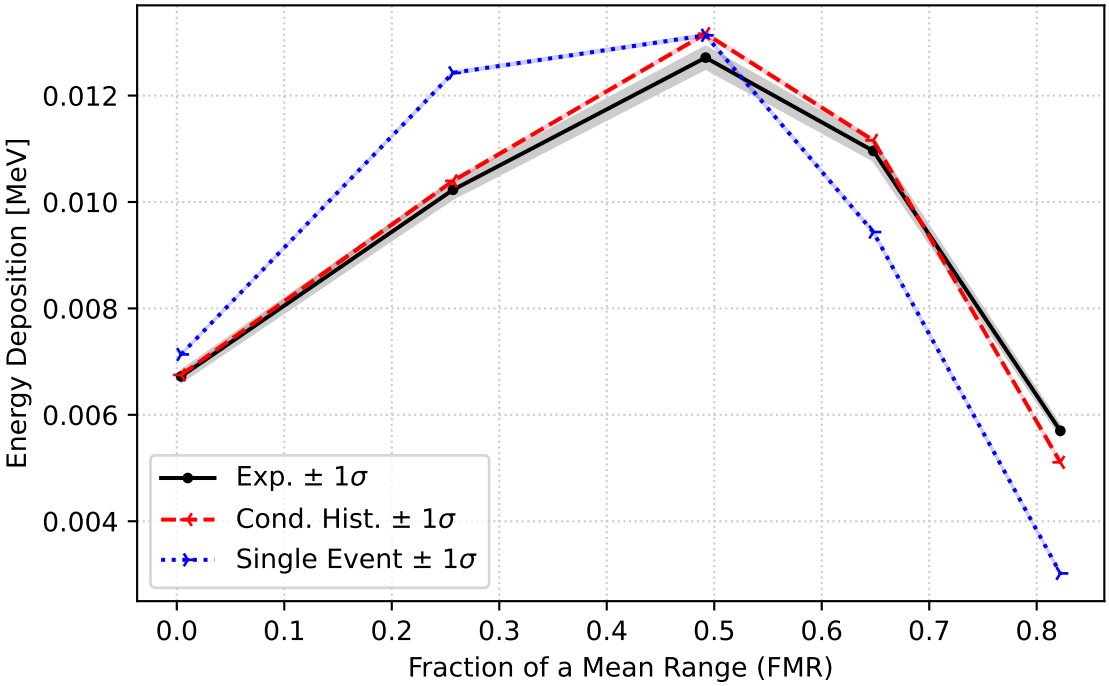

Figure 48: Beryllium 0-degree 1.0 MeV Results

Table 16: Carbon Condensed History Results

Angle	Energy	FMR	Exp. [MeV]	Calc. [MeV]	C/E
0°	1.0 MeV	0.016000	0.02591±2.0%	0.02569±0.1%	0.99
0°	1.0 MeV	0.198000	0.03903±2.0%	0.03842±0.1%	0.98
0°	1.0 MeV	0.378000	0.04730±2.0%	0.04891±0.1%	1.03
0°	1.0 MeV	0.673000	0.03075±2.0%	0.03215±0.2%	1.05
0°	1.0 MeV	0.781000	0.01889±2.0%	0.01875±0.2%	0.99

Table 17: Carbon Single Event Results

Angle	Energy	FMR	Exp. [MeV]	Calc. [MeV]	C/E
0°	1.0 MeV	0.016000	0.02591±2.0%	0.02783±0.1%	1.07
0°	1.0 MeV	0.198000	0.03903±2.0%	0.04565±0.1%	1.17
0°	1.0 MeV	0.378000	0.04730±2.0%	0.05057±0.1%	1.07
0°	1.0 MeV	0.673000	0.03075±2.0%	0.02654±0.2%	0.86
0°	1.0 MeV	0.781000	0.01889±2.0%	0.01348±0.3%	0.71

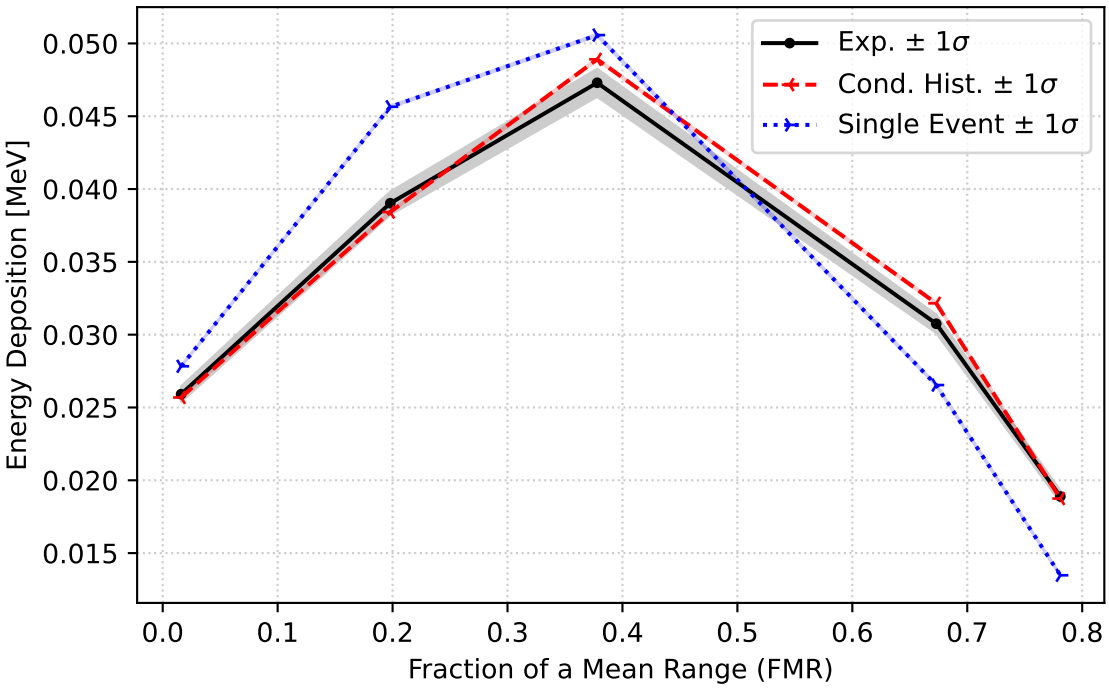

Figure 49: Carbon 0-degree 1.0 MeV Results

Table 18: Copper Condensed History Results

Angle	Energy	FMR	Exp. [MeV]	Calc. [MeV]	C/E
0°	0.3 MeV	0.087000	0.10465±1.3%	0.10744±0.1%	1.03
0°	0.3 MeV	0.178000	0.10860±1.3%	0.11317±0.1%	1.04
0°	0.3 MeV	0.266000	0.08864±1.3%	0.09162±0.1%	1.03
0°	0.3 MeV	0.357000	0.06143±1.3%	0.06293±0.1%	1.02
0°	0.3 MeV	0.453000	0.03598±1.3%	0.03502±0.2%	0.97
0°	0.5 MeV	0.042000	0.07438±1.3%	0.07548±0.1%	1.01
0°	0.5 MeV	0.129000	0.09500±1.3%	0.09921±0.1%	1.04
0°	0.5 MeV	0.173000	0.09083±1.3%	0.09522±0.1%	1.05
0°	0.5 MeV	0.307000	0.06319±1.3%	0.06477±0.1%	1.03
0°	0.5 MeV	0.397000	0.04103±1.3%	0.04127±0.2%	1.01

Table 19: Copper Single Event Results

Angle	Energy	FMR	Exp. [MeV]	Calc. [MeV]	C/E
0°	0.3 MeV	0.087000	0.10465±1.3%	0.10839±0.1%	1.04
0°	0.3 MeV	0.178000	0.10860±1.3%	0.11162±0.1%	1.03
0°	0.3 MeV	0.266000	0.08864±1.3%	0.08897±0.1%	1.00
0°	0.3 MeV	0.357000	0.06143±1.3%	0.06019±0.1%	0.98
0°	0.3 MeV	0.453000	0.03598±1.3%	0.03306±0.2%	0.92
0°	0.5 MeV	0.042000	0.07438±1.3%	0.07763±0.1%	1.04
0°	0.5 MeV	0.129000	0.09500±1.3%	0.09981±0.1%	1.05
0°	0.5 MeV	0.173000	0.09083±1.3%	0.09549±0.1%	1.05
0°	0.5 MeV	0.307000	0.06319±1.3%	0.06424±0.1%	1.02
0°	0.5 MeV	0.397000	0.04103±1.3%	0.04050±0.2%	0.99

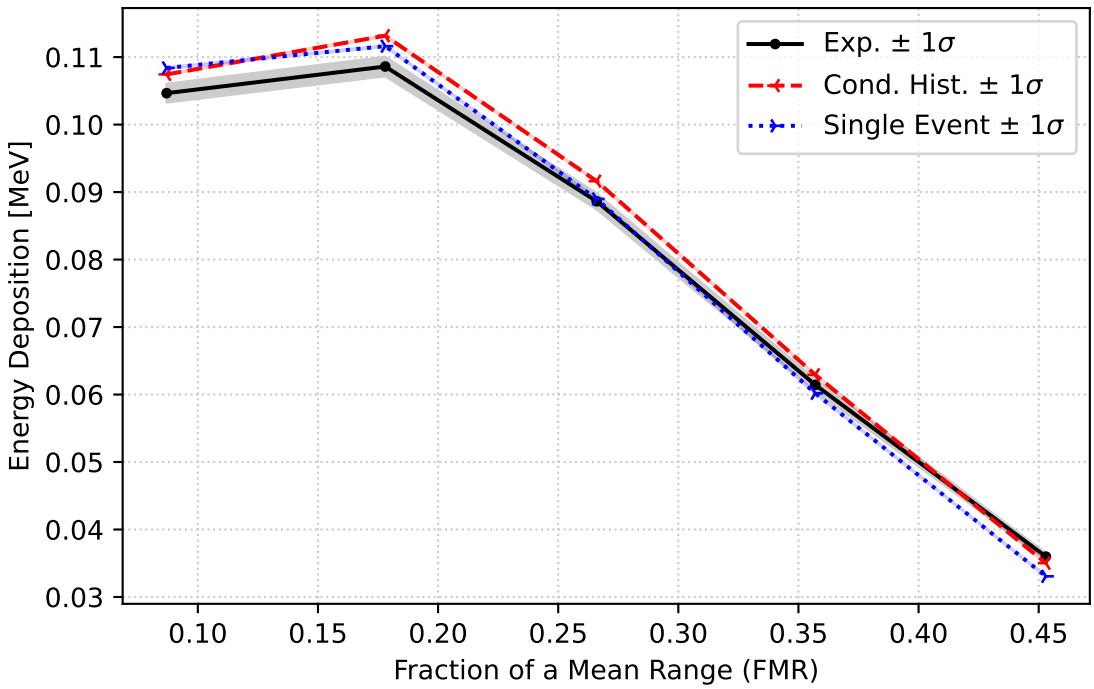

Figure 50: Copper 0-degree 0.3 MeV Results

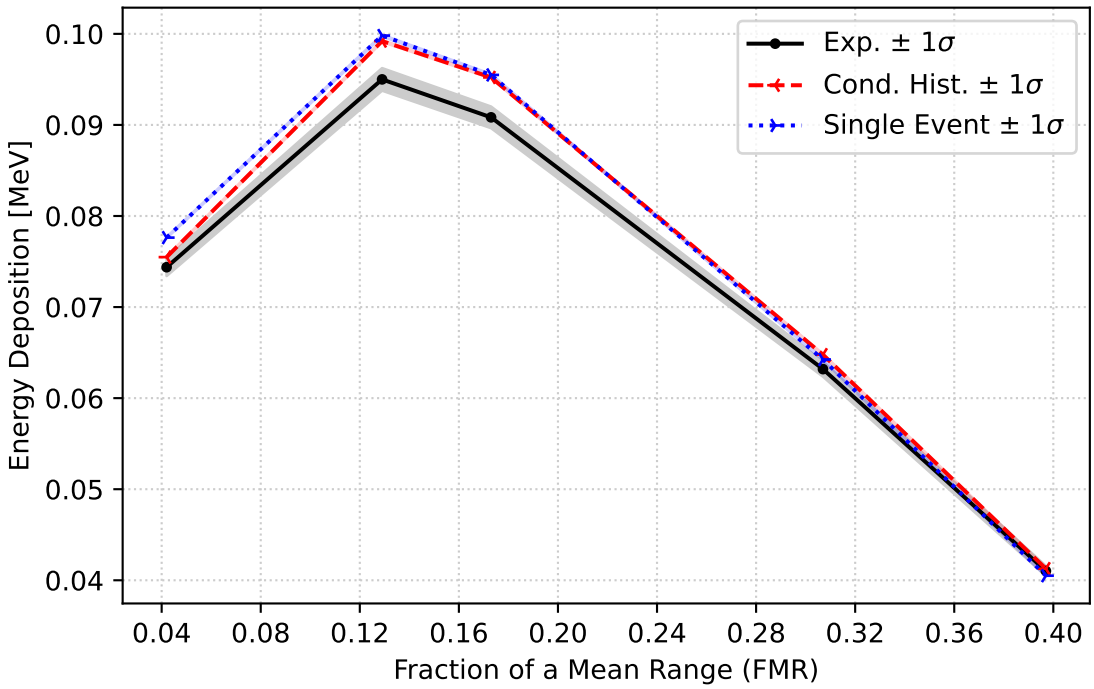

Figure 51: Copper 0-degree 0.5 MeV Results

Table 20: Iron Condensed History Results

Angle	Energy	FMR	Exp. [MeV]	Calc. [MeV]	C/E
0°	0.3 MeV	0.081000	0.08665±1.2%	0.09407±0.1%	1.09
0°	0.3 MeV	0.244000	0.08489±1.2%	0.09241±0.1%	1.09
0°	0.3 MeV	0.305000	0.05203±1.2%	0.05194±0.1%	1.00
0°	0.3 MeV	0.558000	0.01858±1.2%	0.01591±0.3%	0.86
0°	0.3 MeV	0.714000	0.00372±1.2%	0.00223±0.7%	0.60
0°	0.5 MeV	0.039000	0.05848±1.2%	0.06391±0.1%	1.09
0°	0.5 MeV	0.118000	0.07980±1.2%	0.08809±0.1%	1.10
0°	0.5 MeV	0.191000	0.07804±1.2%	0.08509±0.1%	1.09
0°	0.5 MeV	0.270000	0.06592±1.2%	0.07087±0.1%	1.08
0°	0.5 MeV	0.345000	0.05242±1.2%	0.05424±0.1%	1.03
0°	1.0 MeV	0.016000	0.04147±1.2%	0.04221±0.1%	1.02
0°	1.0 MeV	0.048000	0.05438±1.2%	0.05570±0.1%	1.02
0°	1.0 MeV	0.142000	0.06846±1.2%	0.07429±0.1%	1.09
0°	1.0 MeV	0.248000	0.05672±1.2%	0.06359±0.1%	1.12
0°	1.0 MeV	0.388000	0.03501±1.2%	0.03838±0.2%	1.10

Table 21: Iron Single Event Results

Angle	Energy	FMR	Exp. [MeV]	Calc. [MeV]	C/E
0°	0.3 MeV	0.081000	0.08665±1.2%	0.09521±0.1%	1.10
0°	0.3 MeV	0.244000	0.08489±1.2%	0.08928±0.1%	1.05
0°	0.3 MeV	0.305000	0.05203±1.2%	0.04904±0.1%	0.94
0°	0.3 MeV	0.558000	0.01858±1.2%	0.01478±0.3%	0.80
0°	0.3 MeV	0.714000	0.00372±1.2%	0.00205±0.7%	0.55
0°	0.5 MeV	0.039000	0.05848±1.2%	0.06600±0.1%	1.13
0°	0.5 MeV	0.118000	0.07980±1.2%	0.08883±0.1%	1.11
0°	0.5 MeV	0.191000	0.07804±1.2%	0.08411±0.1%	1.08
0°	0.5 MeV	0.270000	0.06592±1.2%	0.06940±0.1%	1.05
0°	0.5 MeV	0.345000	0.05242±1.2%	0.05248±0.1%	1.00
0°	1.0 MeV	0.016000	0.04147±1.2%	0.04347±0.1%	1.05
0°	1.0 MeV	0.048000	0.05438±1.2%	0.05758±0.1%	1.06
0°	1.0 MeV	0.142000	0.06846±1.2%	0.07449±0.1%	1.09
0°	1.0 MeV	0.248000	0.05672±1.2%	0.06291±0.1%	1.11
0°	1.0 MeV	0.388000	0.03501±1.2%	0.03783±0.2%	1.08

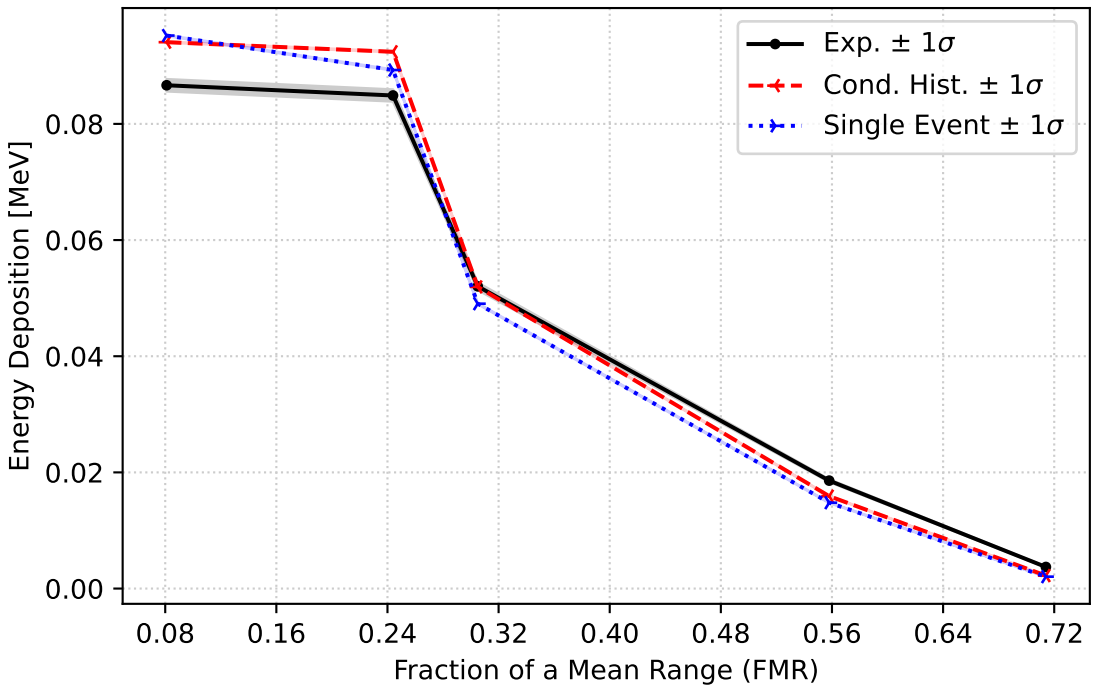

Figure 52: Iron 0-degree 0.3 MeV Results

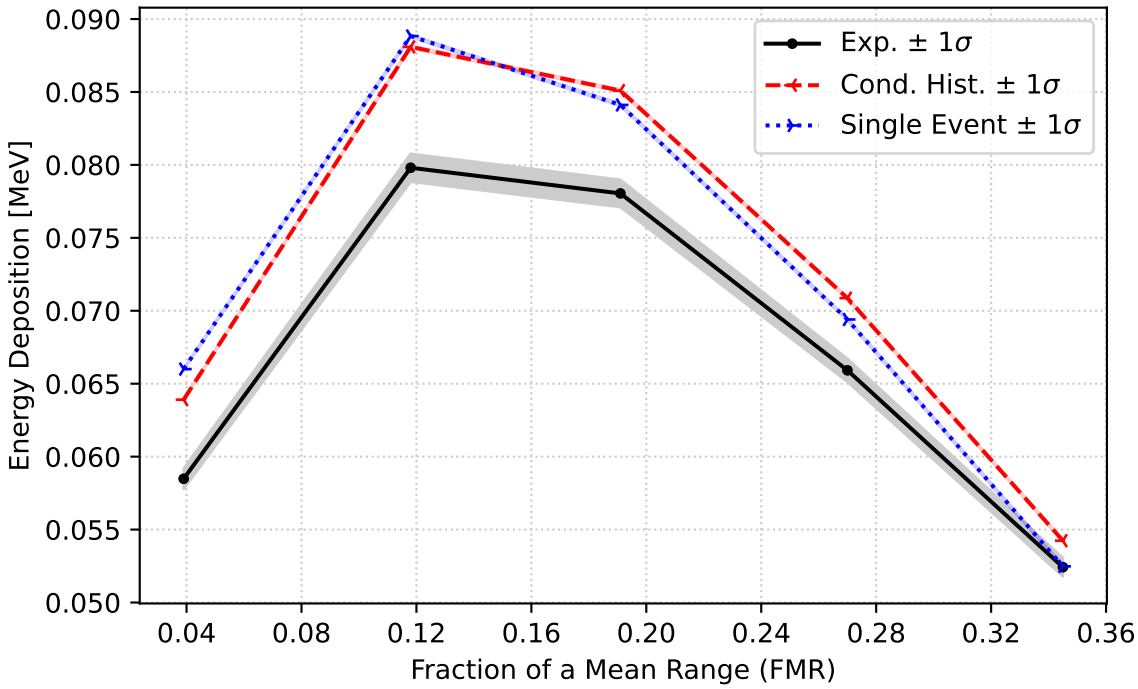

Figure 53: Iron 0-degree 0.5 MeV Results

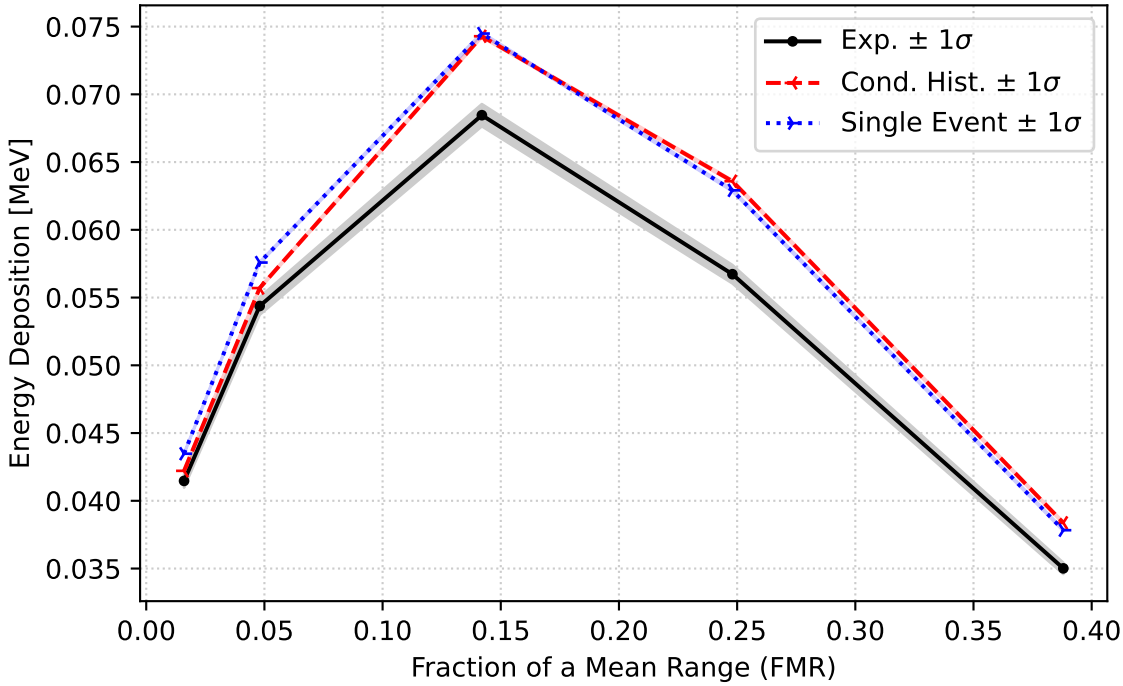

Figure 54: Iron 0-degree 1.0 MeV Results

Table 22: Molybdenum Condensed History Results

Angle	Energy	FMR	Exp. [MeV]	Calc. [MeV]	C/E
0°	0.1 MeV	0.108000	0.04257±1.6%	0.04799±0.1%	1.13
0°	0.1 MeV	0.230000	0.03303±1.6%	0.03820±0.1%	1.16
0°	0.1 MeV	0.264000	0.03170±1.6%	0.03275±0.1%	1.03
0°	0.1 MeV	0.324000	0.02338±1.6%	0.02322±0.1%	0.99
0°	0.1 MeV	0.385000	0.01463±1.6%	0.01483±0.2%	1.01
0°	0.3 MeV	0.019000	0.01776±1.6%	0.02007±0.1%	1.13
0°	0.3 MeV	0.041000	0.02454±1.6%	0.02591±0.1%	1.06
0°	0.3 MeV	0.106000	0.02645±1.6%	0.03000±0.1%	1.13
0°	0.3 MeV	0.210000	0.02057±1.6%	0.02266±0.2%	1.10
0°	0.3 MeV	0.291000	0.01410±1.6%	0.01498±0.2%	1.06
0°	0.5 MeV	0.009000	0.01315±1.6%	0.01403±0.2%	1.07
0°	0.5 MeV	0.028000	0.01733±1.6%	0.01882±0.1%	1.09
0°	0.5 MeV	0.083000	0.02285±1.6%	0.02498±0.1%	1.09
0°	0.5 MeV	0.212000	0.01797±1.6%	0.01865±0.2%	1.04
0°	0.5 MeV	0.293000	0.01256±1.6%	0.01230±0.2%	0.98
0°	1.0 MeV	0.004000	0.01055±1.6%	0.01037±0.2%	0.98
0°	1.0 MeV	0.022000	0.01421±1.6%	0.01426±0.2%	1.00
0°	1.0 MeV	0.088000	0.01998±1.6%	0.02106±0.2%	1.05
0°	1.0 MeV	0.159000	0.01829±1.6%	0.01912±0.2%	1.05
0°	1.0 MeV	0.280000	0.01156±1.6%	0.01184±0.2%	1.02
60°	0.3 MeV	0.019000	0.02576±1.6%	0.02934±0.1%	1.14
60°	0.3 MeV	0.058000	0.02264±1.6%	0.02420±0.1%	1.07
60°	0.3 MeV	0.117000	0.01887±1.6%	0.02100±0.2%	1.11
60°	0.3 MeV	0.171000	0.01702±1.6%	0.01773±0.2%	1.04
60°	0.3 MeV	0.210000	0.01399±1.6%	0.01497±0.2%	1.07
60°	0.5 MeV	0.009000	0.02332±1.6%	0.02635±0.1%	1.13
60°	0.5 MeV	0.057000	0.01813±1.6%	0.02021±0.2%	1.11
60°	0.5 MeV	0.142000	0.01500±1.6%	0.01615±0.2%	1.08
60°	0.5 MeV	0.212000	0.01150±1.6%	0.01221±0.2%	1.06
60°	0.5 MeV	0.253000	0.00954±1.6%	0.00974±0.3%	1.02
60°	1.0 MeV	0.004000	0.02041±1.6%	0.02205±0.2%	1.08
60°	1.0 MeV	0.012000	0.02216±1.6%	0.02490±0.2%	1.12
60°	1.0 MeV	0.043000	0.01728±1.6%	0.01891±0.2%	1.09
60°	1.0 MeV	0.088000	0.01437±1.6%	0.01603±0.2%	1.12
60°	1.0 MeV	0.167000	0.01172±1.6%	0.01263±0.2%	1.08

Table 23: Molybdenum Single Event Results

Angle	Energy	FMR	Exp. [MeV]	Calc. [MeV]	C/E
0°	0.1 MeV	0.108000	0.04257±1.6%	0.04590±0.1%	1.08
0°	0.1 MeV	0.230000	0.03303±1.6%	0.03635±0.1%	1.10
0°	0.1 MeV	0.264000	0.03170±1.6%	0.03128±0.1%	0.99
0°	0.1 MeV	0.324000	0.02338±1.6%	0.02239±0.1%	0.96
0°	0.1 MeV	0.385000	0.01463±1.6%	0.01454±0.2%	0.99
0°	0.3 MeV	0.019000	0.01776±1.6%	0.02030±0.1%	1.14
0°	0.3 MeV	0.041000	0.02454±1.6%	0.02564±0.1%	1.04
0°	0.3 MeV	0.106000	0.02645±1.6%	0.02906±0.1%	1.10
0°	0.3 MeV	0.210000	0.02057±1.6%	0.02182±0.2%	1.06
0°	0.3 MeV	0.291000	0.01410±1.6%	0.01437±0.2%	1.02
0°	0.5 MeV	0.009000	0.01315±1.6%	0.01411±0.1%	1.07
0°	0.5 MeV	0.028000	0.01733±1.6%	0.01888±0.1%	1.09
0°	0.5 MeV	0.083000	0.02285±1.6%	0.02457±0.1%	1.08
0°	0.5 MeV	0.212000	0.01797±1.6%	0.01836±0.2%	1.02
0°	0.5 MeV	0.293000	0.01256±1.6%	0.01227±0.2%	0.98
0°	1.0 MeV	0.004000	0.01055±1.6%	0.01020±0.1%	0.97
0°	1.0 MeV	0.022000	0.01421±1.6%	0.01390±0.1%	0.98
0°	1.0 MeV	0.088000	0.01998±1.6%	0.02046±0.1%	1.02
0°	1.0 MeV	0.159000	0.01829±1.6%	0.01892±0.2%	1.03
0°	1.0 MeV	0.280000	0.01156±1.6%	0.01216±0.2%	1.05
60°	0.3 MeV	0.019000	0.02576±1.6%	0.02717±0.1%	1.05
60°	0.3 MeV	0.058000	0.02264±1.6%	0.02265±0.1%	1.00
60°	0.3 MeV	0.117000	0.01887±1.6%	0.01998±0.2%	1.06
60°	0.3 MeV	0.171000	0.01702±1.6%	0.01686±0.2%	0.99
60°	0.3 MeV	0.210000	0.01399±1.6%	0.01435±0.2%	1.03
60°	0.5 MeV	0.009000	0.02332±1.6%	0.02515±0.1%	1.08
60°	0.5 MeV	0.057000	0.01813±1.6%	0.01928±0.1%	1.06
60°	0.5 MeV	0.142000	0.01500±1.6%	0.01567±0.2%	1.04
60°	0.5 MeV	0.212000	0.01150±1.6%	0.01199±0.2%	1.04
60°	0.5 MeV	0.253000	0.00954±1.6%	0.00969±0.3%	1.02
60°	1.0 MeV	0.004000	0.02041±1.6%	0.02242±0.1%	1.10
60°	1.0 MeV	0.012000	0.02216±1.6%	0.02353±0.1%	1.06
60°	1.0 MeV	0.043000	0.01728±1.6%	0.01821±0.1%	1.05
60°	1.0 MeV	0.088000	0.01437±1.6%	0.01556±0.2%	1.08
60°	1.0 MeV	0.167000	0.01172±1.6%	0.01244±0.2%	1.06

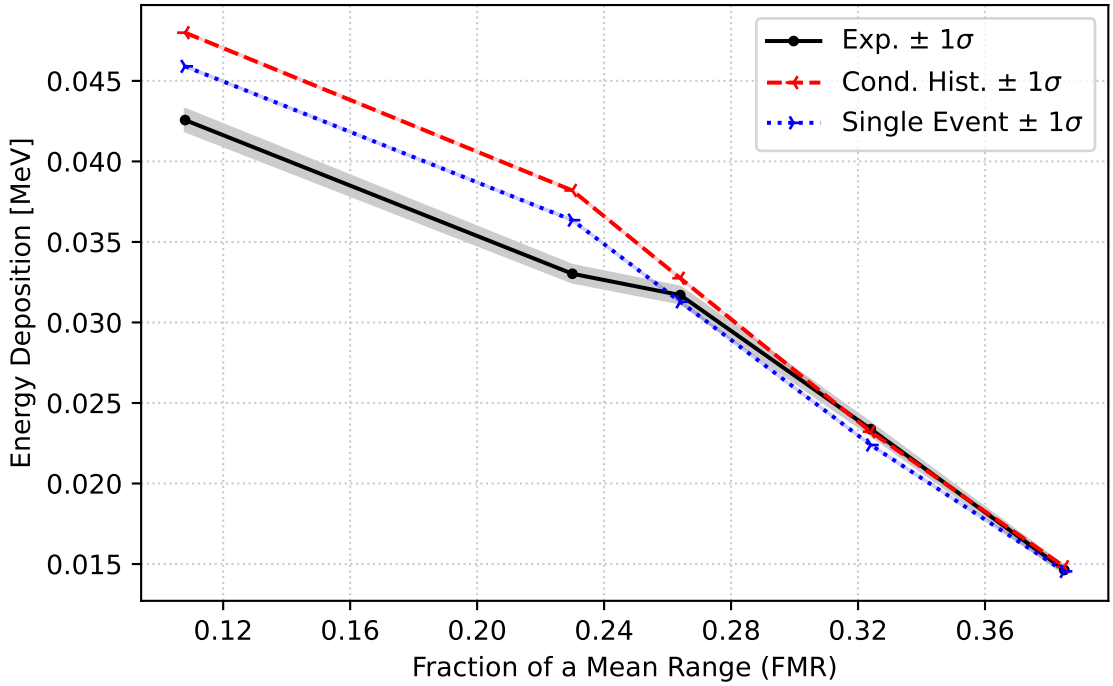

Figure 55: Molybdenum 0-degree 0.1 MeV Results

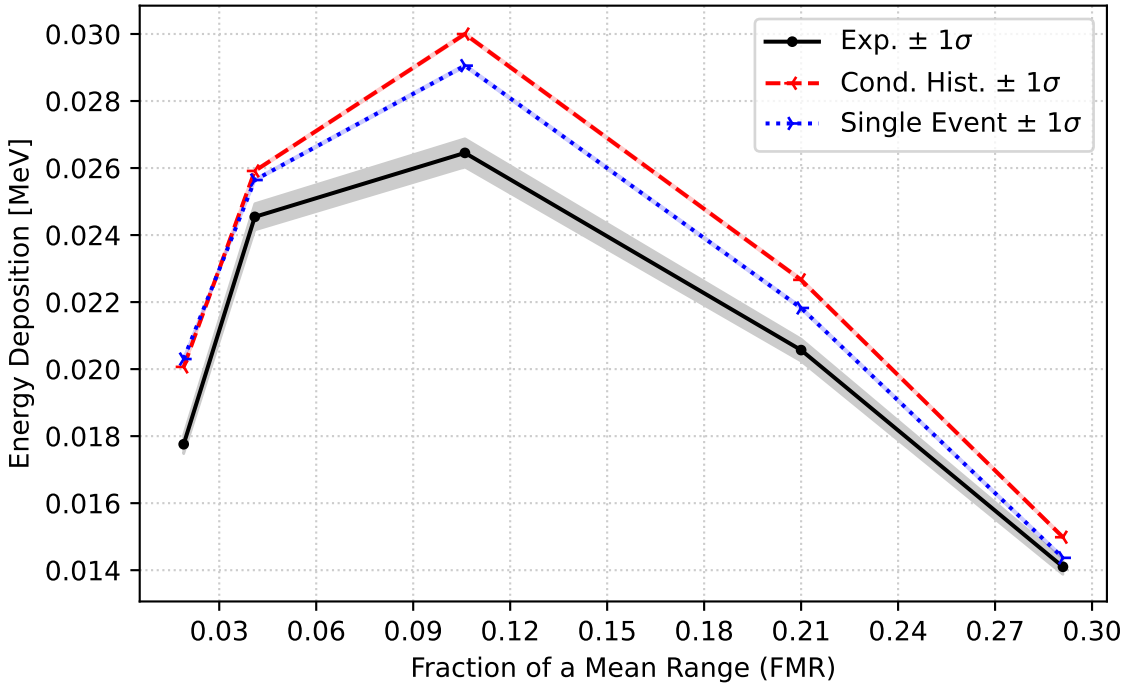

Figure 56: Molybdenum 0-degree 0.3 MeV Results

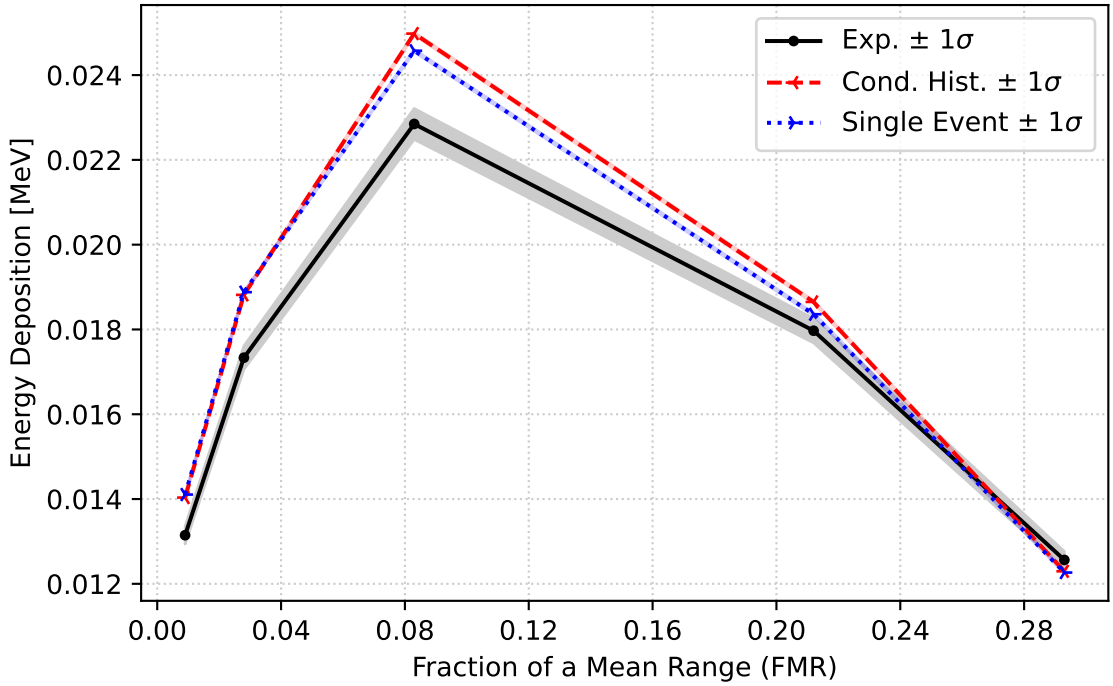

Figure 57: Molybdenum 0-degree 0.5 MeV Results

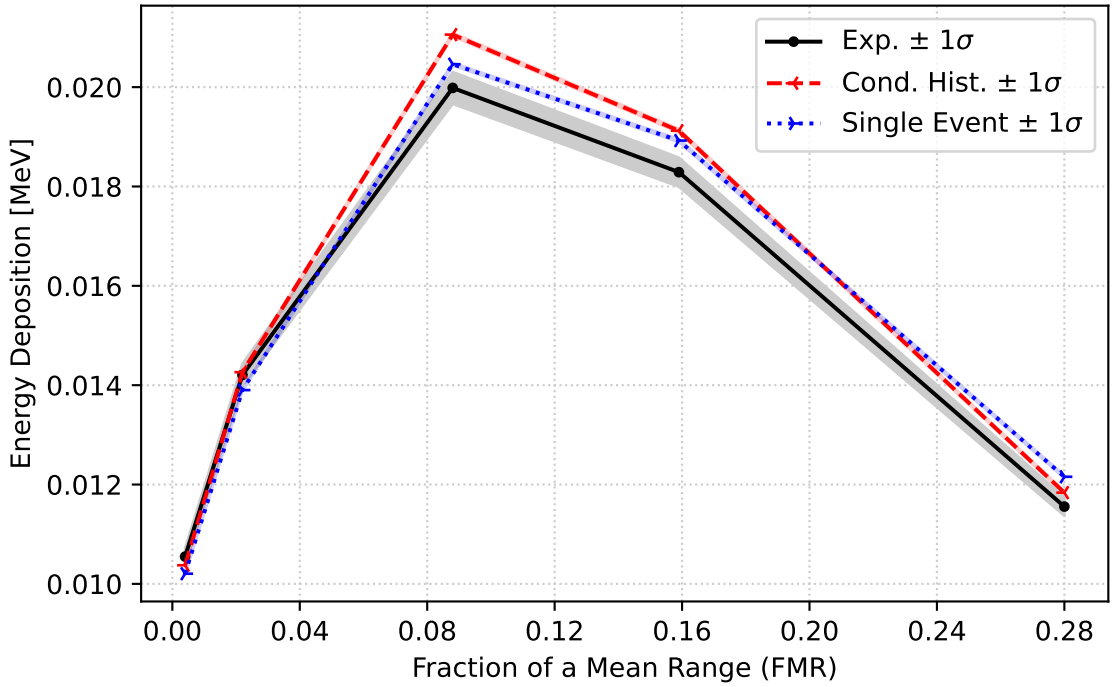

Figure 58: Molybdenum 0-degree 1.0 MeV Results

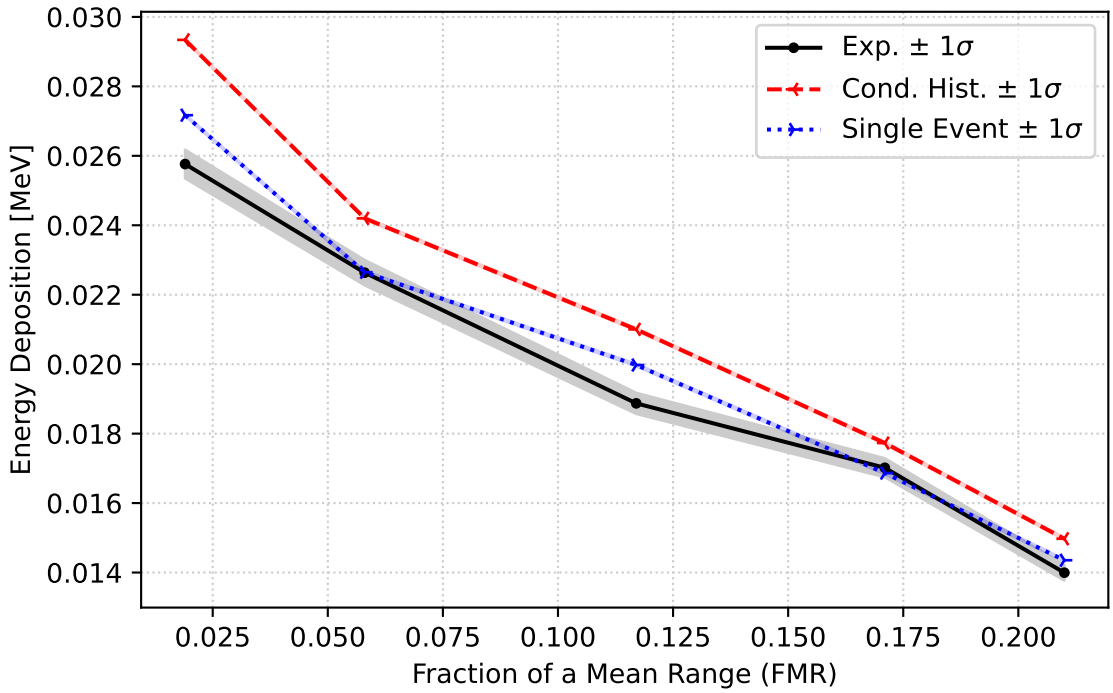

Figure 59: Molybdenum 60-degree 0.3 MeV Results

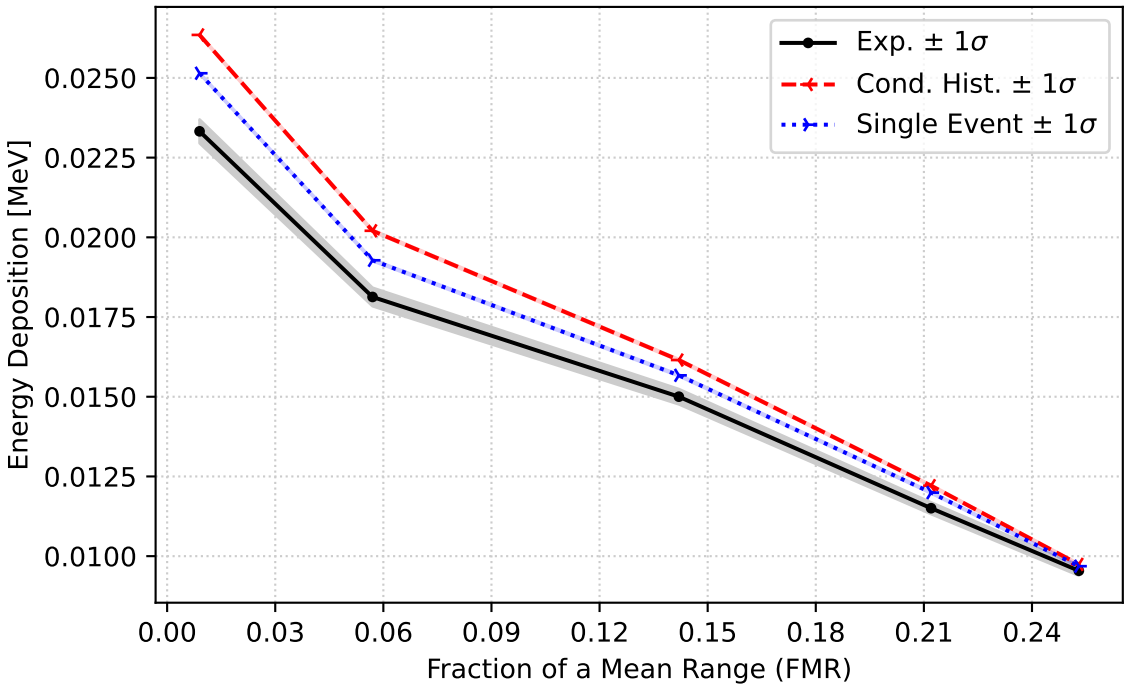

Figure 60: Molybdenum 60-degree 0.5 MeV Results

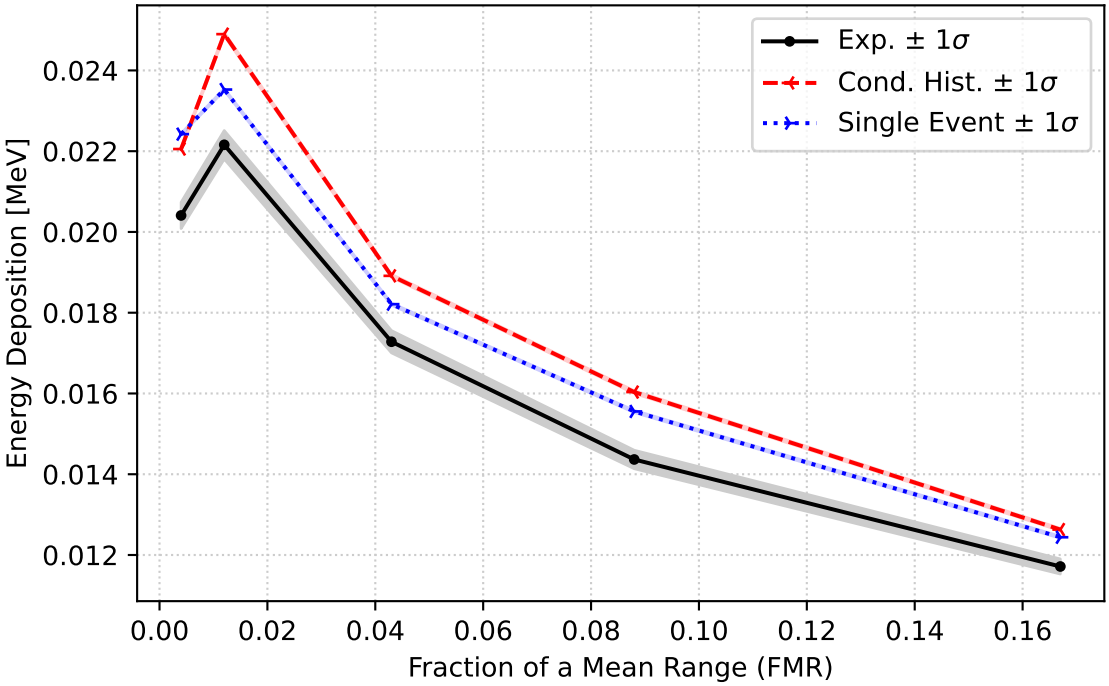

Figure 61: Molybdenum 60-degree 1.0 MeV Results

Table 24: Tantalum Condensed History Results

Angle	Energy	FMR	Exp. [MeV]	Calc. [MeV]	C/E
0°	0.3 MeV	0.069000	0.07911±2.2%	0.08172±0.1%	1.03
0°	0.3 MeV	0.142000	0.06521±2.2%	0.06950±0.1%	1.07
0°	0.3 MeV	0.204000	0.04915±2.2%	0.04710±0.1%	0.96
0°	0.3 MeV	0.292000	0.02267±2.2%	0.02073±0.2%	0.91
0°	0.3 MeV	0.392000	0.00794±2.2%	0.00540±0.5%	0.68
0°	0.5 MeV	0.034000	0.06454±2.2%	0.06262±0.1%	0.97
0°	0.5 MeV	0.100000	0.06653±2.2%	0.07015±0.1%	1.05
0°	0.5 MeV	0.253000	0.02665±2.2%	0.02557±0.2%	0.96
0°	0.5 MeV	0.333000	0.01175±2.2%	0.01011±0.4%	0.86
0°	0.5 MeV	0.488000	0.00166±2.2%	0.00079±1.3%	0.48
0°	1.0 MeV	0.013000	0.04038±1.2%	0.04195±0.1%	1.04
0°	1.0 MeV	0.027000	0.05246±1.2%	0.05599±0.1%	1.07
0°	1.0 MeV	0.057000	0.06206±1.2%	0.06529±0.1%	1.05
0°	1.0 MeV	0.120000	0.05445±1.2%	0.05725±0.1%	1.05
0°	1.0 MeV	0.170000	0.04303±1.2%	0.04471±0.2%	1.04
30°	0.5 MeV	0.034000	0.06488±2.2%	0.06492±0.1%	1.00
30°	0.5 MeV	0.070000	0.06504±2.2%	0.06995±0.1%	1.08
30°	0.5 MeV	0.100000	0.06190±2.2%	0.06465±0.1%	1.04
30°	0.5 MeV	0.144000	0.05081±2.2%	0.05325±0.1%	1.05
30°	0.5 MeV	0.193000	0.03906±2.2%	0.03869±0.2%	0.99
60°	0.5 MeV	0.034000	0.05660±2.2%	0.06360±0.1%	1.12
60°	0.5 MeV	0.070000	0.04948±2.2%	0.05337±0.1%	1.08
60°	0.5 MeV	0.100000	0.04634±2.2%	0.04842±0.2%	1.04
60°	0.5 MeV	0.144000	0.03691±2.2%	0.03914±0.2%	1.06
60°	0.5 MeV	0.193000	0.02698±2.2%	0.02806±0.2%	1.04
60°	1.0 MeV	0.015000	0.05759±2.2%	0.06278±0.1%	1.09
60°	1.0 MeV	0.030000	0.05164±2.2%	0.05337±0.1%	1.03
60°	1.0 MeV	0.043000	0.04915±2.2%	0.05028±0.2%	1.02
60°	1.0 MeV	0.082000	0.04088±2.2%	0.04473±0.2%	1.09
60°	1.0 MeV	0.142000	0.03293±2.2%	0.03478±0.2%	1.06

Table 25: Tantalum Single Event Results

Angle	Energy	FMR	Exp. [MeV]	Calc. [MeV]	C/E
0°	0.3 MeV	0.069000	0.07911±2.2%	0.07791±0.1%	0.98
0°	0.3 MeV	0.142000	0.06521±2.2%	0.06770±0.1%	1.04
0°	0.3 MeV	0.204000	0.04915±2.2%	0.04686±0.1%	0.95
0°	0.3 MeV	0.292000	0.02267±2.2%	0.02131±0.2%	0.94
0°	0.3 MeV	0.392000	0.00794±2.2%	0.00593±0.5%	0.75
0°	0.5 MeV	0.034000	0.06454±2.2%	0.05956±0.1%	0.92
0°	0.5 MeV	0.100000	0.06653±2.2%	0.06811±0.1%	1.02
0°	0.5 MeV	0.253000	0.02665±2.2%	0.02764±0.2%	1.04
0°	0.5 MeV	0.333000	0.01175±2.2%	0.01196±0.4%	1.02
0°	0.5 MeV	0.488000	0.00166±2.2%	0.00109±1.1%	0.66
0°	1.0 MeV	0.013000	0.04038±1.2%	0.03969±0.1%	0.98
0°	1.0 MeV	0.027000	0.05246±1.2%	0.05248±0.1%	1.00
0°	1.0 MeV	0.057000	0.06206±1.2%	0.06237±0.1%	1.01
0°	1.0 MeV	0.120000	0.05445±1.2%	0.05687±0.1%	1.04
0°	1.0 MeV	0.170000	0.04303±1.2%	0.04645±0.2%	1.08
30°	0.5 MeV	0.034000	0.06488±2.2%	0.06149±0.1%	0.95
30°	0.5 MeV	0.070000	0.06504±2.2%	0.06722±0.1%	1.03
30°	0.5 MeV	0.100000	0.06190±2.2%	0.06281±0.1%	1.01
30°	0.5 MeV	0.144000	0.05081±2.2%	0.05298±0.1%	1.04
30°	0.5 MeV	0.193000	0.03906±2.2%	0.03990±0.2%	1.02
60°	0.5 MeV	0.034000	0.05660±2.2%	0.05881±0.1%	1.04
60°	0.5 MeV	0.070000	0.04948±2.2%	0.05058±0.1%	1.02
60°	0.5 MeV	0.100000	0.04634±2.2%	0.04664±0.2%	1.01
60°	0.5 MeV	0.144000	0.03691±2.2%	0.03869±0.2%	1.05
60°	0.5 MeV	0.193000	0.02698±2.2%	0.02858±0.2%	1.06
60°	1.0 MeV	0.015000	0.05759±2.2%	0.06044±0.1%	1.05
60°	1.0 MeV	0.030000	0.05164±2.2%	0.05130±0.1%	0.99
60°	1.0 MeV	0.043000	0.04915±2.2%	0.04817±0.1%	0.98
60°	1.0 MeV	0.082000	0.04088±2.2%	0.04340±0.2%	1.06
60°	1.0 MeV	0.142000	0.03293±2.2%	0.03521±0.2%	1.07

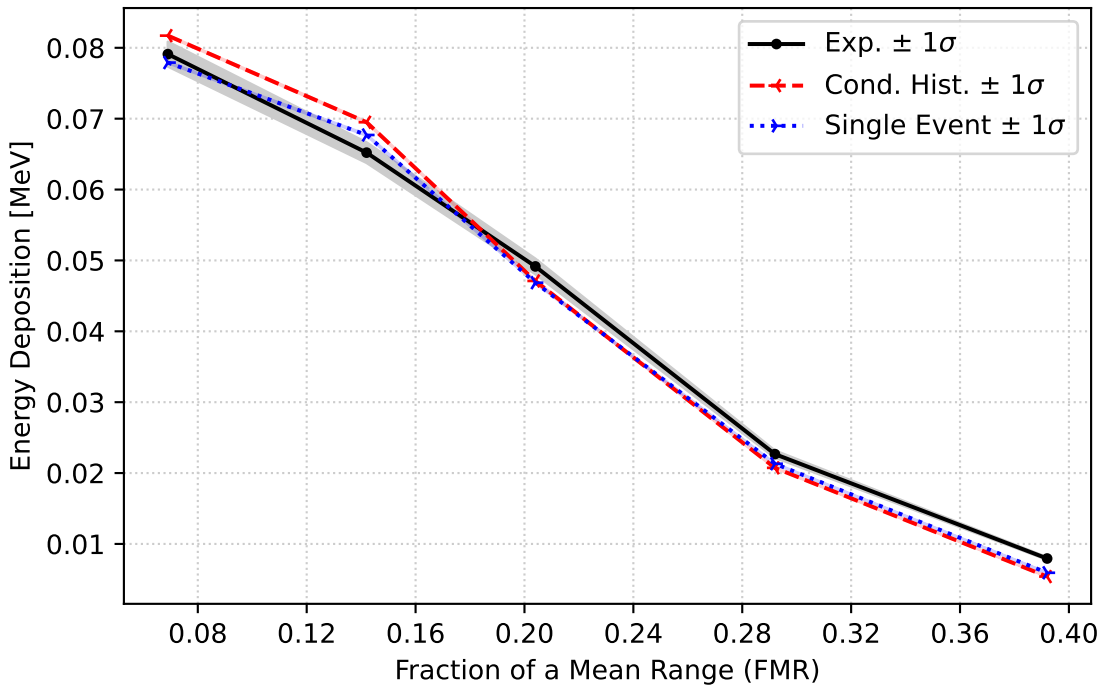

Figure 62: Tantalum 0-degree 0.3 MeV Results

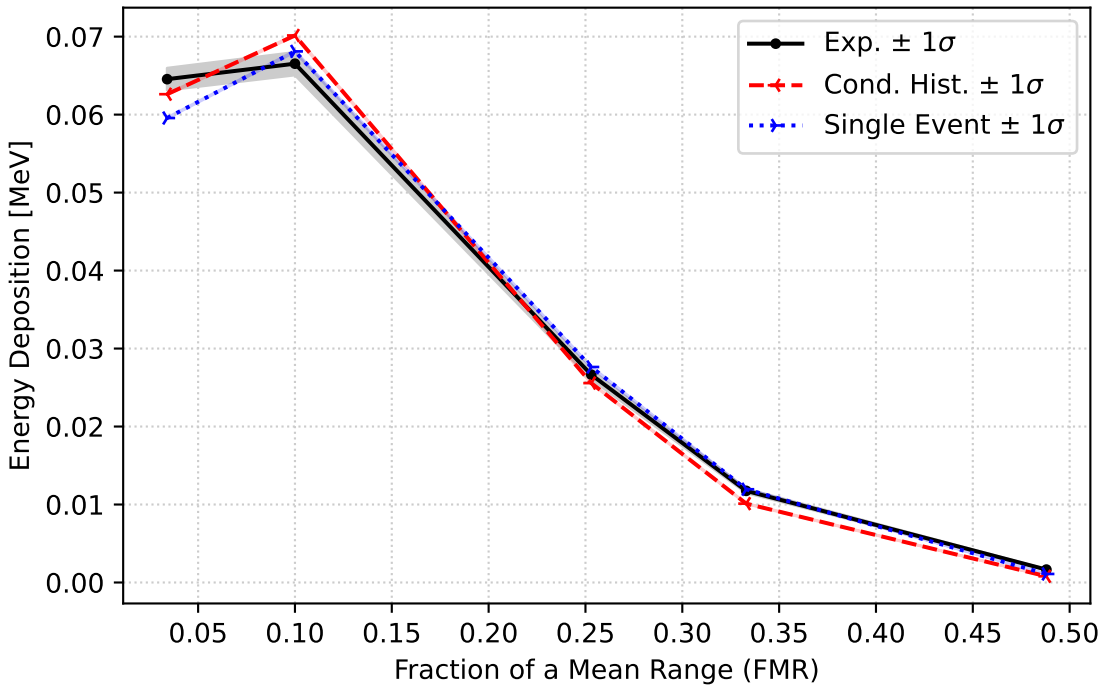

Figure 63: Tantalum 0-degree 0.5 MeV Results

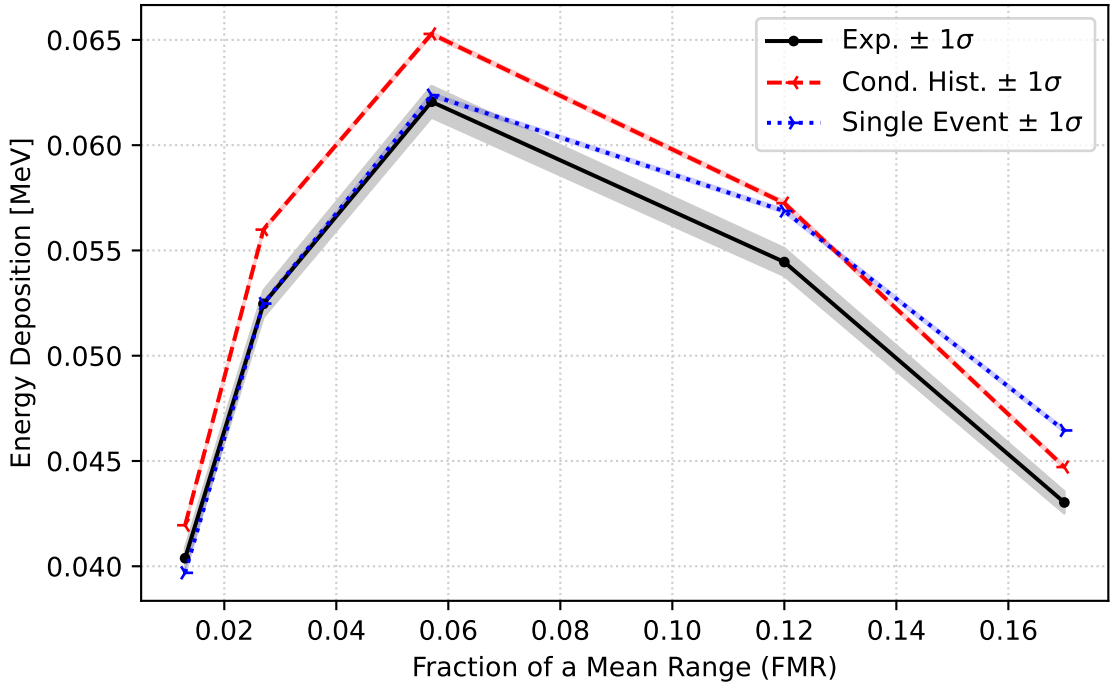

Figure 64: Tantalum 0-degree 1.0 MeV Results

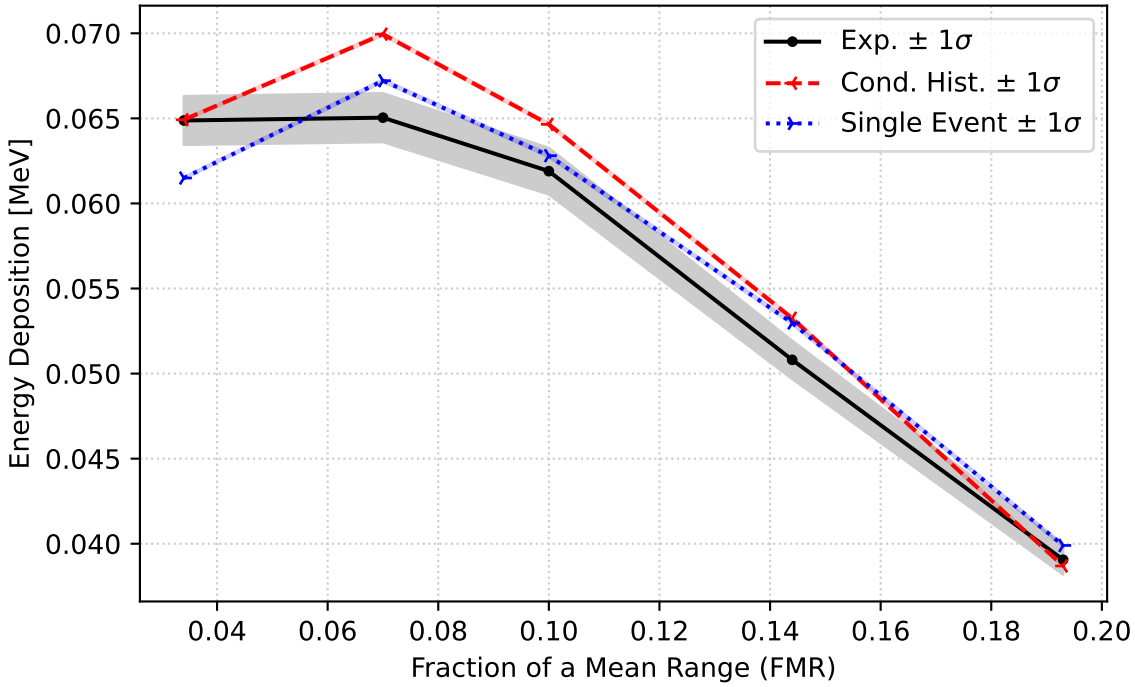

Figure 65: Tantalum 30-degree 0.5 MeV Results

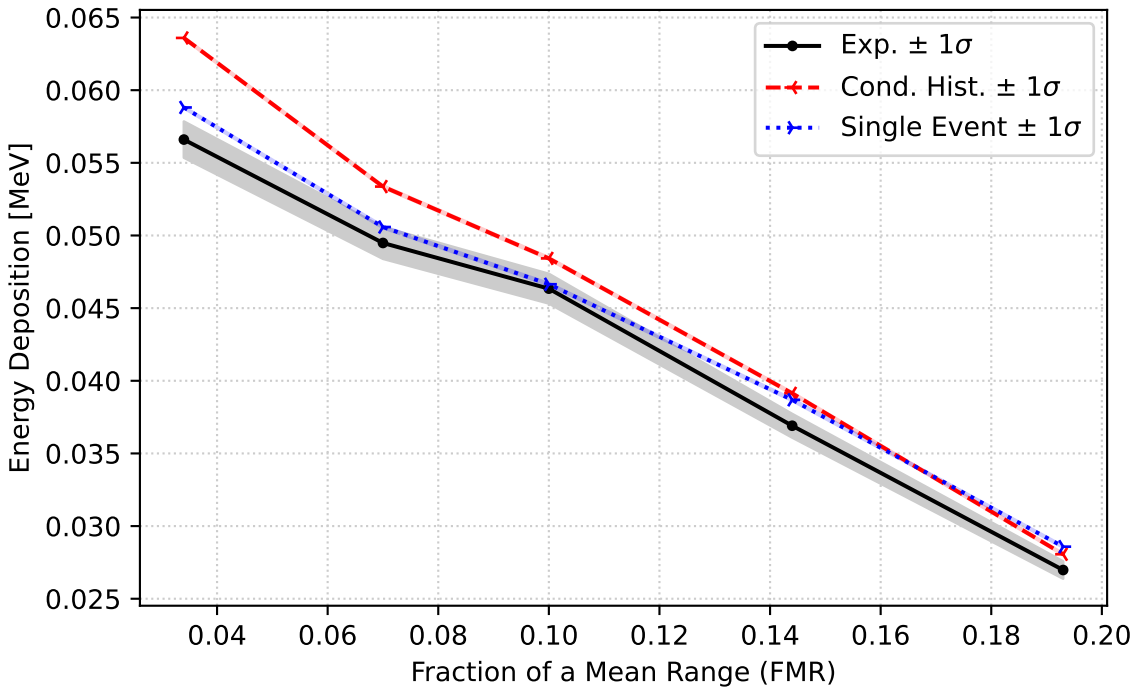

Figure 66: Tantalum 60-degree 0.5 MeV Results

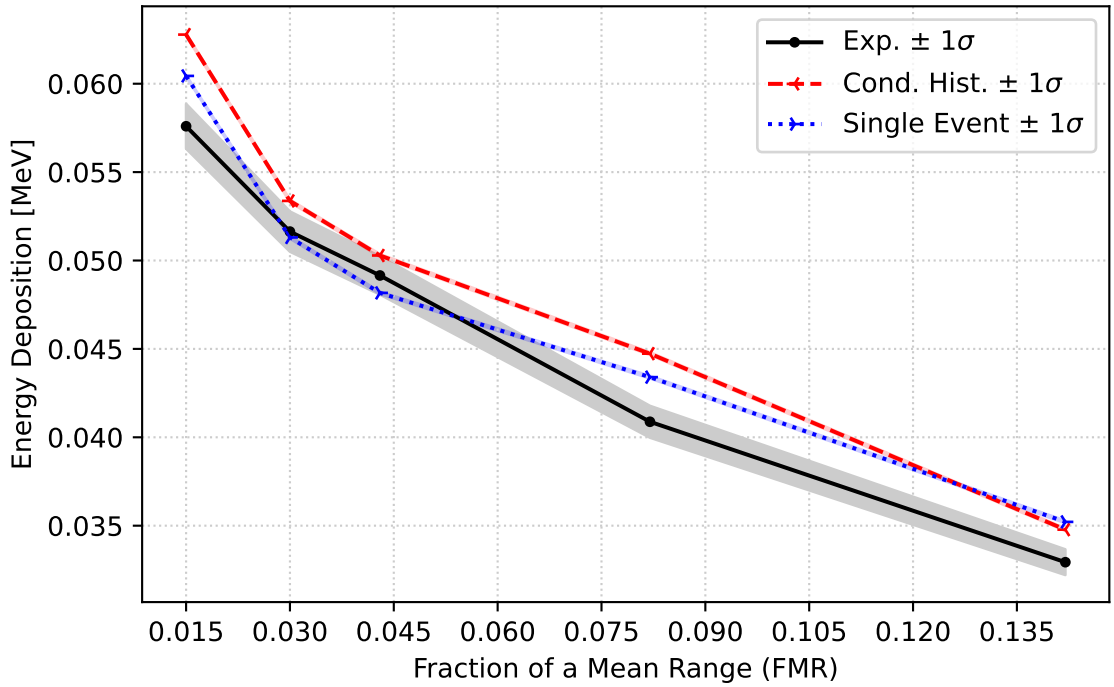

Figure 67: Tantalum 60-degree 1.0 MeV Results

Table 26: Uranium Condensed History Results

Angle	Energy	FMR	Exp. [MeV]	Calc. [MeV]	C/E
0°	0.3 MeV	0.044000	0.06908±1.4%	0.07063±0.1%	1.02
0°	0.3 MeV	0.077000	0.06879±1.4%	0.07263±0.1%	1.06
0°	0.3 MeV	0.135000	0.05421±1.4%	0.05500±0.1%	1.01
0°	0.3 MeV	0.159000	0.04478±1.4%	0.04637±0.1%	1.04
0°	0.3 MeV	0.189000	0.03432±1.4%	0.03578±0.2%	1.04
0°	0.5 MeV	0.023000	0.05318±1.4%	0.05485±0.1%	1.03
0°	0.5 MeV	0.067000	0.06083±1.4%	0.06417±0.1%	1.05
0°	0.5 MeV	0.115000	0.05141±1.4%	0.05276±0.1%	1.03
0°	0.5 MeV	0.141000	0.04257±1.4%	0.04476±0.2%	1.05
0°	0.5 MeV	0.172000	0.03462±1.4%	0.03495±0.2%	1.01
0°	1.0 MeV	0.010000	0.04080±1.4%	0.03768±0.1%	0.92
0°	1.0 MeV	0.023000	0.05052±1.4%	0.05026±0.1%	0.99
0°	1.0 MeV	0.051000	0.05435±1.4%	0.05724±0.1%	1.05
0°	1.0 MeV	0.120000	0.04419±1.4%	0.04593±0.2%	1.04
0°	1.0 MeV	0.194000	0.02475±1.4%	0.02681±0.2%	1.08
60°	1.0 MeV	0.010000	0.05244±1.4%	0.05320±0.1%	1.01
60°	1.0 MeV	0.023000	0.04596±1.4%	0.04656±0.1%	1.01
60°	1.0 MeV	0.040000	0.03992±1.4%	0.04287±0.2%	1.07
60°	1.0 MeV	0.096000	0.03152±1.4%	0.03539±0.2%	1.12
60°	1.0 MeV	0.120000	0.02946±1.4%	0.03106±0.2%	1.05

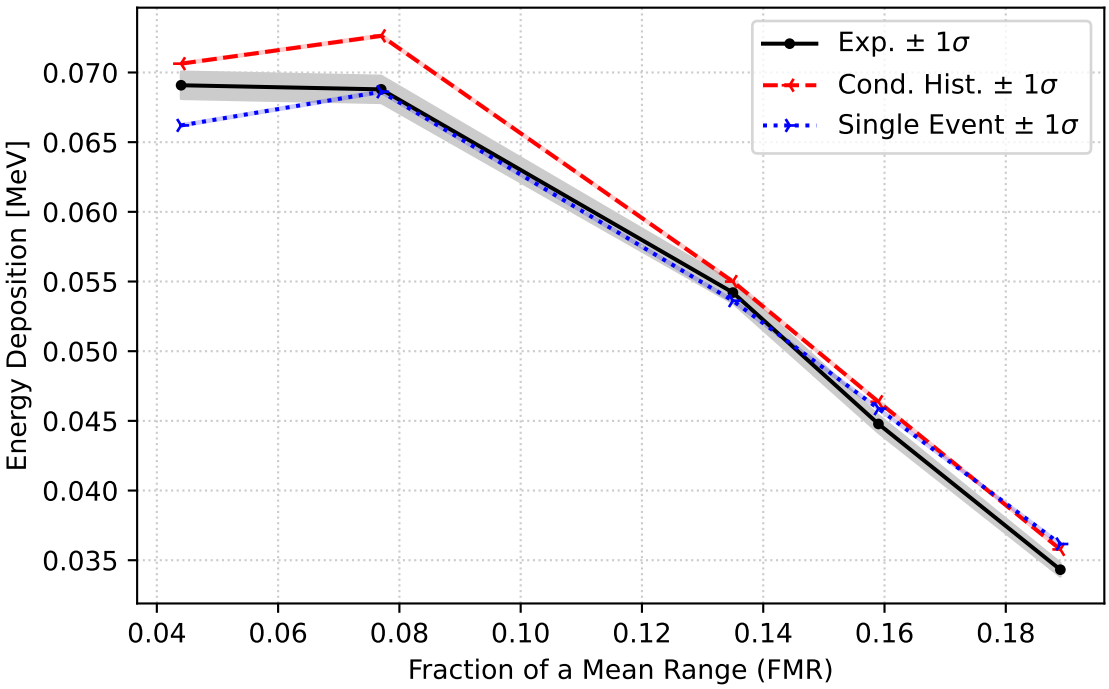

Figure 68: Uranium 0-degree 0.3 MeV Results

Table 27: Uranium Single Event Results

Angle	Energy	FMR	Exp. [MeV]	Calc. [MeV]	C/E
0°	0.3 MeV	0.044000	0.06908±1.4%	0.06620±0.1%	0.96
0°	0.3 MeV	0.077000	0.06879±1.4%	0.06862±0.1%	1.00
0°	0.3 MeV	0.135000	0.05421±1.4%	0.05362±0.1%	0.99
0°	0.3 MeV	0.159000	0.04478±1.4%	0.04588±0.1%	1.02
0°	0.3 MeV	0.189000	0.03432±1.4%	0.03616±0.2%	1.05
0°	0.5 MeV	0.023000	0.05318±1.4%	0.05095±0.1%	0.96
0°	0.5 MeV	0.067000	0.06083±1.4%	0.06095±0.1%	1.00
0°	0.5 MeV	0.115000	0.05141±1.4%	0.05214±0.1%	1.01
0°	0.5 MeV	0.141000	0.04257±1.4%	0.04529±0.2%	1.06
0°	0.5 MeV	0.172000	0.03462±1.4%	0.03680±0.2%	1.06
0°	1.0 MeV	0.010000	0.04080±1.4%	0.03442±0.1%	0.84
0°	1.0 MeV	0.023000	0.05052±1.4%	0.04568±0.1%	0.90
0°	1.0 MeV	0.051000	0.05435±1.4%	0.05430±0.1%	1.00
0°	1.0 MeV	0.120000	0.04419±1.4%	0.04635±0.2%	1.05
0°	1.0 MeV	0.194000	0.02475±1.4%	0.03035±0.2%	1.23
60°	1.0 MeV	0.010000	0.05244±1.4%	0.05005±0.1%	0.95
60°	1.0 MeV	0.023000	0.04596±1.4%	0.04396±0.1%	0.96
60°	1.0 MeV	0.040000	0.03992±1.4%	0.04050±0.1%	1.01
60°	1.0 MeV	0.096000	0.03152±1.4%	0.03452±0.2%	1.10
60°	1.0 MeV	0.120000	0.02946±1.4%	0.03108±0.2%	1.06

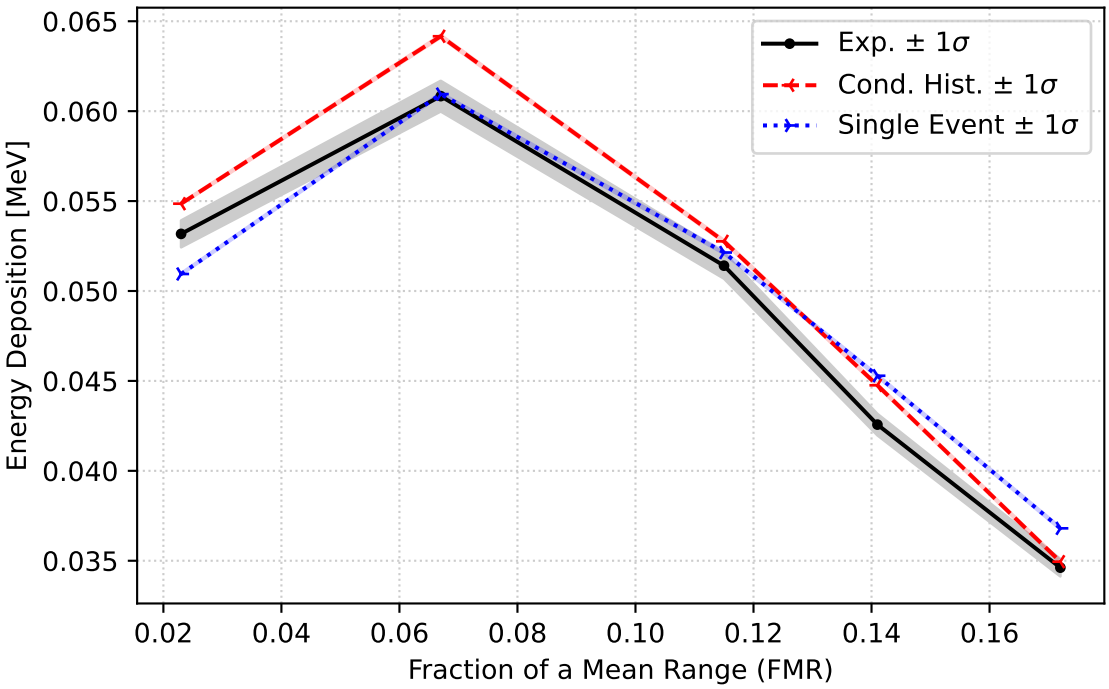

Figure 69: Uranium 0-degree 0.5 MeV Results

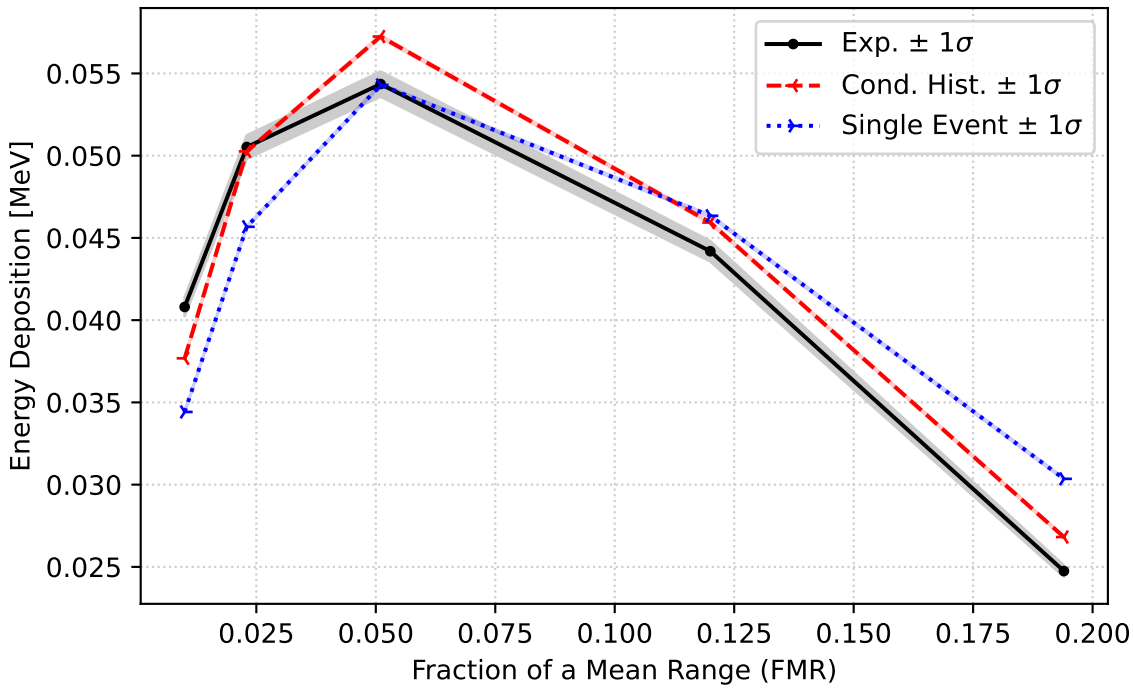

Figure 70: Uranium 0-degree 1.0 MeV Results

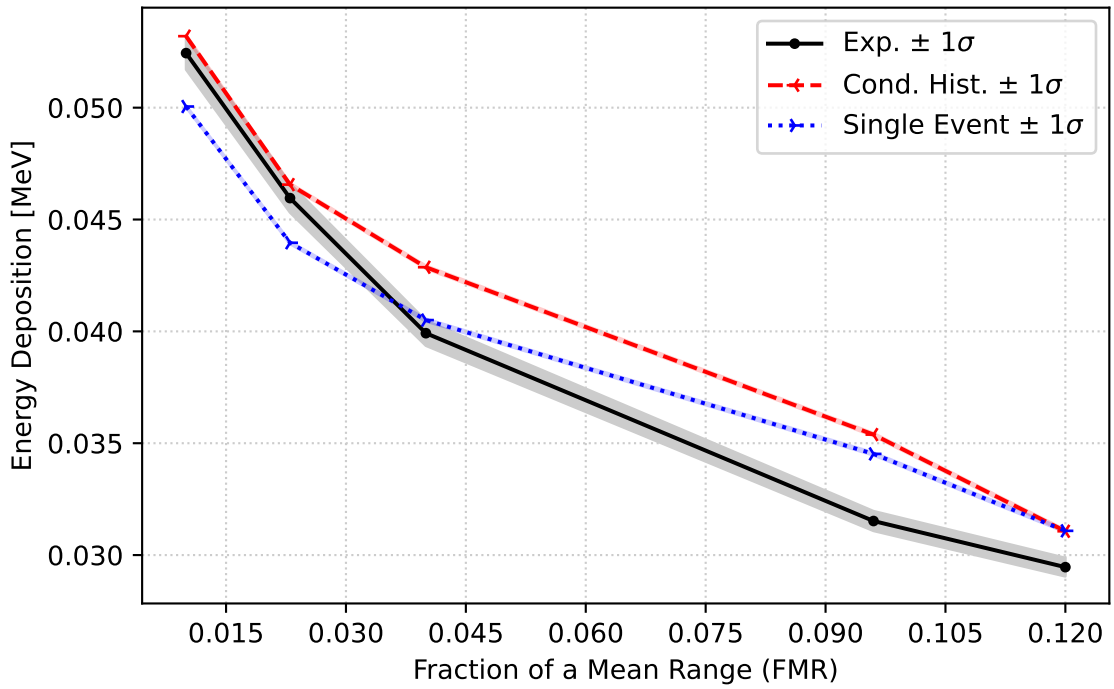

Figure 71: Uranium 60-degree 1.0 MeV Results

Table 28: Rossi-α (ENDF/B-VI.6) Benchmark Results

	Exp. Rossi-α (s^{-1})	Exp. unc.	Calc. Rossi-α (s^{-1})	Calc. unc.
heu-met-fast-001	-1.1100×10^6	2.00×10^4	-1.1388×10^6	1.18×10^4
heu-met-fast-028	-3.8200×10^5	2.00×10^3	-4.1118×10^5	1.89×10^3
heu-met-fast-072-case-1	-3.7266×10^4	4.77×10^2	-4.1394×10^4	2.57×10^2
heu-met-fast-073	-8.9910×10^4	8.17×10^2	-1.0798×10^5	6.93×10^2
heu-met-inter-006-case-1	-3.3810×10^3	7.40×10^1	-3.7778×10^3	1.62×10^1
heu-met-inter-006-case-4	-2.6190×10^4	1.82×10^2	-3.2932×10^4	1.44×10^2
ieu-met-fast-007-case-4	-1.1700×10^5	1.00×10^3	-1.2564×10^5	7.51×10^2
leu-sol-therm-004-case-46	-1.0620×10^2	3.70	-1.1002×10^2	2.49
leu-sol-therm-007-case-30	-1.2680×10^2	2.90	-1.3251×10^2	3.16
pu-met-fast-001	-6.4000×10^5	1.00×10^4	-6.3854×10^5	7.49×10^3
pu-met-fast-006	-2.1400×10^5	5.00×10^3	-2.1642×10^5	3.49×10^3
pu-met-fast-008-case-2	-1.9700×10^5	1.00×10^4	-1.9747×10^5	6.81×10^3
u233-met-fast-001	-1.0000×10^6	1.00×10^4	-1.0939×10^6	7.14×10^3
u233-met-fast-006	-2.7100×10^5	3.00×10^3	-3.0891×10^5	4.22×10^3

4.6 Rossi-α

This test suite executes 1 input per node, where each node uses 114 MPI ranks, with a total Slurm allocation of no more than 45 minutes. An example `VnV.py` execution line is `./VnV.py execute_slurm --nmpi 114 --time 45 --stride=1 --wait --calcdir_name rossi_$DATA`, where `$DATA` is an environment variable that identifies which evaluated nuclear data set to use.

The following figures and tables are results for the Rossi-α Validation Suite. The plots display calculated-to-expected (C/E) values and their uncertainties. The tables provide benchmark and calculated values and uncertainties.

4.6.1 ENDF/B-VI.6

For the Rossi-α (ENDF/B-VI.6) benchmarks, the benchmark data and calculation results are plotted in Fig. 72 as C/E ratios with individual values listed in Table 28.

4.6.2 ENDF/B-VII.0

For the Rossi-α (ENDF/B-VII.0) benchmarks, the benchmark data and calculation results are plotted in Fig. 73 as C/E ratios with individual values listed in Table 29.

4.6.3 ENDF/B-VII.1

For the Rossi-α (ENDF/B-VII.1) benchmarks, the benchmark data and calculation results are plotted in Fig. 74 as C/E ratios with individual values listed in Table 30.

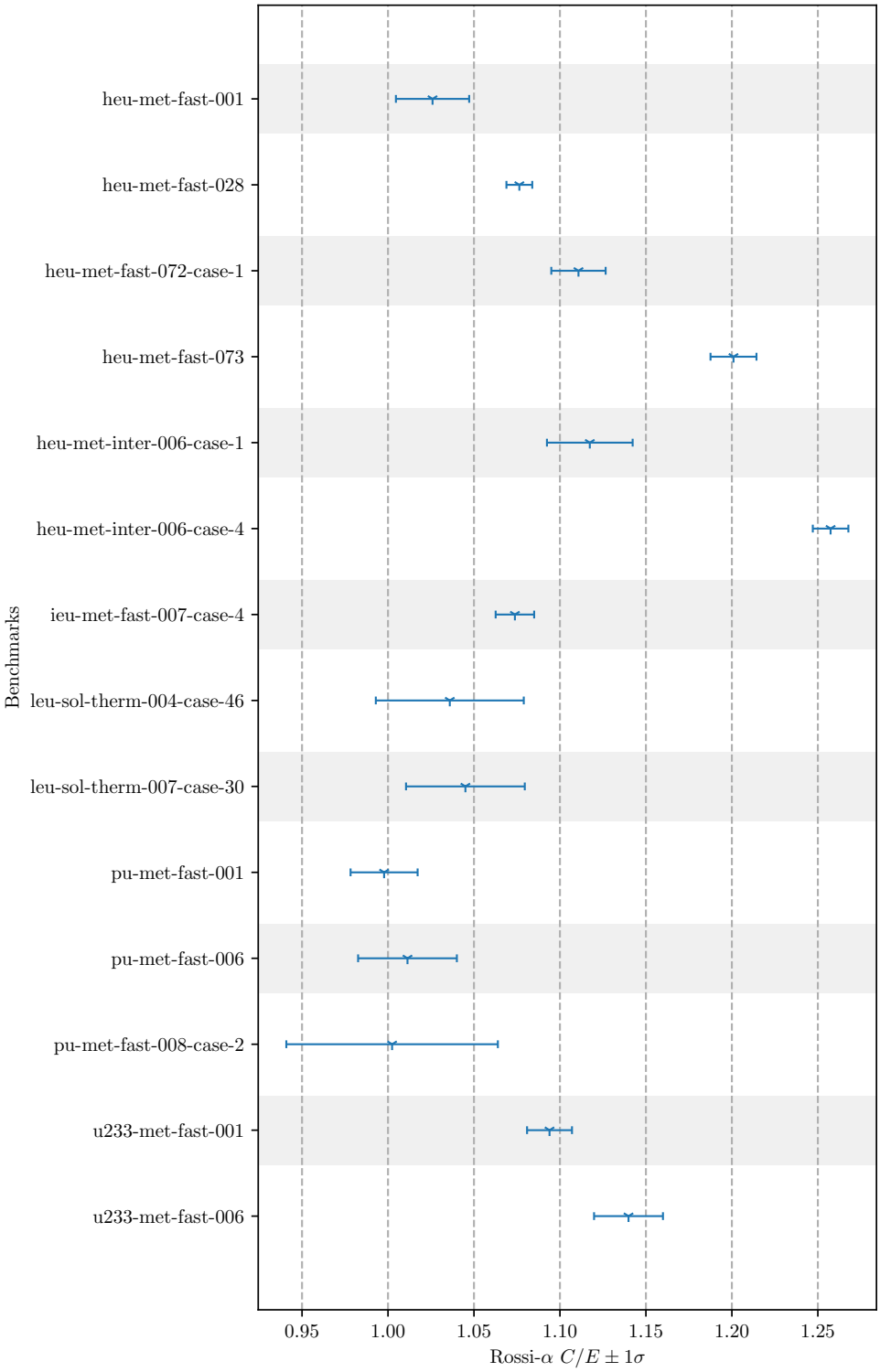

Figure 72: Rossi-α C/E (ENDF/B-VI.6) Benchmark Results

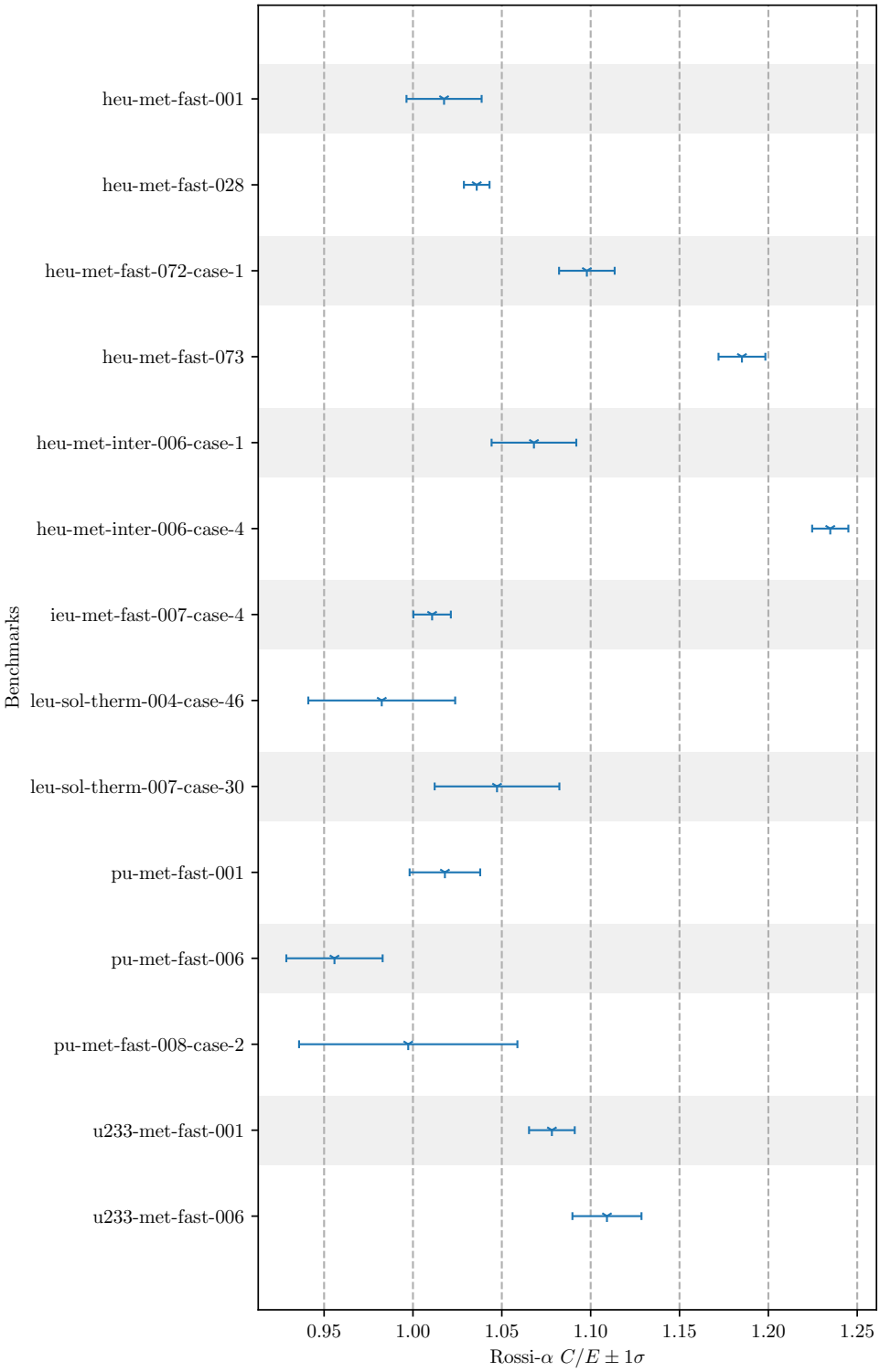

Figure 73: Rossi-α C/E (ENDF/B-VII.0) Benchmark Results

Table 29: Rossi-α (ENDF/B-VII.0) Benchmark Results

	Exp. Rossi-α (s^{-1})	Exp. unc.	Calc. Rossi-α (s^{-1})	Calc. unc.
heu-met-fast-001	-1.1100×10^6	2.00×10^4	-1.1294×10^6	1.17×10^4
heu-met-fast-028	-3.8200×10^5	2.00×10^3	-3.9571×10^5	1.81×10^3
heu-met-fast-072-case-1	-3.7266×10^4	4.77×10^2	-4.0913×10^4	2.56×10^2
heu-met-fast-073	-8.9910×10^4	8.17×10^2	-1.0656×10^5	6.83×10^2
heu-met-inter-006-case-1	-3.3810×10^3	7.40×10^1	-3.6112×10^3	1.58×10^1
heu-met-inter-006-case-4	-2.6190×10^4	1.82×10^2	-3.2340×10^4	1.43×10^2
ieu-met-fast-007-case-4	-1.1700×10^5	1.00×10^3	-1.1826×10^5	7.07×10^2
leu-sol-therm-004-case-46	-1.0620×10^2	3.70	-1.0433×10^2	2.46
leu-sol-therm-007-case-30	-1.2680×10^2	2.90	-1.3280×10^2	3.25
pu-met-fast-001	-6.4000×10^5	1.00×10^4	-6.5150×10^5	7.61×10^3
pu-met-fast-006	-2.1400×10^5	5.00×10^3	-2.0455×10^5	3.28×10^3
pu-met-fast-008-case-2	-1.9700×10^5	1.00×10^4	-1.9648×10^5	6.86×10^3
u233-met-fast-001	-1.0000×10^6	1.00×10^4	-1.0782×10^6	7.01×10^3
u233-met-fast-006	-2.7100×10^5	3.00×10^3	-3.0058×10^5	4.08×10^3

Table 30: Rossi-α (ENDF/B-VII.1) Benchmark Results

	Exp. Rossi-α (s^{-1})	Exp. unc.	Calc. Rossi-α (s^{-1})	Calc. unc.
heu-met-fast-001	-1.1100×10^6	2.00×10^4	-1.1319×10^6	1.17×10^4
heu-met-fast-028	-3.8200×10^5	2.00×10^3	-3.9598×10^5	1.82×10^3
heu-met-fast-072-case-1	-3.7266×10^4	4.77×10^2	-4.1936×10^4	2.60×10^2
heu-met-fast-073	-8.9910×10^4	8.17×10^2	-1.0889×10^5	6.96×10^2
heu-met-inter-006-case-1	-3.3810×10^3	7.40×10^1	-3.6086×10^3	1.58×10^1
heu-met-inter-006-case-4	-2.6190×10^4	1.82×10^2	-3.2352×10^4	1.44×10^2
ieu-met-fast-007-case-4	-1.1700×10^5	1.00×10^3	-1.1802×10^5	7.06×10^2
leu-sol-therm-004-case-46	-1.0620×10^2	3.70	-1.0586×10^2	2.49
leu-sol-therm-007-case-30	-1.2680×10^2	2.90	-1.2048×10^2	2.98
pu-met-fast-001	-6.4000×10^5	1.00×10^4	-6.3207×10^5	7.47×10^3
pu-met-fast-006	-2.1400×10^5	5.00×10^3	-2.0479×10^5	3.34×10^3
pu-met-fast-008-case-2	-1.9700×10^5	1.00×10^4	-2.0254×10^5	7.32×10^3
u233-met-fast-001	-1.0000×10^6	1.00×10^4	-1.0656×10^6	7.03×10^3
u233-met-fast-006	-2.7100×10^5	3.00×10^3	-2.9416×10^5	4.08×10^3

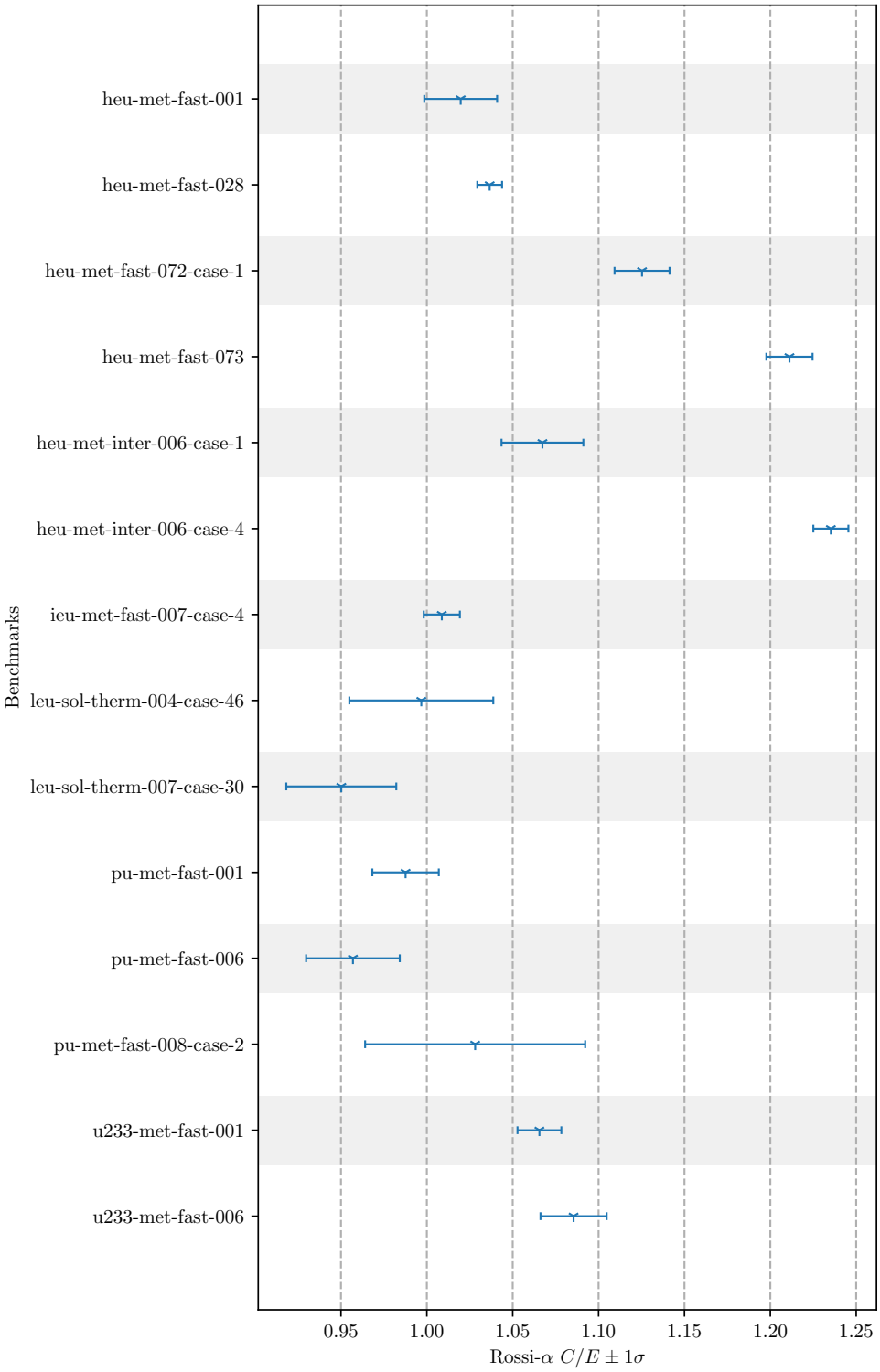

Figure 74: Rossi-α C/E (ENDF/B-VII.1) Benchmark Results

Table 31: Rossi-α (ENDF/B-VIII.0) Benchmark Results

	Exp. Rossi-α (s^{-1})	Exp. unc.	Calc. Rossi-α (s^{-1})	Calc. unc.
heu-met-fast-001	-1.1100×10^6	2.00×10^4	-1.1432×10^6	1.18×10^4
heu-met-fast-028	-3.8200×10^5	2.00×10^3	-4.0089×10^5	1.84×10^3
heu-met-fast-072-case-1	-3.7266×10^4	4.77×10^2	-4.1074×10^4	2.57×10^2
heu-met-fast-073	-8.9910×10^4	8.17×10^2	-1.0488×10^5	6.73×10^2
heu-met-inter-006-case-1	-3.3810×10^3	7.40×10^1	-3.6753×10^3	1.61×10^1
heu-met-inter-006-case-4	-2.6190×10^4	1.82×10^2	-3.1513×10^4	1.40×10^2
ieu-met-fast-007-case-4	-1.1700×10^5	1.00×10^3	-1.1942×10^5	7.13×10^2
leu-sol-therm-004-case-46	-1.0620×10^2	3.70	-1.0743×10^2	2.48
leu-sol-therm-007-case-30	-1.2680×10^2	2.90	-1.2121×10^2	2.96
pu-met-fast-001	-6.4000×10^5	1.00×10^4	-6.5631×10^5	7.67×10^3
pu-met-fast-006	-2.1400×10^5	5.00×10^3	-2.1127×10^5	3.36×10^3
pu-met-fast-008-case-2	-1.9700×10^5	1.00×10^4	-2.1057×10^5	7.39×10^3
u233-met-fast-001	-1.0000×10^6	1.00×10^4	-1.0883×10^6	7.13×10^3
u233-met-fast-006	-2.7100×10^5	3.00×10^3	-2.9376×10^5	4.09×10^3

4.6.4 ENDF/B-VIII.0

For the Rossi-α (ENDF/B-VIII.0) benchmarks, the benchmark data and calculation results are plotted in Fig. 75 as C/E ratios with individual values listed in Table 31.

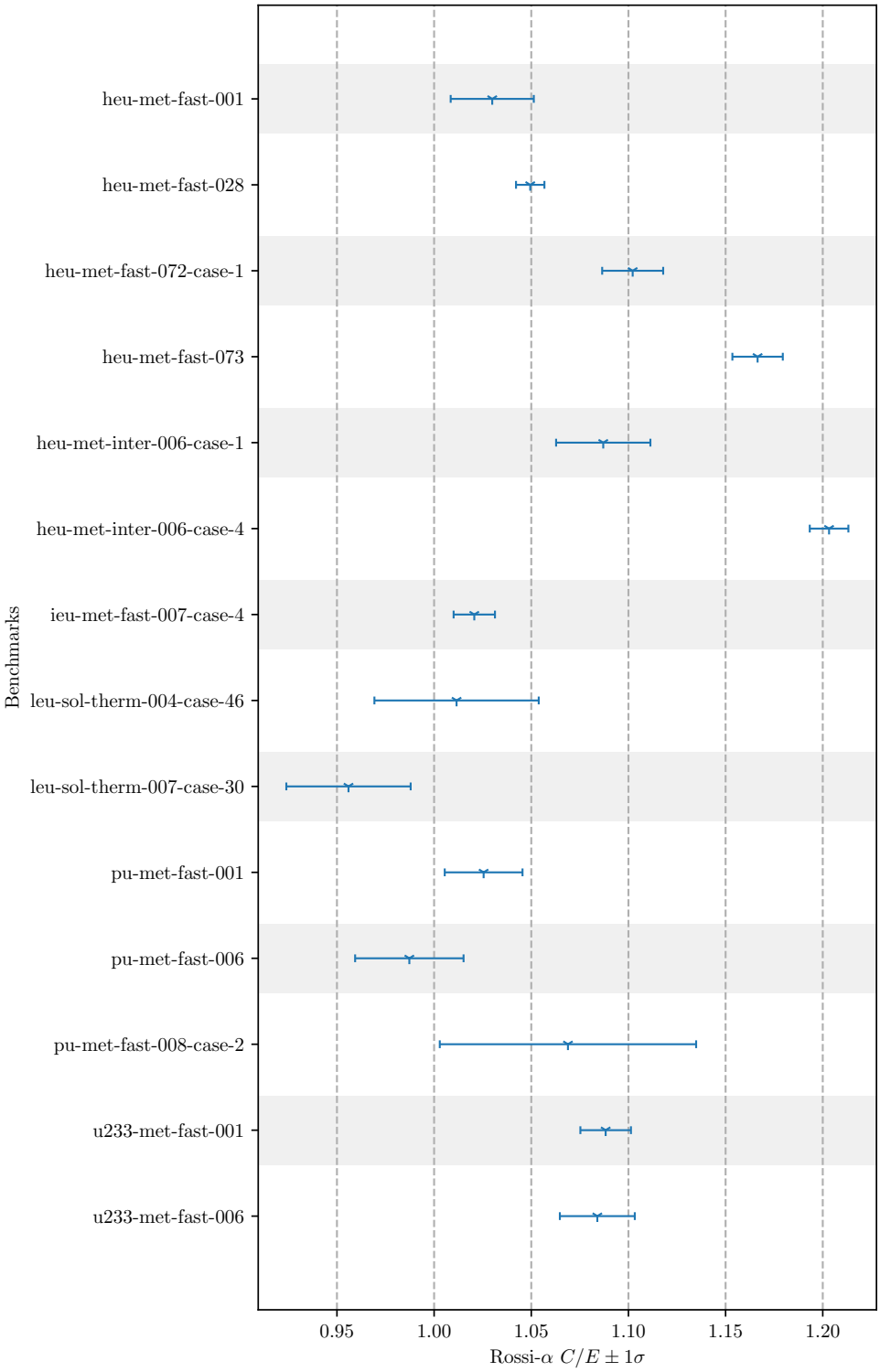

Figure 75: Rossi-α C/E (ENDF/B-VIII.0) Benchmark Results

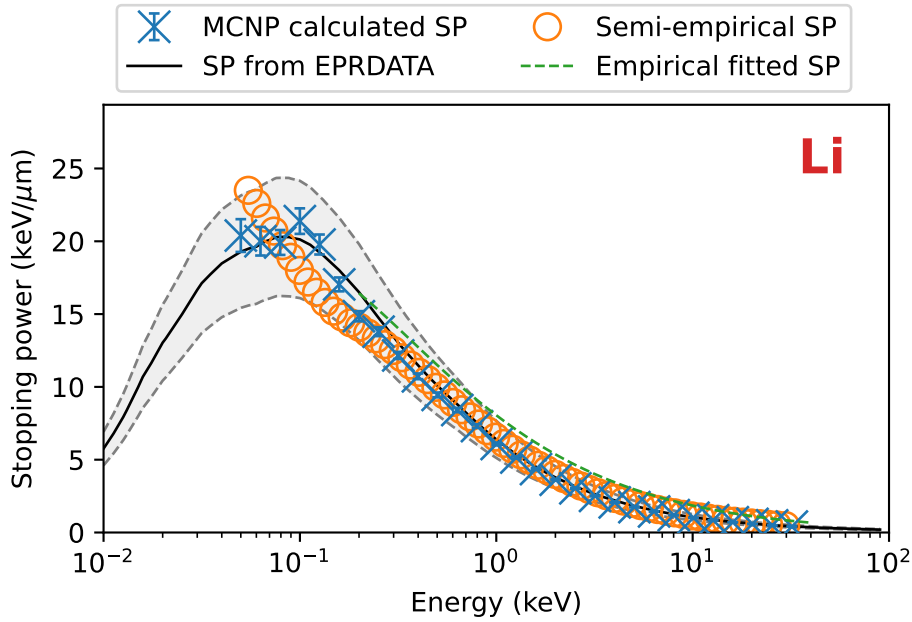

Figure 76: Stopping power results and benchmarks for lithium.

4.7 Electron Stopping Power

Each benchmark problem compares the semi-empirical data computed from experimental electron energy loss functions (ELF) measurements to calculated results using the single event electron transport algorithm using the electron-photon-relaxation data library EPRDATA14 [41]. This test suite executes 1 input per thread using a total of 60 threads, with a total Slurm allocation of no more than 10 minutes. An example `VnV.py` execution line is `./VnV.py execute_slurm -N electron_stopping -j 60 time 10 wait`.

The following figures and tables are results for the Electron Stopping Power Validation Suite. The plots display the calculated and semi-empirical electron stopping powers and their uncertainties, along with stopping powers computed from direct integration of the EPRDATA cross sections and/or an empirical fitting formula where available.

4.7.1 Elements

For the validation electron stopping benchmarks the benchmark data and calculation results for elements are plotted in Figs. 76 through 113. Mean percentage deviation (MPD) data for these benchmarks are plotted in Fig. 114 and in Tab. 32.

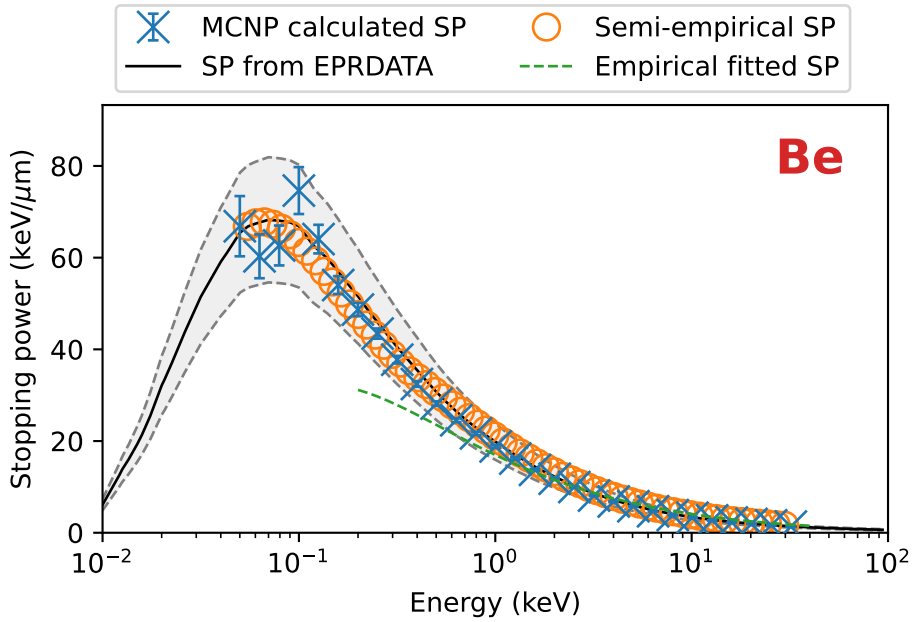

Figure 77: Stopping power results and benchmarks for beryllium.

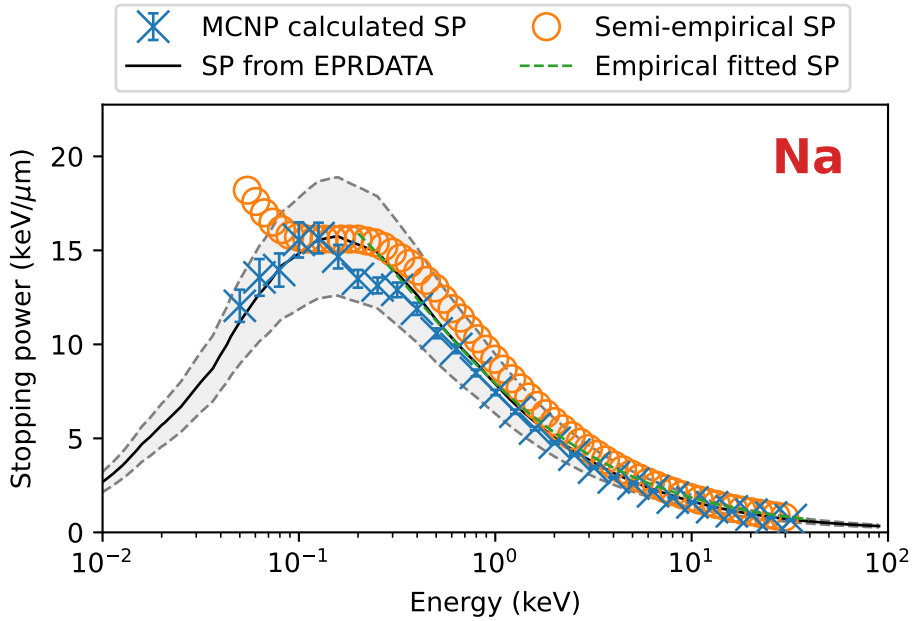

Figure 78: Stopping power results and benchmarks for sodium.

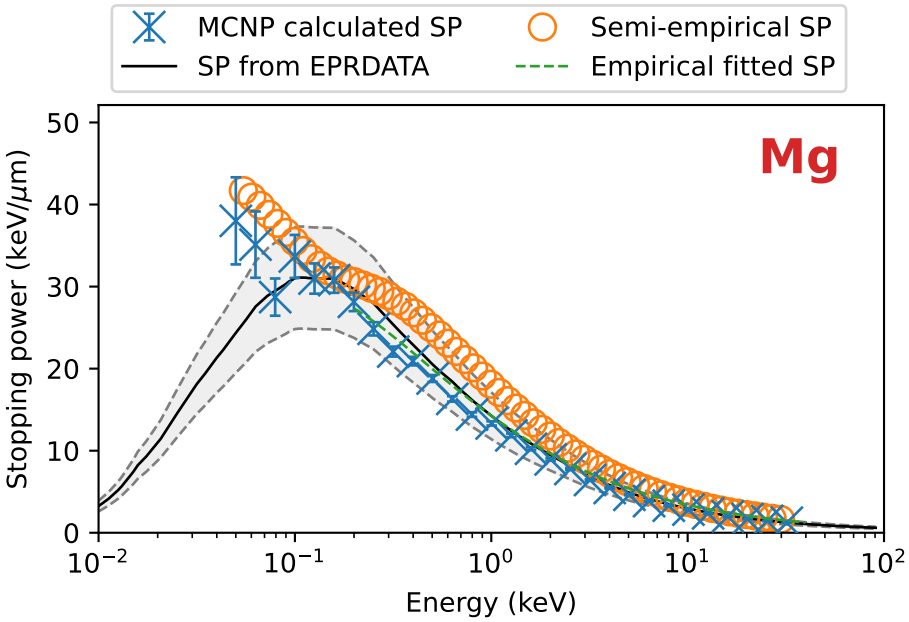

Figure 79: Stopping power results and benchmarks for magnesium.

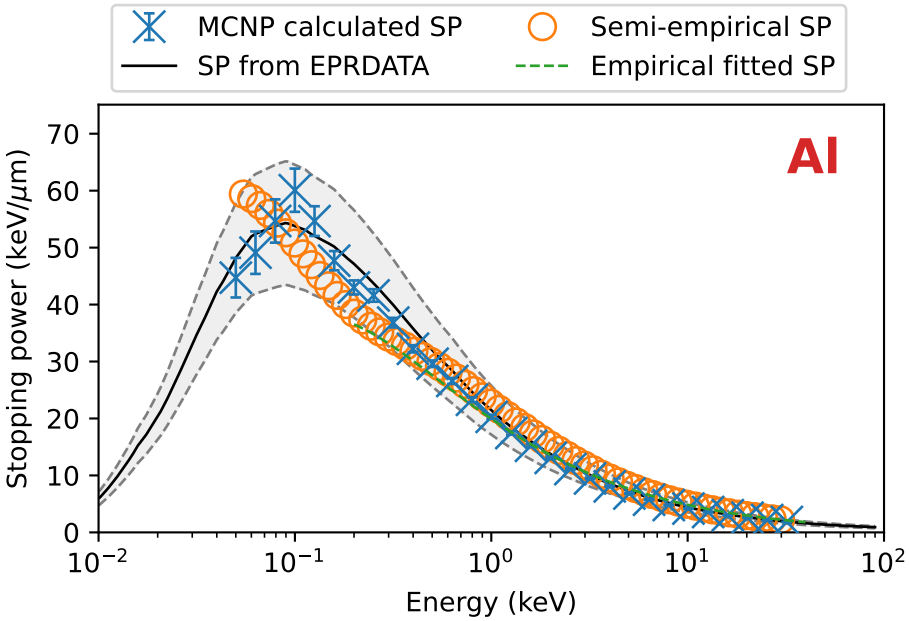

Figure 80: Stopping power results and benchmarks for aluminum.

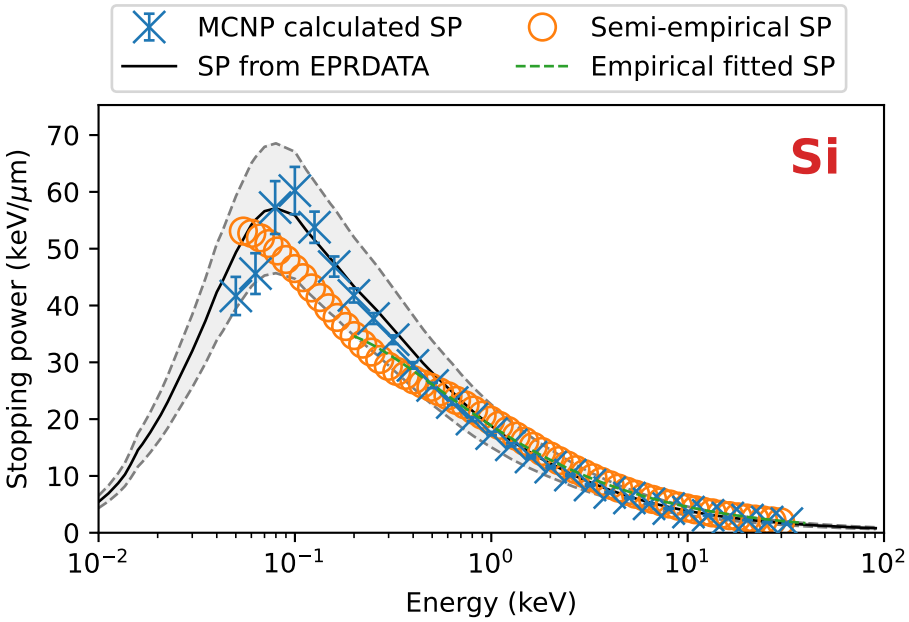

Figure 81: Stopping power results and benchmarks for silicon.

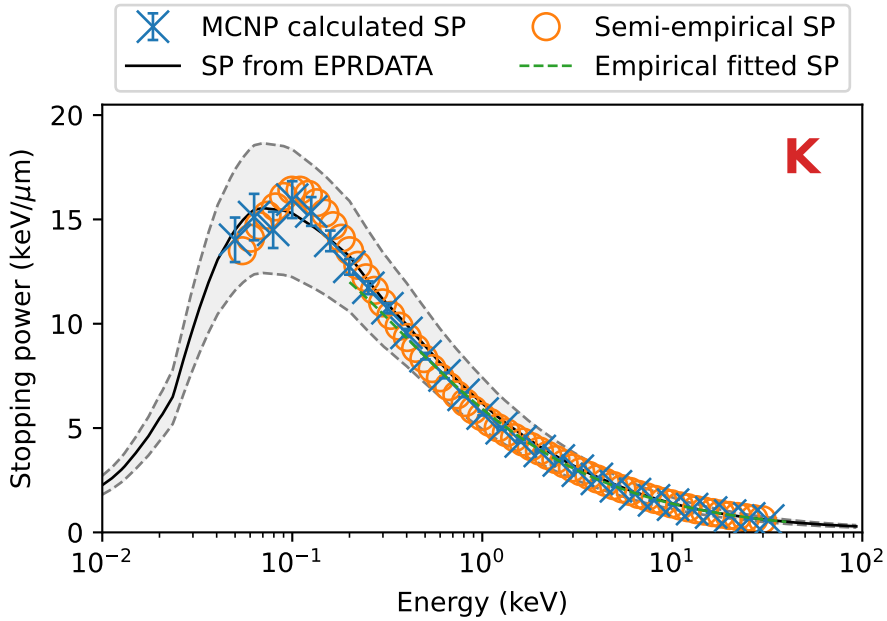

Figure 82: Stopping power results and benchmarks for potassium.

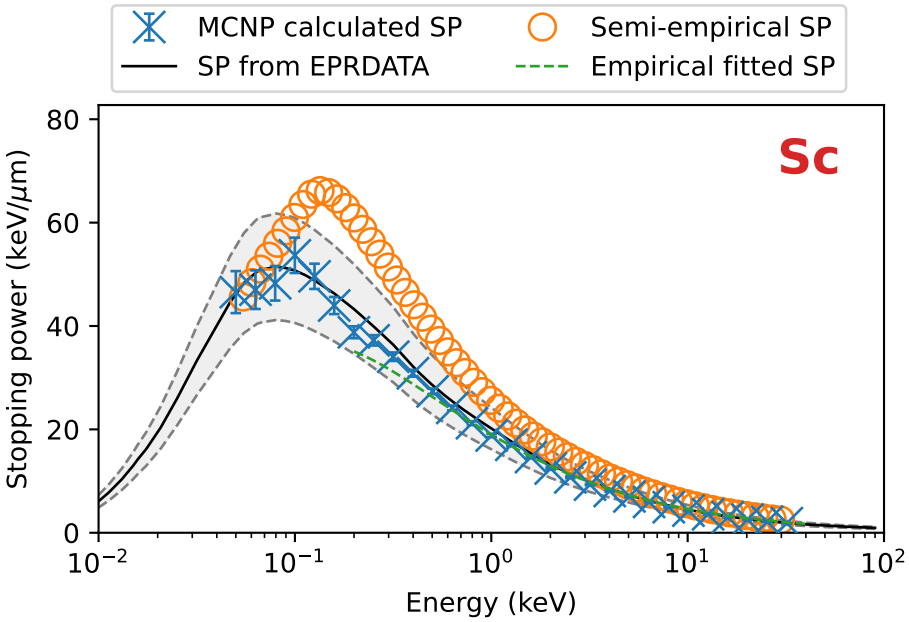

Figure 83: Stopping power results and benchmarks for scandium.

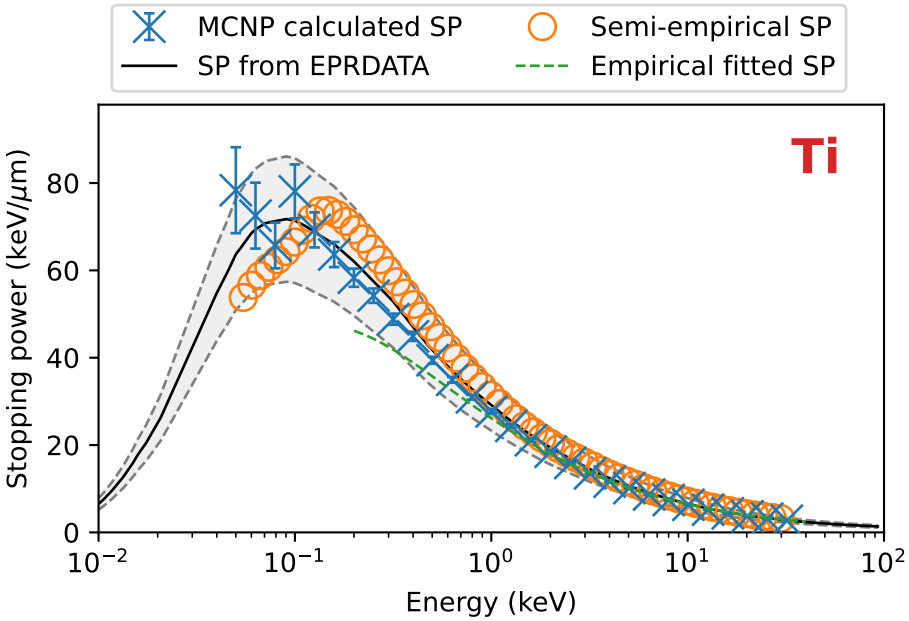

Figure 84: Stopping power results and benchmarks for titanium.

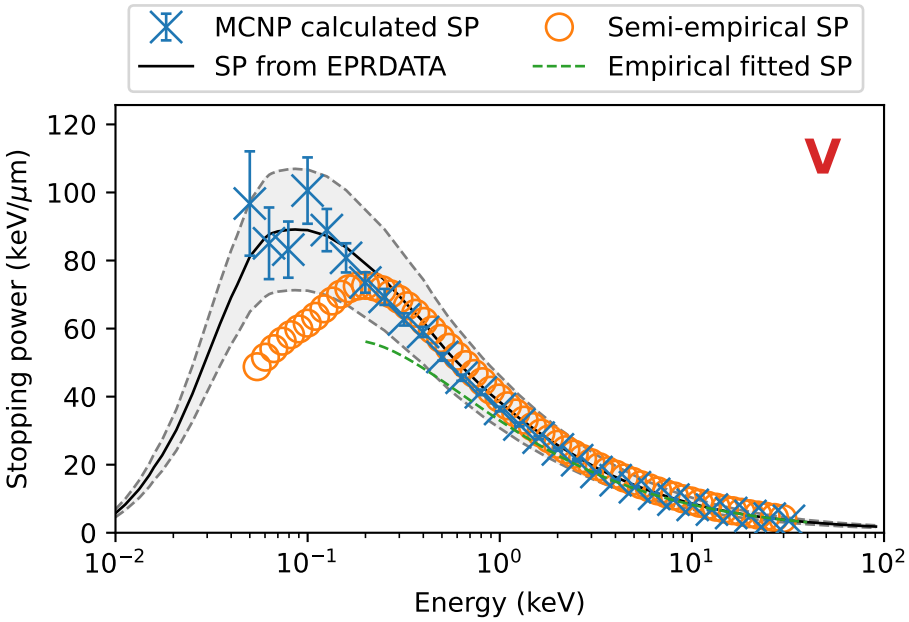

Figure 85: Stopping power results and benchmarks for vanadium.

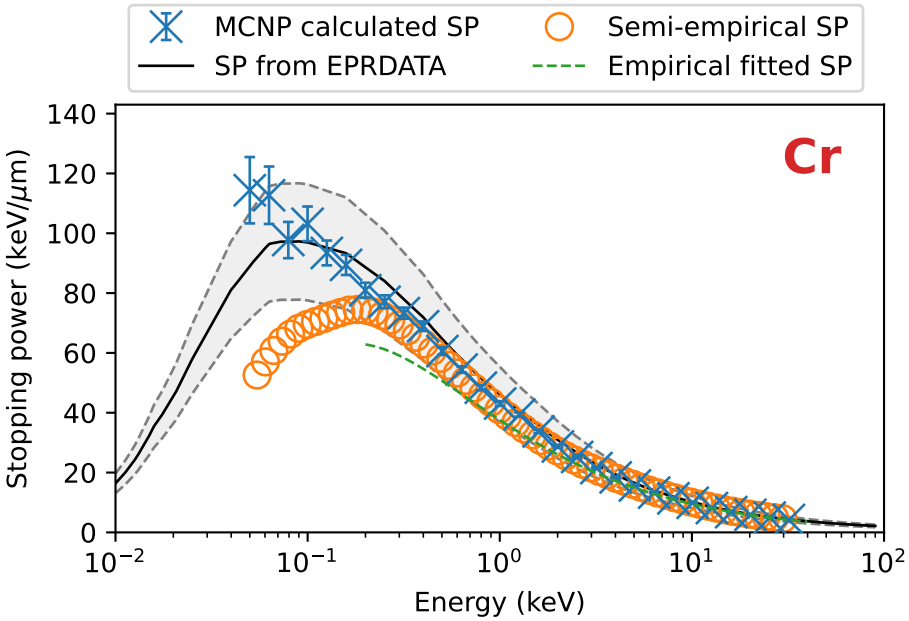

Figure 86: Stopping power results and benchmarks for chromium.

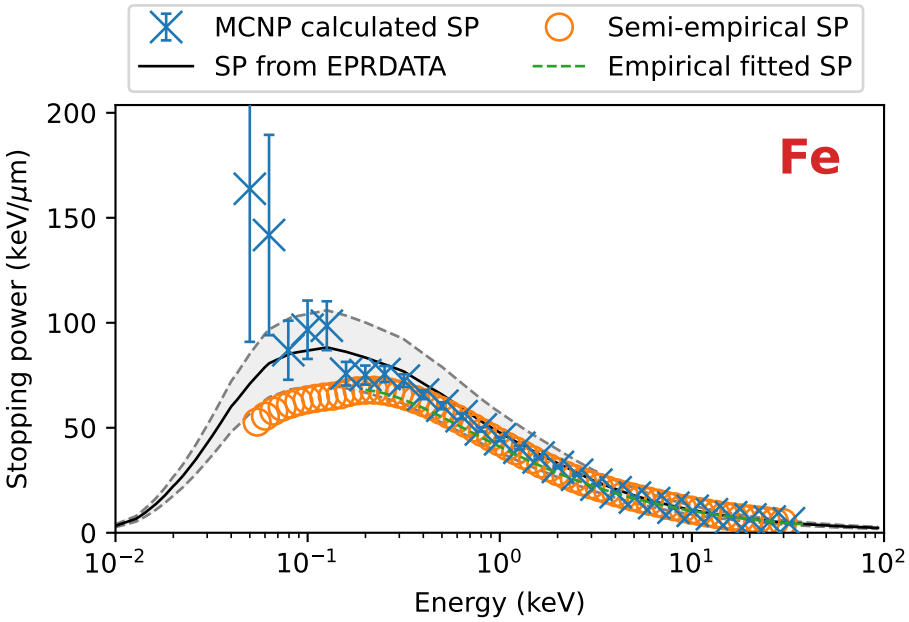

Figure 87: Stopping power results and benchmarks for iron.

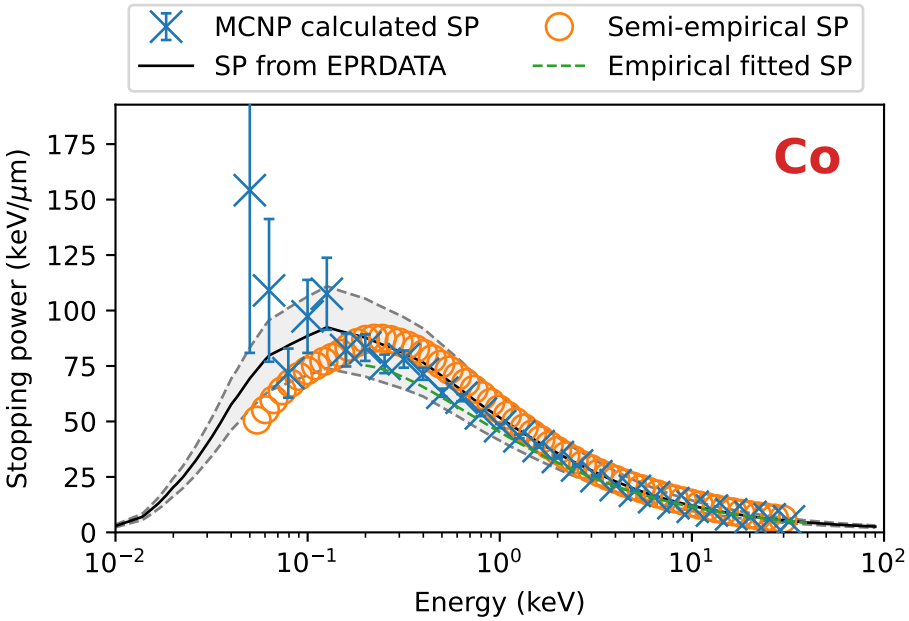

Figure 88: Stopping power results and benchmarks for cobalt.

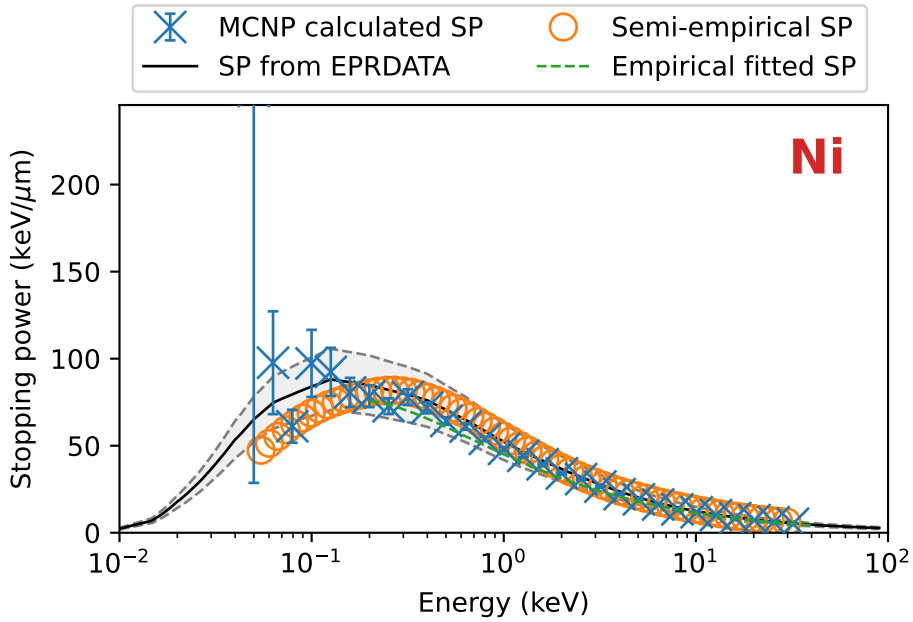

Figure 89: Stopping power results and benchmarks for nickel.

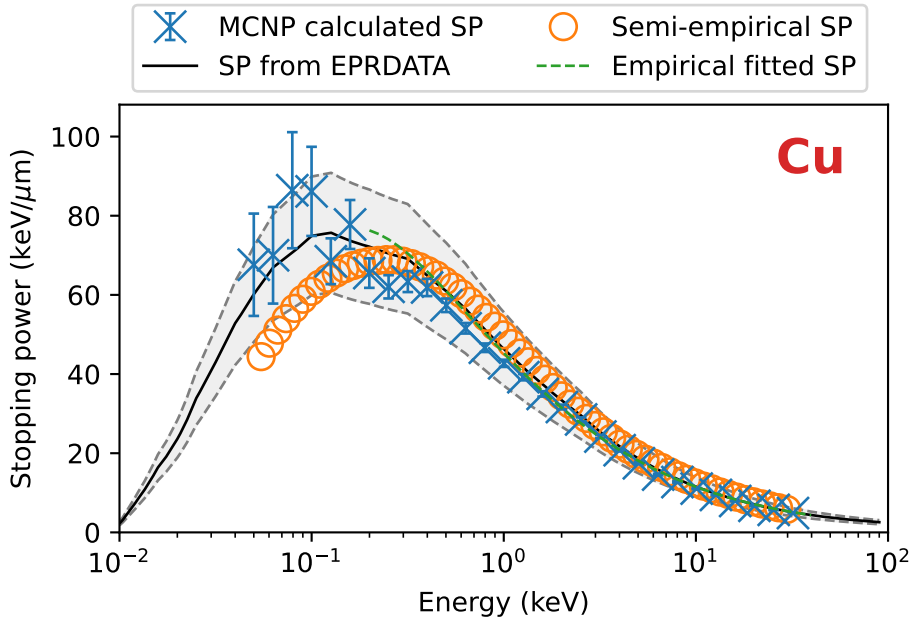

Figure 90: Stopping power results and benchmarks for copper.

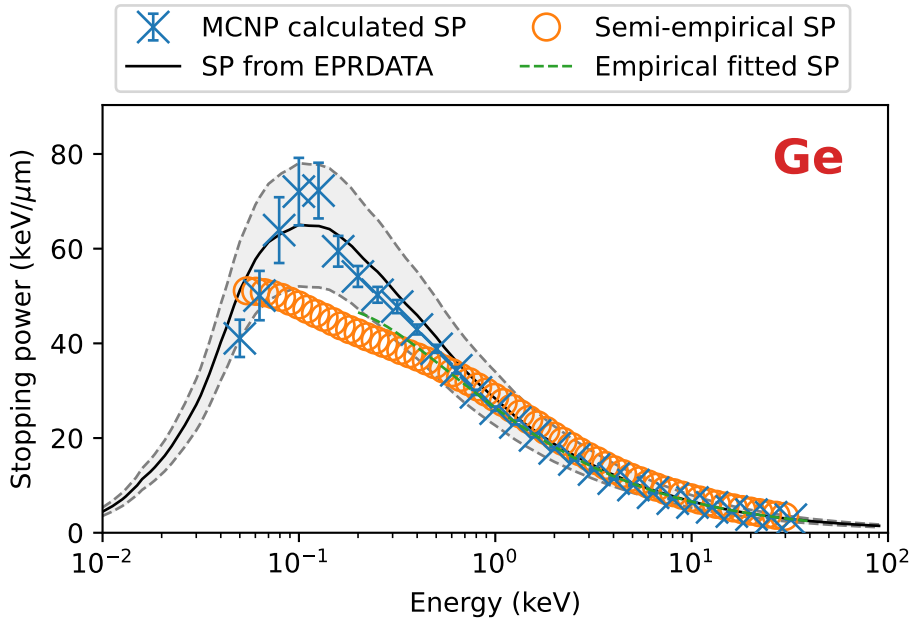

Figure 91: Stopping power results and benchmarks for germanium.

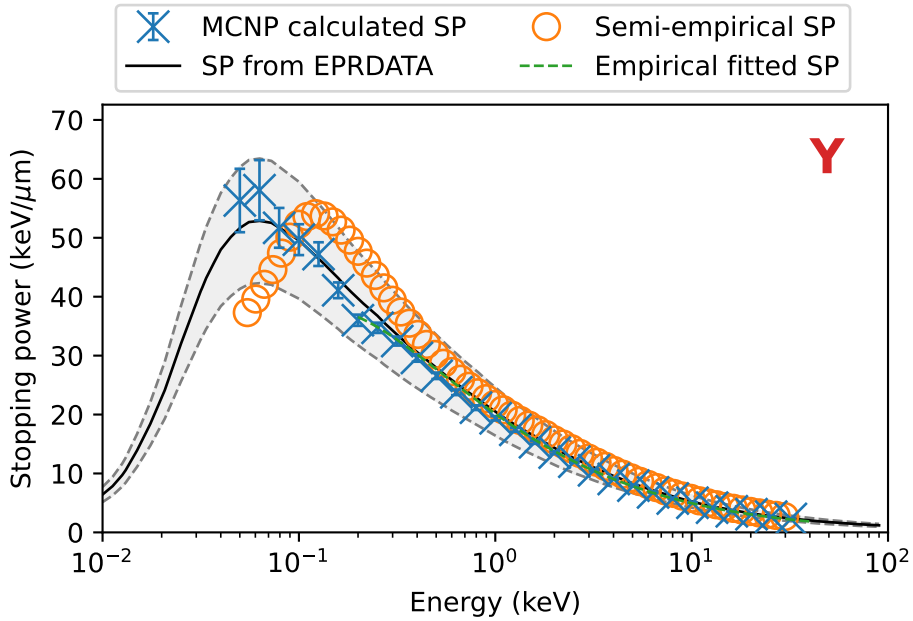

Figure 92: Stopping power results and benchmarks for yttrium.

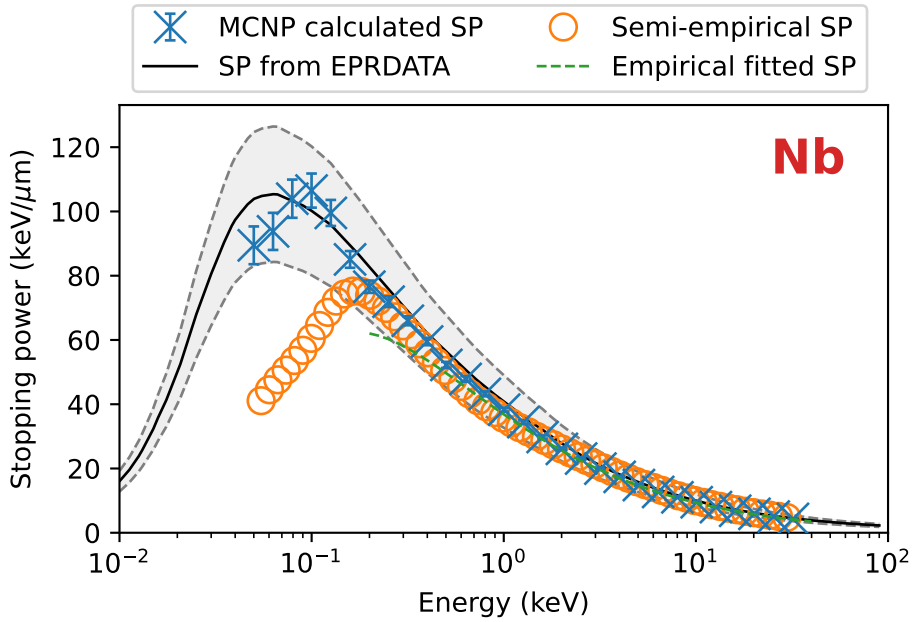

Figure 93: Stopping power results and benchmarks for niobium.

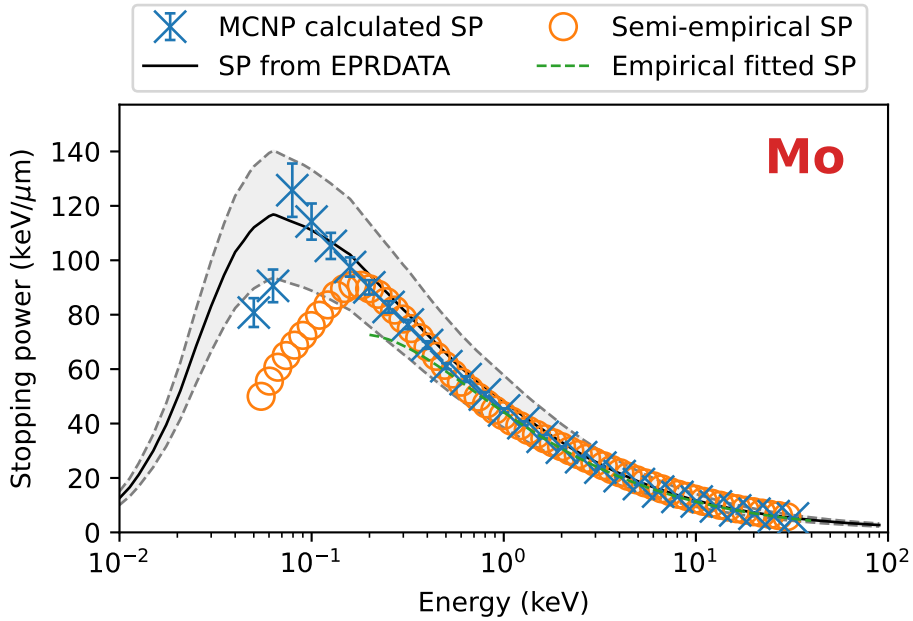

Figure 94: Stopping power results and benchmarks for molybdenum.

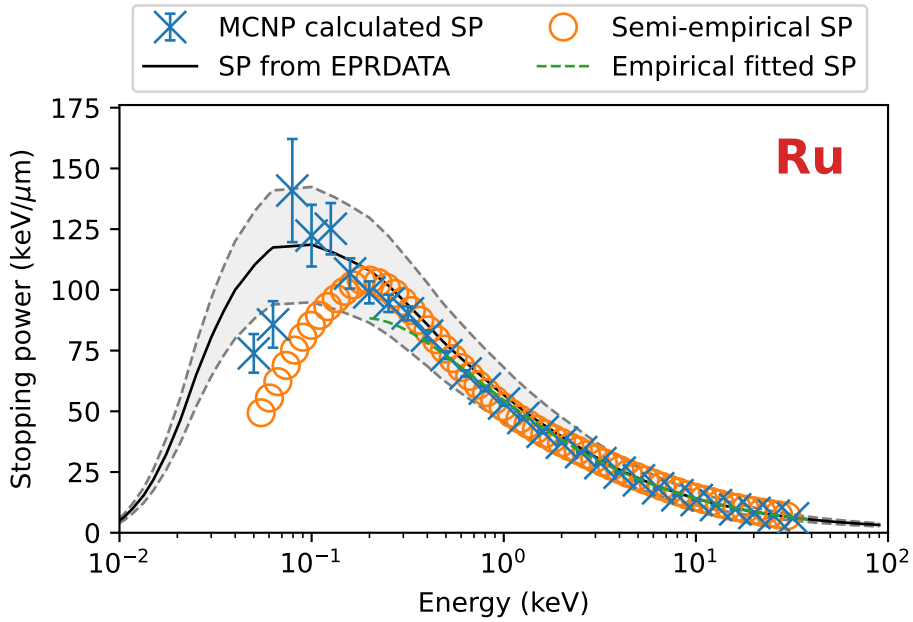

Figure 95: Stopping power results and benchmarks for ruthenium.

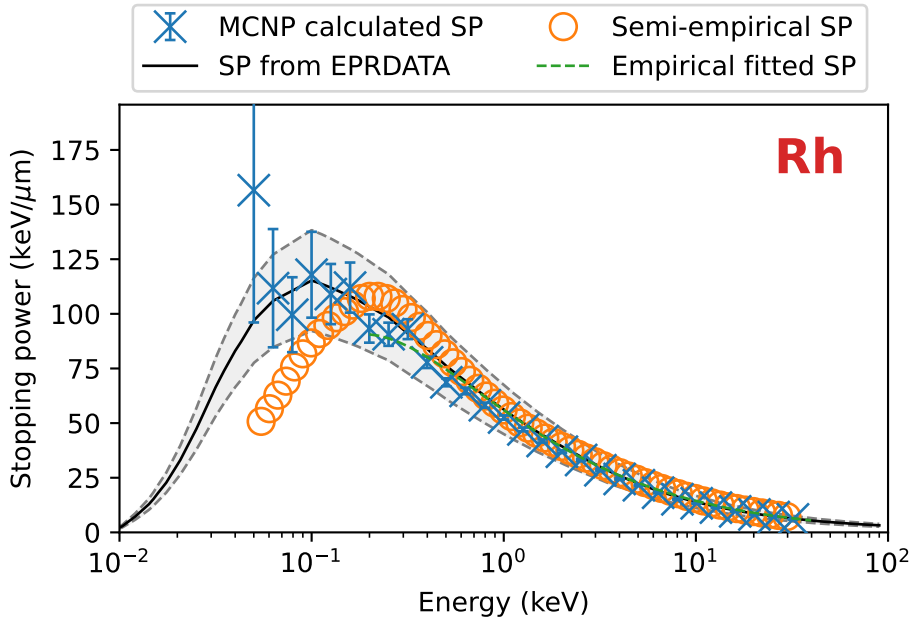

Figure 96: Stopping power results and benchmarks for rhodium.

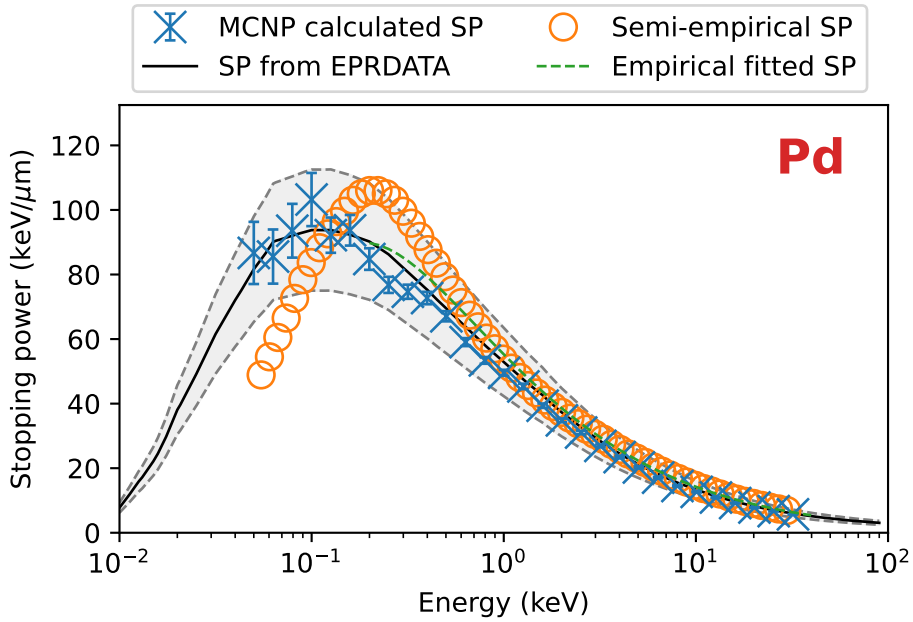

Figure 97: Stopping power results and benchmarks for palladium.

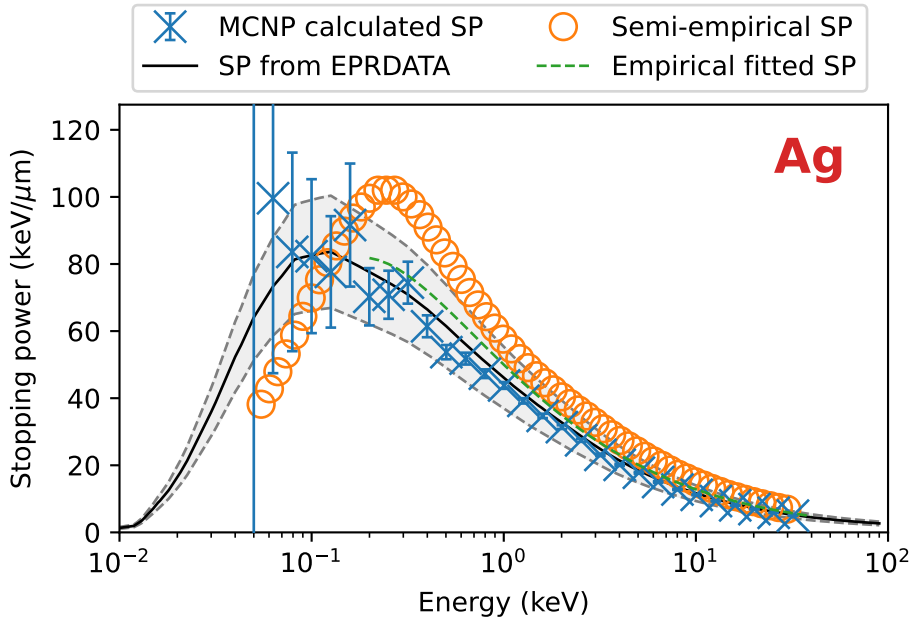

Figure 98: Stopping power results and benchmarks for silver.

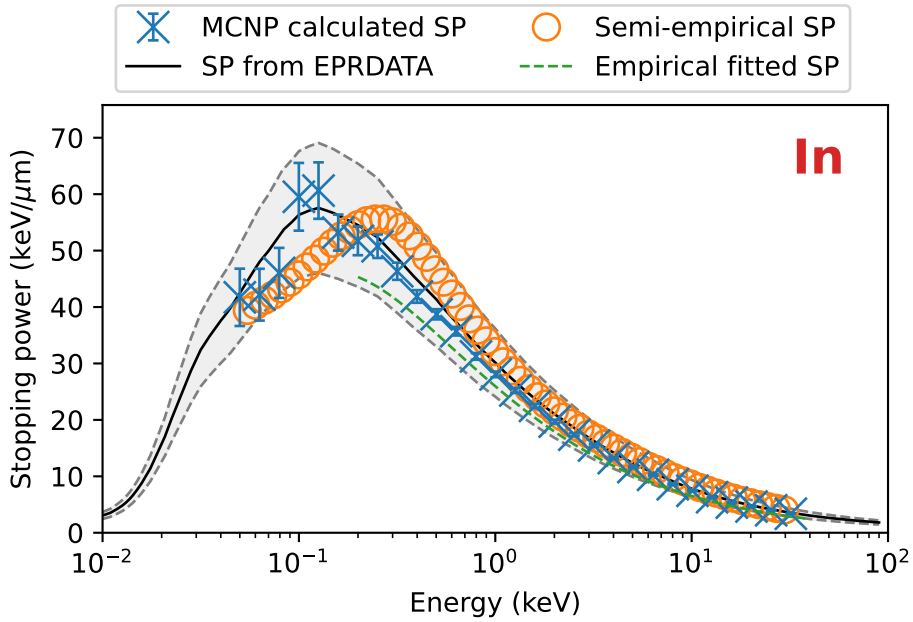

Figure 99: Stopping power results and benchmarks for indium.

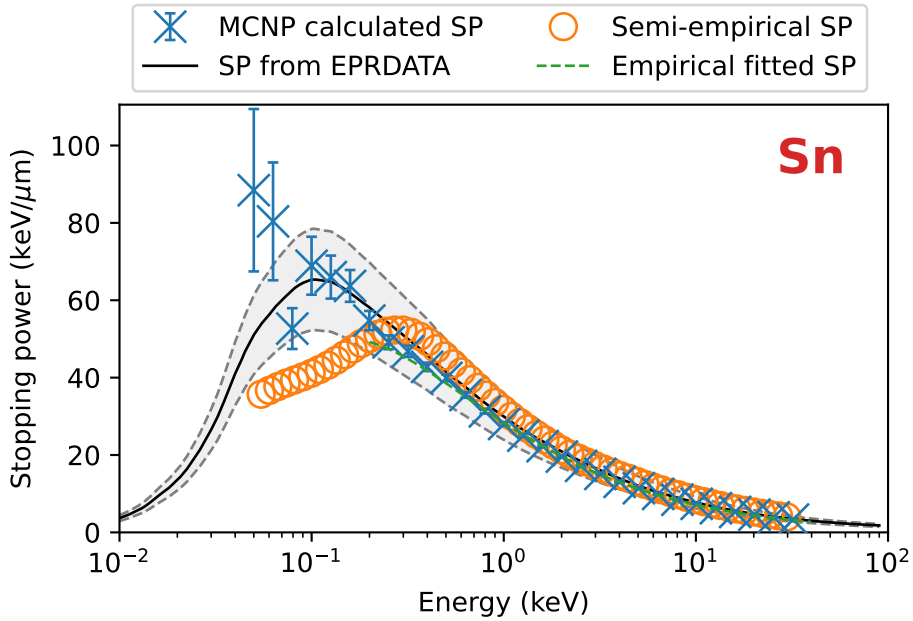

Figure 100: Stopping power results and benchmarks for tin.

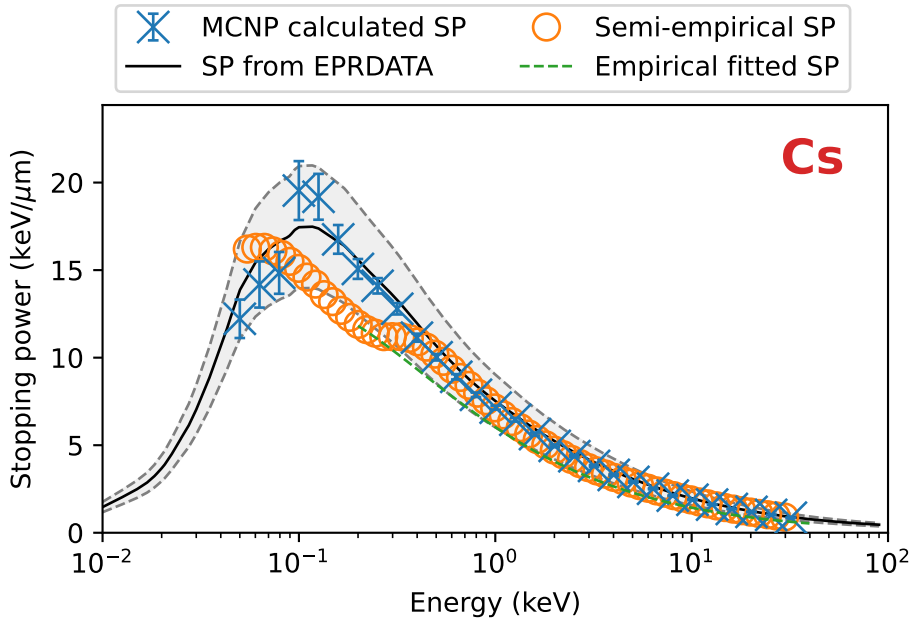

Figure 101: Stopping power results and benchmarks for cesium.

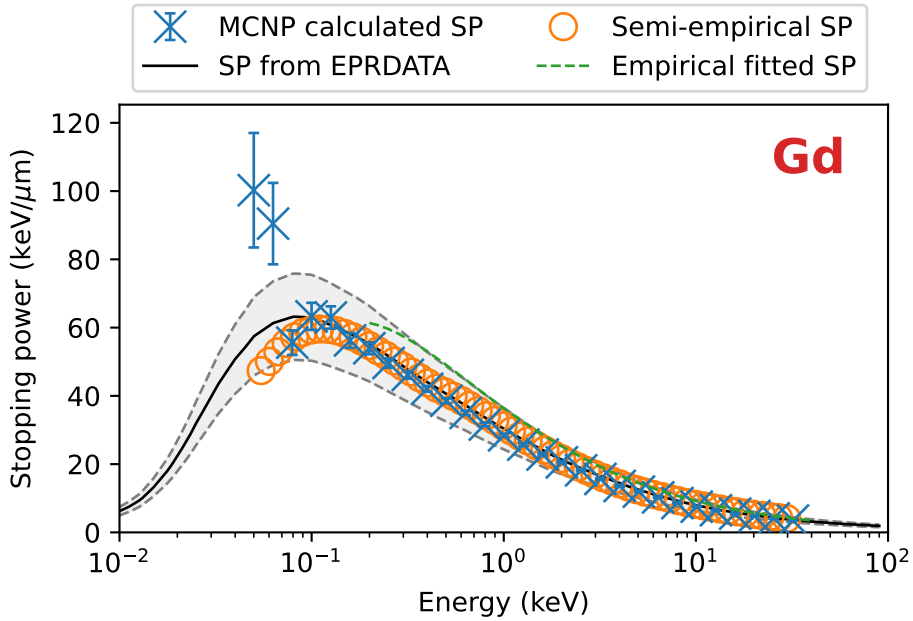

Figure 102: Stopping power results and benchmarks for gadolinium.

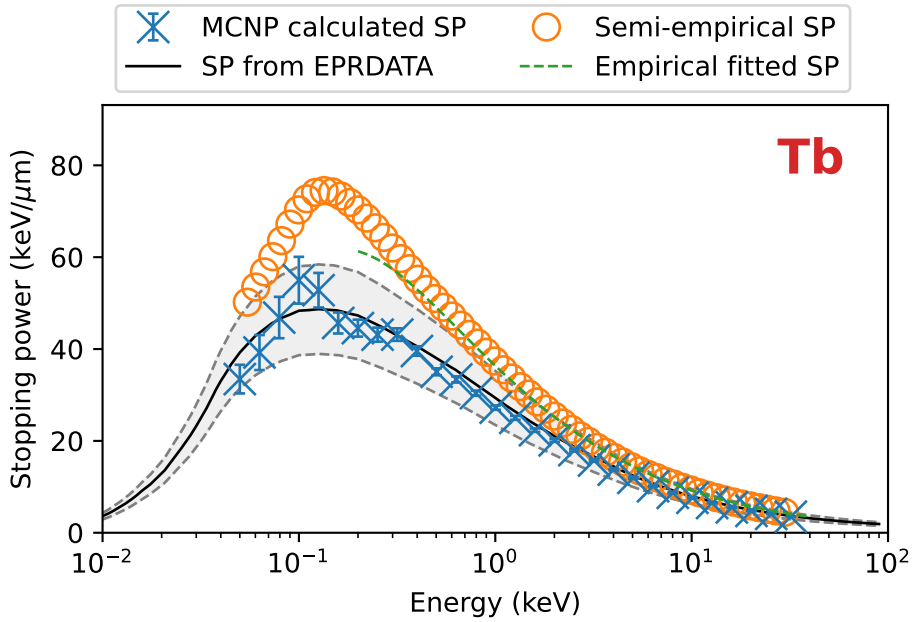

Figure 103: Stopping power results and benchmarks for terbium.

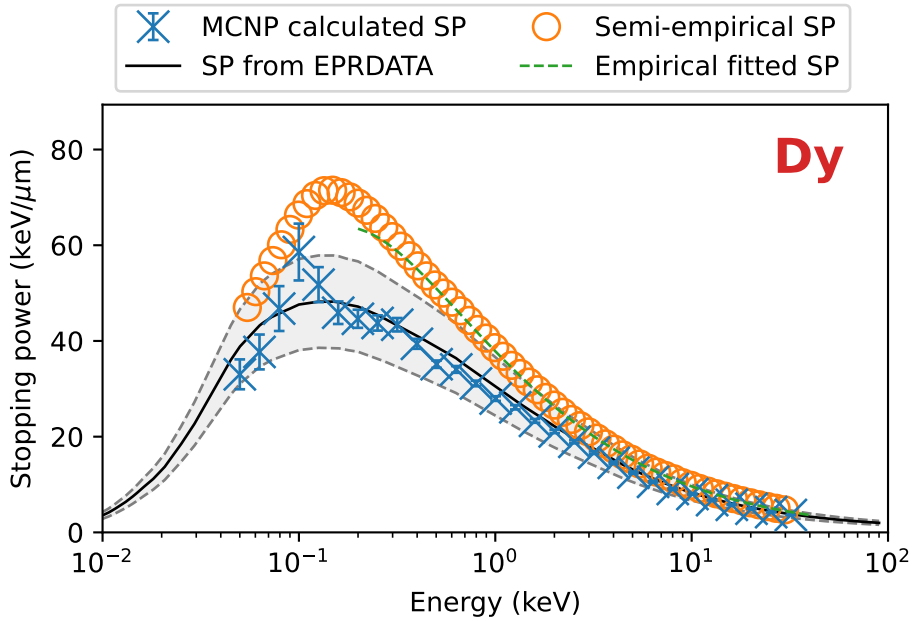

Figure 104: Stopping power results and benchmarks for dysprosium.

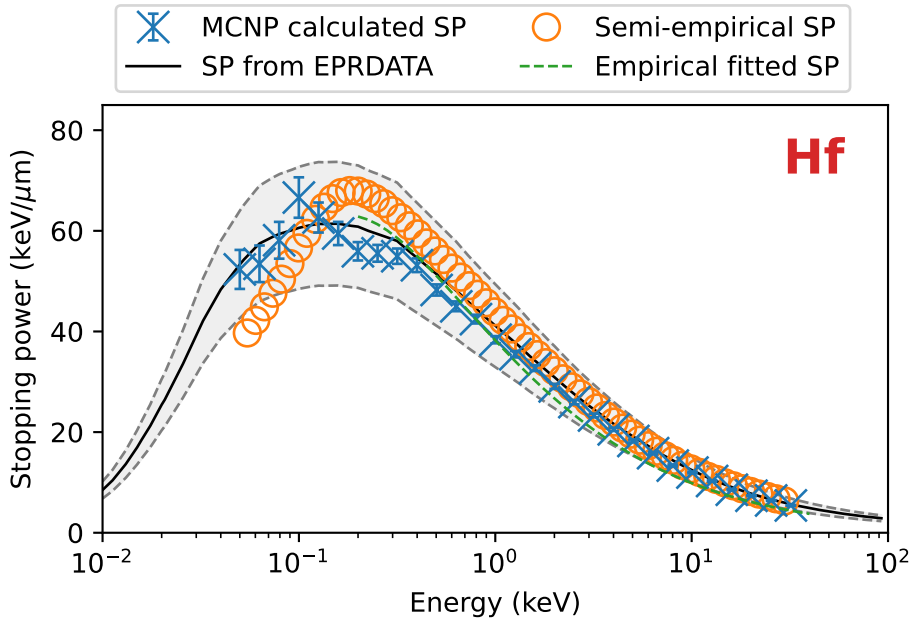

Figure 105: Stopping power results and benchmarks for hafnium.

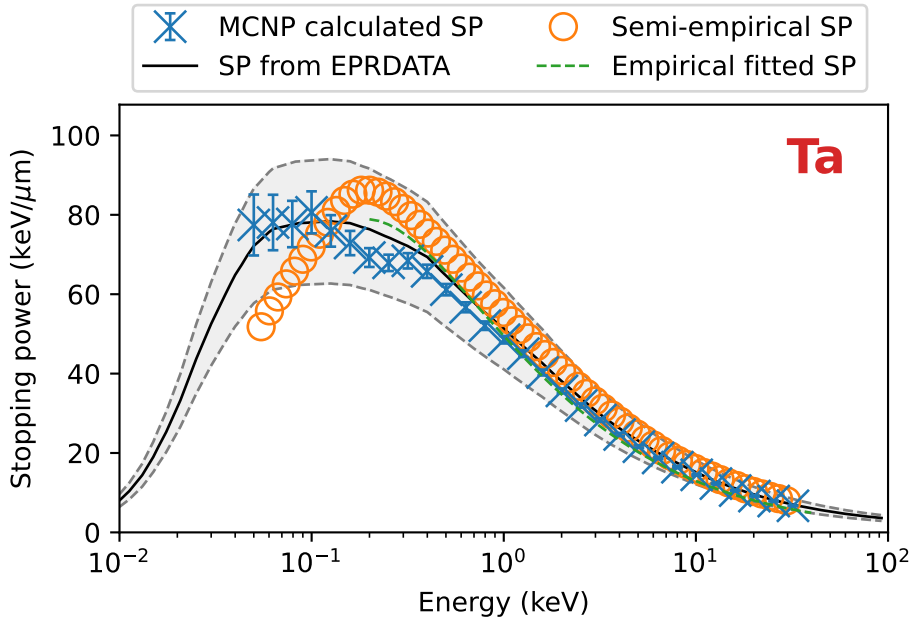

Figure 106: Stopping power results and benchmarks for tantalum.

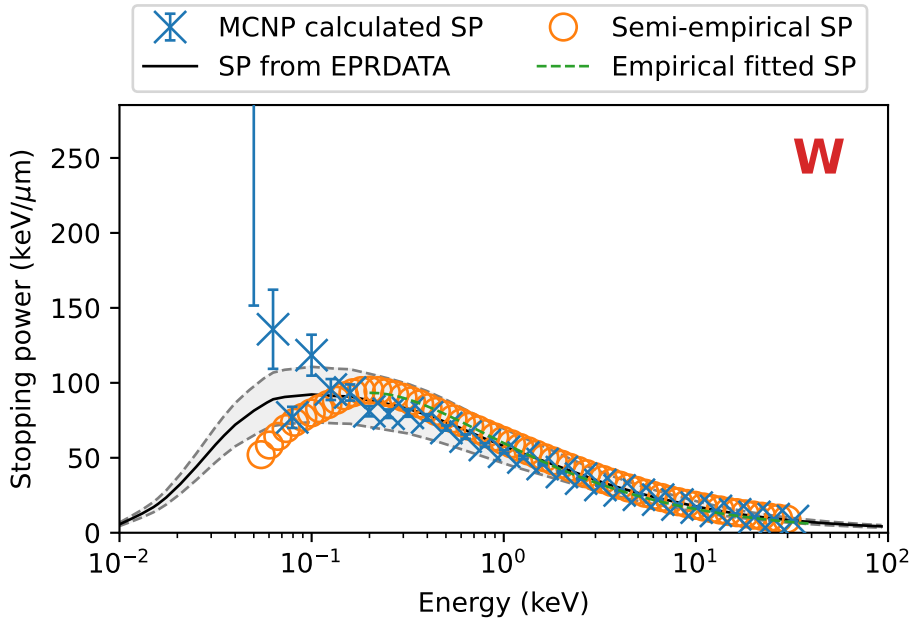

Figure 107: Stopping power results and benchmarks for tungsten.

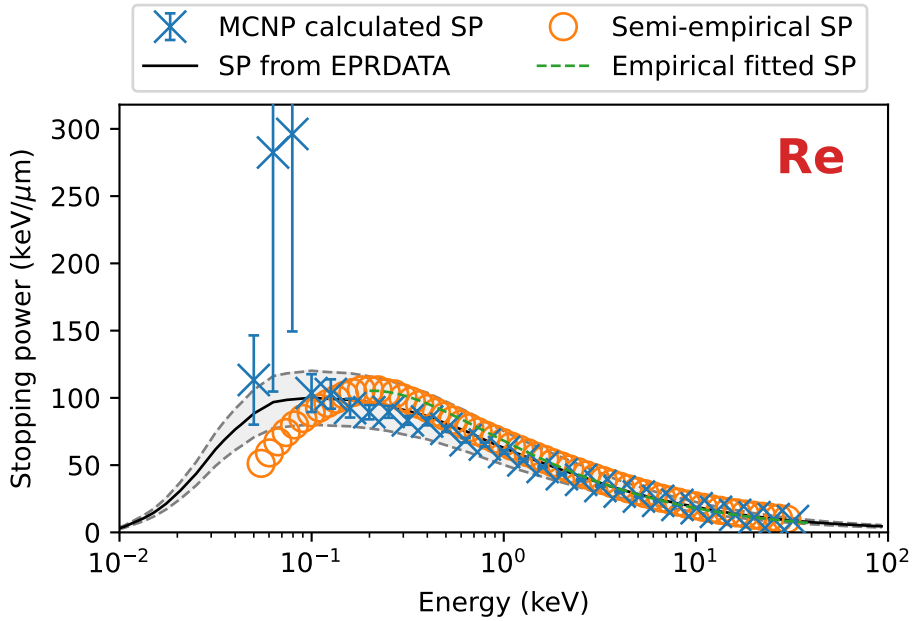

Figure 108: Stopping power results and benchmarks for rhenium.

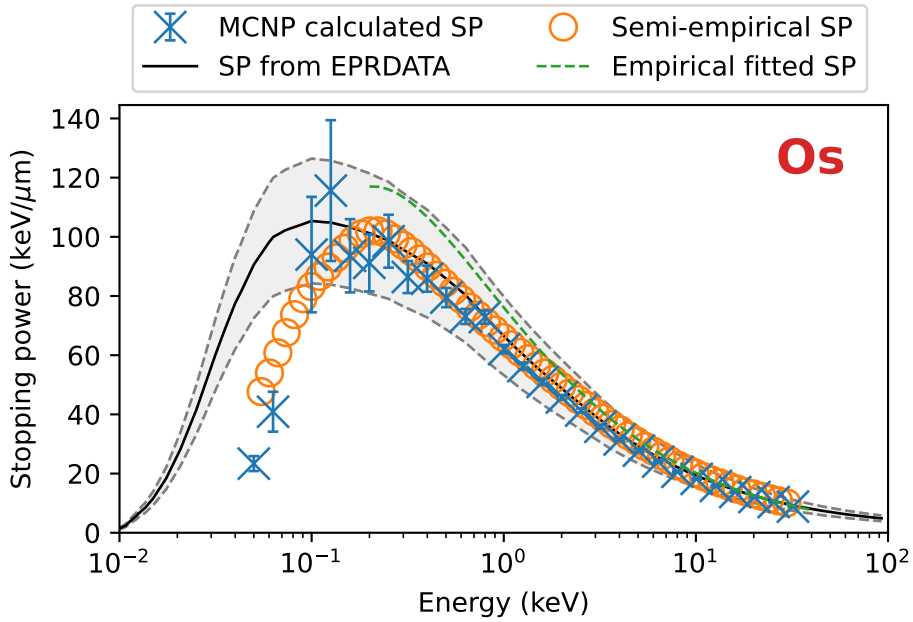

Figure 109: Stopping power results and benchmarks for osmium.

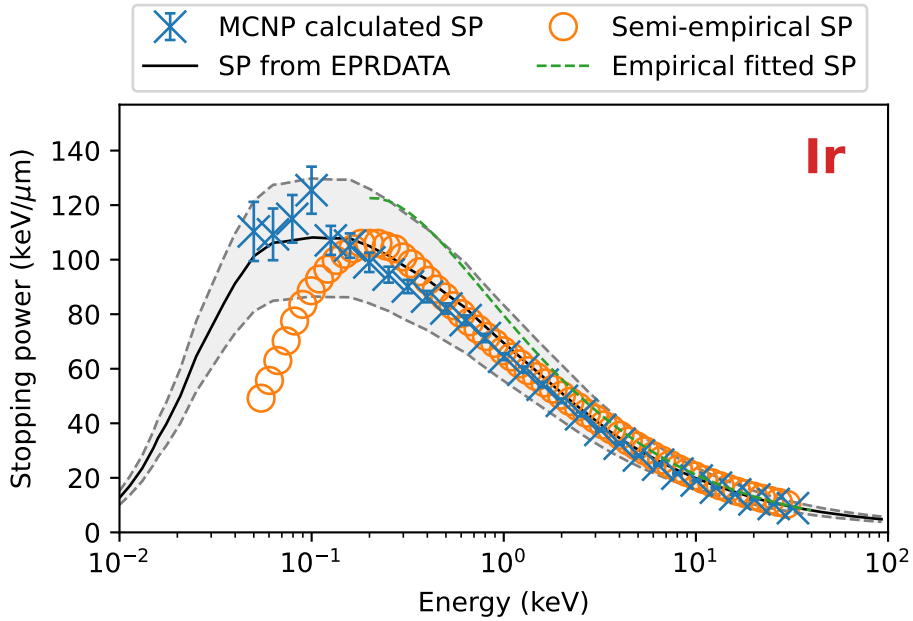

Figure 110: Stopping power results and benchmarks for iridium.

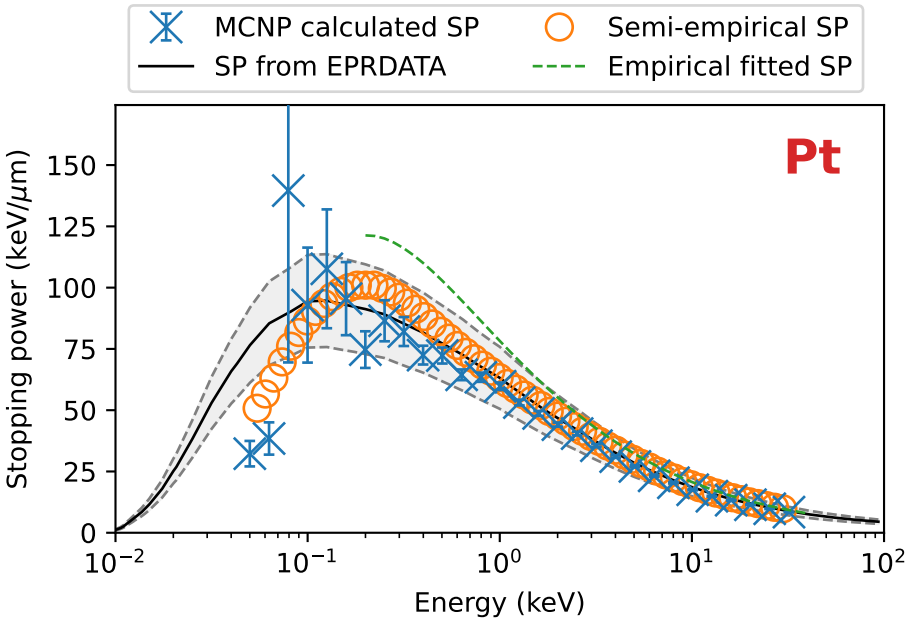

Figure 111: Stopping power results and benchmarks for platinum.

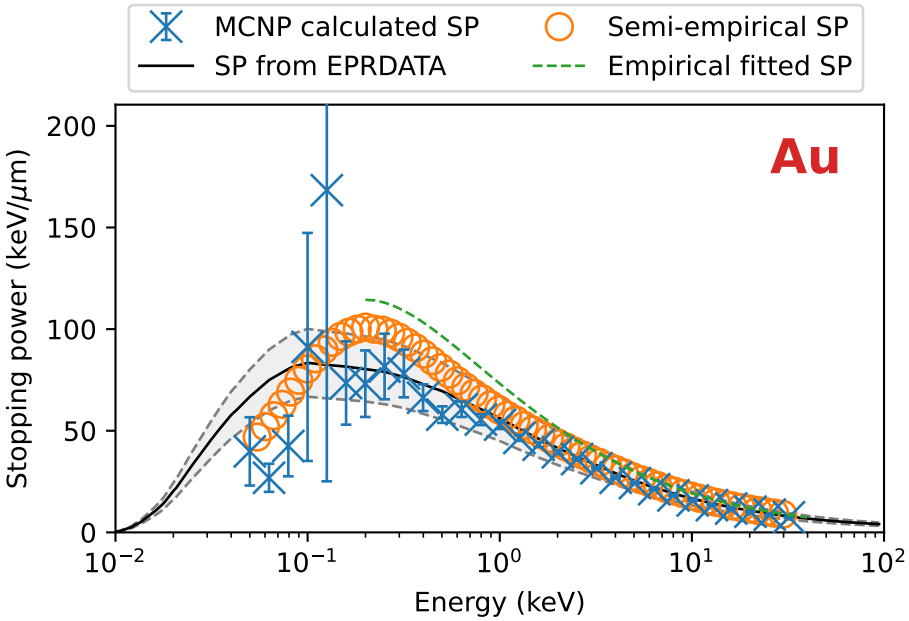

Figure 112: Stopping power results and benchmarks for gold.

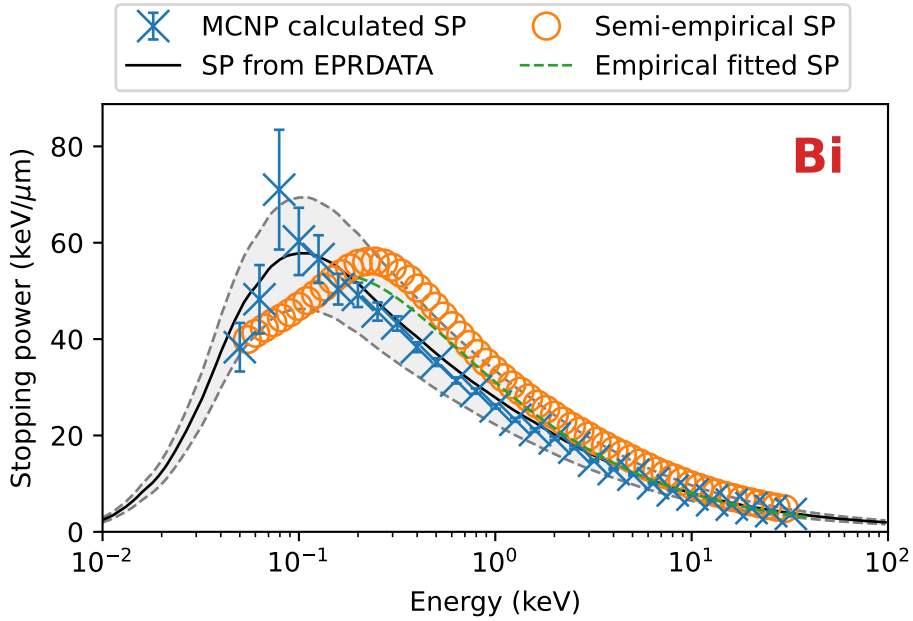

Figure 113: Stopping power results and benchmarks for bismuth.

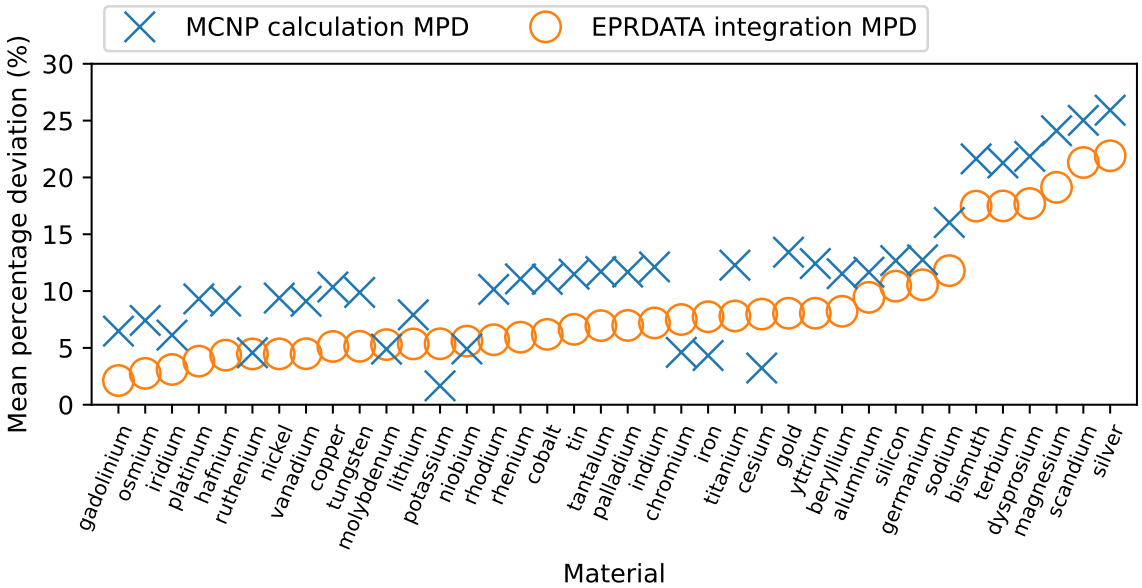

Figure 114: Mean percentage deviation (MPD) for simulated (with MCNP) and integrated (from EPRDATA) electron stopping powers in elemental solids.

Table 32: Elemental stopping powers Benchmark Results

	Calc. MPD (%)	Calc. RMSE (%)	Int. MPD (%)	Int. RMSE (%)
lithium	7.91	8.56	5.35	5.81
beryllium	11.53	12.14	8.22	8.83
sodium	16.03	16.22	11.80	11.96
magnesium	24.11	24.18	19.13	19.26
aluminum	11.66	12.57	9.45	9.99
silicon	12.68	13.31	10.43	11.38
potassium	1.66	2.14	5.36	6.19
scandium	25.02	25.20	21.31	21.49
titanium	12.28	12.43	7.81	8.00
vanadium	9.10	9.37	4.49	5.29
chromium	4.61	5.26	7.50	9.45
iron	4.33	5.12	7.74	9.62
cobalt	11.03	11.31	6.19	6.53
nickel	9.39	9.74	4.48	5.03
copper	10.36	10.70	5.13	5.59
germanium	12.75	13.41	10.56	12.24
yttrium	12.42	12.49	8.05	8.24
niobium	4.90	5.36	5.60	8.06
molybdenum	4.89	5.68	5.29	6.36
ruthenium	4.57	5.53	4.47	5.23
rhodium	10.15	10.76	5.72	6.61
palladium	11.67	12.45	6.98	8.19
silver	25.92	26.10	21.91	22.05
indium	12.13	12.37	7.20	7.67
tin	11.49	11.63	6.63	7.05
cesium	3.23	4.44	7.97	8.72
gadolinium	6.48	6.84	2.13	2.70
terbium	21.27	21.82	17.49	18.21
dysprosium	21.85	22.34	17.70	18.29
hafnium	9.11	9.47	4.36	4.97
tantalum	11.71	11.80	6.96	7.09
tungsten	9.88	9.99	5.14	5.23
rhenium	11.07	11.17	5.94	6.01
osmium	7.42	7.69	2.76	3.07
iridium	6.13	6.78	3.10	3.40
platinum	9.31	9.78	3.84	4.49
gold	13.42	14.26	8.05	8.90
bismuth	21.63	21.70	17.47	17.53

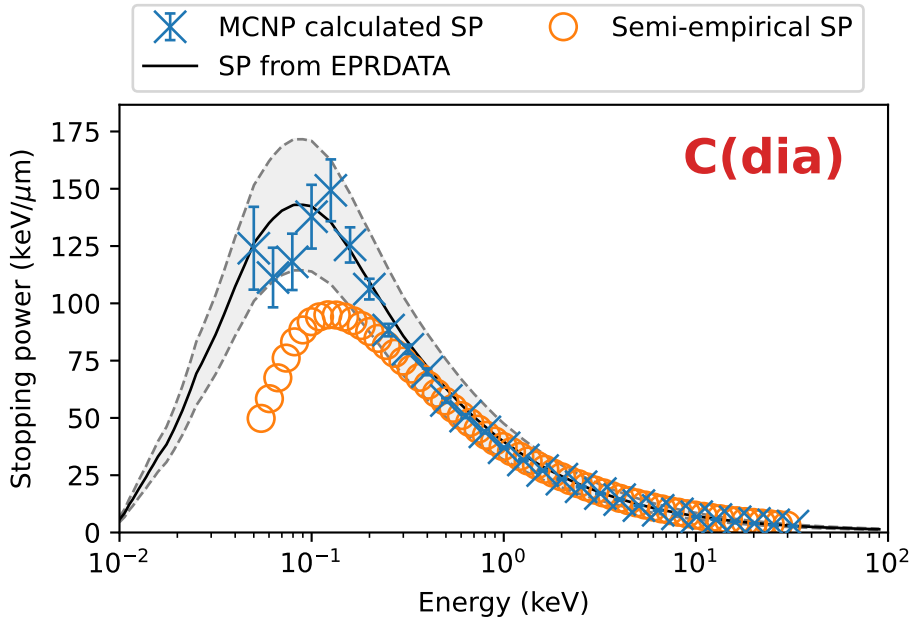

Figure 115: Stopping power results and benchmarks for diamond.

4.7.2 Carbon allotropes

For the validation electron stopping benchmarks the benchmark data and calculation results for carbon allotropes are plotted in Figs. 115 through 117.

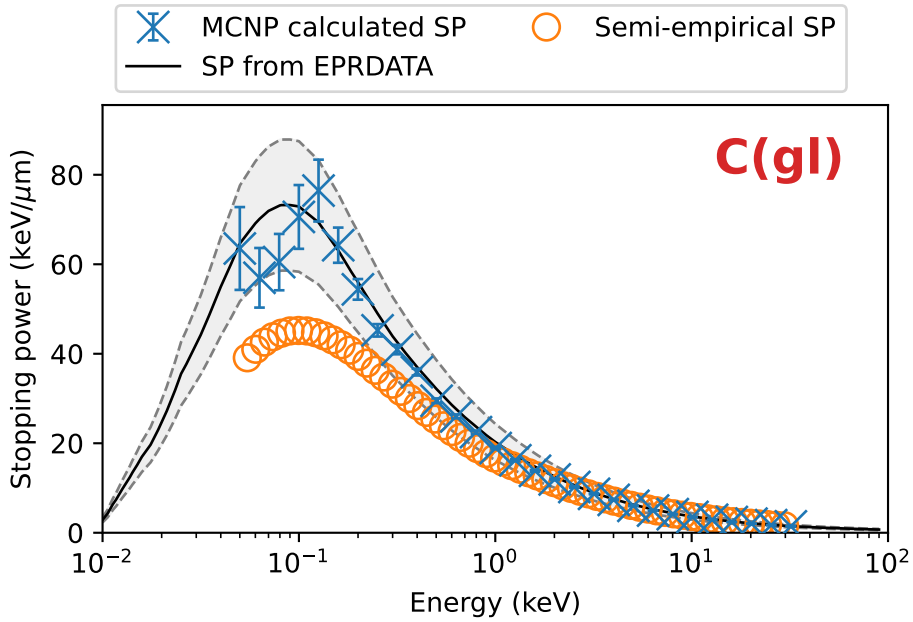

Figure 116: Stopping power results and benchmarks for glassy carbon.

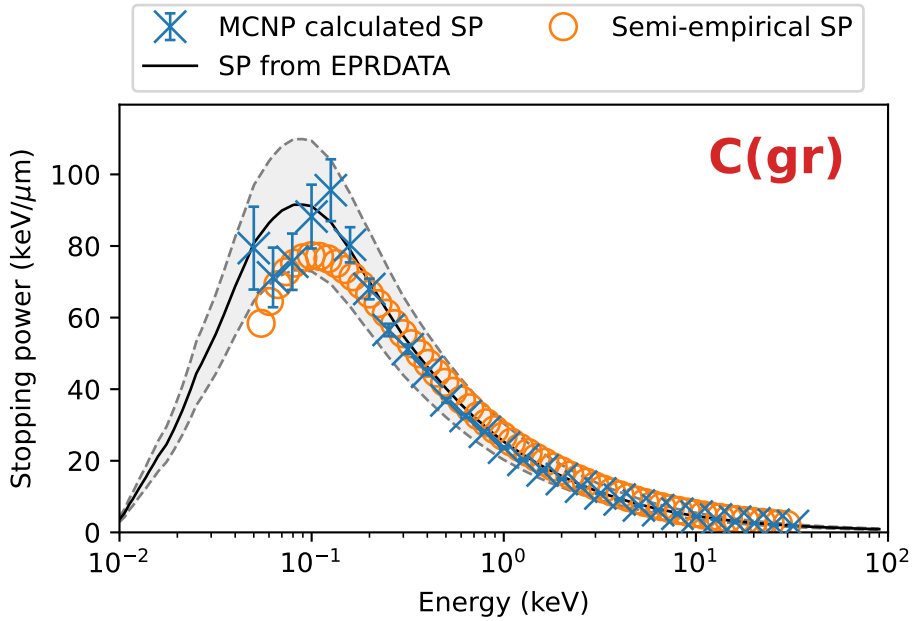

Figure 117: Stopping power results and benchmarks for graphite.

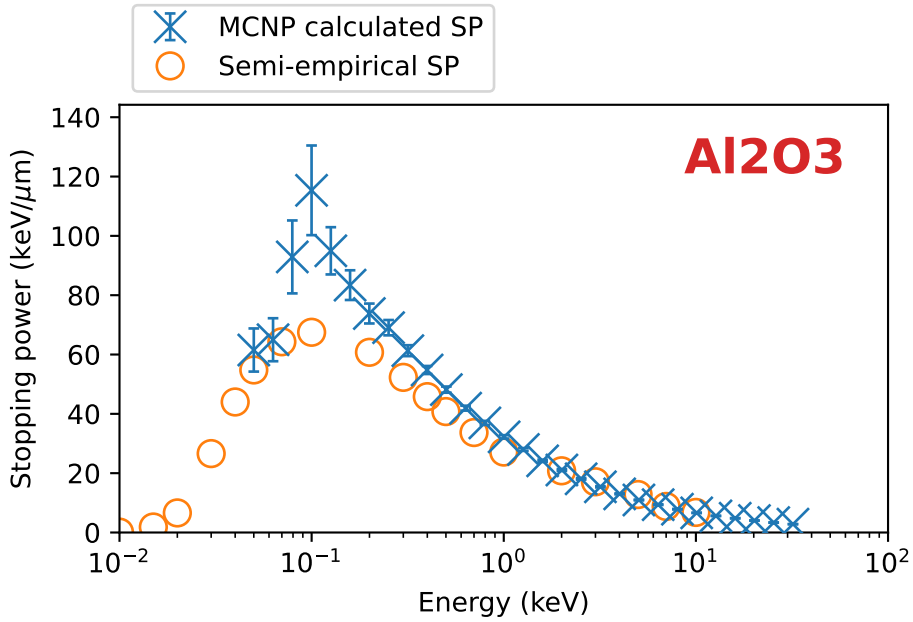

Figure 118: Stopping power results and benchmarks for sapphire.

4.7.3 Compounds

For the validation electron stopping benchmarks the benchmark data and calculation results for compounds are plotted in Figs. 118 through 131.

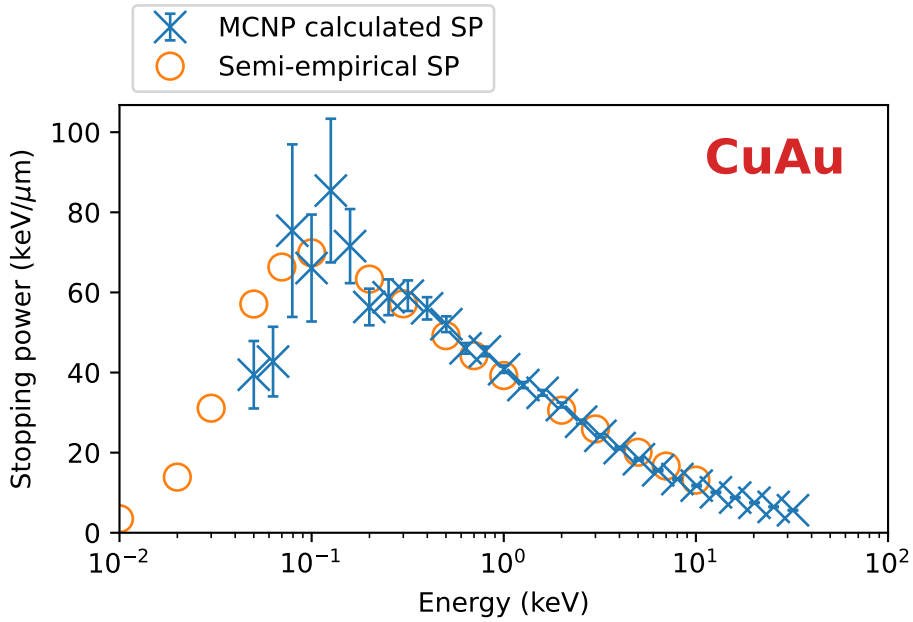

Figure 119: Stopping power results and benchmarks for rose gold.

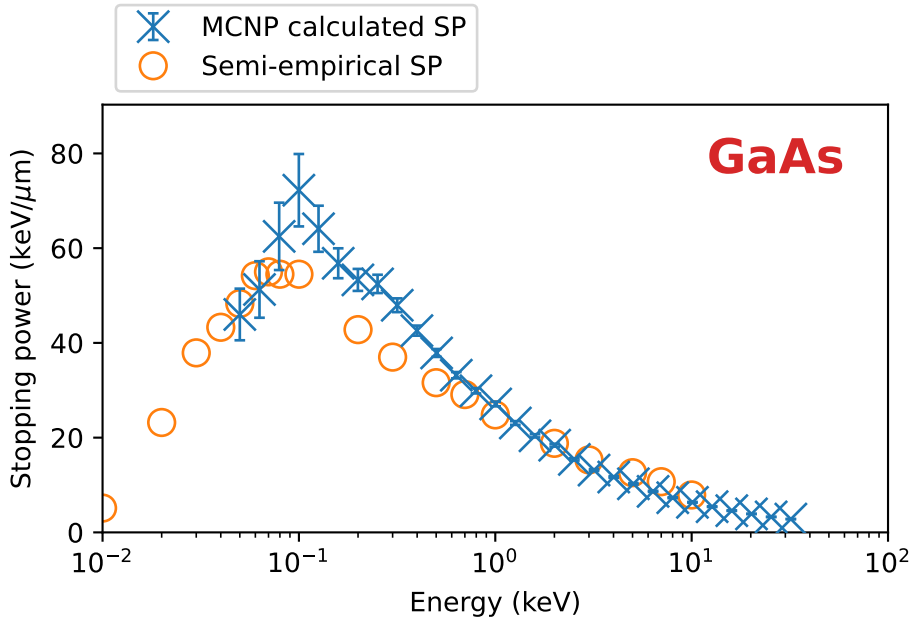

Figure 120: Stopping power results and benchmarks for gallium arsenide.

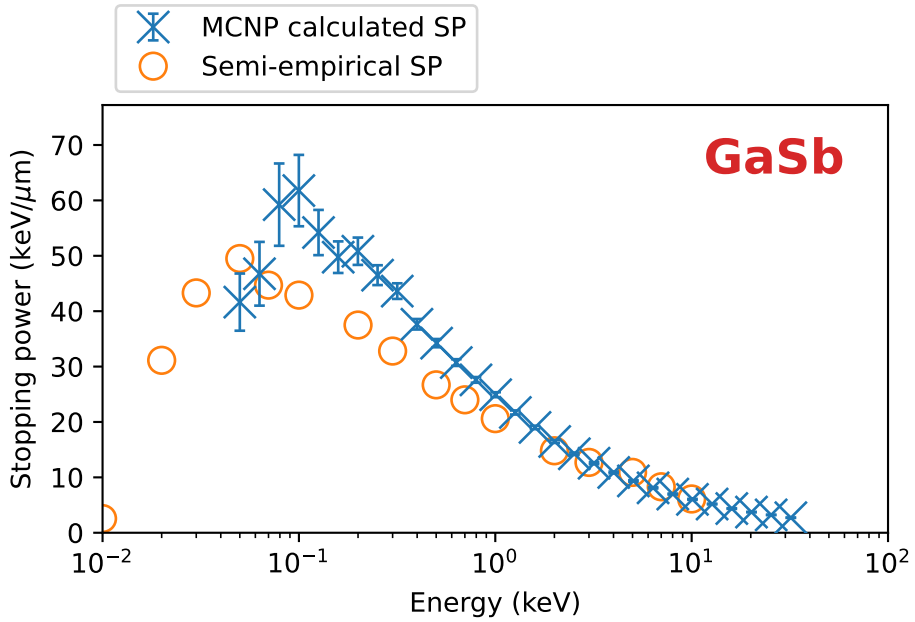

Figure 121: Stopping power results and benchmarks for gallium antimonide.

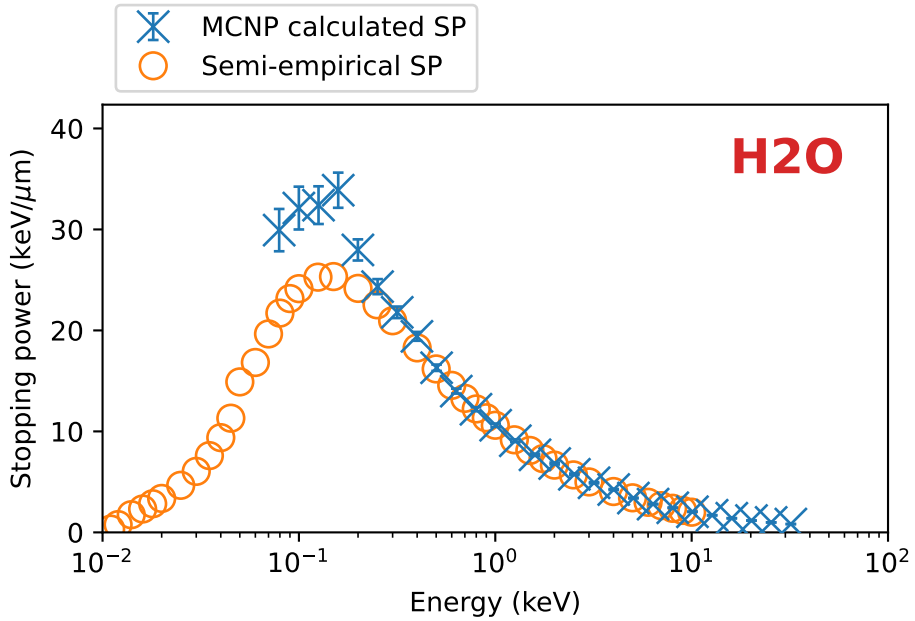

Figure 122: Stopping power results and benchmarks for vitreous ice.

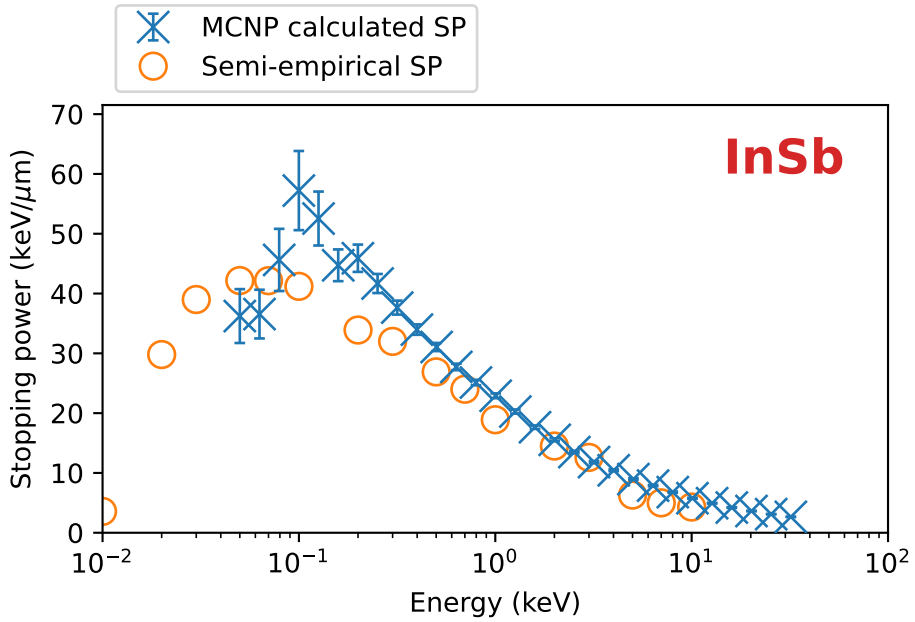

Figure 123: Stopping power results and benchmarks for indium antimonide.

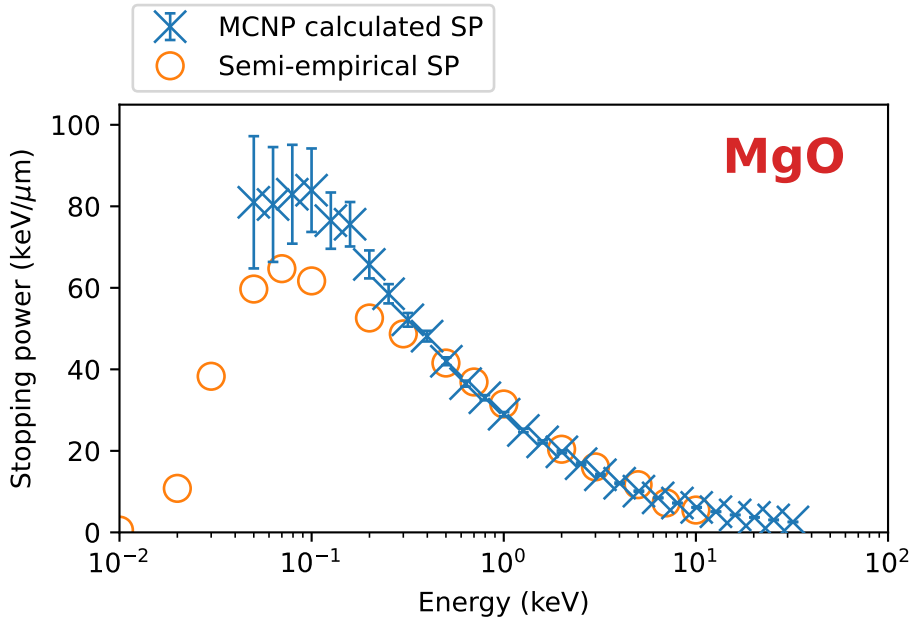

Figure 124: Stopping power results and benchmarks for magnesia.

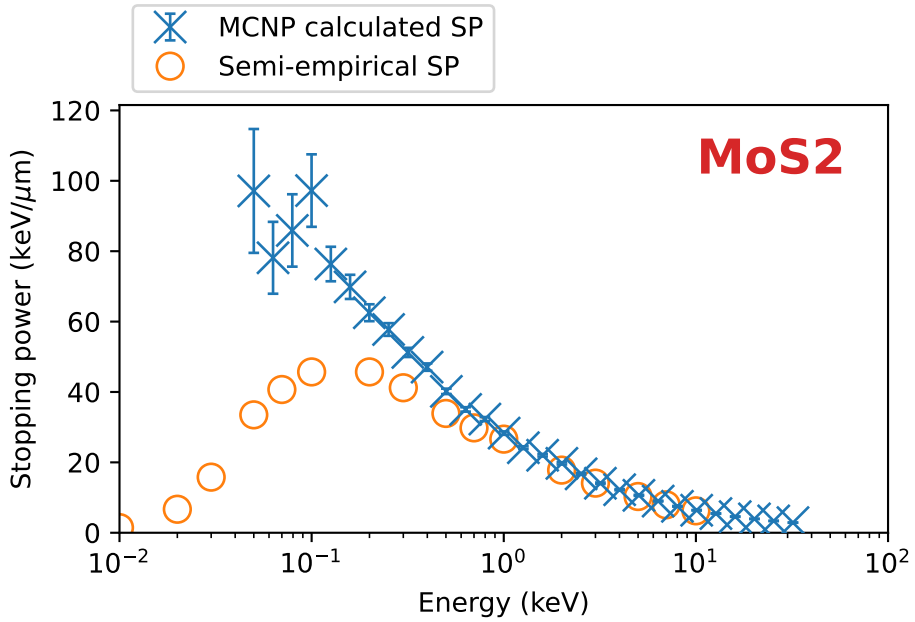

Figure 125: Stopping power results and benchmarks for molybdenum disulfide.

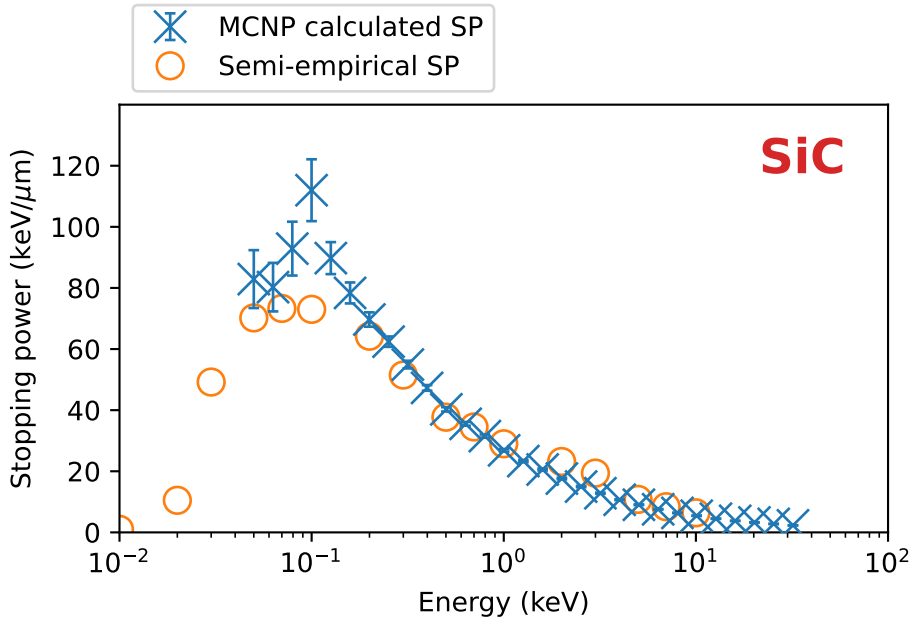

Figure 126: Stopping power results and benchmarks for silicon carbide.

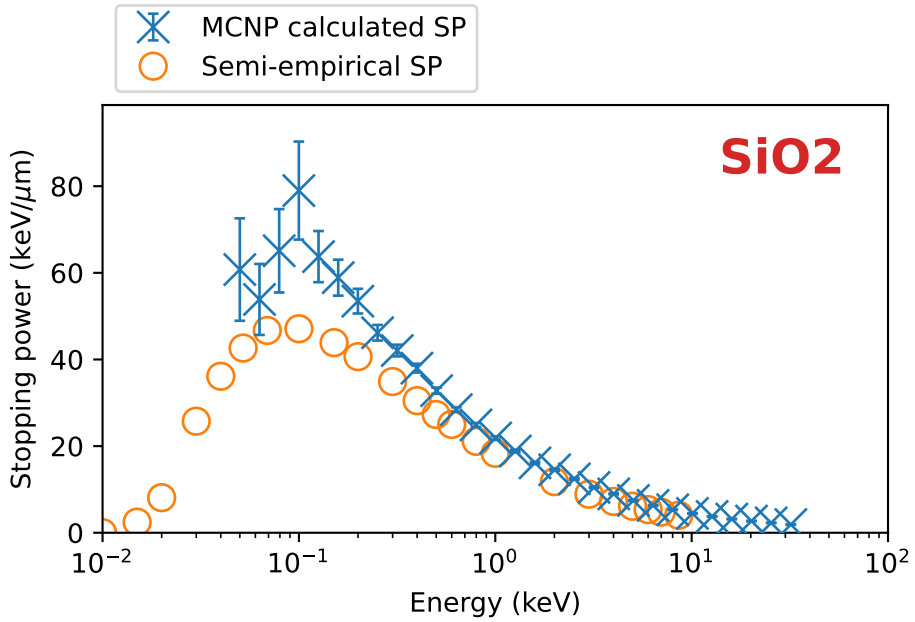

Figure 127: Stopping power results and benchmarks for quartz.

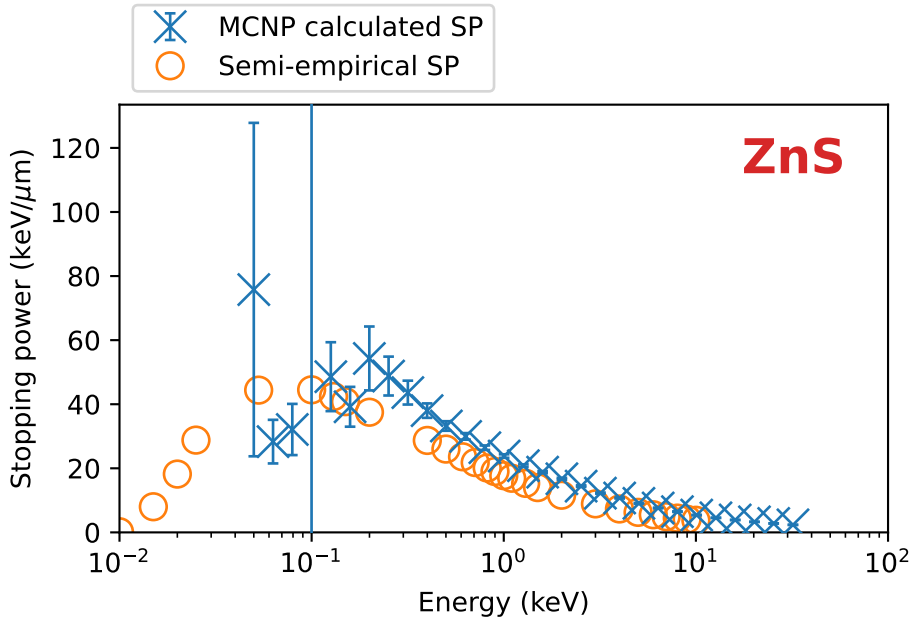

Figure 128: Stopping power results and benchmarks for zinc sulfide.

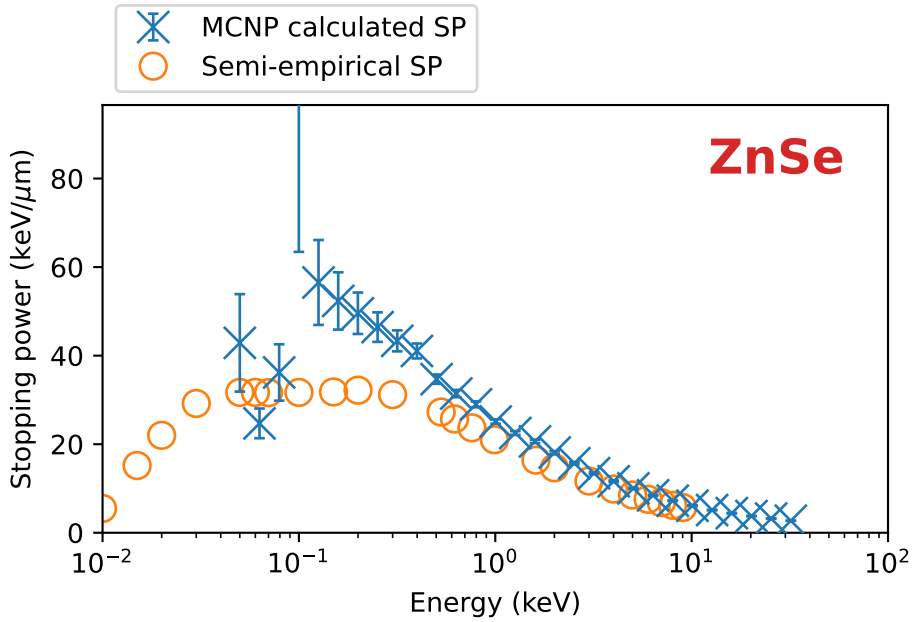

Figure 129: Stopping power results and benchmarks for zinc selenide.

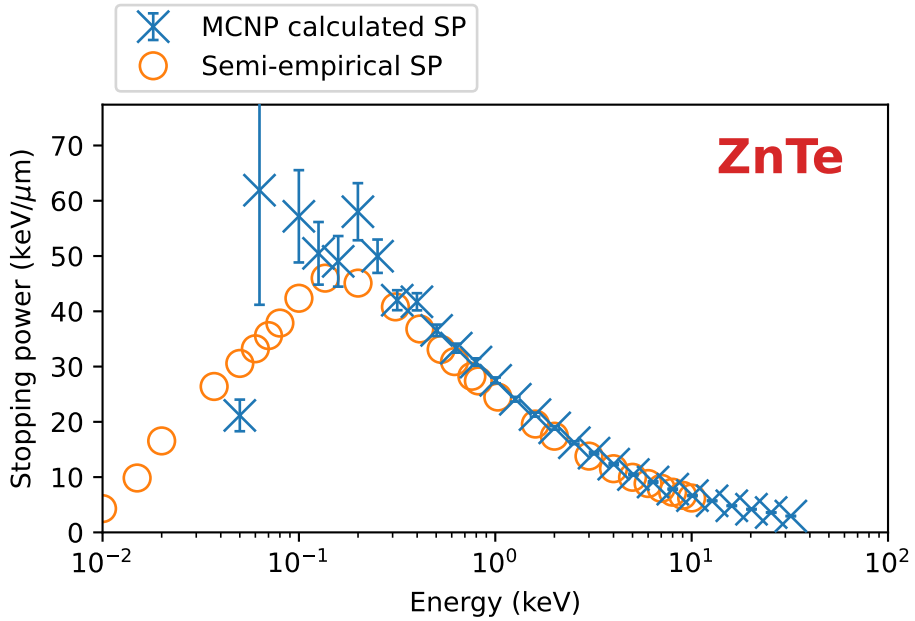

Figure 130: Stopping power results and benchmarks for zinc telluride.

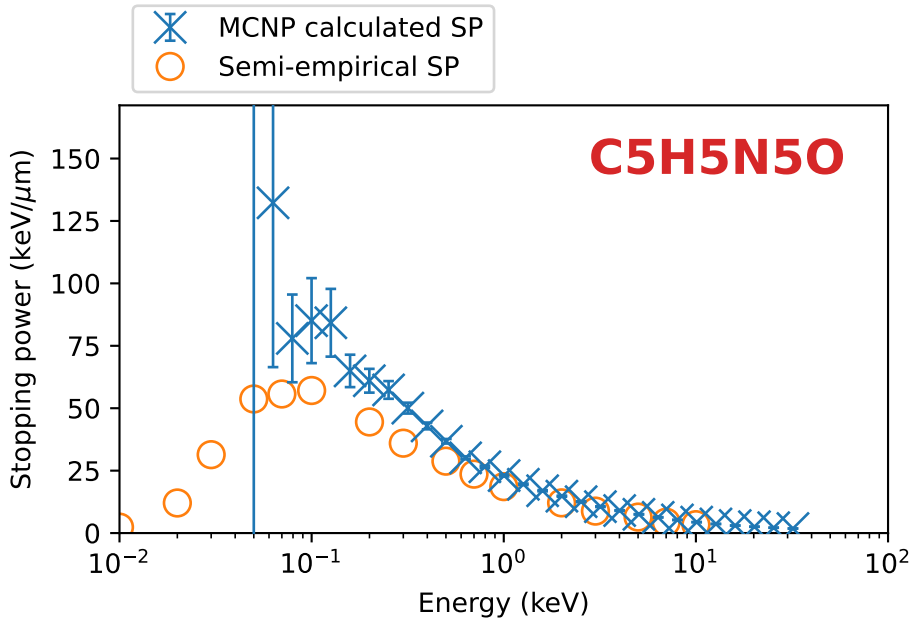

Figure 131: Stopping power results and benchmarks for guanine.

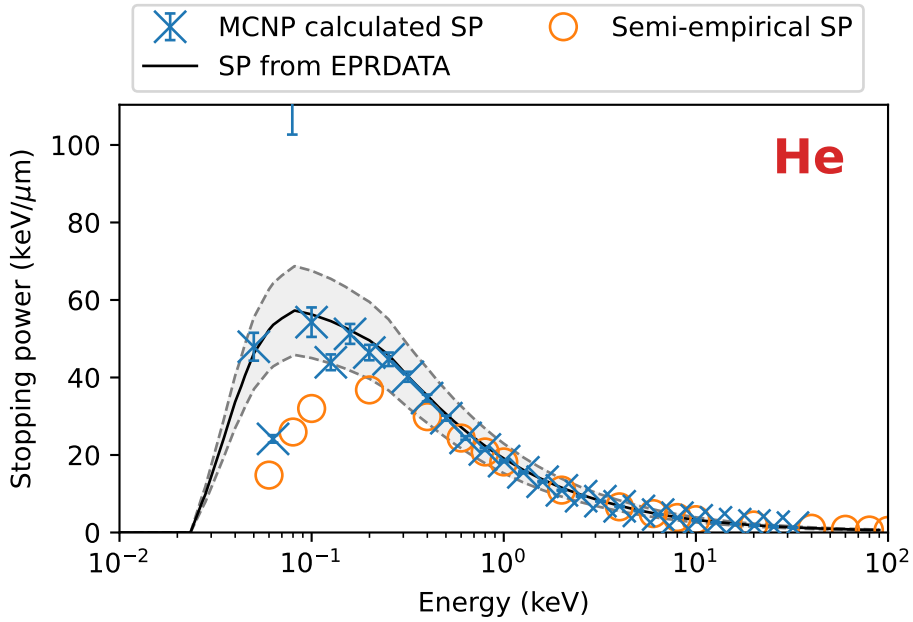

Figure 132: Stopping power results and benchmarks for solid helium.

4.7.4 Rare gas solids

For the validation electron stopping benchmarks the benchmark data and calculation results for rare gas solids are plotted in Figs. 132 through 136.

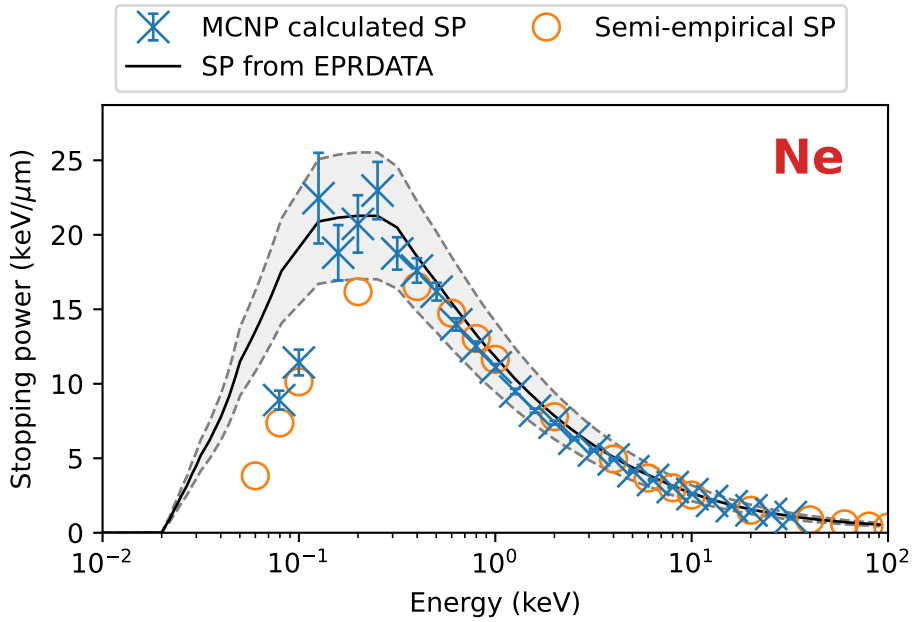

Figure 133: Stopping power results and benchmarks for solid neon.

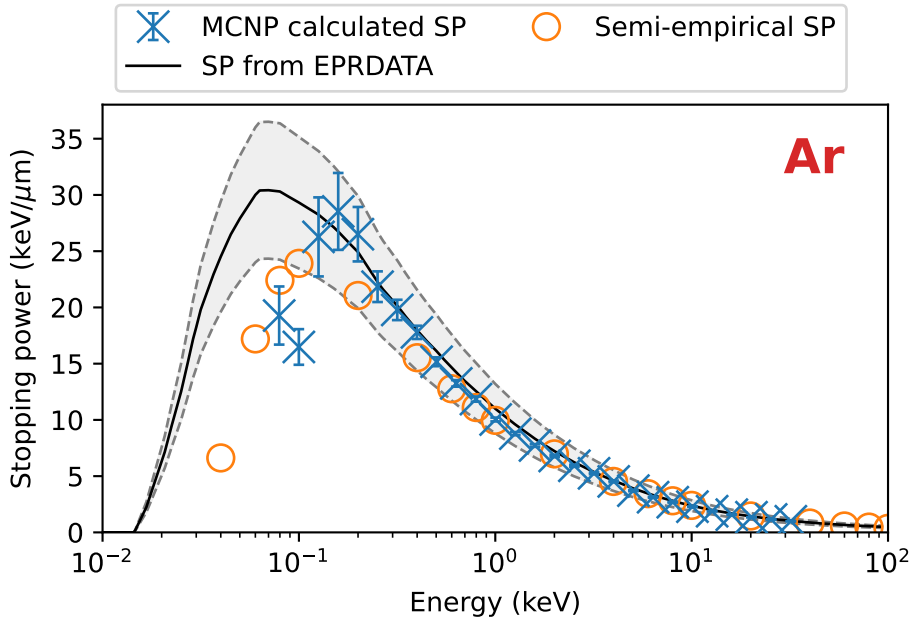

Figure 134: Stopping power results and benchmarks for solid argon.

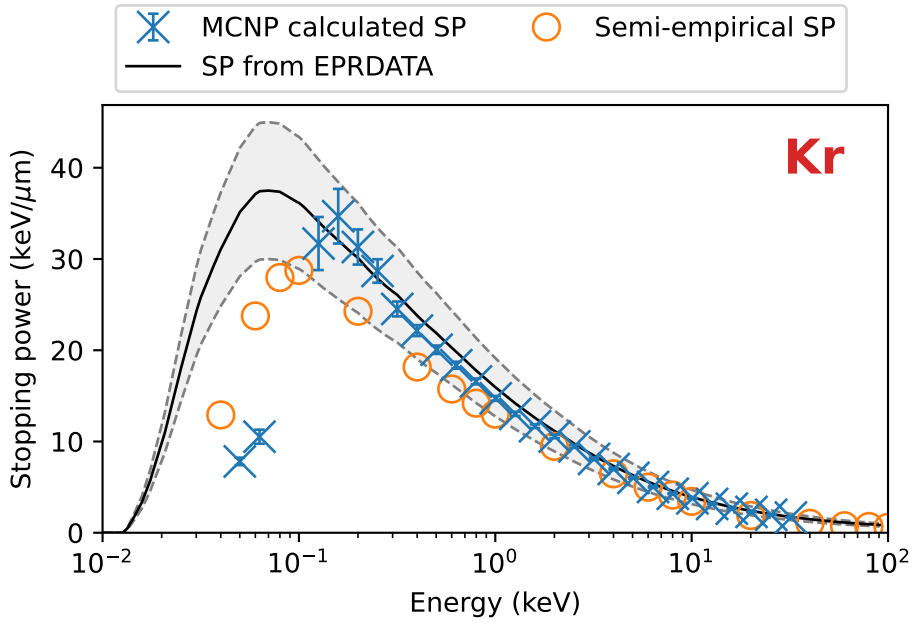

Figure 135: Stopping power results and benchmarks for solid krypton.

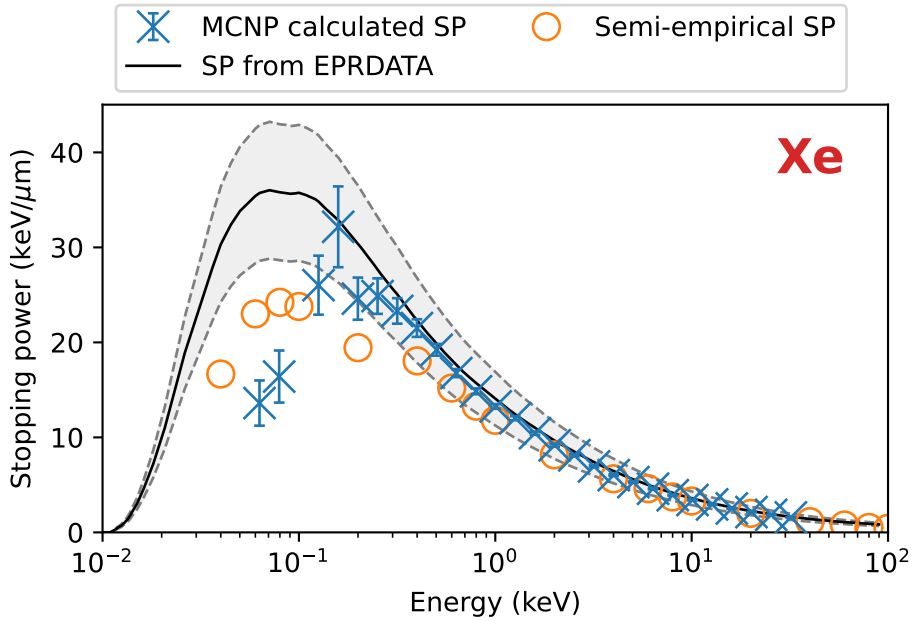

Figure 136: Stopping power results and benchmarks for solid xenon.

5 Verification

5.1 k_{eff} Verification

This test suite executes on 1 node, which uses 14 threads and 8 concurrent jobs, with a total Slurm allocation of no more than 70 minutes. An example `VnV.py` execution line is `./VnV.py execute_slurm --ntrd 14 --jobs 8 --time 70 --wait --calcdir_name verification_keff`.

The following figures and tables are results for the k_{eff} Verification suite, which contains 37 continuous energy and 68 multigroup k-eigenvalue analytic benchmarks. These simple models include k_∞, infinite slab, infinite cylinder, sphere, and two medium reflected infinite slab problems. The plots display ratios of calculated-to-expected (C/E) values and their uncertainties. The tables provide analytic and calculated values and uncertainties.

5.1.1 Continuous Energy

For the analytical k_{eff} continuous energy benchmarks, the benchmark data and calculation results are plotted in Fig. 137 as C/E ratios with individual values listed in Table 33.

5.1.2 Multigroup

For the analytical k_{eff} multigroup benchmarks, the benchmark data and calculation results are plotted in Fig. 138 as C/E ratios with individual values listed in Table 34.

Table 34: Analytical k_{eff} Multigroup Benchmark Results

	Analytic k_{eff}	Calc. k_{eff}	Calc. unc.
mg01	2.612 903	2.612 90	2.34×10^{-9}
mg02	1.000 000	0.999 919	1.05×10^{-4}
mg03	1.000 000	1.000 12	1.05×10^{-4}
mg04	1.000 000	1.000 00	1.14×10^{-4}
mg05	2.290 323	2.290 32	2.71×10^{-9}
mg06	1.000 000	1.000 06	1.01×10^{-4}
mg07	1.000 000	0.999 994	8.92×10^{-5}
mg08	1.000 000	1.000 18	9.38×10^{-5}
mg09	1.000 000	0.999 864	9.73×10^{-5}
mg10	1.000 000	1.000 13	9.59×10^{-5}
mg11	2.250 000	2.250 00	3.84×10^{-9}
mg12	1.000 000	1.000 04	1.05×10^{-4}
mg13	1.000 000	1.000 13	9.19×10^{-5}
mg14	1.000 000	0.999 921	9.15×10^{-5}
mg15	2.330 917	2.330 92	3.84×10^{-9}

Continued on next page

Table 34: Analytical k_{eff} Multigroup Benchmark Results

	Analytic k_{eff}	Calc. k_{eff}	Calc. unc.
mg16	1.000 000	0.999 866	9.59×10^{-5}
mg17	2.256 083	2.256 09	4.90×10^{-9}
mg18	1.000 000	0.999 994	1.00×10^{-4}
mg19	2.232 667	2.232 67	4.50×10^{-9}
mg20	1.000 000	1.000 03	9.83×10^{-5}
mg21	1.133 333	1.133 33	1.80×10^{-9}
mg22	1.000 000	1.000 01	5.02×10^{-5}
mg23	1.000 000	0.999 962	5.33×10^{-5}
mg24	1.000 000	0.999 963	5.56×10^{-5}
mg25	1.000 000	0.999 947	5.46×10^{-5}
mg26	1.000 000	1.000 04	5.24×10^{-5}
mg27	1.000 000	1.000 08	5.44×10^{-5}
mg28	1.000 000	0.999 948	5.31×10^{-5}
mg29	2.180 667	2.180 67	1.93×10^{-9}
mg30	1.000 000	0.999 980	1.06×10^{-4}
mg31	2.500 000	2.500 00	2.71×10^{-9}
mg32	1.000 000	0.999 996	1.06×10^{-4}
mg36	1.000 000	0.999 988	9.46×10^{-5}
mg38	1.205 587	1.205 59	9.62×10^{-10}
mg39	1.000 000	0.999 947	7.10×10^{-5}
mg40	1.227 391	1.227 39	1.80×10^{-9}
mg41	1.000 000	1.000 00	6.93×10^{-5}
mg44	2.683 767	2.683 70	2.87×10^{-5}
mg45	1.000 000	0.999 887	1.06×10^{-4}
mg46	1.000 000	1.000 08	9.25×10^{-5}
mg47	2.216 349	2.216 33	2.62×10^{-5}
mg48	1.000 000	0.999 893	1.02×10^{-4}
mg49	1.000 000	1.000 04	9.29×10^{-5}
mg50	2.662 437	2.662 44	4.02×10^{-5}
mg51	1.000 000	0.999 769	1.79×10^{-4}
mg52	1.000 000	1.000 19	2.02×10^{-4}
mg53	1.631 452	1.631 47	1.36×10^{-5}
mg54	1.000 000	1.000 07	1.12×10^{-4}
mg55	1.000 000	0.999 886	1.27×10^{-4}
mg56	1.365 821	1.365 84	8.08×10^{-6}
mg57	1.633 380	1.633 39	1.19×10^{-5}
mg58	1.000 000	0.999 990	8.66×10^{-5}
mg59	1.000 000	1.000 08	8.37×10^{-5}
mg60	1.000 000	0.999 915	8.81×10^{-5}
mg61	1.000 000	0.999 924	1.09×10^{-4}
mg62	1.034 970	1.034 96	1.68×10^{-5}
mg63	1.000 000	0.999 928	5.58×10^{-5}

Continued on next page

Table 34: Analytical k_{eff} Multigroup Benchmark Results

	Analytic k_{eff}	Calc. k_{eff}	Calc. unc.
mg64	1.000 000	0.999 907	4.80×10^{-5}
mg65	1.000 000	0.999 983	5.05×10^{-5}
mg66	1.000 000	1.000 04	3.83×10^{-5}
mg67	1.000 196	1.000 19	8.74×10^{-5}
mg68	1.000 000	0.999 830	8.74×10^{-5}
mg69	1.000 000	0.999 590	8.75×10^{-5}
mg70	1.631 452	1.631 47	1.36×10^{-5}
mg72	1.000 196	1.000 19	8.69×10^{-5}
mg73	1.000 000	0.999 807	8.68×10^{-5}
mg74	1.600 000	1.600 00	6.84×10^{-6}
mg75	1.600 000	1.599 99	7.48×10^{-6}

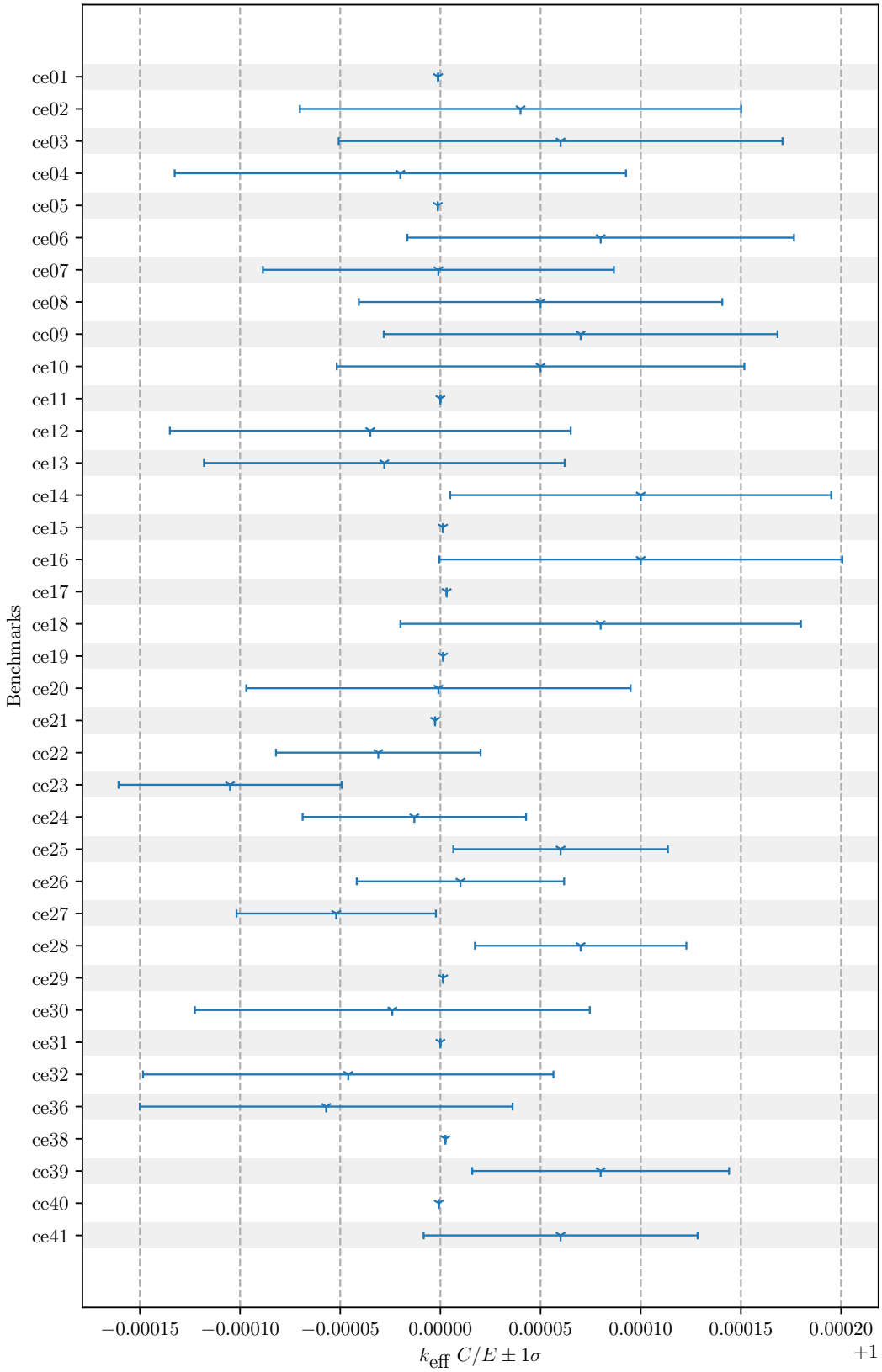

Figure 137: Analytical k_{eff} C/E Continuous Energy Benchmark Results

Table 33: Analytical k_{eff} Continuous Energy Benchmark Results

	Analytic k_{eff}	Calc. k_{eff}	Calc. unc.
ce01	2.612 903	2.612 90	2.35×10^{-9}
ce02	1.000 000	1.000 04	1.10×10^{-4}
ce03	1.000 000	1.000 06	1.11×10^{-4}
ce04	1.000 000	0.999 980	1.13×10^{-4}
ce05	2.290 323	2.290 32	7.71×10^{-14}
ce06	1.000 000	1.000 08	9.65×10^{-5}
ce07	1.000 000	0.999 999	8.76×10^{-5}
ce08	1.000 000	1.000 05	9.07×10^{-5}
ce09	1.000 000	1.000 07	9.83×10^{-5}
ce10	1.000 000	1.000 05	1.02×10^{-4}
ce11	2.250 000	2.250 00	2.36×10^{-9}
ce12	1.000 000	0.999 965	1.00×10^{-4}
ce13	1.000 000	0.999 972	9.00×10^{-5}
ce14	1.000 000	1.000 10	9.51×10^{-5}
ce15	2.330 917	2.330 92	4.08×10^{-9}
ce16	1.000 000	1.000 10	1.01×10^{-4}
ce17	2.256 083	2.256 09	4.30×10^{-9}
ce18	1.000 000	1.000 08	9.99×10^{-5}
ce19	2.232 667	2.232 67	3.97×10^{-14}
ce20	1.000 000	0.999 999	9.59×10^{-5}
ce21	1.133 333	1.133 33	6.80×10^{-10}
ce22	1.000 000	0.999 969	5.11×10^{-5}
ce23	1.000 000	0.999 895	5.56×10^{-5}
ce24	1.000 000	0.999 987	5.58×10^{-5}
ce25	1.000 000	1.000 06	5.36×10^{-5}
ce26	1.000 000	1.000 01	5.18×10^{-5}
ce27	1.000 000	0.999 948	4.97×10^{-5}
ce28	1.000 000	1.000 07	5.28×10^{-5}
ce29	2.180 667	2.180 67	2.35×10^{-9}
ce30	1.000 000	0.999 976	9.86×10^{-5}
ce31	2.500 000	2.500 00	2.35×10^{-9}
ce32	1.000 000	0.999 954	1.02×10^{-4}
ce36	1.000 000	0.999 943	9.30×10^{-5}
ce38	1.205 587	1.205 59	1.18×10^{-9}
ce39	1.000 000	1.000 08	6.41×10^{-5}
ce40	1.227 391	1.227 39	2.15×10^{-9}
ce41	1.000 000	1.000 06	6.84×10^{-5}

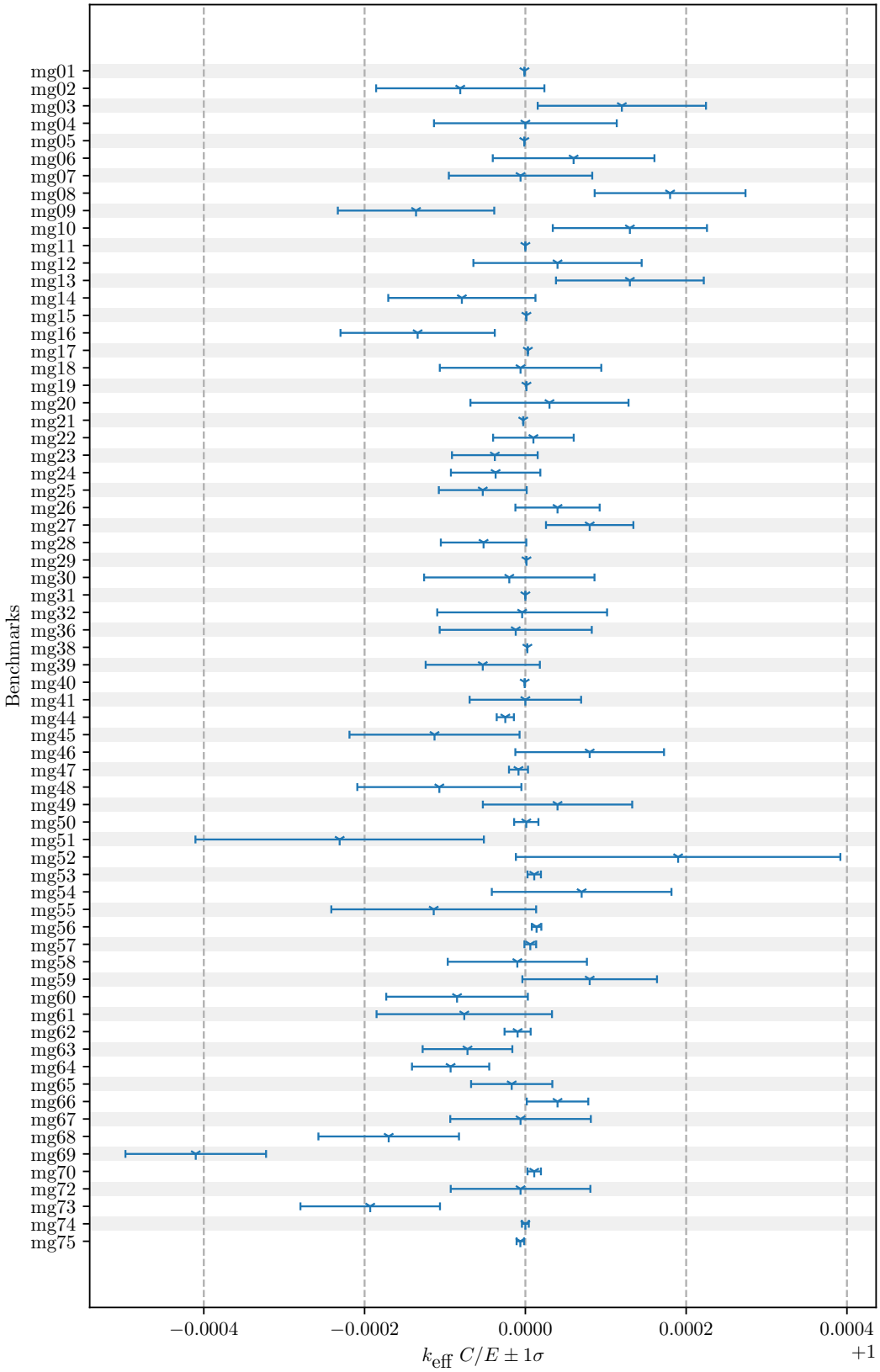

Figure 138: Analytical k_{eff} C/E Multigroup Benchmark Results

5.2 Kobayashi

This test suite executes on 1 node, which uses 114 MPI ranks, with a total Slurm allocation of no more than 100 minutes. An example `VnV.py` execution line is `./VnV.py execute_slurm --nmpi 114 --time 100 --wait --calcdir_name kobayashi`.

The following figures and tables are results from the Kobayashi analytic benchmarks. The plots display C/E values and their uncertainties. The tables provide the benchmark and calculated values and uncertainties as well as their C/E values and uncertainties. This problem set contains 6 benchmarks that were designed to test how 3D discrete ordinates codes deal with ray effects in problems with void and combination of void, purely absorbing, and mixed absorbing/scattering regions. The figures and tables for the purely absorbing problems are identified with an "i" in their moniker ("p1i_ce", "p2i_ce", and "p3i_ce"), while figures and tables for the mixed absorbing/scattering problems are identified with an "ii" in their moniker ("p1ii_ce", "p2ii_ce", and "p3ii_ce").

5.2.1 p1i_ce

For the analytical Kobayashi p1i_ce benchmarks, the benchmark data and calculation results are plotted in Fig. 139 as C/E ratios with individual values listed in Table 35.

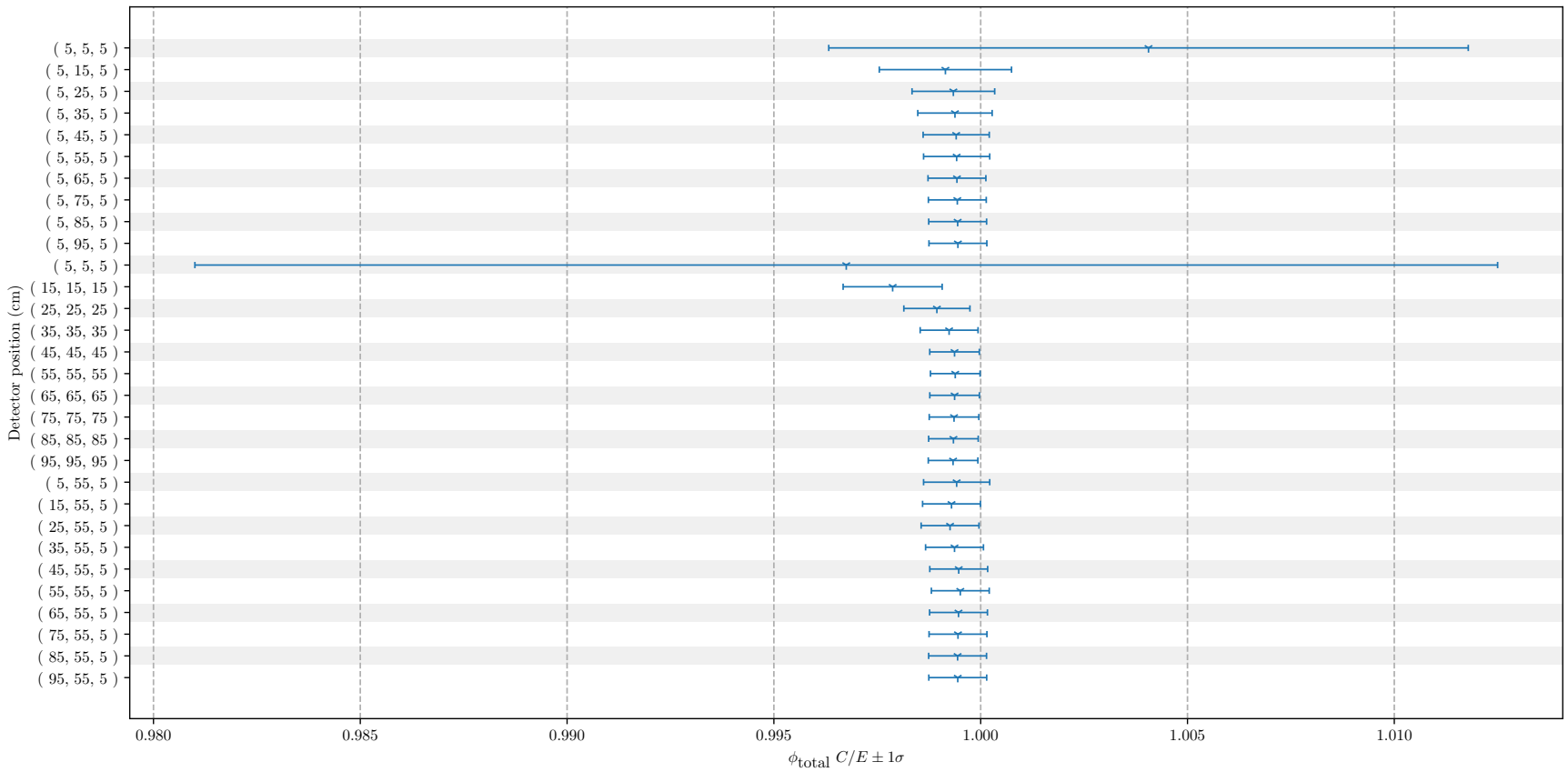

Figure 139: p1i_ce C/E Calculation Benchmark Results

5.2.2 p1ii_ce

For the analytical Kobayashi p1ii_ce benchmarks, the benchmark data and calculation results are plotted in Fig. 140 as C/E ratios with individual values listed in Table 36.

Table 35: p1i_ce Calculation Benchmark Results

Coordinates	Benchmark ϕ_t	Benchmark unc.	Calc. ϕ_t	Calc. unc.	C/E	C/E unc.
(5, 5, 5)	5.9566	0.0000	5.9808	4.6052×10^{-2}	1.0041	7.7312×10^{-3}
(5, 15, 5)	1.3719	0.0000	1.3707	2.1931×10^{-3}	9.9915×10^{-1}	1.5986×10^{-3}
(5, 25, 5)	5.0087×10^{-1}	0.0000	5.0054×10^{-1}	5.0054×10^{-4}	9.9934×10^{-1}	9.9934×10^{-4}
(5, 35, 5)	2.5243×10^{-1}	0.0000	2.5227×10^{-1}	2.2704×10^{-4}	9.9938×10^{-1}	8.9944×10^{-4}
(5, 45, 5)	1.5026×10^{-1}	0.0000	1.5017×10^{-1}	1.2014×10^{-4}	9.9941×10^{-1}	7.9953×10^{-4}
(5, 55, 5)	5.9529×10^{-2}	0.0000	5.9494×10^{-2}	4.7595×10^{-5}	9.9942×10^{-1}	7.9954×10^{-4}
(5, 65, 5)	1.5328×10^{-2}	0.0000	1.5319×10^{-2}	1.0724×10^{-5}	9.9943×10^{-1}	6.9960×10^{-4}
(5, 75, 5)	4.1769×10^{-3}	0.0000	4.1745×10^{-3}	2.9222×10^{-6}	9.9943×10^{-1}	6.9960×10^{-4}
(5, 85, 5)	1.1853×10^{-3}	0.0000	1.1847×10^{-3}	8.2927×10^{-7}	9.9944×10^{-1}	6.9961×10^{-4}
(5, 95, 5)	3.4685×10^{-4}	0.0000	3.4666×10^{-4}	2.4266×10^{-7}	9.9945×10^{-1}	6.9961×10^{-4}
(5, 5, 5)	5.9566	0.0000	5.9372	9.3808×10^{-2}	9.9675×10^{-1}	1.5749×10^{-2}
(15, 15, 15)	4.7075×10^{-1}	0.0000	4.6975×10^{-1}	5.6370×10^{-4}	9.9787×10^{-1}	1.1974×10^{-3}
(25, 25, 25)	1.6997×10^{-1}	0.0000	1.6979×10^{-1}	1.3583×10^{-4}	9.9894×10^{-1}	7.9915×10^{-4}
(35, 35, 35)	8.6833×10^{-2}	0.0000	8.6767×10^{-2}	6.0737×10^{-5}	9.9924×10^{-1}	6.9947×10^{-4}
(45, 45, 45)	5.2513×10^{-2}	0.0000	5.2480×10^{-2}	3.1488×10^{-5}	9.9937×10^{-1}	5.9962×10^{-4}
(55, 55, 55)	1.3338×10^{-2}	0.0000	1.3330×10^{-2}	7.9978×10^{-6}	9.9939×10^{-1}	5.9963×10^{-4}
(65, 65, 65)	1.4587×10^{-3}	0.0000	1.4578×10^{-3}	8.7465×10^{-7}	9.9937×10^{-1}	5.9962×10^{-4}
(75, 75, 75)	1.7536×10^{-4}	0.0000	1.7525×10^{-4}	1.0515×10^{-7}	9.9936×10^{-1}	5.9961×10^{-4}
(85, 85, 85)	2.2461×10^{-5}	0.0000	2.2446×10^{-5}	1.3468×10^{-8}	9.9934×10^{-1}	5.9960×10^{-4}
(95, 95, 95)	3.0103×10^{-6}	0.0000	3.0083×10^{-6}	1.8050×10^{-9}	9.9933×10^{-1}	5.9960×10^{-4}
(5, 55, 5)	5.9529×10^{-2}	0.0000	5.9494×10^{-2}	4.7595×10^{-5}	9.9942×10^{-1}	7.9954×10^{-4}
(15, 55, 5)	5.5025×10^{-2}	0.0000	5.4986×10^{-2}	3.8490×10^{-5}	9.9929×10^{-1}	6.9951×10^{-4}
(25, 55, 5)	4.8075×10^{-2}	0.0000	4.8040×10^{-2}	3.3628×10^{-5}	9.9926×10^{-1}	6.9948×10^{-4}
(35, 55, 5)	3.9677×10^{-2}	0.0000	3.9651×10^{-2}	2.7756×10^{-5}	9.9937×10^{-1}	6.9956×10^{-4}
(45, 55, 5)	3.1637×10^{-2}	0.0000	3.1620×10^{-2}	2.2134×10^{-5}	9.9947×10^{-1}	6.9963×10^{-4}
(55, 55, 5)	2.3530×10^{-2}	0.0000	2.3519×10^{-2}	1.6463×10^{-5}	9.9951×10^{-1}	6.9965×10^{-4}
(65, 55, 5)	5.8372×10^{-3}	0.0000	5.8341×10^{-3}	4.0839×10^{-6}	9.9946×10^{-1}	6.9962×10^{-4}
(75, 55, 5)	1.5673×10^{-3}	0.0000	1.5665×10^{-3}	1.0965×10^{-6}	9.9945×10^{-1}	6.9962×10^{-4}
(85, 55, 5)	4.5311×10^{-4}	0.0000	4.5286×10^{-4}	3.1700×10^{-7}	9.9944×10^{-1}	6.9961×10^{-4}
(95, 55, 5)	1.3708×10^{-4}	0.0000	1.3700×10^{-4}	9.5902×10^{-8}	9.9945×10^{-1}	6.9961×10^{-4}

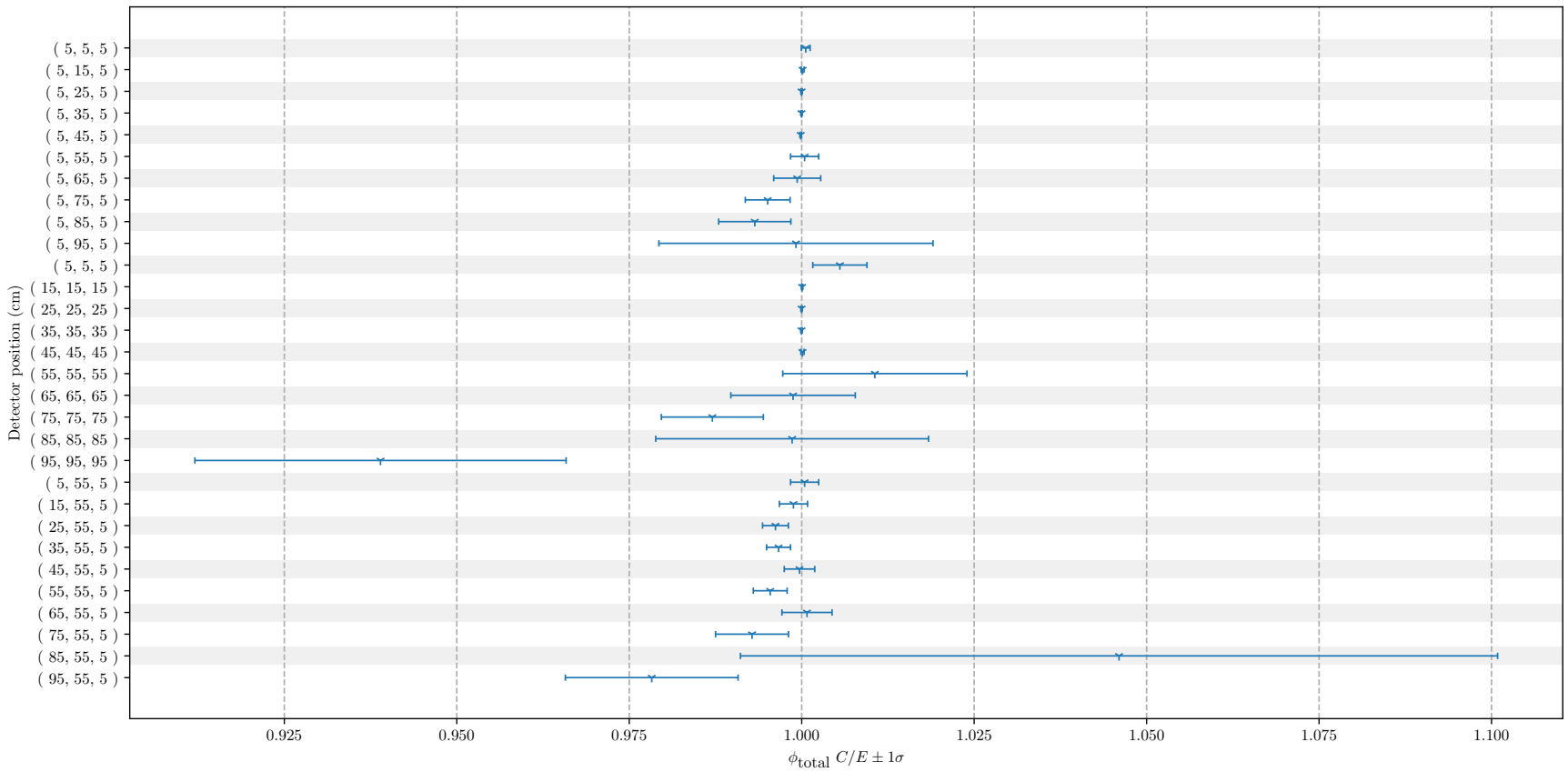

Figure 140: p1ii_ce C/E Calculation Benchmark Results

5.2.3 p2i_ce

For the analytical Kobayashi p2i_ce benchmarks, the benchmark data and calculation results are plotted in Fig. 141 as C/E ratios with individual values listed in Table 37.

Table 36: p1ii_ce Calculation Benchmark Results

Coordinates	Benchmark ϕ_t	Benchmark unc.	Calc. ϕ_t	Calc. unc.	C/E	C/E unc.
(5, 5, 5)	8.2926	1.7414×10^{-3}	8.2974	4.9785×10^{-3}	1.0006	6.3606×10^{-4}
(5, 15, 5)	1.8703	9.3514×10^{-5}	1.8705	3.7411×10^{-4}	1.0001	2.0618×10^{-4}
(5, 25, 5)	7.1399×10^{-1}	2.1420×10^{-5}	7.1397×10^{-1}	7.1397×10^{-5}	9.9998×10^{-1}	1.0440×10^{-4}
(5, 35, 5)	3.8468×10^{-1}	1.5387×10^{-5}	3.8467×10^{-1}	3.8467×10^{-5}	9.9997×10^{-1}	1.0770×10^{-4}
(5, 45, 5)	2.5398×10^{-1}	1.5239×10^{-5}	2.5395×10^{-1}	2.5395×10^{-5}	9.9985×10^{-1}	1.1660×10^{-4}
(5, 55, 5)	1.3722×10^{-1}	1.0017×10^{-4}	1.3728×10^{-1}	2.6083×10^{-4}	1.0004	2.0363×10^{-3}
(5, 65, 5)	4.6591×10^{-2}	5.4512×10^{-5}	4.6561×10^{-2}	1.4899×10^{-4}	9.9935×10^{-1}	3.4050×10^{-3}
(5, 75, 5)	1.5877×10^{-2}	3.1277×10^{-5}	1.5798×10^{-2}	4.1076×10^{-5}	9.9507×10^{-1}	3.2460×10^{-3}
(5, 85, 5)	5.4704×10^{-3}	1.8763×10^{-5}	5.4331×10^{-3}	2.1733×10^{-5}	9.9320×10^{-1}	5.2334×10^{-3}
(5, 95, 5)	1.8508×10^{-3}	1.1457×10^{-5}	1.8493×10^{-3}	3.4951×10^{-5}	9.9917×10^{-1}	1.9871×10^{-2}
(5, 5, 5)	8.2926	1.7414×10^{-3}	8.3385	3.2520×10^{-2}	1.0055	3.9273×10^{-3}
(15, 15, 15)	6.6323×10^{-1}	2.6529×10^{-5}	6.6327×10^{-1}	6.6327×10^{-5}	1.0001	1.0771×10^{-4}
(25, 25, 25)	2.6883×10^{-1}	8.0648×10^{-6}	2.6882×10^{-1}	2.6882×10^{-5}	9.9999×10^{-1}	1.0440×10^{-4}
(35, 35, 35)	1.5668×10^{-1}	7.8342×10^{-6}	1.5668×10^{-1}	1.5668×10^{-5}	9.9997×10^{-1}	1.1180×10^{-4}
(45, 45, 45)	1.0440×10^{-1}	1.1485×10^{-5}	1.0442×10^{-1}	2.0883×10^{-5}	1.0001	2.2828×10^{-4}
(55, 55, 55)	3.0214×10^{-2}	1.8431×10^{-5}	3.0535×10^{-2}	4.0306×10^{-4}	1.0106	1.3354×10^{-2}
(65, 65, 65)	4.0656×10^{-3}	3.0085×10^{-6}	4.0605×10^{-3}	3.6544×10^{-5}	9.9875×10^{-1}	9.0191×10^{-3}
(75, 75, 75)	5.8612×10^{-4}	6.7990×10^{-7}	5.7853×10^{-4}	4.2811×10^{-6}	9.8705×10^{-1}	7.3934×10^{-3}
(85, 85, 85)	8.6606×10^{-5}	1.7148×10^{-7}	8.6486×10^{-5}	1.7038×10^{-6}	9.9861×10^{-1}	1.9772×10^{-2}
(95, 95, 95)	1.1289×10^{-5}	4.3238×10^{-8}	1.0600×10^{-5}	3.0104×10^{-7}	9.3894×10^{-1}	2.6907×10^{-2}
(5, 55, 5)	1.3722×10^{-1}	1.0017×10^{-4}	1.3728×10^{-1}	2.6083×10^{-4}	1.0004	2.0363×10^{-3}
(15, 55, 5)	1.2789×10^{-1}	9.7196×10^{-5}	1.2774×10^{-1}	2.4270×10^{-4}	9.9880×10^{-1}	2.0439×10^{-3}
(25, 55, 5)	1.1358×10^{-1}	9.0866×10^{-5}	1.1315×10^{-1}	1.9235×10^{-4}	9.9620×10^{-1}	1.8717×10^{-3}
(35, 55, 5)	9.5958×10^{-2}	8.4443×10^{-5}	9.5636×10^{-2}	1.4345×10^{-4}	9.9665×10^{-1}	1.7332×10^{-3}
(45, 55, 5)	7.8270×10^{-2}	7.3574×10^{-5}	7.8245×10^{-2}	1.5649×10^{-4}	9.9968×10^{-1}	2.2092×10^{-3}
(55, 55, 5)	5.6703×10^{-2}	6.2940×10^{-5}	5.6444×10^{-2}	1.2418×10^{-4}	9.9543×10^{-1}	2.4529×10^{-3}
(65, 55, 5)	1.8863×10^{-2}	3.5651×10^{-5}	1.8878×10^{-2}	5.8521×10^{-5}	1.0008	3.6335×10^{-3}
(75, 55, 5)	6.4662×10^{-3}	2.0304×10^{-5}	6.4197×10^{-3}	2.7605×10^{-5}	9.9280×10^{-1}	5.2861×10^{-3}
(85, 55, 5)	2.2810×10^{-3}	1.2066×10^{-5}	2.3859×10^{-3}	1.2455×10^{-4}	1.0460	5.4881×10^{-2}
(95, 55, 5)	7.9392×10^{-4}	7.0659×10^{-6}	7.7666×10^{-4}	7.1453×10^{-6}	9.7826×10^{-1}	1.2522×10^{-2}

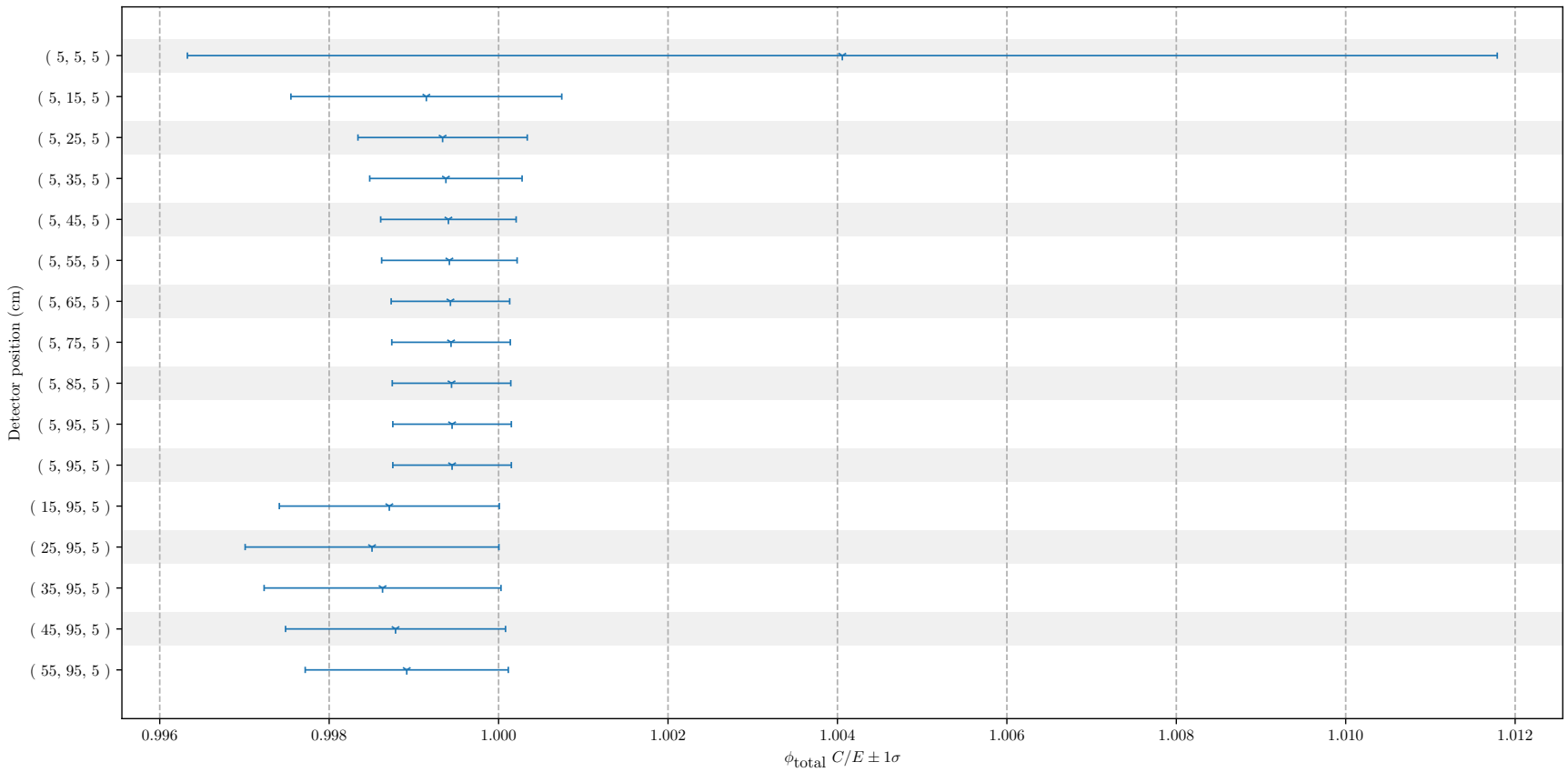

Figure 141: p2i_ce C/E Calculation Benchmark Results

Table 37: p2i_ce Calculation Benchmark Results

Coordinates	Benchmark ϕ_t	Benchmark unc.	Calc. ϕ_t	Calc. unc.	C/E	C/E unc.
(5, 5, 5)	5.9566	0.0000	5.9808	4.6052×10^{-2}	1.0041	7.7312×10^{-3}
(5, 15, 5)	1.3719	0.0000	1.3707	2.1931×10^{-3}	9.9915×10^{-1}	1.5986×10^{-3}
(5, 25, 5)	5.0087×10^{-1}	0.0000	5.0054×10^{-1}	5.0054×10^{-4}	9.9934×10^{-1}	9.9934×10^{-4}
(5, 35, 5)	2.5243×10^{-1}	0.0000	2.5227×10^{-1}	2.2704×10^{-4}	9.9938×10^{-1}	8.9944×10^{-4}
(5, 45, 5)	1.5026×10^{-1}	0.0000	1.5017×10^{-1}	1.2014×10^{-4}	9.9941×10^{-1}	7.9953×10^{-4}
(5, 55, 5)	9.9173×10^{-2}	0.0000	9.9115×10^{-2}	7.9292×10^{-5}	9.9942×10^{-1}	7.9954×10^{-4}
(5, 65, 5)	7.0179×10^{-2}	0.0000	7.0139×10^{-2}	4.9097×10^{-5}	9.9943×10^{-1}	6.9960×10^{-4}
(5, 75, 5)	5.2206×10^{-2}	0.0000	5.2177×10^{-2}	3.6524×10^{-5}	9.9944×10^{-1}	6.9961×10^{-4}
(5, 85, 5)	4.0319×10^{-2}	0.0000	4.0296×10^{-2}	2.8207×10^{-5}	9.9944×10^{-1}	6.9961×10^{-4}
(5, 95, 5)	3.2057×10^{-2}	0.0000	3.2040×10^{-2}	2.2428×10^{-5}	9.9945×10^{-1}	6.9962×10^{-4}
(5, 95, 5)	3.2057×10^{-2}	0.0000	3.2040×10^{-2}	2.2428×10^{-5}	9.9945×10^{-1}	6.9962×10^{-4}
(15, 95, 5)	1.7054×10^{-3}	0.0000	1.7032×10^{-3}	2.2142×10^{-6}	9.9871×10^{-1}	1.2983×10^{-3}
(25, 95, 5)	1.4056×10^{-4}	0.0000	1.4035×10^{-4}	2.1052×10^{-7}	9.9851×10^{-1}	1.4978×10^{-3}
(35, 95, 5)	3.2706×10^{-5}	0.0000	3.2661×10^{-5}	4.5725×10^{-8}	9.9863×10^{-1}	1.3981×10^{-3}
(45, 95, 5)	1.0851×10^{-5}	0.0000	1.0837×10^{-5}	1.4088×10^{-8}	9.9878×10^{-1}	1.2984×10^{-3}
(55, 95, 5)	4.1413×10^{-6}	0.0000	4.1368×10^{-6}	4.9642×10^{-9}	9.9892×10^{-1}	1.1987×10^{-3}

5.2.4 p2ii_ce

For the analytical Kobayashi p2ii_ce benchmarks, the benchmark data and calculation results are plotted in Fig. 142 as C/E ratios with individual values listed in Table 38.

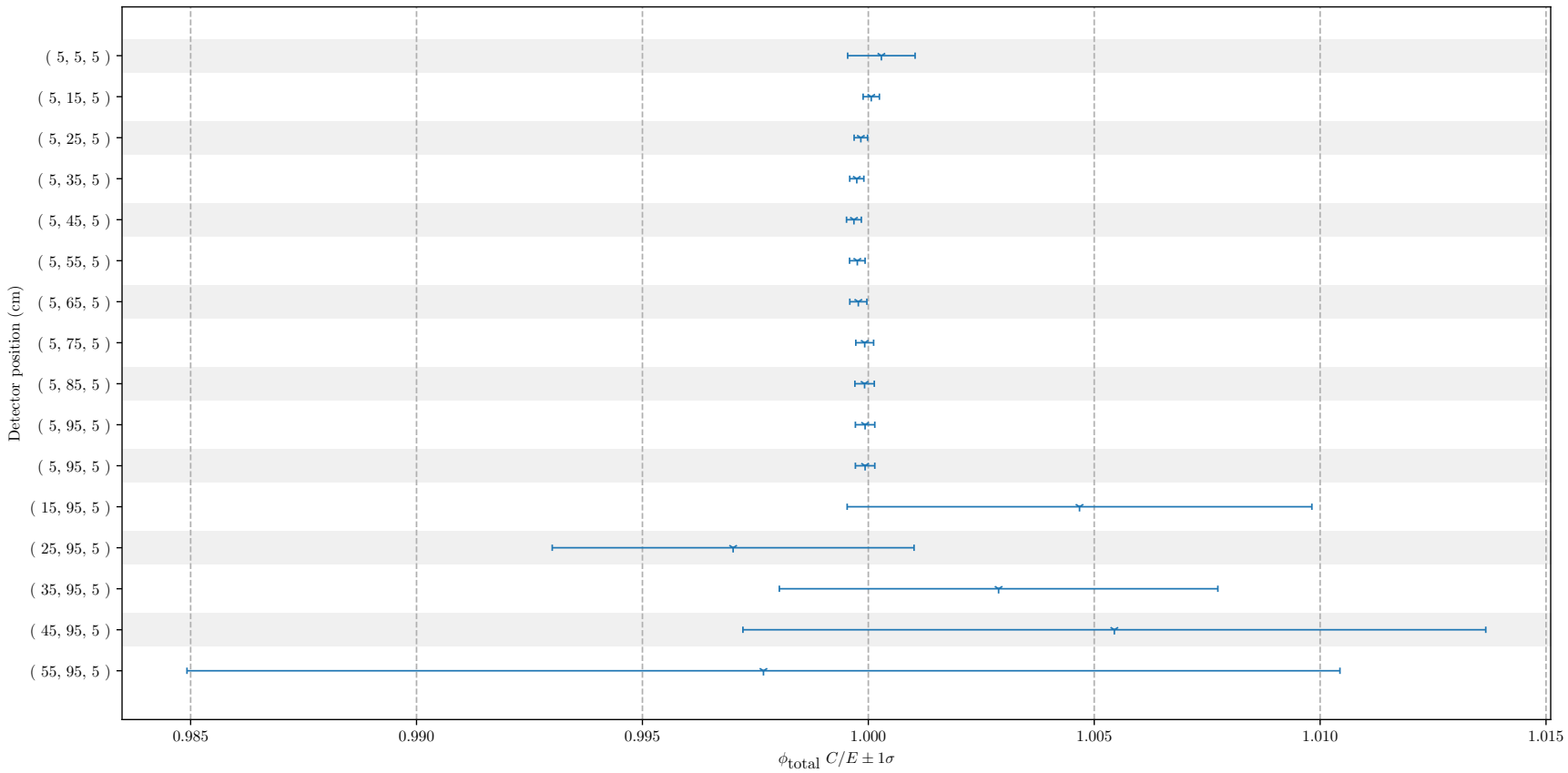

Figure 142: p2ii_ce C/E Calculation Benchmark Results

Table 38: p2ii_ce Calculation Benchmark Results

Coordinates	Benchmark ϕ_t	Benchmark unc.	Calc. ϕ_t	Calc. unc.	C/E	C/E unc.
(5, 5, 5)	8.6170	5.4287×10^{-3}	8.6195	3.4478×10^{-3}	1.0003	7.4647×10^{-4}
(5, 15, 5)	2.1612	3.2418×10^{-4}	2.1614	2.1614×10^{-4}	1.0001	1.8029×10^{-4}
(5, 25, 5)	8.9344×10^{-1}	9.8278×10^{-5}	8.9329×10^{-1}	8.9329×10^{-5}	9.9983×10^{-1}	1.4864×10^{-4}
(5, 35, 5)	4.7745×10^{-1}	5.7294×10^{-5}	4.7733×10^{-1}	4.7733×10^{-5}	9.9974×10^{-1}	1.5617×10^{-4}
(5, 45, 5)	2.8872×10^{-1}	3.7533×10^{-5}	2.8863×10^{-1}	2.8863×10^{-5}	9.9968×10^{-1}	1.6396×10^{-4}
(5, 55, 5)	1.8896×10^{-1}	2.6454×10^{-5}	1.8891×10^{-1}	1.8891×10^{-5}	9.9976×10^{-1}	1.7200×10^{-4}
(5, 65, 5)	1.3103×10^{-1}	2.0964×10^{-5}	1.3100×10^{-1}	1.3100×10^{-5}	9.9978×10^{-1}	1.8864×10^{-4}
(5, 75, 5)	9.4989×10^{-2}	1.6148×10^{-5}	9.4981×10^{-2}	9.4981×10^{-6}	9.9992×10^{-1}	1.9722×10^{-4}
(5, 85, 5)	7.1240×10^{-2}	1.3536×10^{-5}	7.1234×10^{-2}	7.1234×10^{-6}	9.9992×10^{-1}	2.1469×10^{-4}
(5, 95, 5)	5.4481×10^{-2}	1.0351×10^{-5}	5.4477×10^{-2}	5.4477×10^{-6}	9.9993×10^{-1}	2.1469×10^{-4}
(5, 95, 5)	5.4481×10^{-2}	1.0351×10^{-5}	5.4477×10^{-2}	5.4477×10^{-6}	9.9993×10^{-1}	2.1469×10^{-4}
(15, 95, 5)	6.5823×10^{-3}	1.6061×10^{-5}	6.6131×10^{-3}	2.9759×10^{-5}	1.0047	5.1429×10^{-3}
(25, 95, 5)	1.2800×10^{-3}	4.3009×10^{-6}	1.2762×10^{-3}	2.8076×10^{-6}	9.9701×10^{-1}	4.0042×10^{-3}
(35, 95, 5)	4.1341×10^{-4}	1.5007×10^{-6}	4.1461×10^{-4}	1.3267×10^{-6}	1.0029	4.8531×10^{-3}
(45, 95, 5)	1.5555×10^{-4}	7.0619×10^{-7}	1.5640×10^{-4}	1.0635×10^{-6}	1.0054	8.2208×10^{-3}
(55, 95, 5)	6.0277×10^{-5}	3.6106×10^{-7}	6.0137×10^{-5}	6.7955×10^{-7}	9.9768×10^{-1}	1.2760×10^{-2}

5.2.5 p3i_ce

For the analytical Kobayashi p3i_ce benchmarks, the benchmark data and calculation results are plotted in Fig. 143 as C/E ratios with individual values listed in Table 39.

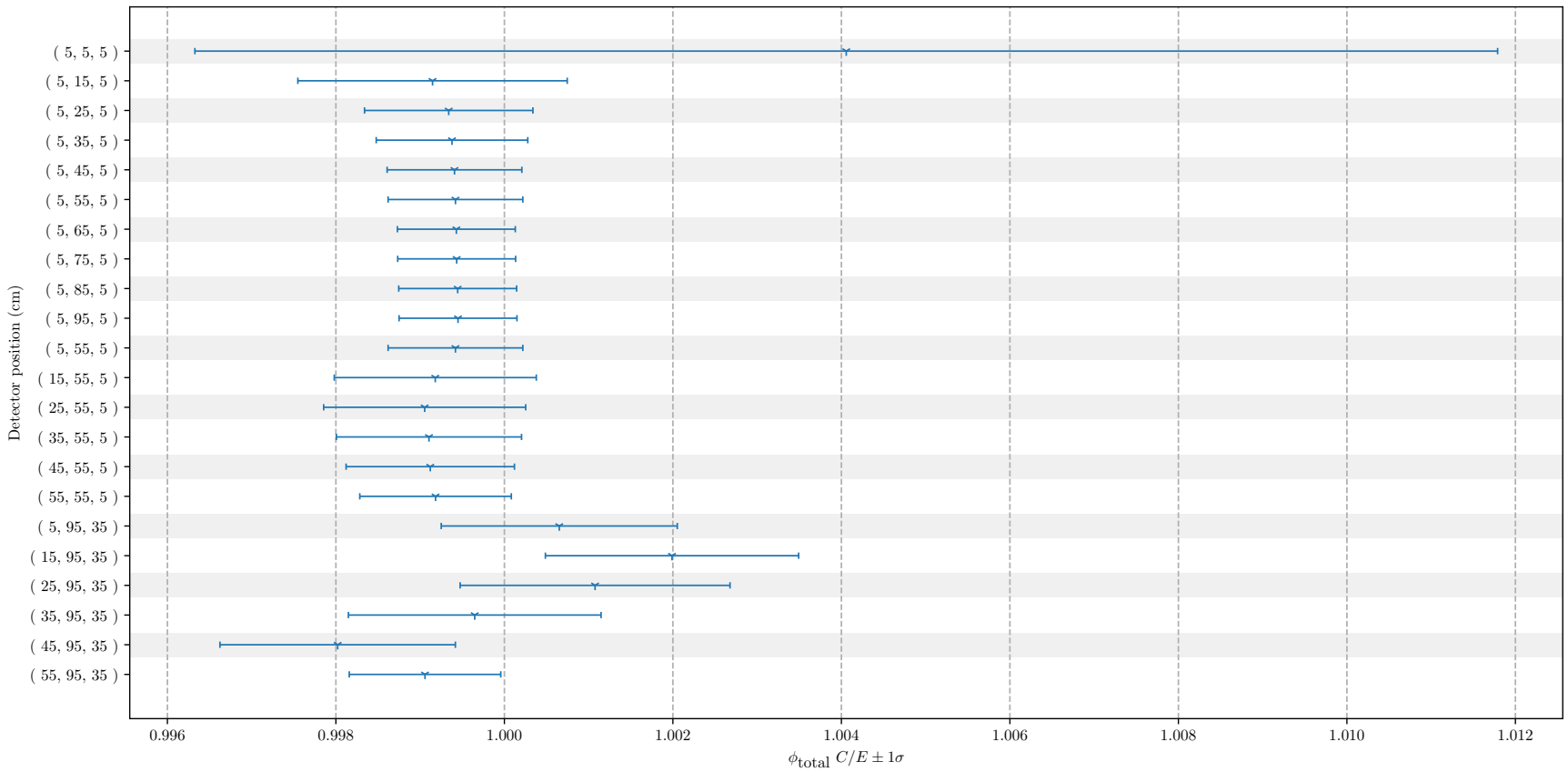

Figure 143: p3i_ce C/E Calculation Benchmark Results

Table 39: p3i_ce Calculation Benchmark Results

Coordinates	Benchmark ϕ_t	Benchmark unc.	Calc. ϕ_t	Calc. unc.	C/E	C/E unc.
(5, 5, 5)	5.9566	0.0000	5.9808	4.6052×10^{-2}	1.0041	7.7312×10^{-3}
(5, 15, 5)	1.3719	0.0000	1.3707	2.1931×10^{-3}	9.9915×10^{-1}	1.5986×10^{-3}
(5, 25, 5)	5.0087×10^{-1}	0.0000	5.0054×10^{-1}	5.0054×10^{-4}	9.9934×10^{-1}	9.9934×10^{-4}
(5, 35, 5)	2.5243×10^{-1}	0.0000	2.5227×10^{-1}	2.2704×10^{-4}	9.9938×10^{-1}	8.9944×10^{-4}
(5, 45, 5)	1.5026×10^{-1}	0.0000	1.5017×10^{-1}	1.2014×10^{-4}	9.9941×10^{-1}	7.9953×10^{-4}
(5, 55, 5)	9.9173×10^{-2}	0.0000	9.9115×10^{-2}	7.9292×10^{-5}	9.9942×10^{-1}	7.9954×10^{-4}
(5, 65, 5)	4.2262×10^{-2}	0.0000	4.2238×10^{-2}	2.9567×10^{-5}	9.9943×10^{-1}	6.9960×10^{-4}
(5, 75, 5)	1.1470×10^{-2}	0.0000	1.1464×10^{-2}	8.0247×10^{-6}	9.9943×10^{-1}	6.9960×10^{-4}
(5, 85, 5)	3.2466×10^{-3}	0.0000	3.2448×10^{-3}	2.2714×10^{-6}	9.9945×10^{-1}	6.9961×10^{-4}
(5, 95, 5)	9.4832×10^{-4}	0.0000	9.4780×10^{-4}	6.6346×10^{-7}	9.9945×10^{-1}	6.9961×10^{-4}
(5, 55, 5)	9.9173×10^{-2}	0.0000	9.9115×10^{-2}	7.9292×10^{-5}	9.9942×10^{-1}	7.9954×10^{-4}
(15, 55, 5)	2.4504×10^{-2}	0.0000	2.4484×10^{-2}	2.9381×10^{-5}	9.9918×10^{-1}	1.1990×10^{-3}
(25, 55, 5)	4.5448×10^{-3}	0.0000	4.5405×10^{-3}	5.4486×10^{-6}	9.9905×10^{-1}	1.1989×10^{-3}
(35, 55, 5)	1.4296×10^{-3}	0.0000	1.4283×10^{-3}	1.5712×10^{-6}	9.9910×10^{-1}	1.0990×10^{-3}
(45, 55, 5)	2.6485×10^{-4}	0.0000	2.6461×10^{-4}	2.6461×10^{-7}	9.9912×10^{-1}	9.9912×10^{-4}
(55, 55, 5)	9.1421×10^{-5}	0.0000	9.1346×10^{-5}	8.2212×10^{-8}	9.9918×10^{-1}	8.9926×10^{-4}
(5, 95, 35)	3.2706×10^{-5}	0.0000	3.2727×10^{-5}	4.5818×10^{-8}	1.0007	1.4009×10^{-3}
(15, 95, 35)	2.6842×10^{-5}	0.0000	2.6895×10^{-5}	4.0342×10^{-8}	1.0020	1.5030×10^{-3}
(25, 95, 35)	1.7002×10^{-5}	0.0000	1.7020×10^{-5}	2.7232×10^{-8}	1.0011	1.6017×10^{-3}
(35, 95, 35)	3.3798×10^{-5}	0.0000	3.3786×10^{-5}	5.0679×10^{-8}	9.9965×10^{-1}	1.4995×10^{-3}
(45, 95, 35)	6.0489×10^{-6}	0.0000	6.0370×10^{-6}	8.4517×10^{-9}	9.9802×10^{-1}	1.3972×10^{-3}
(55, 95, 35)	3.3646×10^{-6}	0.0000	3.3614×10^{-6}	3.0253×10^{-9}	9.9906×10^{-1}	8.9915×10^{-4}

5.2.6 p3ii_ce

For the analytical Kobayashi p3ii_ce benchmarks, the benchmark data and calculation results are plotted in Fig. 144 as C/E ratios with individual values listed in Table 40.

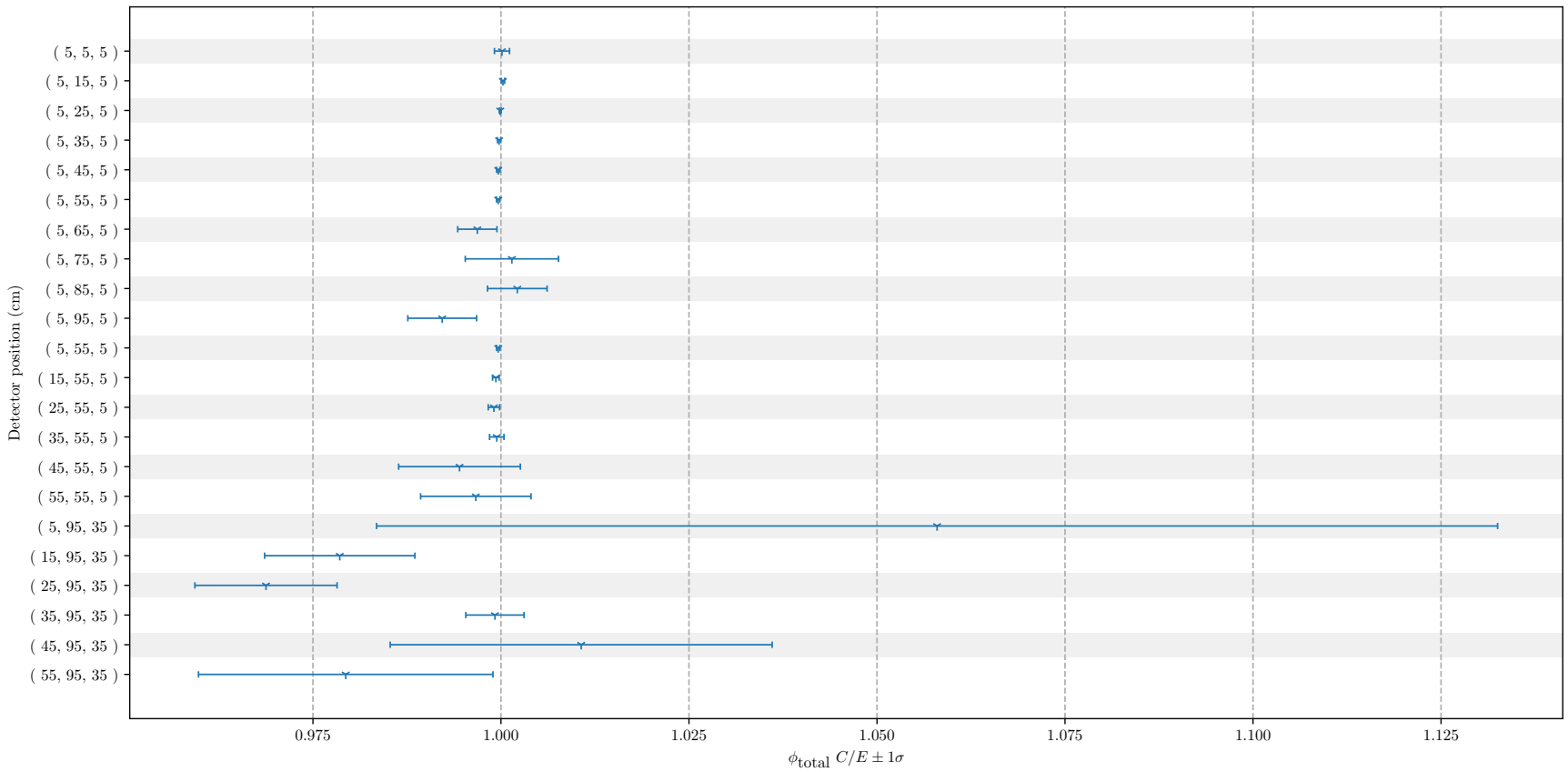

Figure 144: p3ii_ce C/E Calculation Benchmark Results

Table 40: p3ii_ce Calculation Benchmark Results

Coordinates	Benchmark ϕ_t	Benchmark unc.	Calc. ϕ_t	Calc. unc.	C/E	C/E unc.
(5, 5, 5)	8.6158	3.7909×10^{-3}	8.6169	7.7552×10^{-3}	1.0001	1.0019×10^{-3}
(5, 15, 5)	2.1613	2.1613×10^{-4}	2.1619	4.3237×10^{-4}	1.0003	2.2367×10^{-4}
(5, 25, 5)	8.9378×10^{-1}	7.1503×10^{-5}	8.9370×10^{-1}	8.9370×10^{-5}	9.9990×10^{-1}	1.2805×10^{-4}
(5, 35, 5)	4.7805×10^{-1}	3.8244×10^{-5}	4.7793×10^{-1}	9.5586×10^{-5}	9.9975×10^{-1}	2.1535×10^{-4}
(5, 45, 5)	2.8942×10^{-1}	2.6048×10^{-5}	2.8932×10^{-1}	5.7864×10^{-5}	9.9964×10^{-1}	2.1924×10^{-4}
(5, 55, 5)	1.9270×10^{-1}	1.9270×10^{-5}	1.9263×10^{-1}	3.8525×10^{-5}	9.9963×10^{-1}	2.2352×10^{-4}
(5, 65, 5)	1.0498×10^{-1}	8.0836×10^{-5}	1.0465×10^{-1}	2.6163×10^{-4}	9.9686×10^{-1}	2.6077×10^{-3}
(5, 75, 5)	3.3754×10^{-2}	3.6117×10^{-5}	3.3803×10^{-2}	2.0620×10^{-4}	1.0015	6.2021×10^{-3}
(5, 85, 5)	1.0816×10^{-2}	1.7630×10^{-5}	1.0839×10^{-2}	3.9021×10^{-5}	1.0022	3.9604×10^{-3}
(5, 95, 5)	3.3963×10^{-3}	9.3399×10^{-6}	3.3698×10^{-3}	1.2468×10^{-5}	9.9219×10^{-1}	4.5740×10^{-3}
(5, 55, 5)	1.9270×10^{-1}	1.9270×10^{-5}	1.9263×10^{-1}	3.8525×10^{-5}	9.9963×10^{-1}	2.2352×10^{-4}
(15, 55, 5)	6.7215×10^{-2}	1.2771×10^{-5}	6.7169×10^{-2}	2.6868×10^{-5}	9.9932×10^{-1}	4.4253×10^{-4}
(25, 55, 5)	2.2180×10^{-2}	6.2104×10^{-6}	2.2159×10^{-2}	1.5511×10^{-5}	9.9906×10^{-1}	7.5322×10^{-4}
(35, 55, 5)	9.9065×10^{-3}	3.2691×10^{-6}	9.9009×10^{-3}	8.9108×10^{-6}	9.9944×10^{-1}	9.5806×10^{-4}
(45, 55, 5)	3.3907×10^{-3}	6.6118×10^{-6}	3.3720×10^{-3}	2.6639×10^{-5}	9.9449×10^{-1}	8.0923×10^{-3}
(55, 55, 5)	1.0563×10^{-3}	3.4541×10^{-6}	1.0528×10^{-3}	6.9482×10^{-6}	9.9666×10^{-1}	7.3410×10^{-3}
(5, 95, 35)	3.4480×10^{-4}	2.7343×10^{-6}	3.6480×10^{-4}	2.5536×10^{-5}	1.0580	7.4533×10^{-2}
(15, 95, 35)	2.9183×10^{-4}	1.9231×10^{-6}	2.8557×10^{-4}	2.2274×10^{-6}	9.7857×10^{-1}	9.9923×10^{-3}
(25, 95, 35)	2.0579×10^{-4}	1.0886×10^{-6}	1.9936×10^{-4}	1.6348×10^{-6}	9.6876×10^{-1}	9.4534×10^{-3}
(35, 95, 35)	2.6209×10^{-4}	1.9656×10^{-7}	2.6188×10^{-4}	9.9513×10^{-7}	9.9920×10^{-1}	3.8702×10^{-3}
(45, 95, 35)	1.0537×10^{-4}	4.2358×10^{-7}	1.0649×10^{-4}	2.6410×10^{-6}	1.0107	2.5392×10^{-2}
(55, 95, 35)	4.4496×10^{-5}	1.9578×10^{-7}	4.3578×10^{-5}	8.4977×10^{-7}	9.7936×10^{-1}	1.9578×10^{-2}

References

[Citing pages are listed after each reference.]

1. R. D. Mosteller, "Comparison of Results from the MCNP Criticality Validation Suite Using ENDF/B-VI and Preliminary ENDF/B-VII Nuclear Data," in *AIP Conference Proceedings*, vol. 769, no. 1. American Institute of Physics, 2005, pp. 458–461, Also: LA-UR-04-6489. DOI: 10.1063/1.1945047 [Pages 3 and 14]

2. "International Criticality Safety Benchmark Evaluation Project Handbook 2015," OECD Nuclear Energy Agency, Paris, France, Tech. Rep. ICSBEP-2015, 2015. DOI: 10.1787/936dd0d6-en [Page 3]

3. J. S. Coursey, D. J. Schwab, J. J. Tsai, and R. A. Dragoset, "Atomic Weights and Isotopic Compositions (version 4.1)," National Institute of Science and Technology, Gaithersburg, MD, 2015. URL: http://physics.nist.gov/Comp [Page 3]

4. M. Berglund and M. E. Wieser, "Isotopic compositions of the elements 2009 (IUPAC Technical Report)," *Pure and Applied Chemistry*, vol. 83, no. 2, pp. 397–410, 2011. DOI: 10.1351/PAC-REP-10-06-02 [Page 3]

5. R. D. Mosteller, F. B. Brown, and B. C. Kiedrowski, "An Expanded Criticality Validation Suite for MCNP," in *American Nuclear Society Summer Meeting*, Hollywood, FL, USA, Jun. 2011, Also: LA-UR-11-00240. URL: https://permalink.lanl.gov/object/tr?what=info:lanl-repo/lareport/LA-UR-11-00240 [Page 3]

6. J. T. Goorley, M. R. James, T. E. Booth, F. B. Brown, J. S. Bull, L. J. Cox, J. W. Durkee, Jr., J. S. Elson, M. L. Fensin, R. A. Forster, III, J. S. Hendricks, H. G. Hughes, III, R. C. Johns, B. C. Kiedrowski, R. L. Martz, S. G. Mashnik, G. W. McKinney, D. B. Pelowitz, R. E. Prael, J. E. Sweezy, L. S. Waters, T. A. Wilcox, and A. J. Zukaitis, "Initial MCNP6 Release Overview - MCNP6 Version 1.0," Los Alamos National Laboratory, Los Alamos, NM, USA, Tech. Rep. LA-UR-13-22934, Rev. 1, Jun. 2013. DOI: 10.2172/1086758 [Pages 4 and 5]

7. A. Sandoval, H. H. Gutbrod, W. G. Meyer, R. Stock, C. Lukner, A. M. Poskanzer, J. Gosset, J.-C. Jourdain, C. H. King, G. King, N. Van Sen, G. D. Westfall, and K. L. Wolf, "Spectra of p, d, and t from Relativistic Nuclear Collisions," *Physical Review C*, vol. 21, no. 4, pp. 1321–1343, Apr. 1980. DOI: 10.1103/PhysRevC.21.1321 [Page 4]

8. Y. Iwata, T. Murakami, H. Sato, H. Iwase, T. Nakamura, T. Kurosawa, L. Heilbronn, R. M. Ronningen, K. Ieki, Y. Tozawa, and K. Niita, "Double-differential Cross Sections for the Neutron Production from Heavy-ion Reactions at Energies $E/A = 290$–600 MeV," *Physical Review C*, vol. 64, no. 5, pp. 054 609–054 619, Oct. 2001. DOI: 10.1103/PhysRevC.64.054609 [Page 5]

9. H. Iwase, Y. Iwata, T. Nakamura, K. Gudima, S. Mashnik, A. Sierk, and R. Prael, "Neutron Spectra from Intermediate-energy Nucleus-nucleus Reactions," in *Proceedings of the International Conference on Nuclear Data for Science and Technology (ND2004) via AIP Conference Proceedings*, R. C. Haight, M. B. Chadwick, T. Kawano, and P. Talou, Eds., vol. 769, no. 1. Santa Fe, NM, USA. September 26–October 1, 2004: American Institute of Physics, 2005, pp. 1066–1069, also: LA-UR-05-0367. DOI: 10.1063/1.1945191 [Page 5]

10. L. Heilbronn, C. J. Zeitlin, Y. Iwata, T. Murakami, H. Iwase, T. Nakamura, T. Nunomiya, H. Sato, H. Yashima, R. M. Ronningen, and K. Ieki, "Secondary Neutron-production Cross Sections from Heavy-ion Interactions Between 230 and 600 MeV/Nucleon," *Nuclear Science and Engineering*, vol. 157, no. 2, pp. 142–158, Oct. 2007. DOI: 10.13182/NSE07-A2719 [Page 5]

11. R. M. Ronningen, I. Remec, and L. H. Heilbronn, "Benchmarking Heavy Ion Transport Codes FLUKA, HETC-HEDS MARS15, MCNPX, and PHITS," Michigan State University, East Lansing, MI, USA, Tech. Rep. DE-FG02-08ER41548, Jun. 2013. DOI: 10.2172/1082753 [Page 5]

12. S. Nagamiya, M. C. Lemaire, E. Moeller, S. Schnetzer, G. Shapiro, H. Steiner, and I. Tanihata, "Production of Pions and Light Fragments at Large Angles in High-energy Nuclear Collisions," *Physical Review C*, vol. 24, no. 3, pp. 971–1009, Sep. 1981. DOI: 10.1103/PhysRevC.24.971 [Page 6]

13. M. C. Lemaire, S. Nagamiya, O. Chamberlain, G. Shapiro, S. Schnetzer, H. Steiner, and I. Tanihata, "Tables of Light-fragment Inclusive Cross Sections in Relativistic Heavy Ion Collisions. Part I. C + C, C + Pb, Ne + NaF, Ne + Cu, Ne + Pb $\rightarrow \pi^{\pm}$, p, d, t, ^{3}He; $E_{\mathrm{BEAM}} = 800$ MeV/A," Lawrence Berkeley National Laboratory, Berkeley, CA, USA, Tech. Rep. LBL-8463, Nov. 1978. DOI: 10.2172/6313624 [Page 6]

14. N. I. of Standards and Technology, "CODATA Recommended Values of the Fundamental Physical Constants: 2018," U.S. Department of Commerce, Washington, D.C., USA, Tech. Rep. NIST SP 961, 2019. URL: https://physics.nist.gov/cuu/pdf/wall_2018.pdf [Page 6]

15. C. Wong, J. D. Anderson, P. Brown, L. F. Hansen, J. L. Kammerdiener, C. Logan, and B. Pohl, "Livermore Pulsed Sphere Program: Program Summary through July 1971," Lawrence Livermore National Laboratory, Livermore, CA, USA, Tech. Rep. UCRL-51144, Rev. 1, Feb. 1972. [Pages 6 and 7]

16. J. A. Kulesza and R. L. Martz, "Evaluation of Pulsed Sphere Time-of-Flight and Neutron Attenuation Experimental Benchmarks Using MCNP6's Unstructured Mesh Capabilities," *Nuclear Technology*, vol. 195, no. 1, pp. 44–54, Jul. 2016, Los Alamos National Laboratory Tech. Rep. LA-UR-15-27014. DOI: 10.13182/NT15-121 [Page 6]

17. J. D. Court, R. C. Brockhoff, and J. S. Hendricks, "Lawrence Livermore Pulsed Sphere Benchmark Analysis of MCNP™ ENDF/B-VI," Los Alamos National Laboratory, Los Alamos, NM, USA, Tech. Rep. LA-12885, Dec. 1994. [Page 6]

18. R. D. Mosteller, S. C. Frankle, and P. G. Young, "Data Testing of ENDF/B-VI with MCNP: Critical Experiments, Thermal-Reactor Lattices, and Time-of-Flight Measurements," Los Alamos National Laboratory, Los Alamos, NM, USA, Tech. Rep. LA-UR-96-2143, Jun. 1996. [Page 6]

19. J. A. Bucholz and S. C. Frankle, "Improving the LLNL Pulsed Sphere Experiments Database and MCNP Models," Los Alamos National Laboratory, Los Alamos, NM, USA, Tech. Rep. LA-UR-03-0609, Jan. 2003. URL: https://mcnp.lanl.gov/pdf_files/la-ur-03-0609.pdf [Page 6]

20. J. A. Bucholz and S. C. Frankle, "Improving the LLNL Pulsed Sphere Experiments Database and MCNP Models," Los Alamos National Laboratory, Los Alamos, NM, USA, Presentation LA-UR-03-3537, 2003. URL: http://permalink.lanl.gov/object/tr?what=info:lanl-repo/lareport/LA-UR-03-3537 [Page 6]

21. S. C. Frankle, "Possible Impact of Additional Collimators on the LLNL Pulsed Sphere Experiments (U)," Los Alamos National Laboratory, Los Alamos, NM, USA, Tech. Rep. LA-UR-05-5877, Jul. 2005. [Page 6]

22. S. C. Frankle, "LLNL Pulsed Sphere Measurements and Detector Response Functions (U)," Los Alamos National Laboratory, Los Alamos, NM, USA, Tech. Rep. LA-UR-05-5878, Jul. 2005. [Page 6]

23. S. C. Frankle, "README file for Running a LLNL Pulsed-Sphere Benchmark Calculation (U)," Los Alamos National Laboratory, Los Alamos, NM, USA, Tech. Rep. LA-UR-05-5879, Jul. 2005. [Page 6]

24. G. J. Lockwood, L. E. Ruggles, G. H. Miller, and J. A. Halbleib, "Calorimetric Measurement of Electron Energy Deposition in Extended Media—Theory vs. Experiment," Sandia National Laboratories, Albuquerque, NM, USA, Tech. Rep. SAND79-0414, Jan. 1980. DOI: 10.2172/5516784 [Page 9]

25. G. J. Lockwood, L. E. Ruggles, G. H. Miller, and J. A. Halbleib, "Electron Energy and Charge Albedos—Calorimetric Measurement vs. Monte Carlo Theory," Sandia National Laboratories, Albuquerque, NM, USA, Tech. Rep. SAND80-1968, Nov. 1981. DOI: 10.2172/5018508 [Page 9]

26. J. Sempau, J. M. Fernández-Varea, E. Acosta, and F. Salvat, "Experimental Benchmarks of the Monte Carlo Code PENELOPE," *Nuclear Instruments and Methods in Physics Research Section B: Beam Interactions with Materials and Atoms*, vol. 207, no. 2, pp. 107–123, Jun. 2003. DOI: 10.1016/S0168-583X(03)00453-1 [Page 9]

27. O. Kadri, V. N. Ivanchenko, F. Gharbi, and A. Trabelsi, "GEANT4 Simulation of Electron Energy Deposition in Extended Media," *Nuclear Instruments and Methods in Physics Research Section B: Beam Interactions with Materials and Atoms*, vol. 258, no. 2, pp. 381–387, May 2007. DOI: 10.1016/j.nimb.2007.02.088 [Page 9]

28. H. G. Hughes, III, "Recent Developments in Low-energy Electron/Photon Transport for MCNP6," Los Alamos National Laboratory, Los Alamos, NM, USA, Tech. Rep. LA-UR-12-24213, Rev. 4, Jul. 2013. URL: https://mcnp.lanl.gov/pdf_files/la-ur-12-24213v4.pdf [Page 9]

29. D. A. Dixon and H. G. Hughes, III, "Validation of MCNP6 for Electron Energy Deposition in Extended Media," Los Alamos National Laboratory, Los Alamos, NM, USA, Presentation LA-UR-15-28708, Nov. 2015. URL: http://permalink.lanl.gov/object/tr?what=info:lanl-repo/lareport/LA-UR-15-28708 [Page 9]

30. D. A. Dixon and H. G. Hughes, III, "A Complete Reporting of MCNP6 Validation Results for Electron Energy Deposition in Single-layer Extended Media for Source Energies $\leq$ 1-MeV," Los Alamos National Laboratory, Los Alamos, NM, USA, Tech. Rep. LA-UR-16-22749, May 2016. DOI: 10.2172/1253497 [Page 9]

31. D. A. Dixon, "A New MCNP6 Electron-Photon Transport Validation Test: The Lockwood Energy Deposition Experiment," Los Alamos National Laboratory, Los Alamos, NM, USA, Tech. Rep. LA-UR-16-23838, Jun. 2016. [Page 9]

32. D. A. Dixon, "An Update to the Computation of the Goudsmit-Saunderson Distribution in MCNP® Version 6.2," Los Alamos National Laboratory, Los Alamos, NM, USA, Tech. Rep. LA-UR-16-27959, Oct. 2016. DOI: 10.2172/1330070 [Page 9]

33. D. A. Dixon, "An Update to the Lockwood Energy Deposition Validation Suite for the MCNP® Version 6.2 Electron-photon Transport Algorithms," Los Alamos National Laboratory, Los Alamos, NM, USA, Tech. Rep. LA-UR-17-23433, Apr. 2017. [Page 9]

34. R. D. Mosteller and B. C. Kiedrowski, "A Rossi Alpha Validation Suite for MCNP," Los Alamos National Laboratory, Los Alamos, NM, USA, Tech. Rep. LA-UR-11-01162, Feb. 2011. [Page 10]

35. G. E. McKenzie, IV, "Validation of MCNP® Rossi-alpha Calculations using Recent Measurements," Los Alamos National Laboratory, Los Alamos, NM, USA, Tech. Rep. LA-UR-19-25525, Rev. 1, Aug. 2019. [Page 10]

36. M. A. Lively, D. Perez, B. P. Uberuaga, and X. Tang, "Validation of the Single-Event Method for Low-Energy Electron Transport Via Stopping Power Calculations with MCNP," *Radiation Physics and Chemistry*, vol. 216, p. 111483, Mar. 2024, Los Alamos National Laboratory Tech. Rep. LA-UR-23-29803, Rev. 1. DOI: 10.1016/j.radphyschem.2023.111483 [Page 11]

37. A. Sood, R. A. Forster, III, and D. K. Parsons, "Analytical Benchmark Test Set for Criticality Code Verification," *Progress in Nuclear Energy*, vol. 42, no. 1, pp. 55–106, 2003, Los Alamos National Laboratory Tech. Rep. LA-UR-01-3082. DOI: 10.1016/S0149-1970(02)00098-7 [Page 11]

38. K. Kobayashi, N. Sugimura, and Y. Nagaya, "3D radiation transport benchmark problems and results for simple geometries with void region," *Progress in Nuclear Energy*, vol. 39, no. 2, pp. 119–144, 2001. DOI: 10.1016/S0149-1970(01)00007-5 [Pages 11 and 13]

39. J. A. Kulesza and R. L. Martz, "Evaluation of the Kobayashi Analytical Benchmark using MCNP6's Unstructured Mesh Capabilities," *Nuclear Technology*, vol. 195, no. 1, pp. 55–70, Jul. 2016, Los Alamos National Laboratory Tech. Rep. LA-UR-15-27089. DOI: 10.13182/NT15-122 [Page 12]

40. B. E. Toth and F. B. Brown, "MCNP5 Benchmark Calculations for 3-d Radiation Transport in Simple Geometries with Void Regions," Los Alamos National Laboratory, Los Alamos, NM, USA, Tech. Rep. LA-UR-03-5974, Aug. 2003. URL: http://permalink.lanl.gov/object/tr?what=info:lanl-repo/lareport/LA-UR-03-5974 [Page 12]

41. H. G. Hughes, III, "Improvements in Electron-photon-relaxation Data for MCNP6," Los Alamos National Laboratory, Los Alamos, NM, USA, Tech. Rep. LA-UR-16-20840, 2016. URL: http://permalink.lanl.gov/object/tr?what=info:lanl-repo/lareport/LA-UR-16-20840 [Pages 81 and 123]